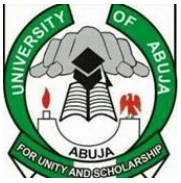

PREDICTING CONCENTRATED FLOW EROSION IN DATA SPARSE REGIONS

MGBANYI, LIBERTY LAZARUS ORAPINE, BSc., MSc.

Thesis submitted to The University of Nottingham

for the Degree of Doctor of Philosophy

February 2020

ABSTRACT

This PhD explores the possibility of using the Compound Topographic Index (CTI), which traditionally requires high-resolution data to predict concentrated flow erosion, to predict susceptibility to concentrated flow erosion in data-sparse regions. To achieve this, the PhD had to focus on a number of issues. The first is the accuracy of slopes derived from DEMs of low resolution over large topographic areas. Slope is vital input to many erosion models, including the CTI, but its accuracy is shown here to be dependent on the slope equation used and the terrain ruggedness. This was found to be problematic on high-resolution DEMS but, when using low resolution DEMs, the topography is generally much less rugged and so it is possible to use a single equation to calculate representative slopes. This slope calculation was used to determine CTI at a study site at Mount St Helens, USA, across a range of DEMs with different spatial resolutions. The results confirm earlier research in that they demonstrate that a terrain model's ability to predict gully locations and centre-line coordinates declines with coarsening DEM resolution. In an attempt to improve model performance for low resolution data, the CTI was adapted using a fuzzy logic approach and the fuzzy-CTI model was compared to the original CTI first, at Mount St Helens, across a range of DEM resolutions, and second, using data already available from the www for a study area in South Africa. In all cases, the fuzzy logic approach showed a small improvement over the original CTI, but both still gave relatively poor predictions (~50% accuracy) of gully locations when using coarse, 30 m resolution data. It was then found that the accuracy of the fuzzy CTI could be improved in two ways. First, by setting a threshold value rather than taking any positive value as indicating that a gully would be present at a given node in the DEM. This reduced the number of false positives and improved the accuracy of fuzzy CTI to >70%. A ROC curve validation approach than allowed the most appropriate threshold value for a given study site to be determined, quantitatively. The second way that accuracy was improved was to apply the fuzzy CTI to specific environment units. This revealed that in areas with weak soil structures and/or cropland land-cover, the predictive performance of the fuzzy CTI improved further. In contrast, where soils were strong and/or forest cover was present, predictive performance was poor because gullies were often predicted where they were not observed, most likely because of the stabilising effects of current environmental conditions. It follows that areas such as these are topographically-susceptible to gully formation and could suffer serious gullying if land use were changed (e.g. from forest to cropland) and/or soil structure was weakened. Finally, the results are discussed, including key conclusions and areas for future analysis. Of particular note is the difficulty in validating a model of gully susceptibility using data on gully presence/absence because some areas may be susceptible to gullies even though gullies have not yet formed. The results are an important step toward developing a terrain model capable of accurately delineating areas susceptible using low-resolution DEMs that are available globally. However, it must be remembered that topography alone is insufficient to predict exactly where and when a gully will actually form.

ACKNOWLEDGEMENT AND APPRECIATION

First and foremost, I give thanks to GOD almighty who made way for me to come to the University of Nottingham and continued blessing me and my family with good health and protection during my PhD.

I must say that I am a mosaic of numerous favours and blessing from several sources made possible by God through men and women whom I must not rescind to thank and acknowledge. However, this acknowledgement is not by any means an exhaustive compilation of all the good wills from good people towards me directly or indirectly contributing to this milestone achievement. This will be too numerous to mention here, but I rest in the fact that God said "I will bless those who bless you……" Genesis 12:3, KJV and therefore thank you very much and your blessings will never elude you.

The first part of the mosaic started with my parents who encouraged and educated me on the importance of education, with many prayers for me to go to school amidst the poor economic status. My father understood the importance of training a child so that when they grow old, they may not depart from it: "No discipline is enjoyable while it is happening—it's painful! But afterward there will be a peaceful harvest of right living for those who are trained in this way". My mother's prayer for me resounds in my ears all the time. She had always tried her best to support my early years of education but, when it was obvious she could not, she prayed for me saying "Though I do not have means to further your studies, God will make a way for you when there seems to be no way, He will give you brothers, sisters, friends, Fathers and Mothers wherever you go and God will be your helper even through them". This prayer has been answered in my life, times without number.

The University of Nottingham is the right place to be by someone in search of sound academic experience. I will not be at this stage of writing this acknowledgement if it were not the diligent support and hard work of my supervisors, Professor Colin R. Thorne and Associate Professor Matthew Johnson. They were all always ready to support my PhD journey. Their constructive reviews of my work along with that of my internal assessor, Associate Professor Gary Priestnall, are highly appreciated. The entire school of Geography, University of Nottingham (staff and students) provided an atmosphere that made it possible for me to achieve this thesis, especially during periods of extenuating circumstances. Thanks also to Adam Mosbrucker of the USGS and Associate Professor Gary Priestnall for providing GIS data on Mount Saint Helens, which was useful for my studies.

Special thanks to the Federal Republic of Nigeria who via the Tertiary Education Trust Fund of Nigeria (TETFUND) has provided funding for this study. I thank the then Vice Chancellor of the University of Abuja Professor Michael Adikwu who

brought possibility and opportunity to University of Abuja through his excellent administration making it possible for many colleagues and I to benefit from TETFUND PhD sponsorship. I also thank the Department of Geography and Environmental Management of the University of Abuja then headed by Prof S.P Ejaro, currently being headed by Professor M.M Alhassan and the Faculty of Social Science then headed by Professor Rhoda Mundi, currently being headed by Professor Y.A Zoaka for any form of support known or unknown that they have administratively rendered to me while on this PhD Journey.

Thanks to my lovely wife for her unwavering support and encouragements – she worked hard to support our living expense in the midst of insufficient funds. I thank my children for always asking me “Daddy when are you going to finish”. For them too it has been a rough journey. I thank my elder sister Mwuese Mgbanyi for her encouragement and support, starting from my early journey toward education without which I will not be talking of a PhD today.

I remain grateful to Eileen Thorne for all her support via providing a family and friendly atmosphere through her visits and our visits, taking my family out, and various gifts to the children on their birthdays, Easter, and Christmas. Throughout my studies in Nottingham, when I was unable to take break from research to relieve the pressure, she ensured that opportunity was created for me to take a break and do outing with my family. To my Good Neighbours Mr and Mrs Joseph Ford, and Mr and Mrs Phil, I say thank you for your care and love throughout the time of my PhD.

I thank Trent Vineyard Church and our small group for always being a place of spiritual refreshment, family, care and love. You have been an instrument of God, the oil that lubricated the front between my spiritual and the secular.

TABLE OF CONTENTS

ABSTRACT ..... **II**

ACKNOWLEDGEMENT AND APPRECIATION ..... **III**

TABLE OF CONTENTS ..... **V**

LIST OF FIGURES ..... **IX**

LIST OF TABLES ..... **XV**

CHAPTER 1: INTRODUCTION **1**

1.1. The Global Problem of Gullying **1**

1.2. Aim and objectives **2**

1.3. Gullying and its prediction **4**

1.3.1. Definition of topographic attributes relevant to understanding overland flow erosion 4
1.3.2. Fluvial implications of land surface curvature 7
1.3.3. Stream power and the Compound Topographic Index (CTI) 7
1.3.4. Modelling gullying with topographic data and the Compound Topographic Index (CTI) 11
1.3.5. Approaches to modelling gullying 14
1.3.6. Gully prediction using topographic data and the future utility of the CTI 20

CHAPTER 2: INVESTIGATING VARIATION OF TWO OF THE MOST POPULAR SLOPE DERIVATION METHODS WITH TERRAIN RUGGEDNESS **23**

2.1. Introduction and aim **23**

2.2. Literature Review **23**

2.2.1. Approaches to terrain analysis and slope fitting 23
2.2.2. Zevenbergen and Thorne method 28
2.2.3. Horn (1981) method 33
2.2.4. Quantifying topographic ruggedness 35

2.3. Chapter objectives **38**

2.4. Methodology **40**

2.4.1. Introduction to the methods 40
2.4.2. Mount St Helens 40
2.4.3. Comparing the Horn and Zevenbergen and Thorne slope calculation methods (Objective 2.1) 42
2.4.4. Comparison of calculated slopes with field measurements (Objective 2.2) 46
2.4.5. Investigation of whether slope accuracy is related to terrain ruggedness based on cross-sectional data (Objective 3) 49

2.4.6. Investigation of how calculated slopes are affected by ruggedness and grid resolution (Objectives 3 and 4) 52

2.5. Results 53

2.5.1. Comparison of slopes calculated using the Horn and Z&T methods (Objective 1) 53
2.5.2. Comparison of calculated slopes with field measurements (Objective 2) 66
2.5.3. Investigation of whether slope accuracy is related to terrain ruggedness and grid resolution (Objectives 3 and 4) 69

2.6. Discussion 81

CHAPTER 3: PREDICTING CONCENTRATED OVERLAND FLOW AND GULLYING 85

3.1. Introduction 85

3.2. Literature review 86

3.2.1. Influence of data resolution on terrain analyses for gully prediction 86
3.2.2. Threshold CTI values for gully initiation 88
3.2.3. Specific and relative values of threshold CTIs in the USA 90
3.2.4. DEM of difference (DoD) concept and technique 96

3.3. Chapter Objective 99

3.4. Methodology 101

3.4.1. Historical DEMs at Mount Saint Helens 101
3.4.2. Field mapped gullies, CTI threshold gullies and gullies extracted from DoDs as ground truth 103
3.4.3. Using the DEM of Difference (DOD) to detect areas of gully erosion 105
3.4.4. Principle behind validating a model using the Receiver Operator Characteristics (ROC) 110

3.5. Results 114

3.5.1. Melton Farm 114
3.5.2. Symbology and visualisation of the CTI at Mount Saint Helens 118
3.5.3. Prediction performance evaluation of CTI using observed gullies at Mt St Helens 123
3.5.4. Comparing and Ranking the predictive abilities based on their Accuracies 131

3.6. Discussion and conclusion 131

CHAPTER 4: NEW VERSION OF THE CTI MODEL, BASED ON FUZZY LOGIC 134

4.1. Introduction 134

4.2. Chapter Objectives 134

4.3. Literature review 134

4.3.1. Topographic modelling with continuous variables 134

4.3.2. Using fuzzy logic in topographic analysis 136
4.3.3. Fuzzy logic and land surface erosion modelling 138

4.4. Methodology 140

4.4.1. Expert-based knowledge concerning topographic parameters 140
4.4.2. Expert knowledge-based rules and knowledge-based systems. 141
4.4.3. Fuzzification 143
4.4.4. Fuzzy Rule evaluation 146
4.4.5. Validation of fuzzy CTI, comparison with the original CTI and effect of DEM quality at Mount Saint Helens and Eastern Cape Province of South Africa. 148
4.4.6. Field gullies in South Africa and data availability 149

4.5. Results 153

4.5.1. Visual comparison of original CTI and fuzzy CTI predictions based on the 5m, LiDAR-based DEM 153
4.5.2. Selected comparisons of ROC performance parameters and curves 156
4.5.3. Fuzzy CTI versus original CTI based on the 30 m LiDAR DEM and USGS SRTM 30 m DEM at Mount St Helens 159
4.5.4. Predicting and validating gullying in Eastern Cape Province of South Africa. 163

4.6. Discussion and conclusion 166

CHAPTER 5: CONTROLS ON WHETHER AND WHERE GULLIES ARE OBSERVED WITHIN A TOPOGRAPHICALLY-SUSCEPTIBLE AREA 170

5.1. Introduction 170

5.2. Objective 170

5.3. Literature review 171

5.3.1. Environmental influences on gullying 171
5.3.2. Influence of a soil property-based soil erodibility index on the threshold CTI 172
5.3.3. Dispersion Ratio 173
5.3.4. Clay Ratio (CR) 174
5.3.5. Modified Clay Ratio 175
5.3.6. Critical Level of Soil Organic Matter Content 175
5.3.7. Sodium absorption ratio (SAR) and exchangeable sodium percentage (ESP) 177
5.3.8. Land use and vegetation cover impacts on gullying 178

5.4. Methodology 179

5.4.1. Methodological overview 179
5.4.2. Environmental descriptors 179

5.5. Results and discussion 182

5.5.1. Exploration of the benefits of considering land cover 182

5.5.2. Exploration of the benefits of considering soil conditions 190
5.5.3. Prediction of gullies at sub-Provincial scale in the Eastern Cape Province 193
5.5.4. Analysis of variance of fuzzy CTI with subsets of environmental descriptors 196
5.5.5. Discussion and Conclusion 198
CHAPTER 6: DISCUSSION AND CONCLUSIONS 200

6.1. Major findings of the study and their implications 200

6.2. Fuzzy CTI and constraints on modelling 202

6.3. Implications for land management 205

6.4. Future research 206

APPENDICES 210

REFERENCES 234

LIST OF FIGURES

Figure 1.1: Illsutation of topographic attributes (https://www.spatialanalysisonline.com/HTML/profiles_and_curvature.htm) 5

Figure 1.2: Diagrammatic presentation of profile and planform curvature. For profile curvature, A(-) represents a convex profile, implying accelerating flow, B(+) represents a concave profile, implying decelerating flow, and C(0) indicates that the profile is linear, implying uniform flow. For plan curvature, D(+) represents a convex planform, implying diverging flow, E(-) represents a concave planform, implying converging flow, and C(0) represents a linear planform with uniform flow (source: ArcGIS instruction manual). 7

Figure 1.3: Concentration of flow in swales due to topographic control, after Thorne (1984b). 8

Figure 1.4: Concentrated flow and ephemeral gully caused by converging furrow flows on plowed field after Thorne (1984b). 9

Figure 1.5: Field measurent of PlanC, where W = A + B, and H = swale depth. 10

Figure 2.1: 3 x 3 elevation sub-matrix, adapted from Zevenbergen and Thorne (1987) 29

Figure 2.2. Horn's 3 × 3 neighbourhood matrix notation. 33

Figure 2.3: (a) Zevenbergen and Thorne (1987) and (b) Horn (1981) slope calcualtion methods as illustrated by Jenness (2013). 35

Figure 2.4: Visual representation of the three most common terrain ruggedness calculation methods. After Sappington et al. (2007). 36

Figure 2.5: Correlations of slope to ruggedness parameterised using the LSRI, TRI and VRM. After Sappington et al. (2007). 37

Figure 2.6: Diagrammatic representation of how to compute VRM (Sappington *et al.*, 2007). 38

Figure 2.7: LiDAR-derived DEM of the Upper North Fork Toutle River (UNFTR) basin, downstream from Mount St Helens. Spatial resolution = 1 m. Data acquired in 2009 and provided by the USGS. 41

Figure 2.8: Trigonometric and Pythagoras approach to derivation of the field surveyed slopes. 49

Figure 2.9: Proportion of cells where raw slopes computed using Horn are the same, less or more than those computed using Z&T. 54

Figure 2.10: (a) maximum and variance and b) mean and standard deviation of raw Horn and Zevenbergen and Thorne slopes, as a function of DEM resolution. 56

Figure 2.11: Proportions of cells where rounded up slopes computed using Horn are the same as, less than, and more than those computed using Z&T. 57

Figure 2.12: Correlation between slopes calculated using the Horn and Z&T methods at grid resolutions of (a) 5m, (b) 10m, (c) 15m, (d) 20m, (e) 25m, and (f) 30m. 59

Figure 2.13: Frequencies of cell for each geomorphological slope class and DEM grid resolutions of (a) 5m, (b) 10m, (c) 15m, (d) 20m, (e) 25m and (f) 30m....61

Figure 2.14. Percentage differences between Z&T and Horn slopes according to geomorphological slope class....63

Figure 2.15: Mean percentage differences between Z&T and Horn slopes in each geomorphological slope class at DEM resolutions of: (a) 5m, (b) 10m, (c) 15m, (d) 20m, (e) 25m, and (f) 30m.....65

Figure 2.16. Field surveyed and DEM-based elevations along cross-sections (a) NF100, (b) NF110, (c) NF300, and (d) NF310....66

Figure 2.17. Comparisons of field and computed slopes along cross-section NF100 at 1m resolution. (a)2D Slope vs field slope, (b)Zevenbergen & Thorne vs field slope and (c) Horn vs Field slope. Purple line = 1:1 line of perfect agreement, Yellow line = the regression line passing through the origin, light blue line = the regression line pass through the y- intercept. 67

Figure 2.18. Absolute differences between slopes computed using the Horn and Z&T methods plotted as a function of VRM for DEM resolutions of (a) 5m, (b) 10m, (c) 15m, (d) 20m, (e) 25m, and (f) 30m. Note: while indicative trend lines are fitted to the data, all the r2 values are very small.....70

Figure 2.19. Percentage differences between raw slopes computed using the Horn and Z&T methods plotted as a function of VRM for DEM resolutions of (a) 5m, (b) 10m, (c) 15m, (d) 20m, (e) 25m, and (f) 30m. 71

Figure 2.20. Percentage differences between slopes calculated using the H and Z&T methods grouped by VRM class for the (a) 1m ,(b) 10m, and (c) 30m grids. 72

Figure 2.21.Graphs of slopes calculated using the Horn method plotted against Z&T slopes for ruggedness categories of: (a) VRM = 1, (b) VRM = 2, (c) VRM = 3, (d) VRM = 4, (e) VRM = 5, (f) VRM = 6, (g) VRM = 7, and (8) VRM = 8.....73

Figure 2.22: Correlation coefficients and Coefficients of determination between Horn and Z&T slopes (a) for VRM dervied from 1m grid resolution DEM, and (b) grouped by VRM class. 75

Figure 2.23**:** Plots of correlations between slopes calculated using Horn and Z&T plotted as a function of VRM at the DEM resolutions indicated on the VRM axis. Note: while indicative regression lines are fitted to the data, all the r^2 values are very small. 77

Figure 2.24: Plot of overall mean VRM values as a function of DEM grid size. 80

Figure 3.1: Maps showing CTI values greater than 10 (green) and known gullies (blue) at Ellis Farm, Site 2A. (a) Field surveyed data at 6.1m resolution (b), USGS elevation date resampled to 6.1m (c), Field surveyed data at 10m resolution and (d) USGS elevation date to 10m. After Parker *et al.* (2007). 92

Figure 3.2: The CTI gully threshold set at (a) 10 m, (b) 50 m, (c) 62m, (d) 75m, (e) 87 m and (f) 100 m. After Parker *et al.* (2007). 93

Figure 3.3: Map of height differences between Zevenbergen's field-surveyed DEM and the USGS 10m DEM for Ellis Site2 A. Cells in which the field-surveyed DEM is lower than in the USGS DEM are orange, while those in which the field-surveyed DEM is higher than the USGS DEM are blue. After Parker *et al.* (2007). 94

Figure 3.4: Map showing observed and predicted gully locations at the Ellis Farm Site2A. Cells with CTI values ≥62 (green) are predicted to contain a gully according to a GIS-based application of the CTI method. These cells match well to known field gully locations (blue polyline) and original predictions made by Zevenbergen (purple polyline). After Parker *et al.* (2007). 95

Figure 3.5: The principles underpinning the concept of a DEM of Difference. After Wheaton (2012). 99

Figure 3.6. Hillshade of the 2003, 5m DEM of the south valley side of the North Fork Toutle River at Mount St. Helens near Bear Creek. 102

Figure 3.7: Hillshade of the 2009, 5m DEM of the south valley side of the North Fork Toutle River at Mount St. Helens near Bear Creek. 102

Figure 3.8. An image of gullies from a DEM of Melton farm 104

Figure 3.9: The model built in ArcGIS model builder to evaluate the models and the validations respectively. 110

Figure 3.10. (a) ROC curves for CTI predictions of gullying at Melton Farm, with grid resolutions of 1, 5 & 30m. (b) Areas under ROC curves (i.e. Accuracy values) for the CTI model at Melton, using the 1m, 5m & 30m DEMs. 114

Figure 3.11. ROC curves for CTI predictions of gullying (a) with a threshold CTI = 36 and (b) with the threshold set to zero, for DEM resolutions of 1m, 5m and 30m. Note that the curve for 5m must be ignored as, for the purpose of revealing the influence of grid resolution, gullies predicted using this grid resolution were used as 'ground truth' for the presence of gullies at the Melton site, ensuring perfect agreement between predicted and observed gullying. 117

Figure 3.12. Hillshade of the study area at Mount St Helens based on the 2003 DEM at a grid resolution of 5m. The drainage pathways for concentrated overland flow (swales) and drainage divides (ridges) existing in 2003 are clearly visible. 118

Figure 3.13: Gullies predicted using CTI1 values calculated using the 2003, 5m DEM and plotted as white lines added to (a) the DEM and (b) the hillshade.....119

Figure 3.14: CTI values calculated using the 2003, 5m DEM displayed using 'per cent clip' stretch. 120

Figure 3.15: CTI values calculated using the 2003, 5m DEM displayed using 'standard deviation'. 121

Figure 3.16: CTI values calculated using the 2003, 5m DEM displayed using 'custom stretch'. 121

Figure 3.17: CTI values calculated using the 2003, 5m DEM displayed using 'minimum-maximum'. 122

Figure 3.18: CTI values calculated using the 2003, 5m DEM displayed using 'histogram equalize '.....122

Figure 3.19: (a) ROC curve for predictions based on CTI1 and validation by G1 at 5, 10, 15, 20, 25 and 30 m resolution, (b) AUC values for prediction by CTI1 and validation by G1 at 5, 10, 15, 20, 25 and 30 m resolution. 124

Figure 3.20**.** (a) ROC curve for CTI2 and validation by G1 at 5, 10, 15, 20, 25 and 30 m resolution, (b) ROC AUC values for CTI2 and validation by G1 at 5, 10, 15, 20, 25 and 30 m resolution. 126

Figure **3.21**: (a) ROC curve for predictions using CTI2 and validation using G2 at 5, 10, 15, 20, 25 and 30 m grid resolutio. (b) ROC AUC results for CTI2 as validated using G2 at 5, 10, 15, 20, 25 and 30 m grid resolutions. 128

Figure 3.22**:** (a) ROC curves for prediction of gullies using CTI and validation using G2 at 5, 10, 15, 20, 25 and 30 m resolutions. (b) AUCs for CTI1 and validation using G2 at 5, 10, 15, 20, 25 and 30 m resolutions. 130

Figure 3.23**.** Areas under the ROC curves for prediction of gully suceptibility based on validation Versions 1 to 4 at Mount St Helens, under a range of grid resolutions.....131

Figure 4.1: Visualisation of (a) classical binary logic and (b) fuzzy logic. Reproduced from Negnevitsky (2005).....136

Figure 4.2: Flow chart of gully detection algorithm proposed by Noto *et al.* (2017). This is part II, which supports identification of the gully boundary through image analysis. 139

Figure 4.3: Hedge expressions and their graphical representations. After Negnevitsky (2005) 145

Figure 4.4: Fuzzy Membership type and Hedges in ArcGIS 10.4. 146

Figure 4.5: Graphical representation of fuzzy overlay types. After Negnevitsky (2005) 148

Figure 4.6: Study Area of the Eastern Cape province, showing LGAs.....151

Figure 4.7: A gully example in the South African study site. After Kakembo *et al.* (2009).....152

Figure 4.8**.** Areas predicted to be susceptible to concentrated flow erosion (gullying) using (a, b) the original and (c, d) fuzzy CTIs. Maps (a, c) use the 'standard deviation' stretch while (b, d) use 'histogram equalize' stretch.....154

Figure 4.9. Visulization of (a) fuzzy CTI and (b) original CTI using the 'standard deviation' stretch symbology. 155

Figure 4.10. Comparison of ROC curves for the fuzzy CTI (Fuzzy CTI at 30m LiDAR and Fuzzy CTI at 30m USGS SRTM) and the original CTI(CTI1 at 30m LiDAR and CTI1 at 30m USGS SRTM) validated by DoD gully (a) without threshold(CTI1_G1) and (b) with threshold(CTI1_G2).....160

Figure 4.11. ROC curves for prediction of gullying over the whole of the Eastern Cape Province of South Africa using the original and fuzzy CTIs.....163

Figure 4.12. Fuzzy CTI prediction performance and possible threshold values. (a) ROC curve for the fuzzy CTI (with a cutoff) and (b) True Positive rate (Sensitivity) as a function of fuzzy CTI cutoff (%). 164

Figure 4.13. TPR as a function of value selected for the threshold fuzzy CTI.....166

Figure 5.1. Critical organic matter levels for maintenance of physical soil stability and suppression of erosion/degradation. After Pieri (1992).....176

Figure 5.2. Soil Textural Class for the study area in the Eastern Cape province, South Africa.....180

Figure 5.3. ROC curves for original and fuzzy CTI models (without threshold values) for the Eastern Cape Province specific to land covers of: (a) bare soil, (b) crops, (c) grass, (d) shrubs, (e) trees, and (f) lichens, mosses and sparse vegetation. In most cases, AUC values for fuzzy CTI are slightly higher than for the original CTI. While all AUCs are

relatively low when no threshold CTI is used, fuzzy CTI out-performs the original CTI, albeit only by a small margin under all land covers except (f). 183

Figure 5.4. (a)Sensitivity and (b) Accuracy under different land covers for a range of threshold values for fuzzy CTI. 186

Figure 5.5. (a)Sensitivity and (b) Accuracy under levels of soil organic matter content for a range of threshold values for fuzzy CTI. Note: St1 = loss of soil structure and high susceptibility to erosion (i.e. physically degraded soil), St2 = instability and high risk of loss of soil structure, St3 = no/low immediate risk of structural decline, and, St4 = soils with enough organic matter. 192

Figure 5.6. ROC curves for original and fuzzy CTI (with no threshold CTI value) applications in selected administrative districts of the Eastern Cape: (a) Alfred_Nzo, (b) Amathole; (c) Buffalo City (d) Chris Hani, (e) Joe Gqabi, (f) Nelson Mandela Bay, (g) OR Tambo, and (h) Sarah Baartma..... 195

Figure 5.7. Bar chart allowing direct comparison of the predictive performances of the original and fuzzy CTI models (as indicated by area under the ROC curve) when applied in selected administrative units of the Eastern Cape province of South Africa..... 196

LIST OF TABLES

Table 1.1: Primary topographic attributes (Moore *et al.*, 1991). 6

Table 1.2: Characteristics of different cropland erosion processes. After Laflen et al. (1985). 11

Table 1.3: Soil Erosion and Sediment Transport models. After Merritt *et al.* (2003) 16

Table 1.4: Model scopes and their potential to predict gullying. After Merritt *et al.* (2003) 17

Table 2.1. Eight slope algorithms investigated by Jones (1998b). 25

Table 2.2. Slope calculation methods implemented in GIS platforms 26

Table 2.3: Coordinates in the 3 x 3 elevation sub-matrix 30

Table 2.4: LiDAR-based DEMs available for the UNFTR basin at Mount Saint Helens, USA. 42

Table 2.5: An example of the input and output values when using the round up tool in ArcGIS10.4. 43

Table 2.6. Classification of slope angles proposed by (Young and Clayton, 1972). 46

Table 2.7. USGS cross-section names and ruggedness statistics for the 2009 LiDAR DEM (1 m). 50

Table 2.8. Reclassification of VRM values 52

Table 2.9. Differences and zonal statistics of differences between raw H and Z&T slopes 55

Table 2.10: Differences and zonal statistics of differences between rounded up Horn and Z&T slopes 58

Table 2.11: Results of paired-sample t-tests on slopes calculated using the Horn and Z&T methods 60

Table 2.12: Geomorphological classification of slopes at various resolutions 62

Table 2.13. Breaking down the data by DEM resolution shows that the shapes of the histograms are similar for all grid sizes (Figure 2.15). 64

Table 2.14. Statistics for raw differences between H and Z&T grouped by VRM class 79

Table 3.1: Critical CTI values and available information on crop and soil type for sites in the Parker *et al.* (2007) study. After Parker *et al.* (2007). 89

Table 3.2: DEMs of Difference (DoD) generated for the study site at Mount St. Helens. 103

Table 3.3. Matrix for the validation runs of CTI1 and CTI2, by G1 and G2. 107

Table 3.4. Receiver operator characteristics matrix or cross-tabulation 111

Table 3.5: Test statistics for areas under the ROC curves at different grid resolutions. 114

Table 3.6. Test statistics for areas under ROC curves in Figure 3.11. 117

Table 3.7. CTI1_G1 of prediction performance evaluation at Mount St Helens. 123

Table 3.8: Test statistics for Areas Under the ROC Curves for CTI1_G1 presented in Figure 3.19 124

Table 3.9: Prediction performance using CTI2 (with critical flow accumulation value) and G1 (without a minimum difference in the DoD). 126

Table 3.10. Areas Under the ROC Curves for CTI2_G1 presented in Figure 3.20. 127

Table 3.11. Areas Under the ROC Curves for CTI2_G2 presented in Figure 3.21. 128

Table 3.12: Prediction performance of the CTI2_G1 model at Mount St Helens through ROC. 129

Table 3.13. Areas Under the Curves for CTI1_G2 presented in Figure 3.30. 130

Table 4.1. Validation matrix for applications of original and fuzzy CTIs and validation using G1 and G2 DoDs. 149

Table 4.2: Gullies observed Provinces of South Africa 151

Table 4.3: ROC performance Parameter of versions 5 and 6 (which both use fuzzy CTI) 156

Table 4.4: Areas Under the ROC Curves for validation of fuzzy and original CTI methods. 158

Table 4.5. Predictive Accuracy of fuzzy CTI and original CTI models when applied to LiDAR-based and STRM-based DEMs, both with 30 m grid sizes, and validated using G1 and G2 160

Table 4.6. Confusion matrix for TPs, FPs and TPR as a function of the value selected for the threshold fuzzy CTI. 165

Table 5.1. List of soil erodibility indices in water and wind research. After Song et al. (2005) 173

Table 5.2. Reclassification of critical level of soil organic matter content. 180

Table 5.3. *Accuracy* and *Sensitivity* values for fuzzy CTI under different land covers, using no threshold CTI value and a range of possible threshold CTI values. 185

Table 5.4. Values of FN, FP, TN, TP and *Prevalence* for the five land use types.....189

Table 5.5. Accuracy and Sensitivity values for fuzzy CTI in areas with different levels of soil organic matter content, using no threshold CTI and a range of possible threshold CTI values. 191

Table 5.6. Values of FN, FP, TN, TP and *Prevalence* for the four soil organic matter contents 193

Table 5.7. Summary results for fuzzy CTI applications with different Environmental Descriptors, based on post hoc tests for multiple comparisons of means of fuzzy CTI using the least small difference (LSD) approach.....197

CHAPTER 1: INTRODUCTION

1.1. The Global Problem of Gullying

Gullies form because of the concentration of overland run-off, usually after heavy rainfall. Precipitation falling on the land surface is drained to topographic lows, moving downslope due to gravity (Moore *et al.*, 1988b; Moore *et al.*, 1988a). If precipitation falls on an impermeable surface, or the infiltration capacity of soil has been exceeded, or the ground is saturated, water will move downslope on the surface of the land as 'overland flow'. Unconcentrated overland flow washes evenly over the land surface, but it is usual for overland flow to become concentrated due to irregularities in the topography of the land surface (Laflen *et al.*, 1985). Where water becomes concentrated with sufficient duration and magnitude, its erosional power per unit flow width increases, initiating erosion of the land surface. This creates a channel, called a gully, which further accentuates flow convergence and concentration of the surface runoff. Gully channels tend to increase in cross-sectional size with distance downslope and through time they often extend headward in the upslope direction – a process termed 'head-cutting' (Thorne *et al.*, 1986; Montgomery and Dietrich, 1989). Anthropogenic alterations to the land surface can instigate the development of gullies, with detrimental impacts on soil health and land productivity (Morgan, 2005). In particular, agricultural activities that alter land slopes, reduce vegetation cover, and/or create ridges and furrows can concentrate overland flow on easily-eroded ground, causing gullies to form and grow rapidly.

Farming often has severe, negative consequences for agricultural land, due to the loss of formerly productive soils (Smith, 1993; Vandekerckhove *et al.*, 1998; Woodward, 1999; Poesen *et al.*, 2003; Morgan, 2005). Consequently, prediction of agricultural soil loss has been the focus of extensive research. Empirical modelling of soil erosion, employing extensive field instrumentation and long-term monitoring, has informed our understanding of soil loss and is widely used to predict rates of degradation in agricultural land (Laflen and Flanagan, 2013). However, most soil loss equations and models predict spatially-averaged, annualised rates of soil loss, usually at the field-scale, and these approaches rarely

include gullying explicitly. Examples include the widely used Universal Soil Loss Equation (USLE) and derivatives thereof (e.g. RUSLE, MUSLE), and the more recent Water Erosion Prediction Project (WEPP) (Renard *et al.*, 1991; Cochrane and Flanagan, 1999, 2003). These models require parameterised environmental data, usually including a combination of rainfall erosivity (based on rainfall energy and intensity); soil erodibility, and the distribution of slopes across the land surface. In addition, information concerning the agricultural cycle and crop type are usually necessary.

Less Economically Developed Countries (LEDCs) are at particular risk of gullying due to climate change, land-use change, poor agricultural practices and widespread farming intensification (Young, 1999), but in these areas the data required to apply most predictive models are unavailable (Kinnell, 2010; Laflen and Flanagan, 2013). Therefore, there is an urgent need to provide a pragmatic and rapid predictive tool for assessing gullying potential in data sparse, developing regions, to inform planning, agricultural practices and environmental management decision-making.

Given the difficulty in applying existing empirical models (Laflen *et al.*, 1985) to developing areas, where input data is sparse but the risk of gullying is high, alternative methods need to be developed to identify areas susceptible to gullying. Here it is hypothesised that detailed data is required to apply existing models of soil loss from agricultural areas because they focus on predicting the *quantities* of sediment lost after agriculture has commenced. If the focus were instead on identifying areas that are *susceptible* to gullying, and then taking steps to avoid soil loss (by either protecting susceptible areas from agricultural development or at least applying soil conservation measures from the outset), rather than attempting to predict the extents or the specific, metre-scale locations of individual gully channels, the data requirements for successful model application could be reduced.

1.2. **Aim and objectives**

Given that the substantial and detailed data inputs required to model and predict gullying using available methods are unavailable in many areas where such model

applications are most needed, there is an urgent need for investigation into the efficacy of simpler approaches to identifying gully susceptibility in data-sparse regions. Therefore, the aim of the research reported in this thesis is to develop a GIS-based approach that identifies (at a regional scale) areas that are susceptible to gullying, where susceptibility herein implies that the topography of the land will concentrate overland flow - promoting gully erosion and, where flow concentration is greater, the susceptibility to gullying will increase. Hence, susceptibility as used herein, means topographic-susceptibility. This is distinct from predicting gully locations because when attempting to avoid gullies forming in the first place (through making better land-use management planning decisions) the precise location where a gully would form is not in itself significant. It is sufficient to identify that an area is topographically-susceptible to gullying, even though a gully has not to date ever formed, because other environmental controls have, thus far, prevent concentrated overland flow from being able to initiate erosion. The aim is to produce a new method for reliably predicting regional scale susceptibility to gullying, using globally available, low resolution datasets, so that this approach can provide useful indications of areas where gullies are more likely to develop and cause unacceptably high rates of soil loss in LEDCs. Reliability will be tested by comparing the predictive power of the new method in large areas that are susceptible to gullying, but which have different environmental conditions that make it more likely (e.g. croplands/weak soils) or less likely (e.g. forest land-cover/strong soils) that gullies will be observed.

The objectives pursued to achieve this aim are:

1. To determine how different measures of slope affect terrain analysis, and the implications of DEM resolution and terrain ruggedness for slope calculation.
2. To determine the effect of a Digital Elevation Model's (DEM) grid resolution when calculating the Compound Topographic Index (CTI), which for decades has proved useful in identifying pathways for concentrated overland flow.
3. To explore how fuzzification of the CTI affects its accuracy when applied using fine and coarse resolution DEMs.

4. To examine how other readily-available environmental descriptors can be combined with knowledge of the distribution of concentration of overland flow, to inform prediction of susceptibility to concentrated flow erosion (gullying) and the likelihood of gullies being observed in the landscape.

Each objective is addressed in its own chapter. Work tackling objective 1 is presented in Chapter 2; objective 2 is dealt with in Chapter 3; objective 3 in Chapter 4 and finally; objective 4 in Chapter 5. Each of these chapters has its own introduction, objectives, methodology, results and discussion sections. Chapter 6 provides an over-arching discussion of all the research results and considers the extent to which the thesis has achieved the overall aim (as stated above). It also summarises the main conclusions. The remainder of this chapter provides an overview of literature relevant to the overall aim and objectives stated above.

1.3. **Gullying and its prediction**

1.3.1. **Definition of topographic attributes relevant to understanding overland flow erosion**

Land surface topography influences many of the environmental factors that govern soil erodibility, and it also affects many of the geomorphological processes that, in turn, alter the topography. When interpreting the landscape, a digital representation of the terrain, such as a Digital Elevation Model (DEM), provides the basis on which the topography can be parameterised. Parameters derived from a DEM, termed *topographic indices* or *attributes*, are used to study earth surface processes and landforms, and greatly aid understanding of the role of topography in driving geomorphological processes.

The primary topographic attributes are usually considered to be: slope magnitude, slope aspect, planform curvature, and profile curvature (Zevenbergen and Thorne, 1987; Thorne *et al.*, 1987; Zevenbergen, 1987) (Figure 1.1). Slope magnitude (herein referred to as 'slope') is defined as the rate of change of elevation with distance downslope. It is a critical topographic attribute that influences the speed of overland flow and entrainment/movement of sediment by regulating the stream

power available to drive flow and sediment transport (Thorne *et al.*, 1986; Thorne *et al.*, 1987). Because nearly all landscapes are composed of slopes, their study is the core of geomorphology (Finlayson and Statham, 1980). The direction or orientation of the slope is called the slope aspect (herein 'aspect') and defines the planimetric direction of downslope movement. The upslope area contributing surface runoff to the flow at any point in a drainage basin depends on how aspect varies throughout the basin. Slope and aspect are first derivatives of elevation, the first being in the downslope direction and the second being orthogonal to that direction. Planform curvature depends on the distribution of slope and aspect laterally around a point, indicating whether flow is concentrating or diverging, while profile curvature is the distribution of slope and aspect longitudinally, indicating whether flow is accelerating or decelerating (Figure 1.1).

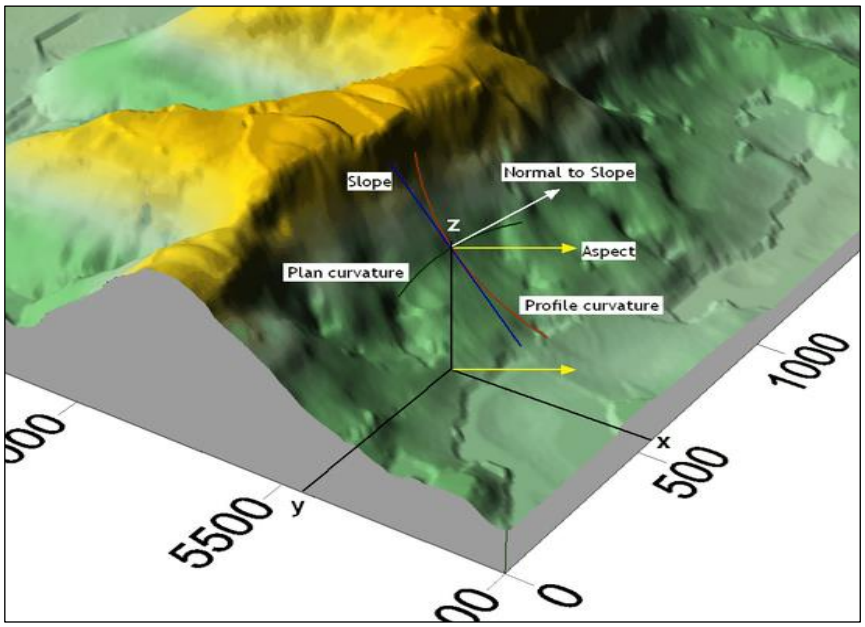

Figure 1.1: Illsutation of topographic attributes (https://www.spatialanalysisonline.com/HTML/profiles_and_curvature.htm)

There are many approaches for fitting a surface to digital terrain data and generating topographic indices or attributes, many of which were developed before the widespread availability of high spatial resolution satellite and aerial imagery (Tobler, 1969; Sharpnack, 1969; Rhind, 1972; Young, 1978; Evans, 1980; Horn, 1981; Zevenbergen and Thorne, 1987). Moore *et al.* (1991)considered the hydrological

significance of a range of topographic attributes and their relevant links, as summarised in Table 1.1.

Table 1.1: Primary topographic attributes (Moore *et al.*, 1991).

Attribute	Definition	Hydrologic significance
Altitude	Elevation	Climate, vegetation type, potential energy
Upslope height	Mean height of upslope area	Potential energy
Aspect	Slope azimuth	Solar irradiation
Slope	Gradient	Overland and subsurface flow velocity and runoff rate
Upslope slope	Mean slope of upslope area	Runoff velocity
Dispersal slope	Mean slope of dispersal area	Rate of soil drainage
Catchment slope*	Average slope over the catchment	Time of concentration
Upslope area	Catchment area above a short length of contour	Runoff volume, steady-state runoff rate
Dispersal area	Area downslope from a short length of contour	Soil drainage rate
Catchment area*	Area draining to catchment outlet	Runoff volume
Specific catchment area	Upslope area per unit width of contour	Runoff volume, steady-state runoff rate
Flow path length	Maximum distance of water flow to a point in the catchment	Erosion, rales, sediment yield, time of concentration
Upslope length	Mean length of flow paths to a point in the catchment	Flow acceleration, erosion rates
Dispersal length	Distance from a point in the catchment to the outlet	Impedance of soil drainage
Catchment length*	Distance from highest point to outlet	Overland flow attenuation
Profile curvature	Slope profile curvature	Flow acceleration, erosion/ deposition rate
Plan curvature	Contour curvature	Converging/diverging flow, soil water content

* defined at points within the catchment. Over the last two decades, improved data accessibility, advanced computational capacity, increasing resolution and greater spatial coverage of digital terrain information have generated increasing interest in topographic attributes.

1.3.2. **Fluvial implications of land surface curvature**

Profile curvature is the curvature of the land surface in the longitudinal direction. It represents the second derivative of elevation in the downslope direction. By affecting flow acceleration and deceleration, profile curvature can influence patterns of land surface degradation and aggradation. Planform curvature is the curvature of the land surface transverse to the direction of steepest slope, and it controls flow convergence and divergence (Figure 1.2).

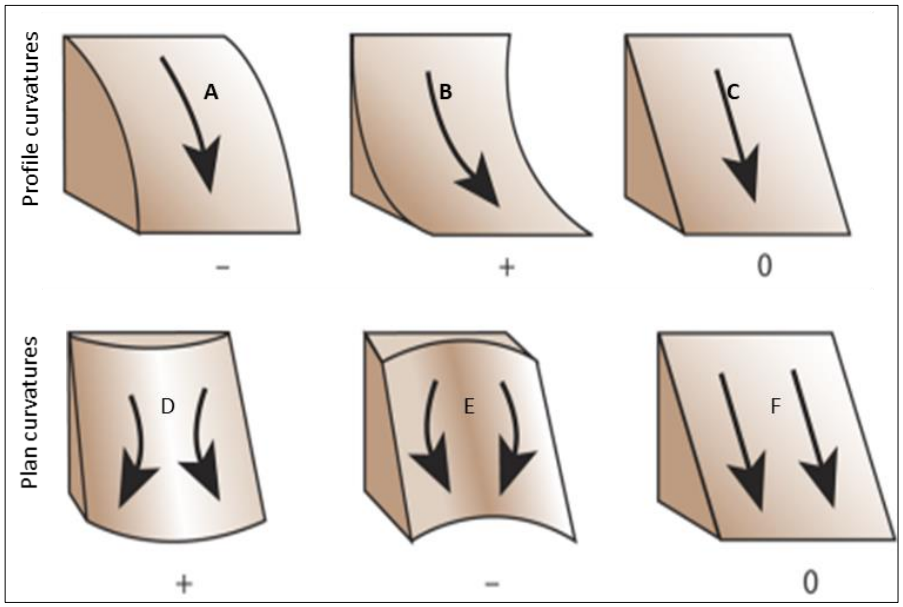

Figure 1.2: Diagrammatic presentation of profile and planform curvature. For profile curvature, A(-) represents a convex profile, implying accelerating flow, B(+) represents a concave profile, implying decelerating flow, and C(0) indicates that the profile is linear, implying uniform flow. For plan curvature, D(+) represents a convex planform, implying diverging flow, E(-) represents a concave planform, implying converging flow, and C(0) represents a linear planform with uniform flow (source: ArcGIS instruction manual).

1.3.3. **Stream power and the Compound Topographic Index (CTI)**

Surface runoff exerts a tangential shear force on the underlying land surface that can, if of sufficient magnitude, entrain particles of soil or sediment from that surface. The capacity of such a shear flow to entrain bed particles and move them downslope can be represented by its stream power, which is defined as:

$$\text{Stream Power } (\omega) = \rho g Q S \qquad \text{Equation 1.1}$$

where, ω = stream power per unit distance downstream, ρ = water density, g = gravitational acceleration, Q = volumetric discharge, and S = energy slope. Because gravity and the density of water are almost constant, the magnitude of stream power can, for practical purposes, be represented by the product of discharge and slope. Further, drainage area has been used as a surrogate for discharge and multiplied by local slope to represent local stream power (Knighton, 1999; Kakembo *et al.*, 2009; Wells *et al.*, 2016). Where upstream contributing area and slope are large enough to sustain flow and erode sediments, a gully will form (Vandaele and Poesen, 1995; Vandaele *et al.*, 1996a; Desmet *et al.*, 1999). This is especially likely in flow convergent zones (e.g. swales or hollows) because the discharge and stream power per unit bed width (which is termed specific stream power) are higher where the flow is concentrated (Zevenbergen, 1989; Vandaele *et al.*, 1997) (Figure 1.3).

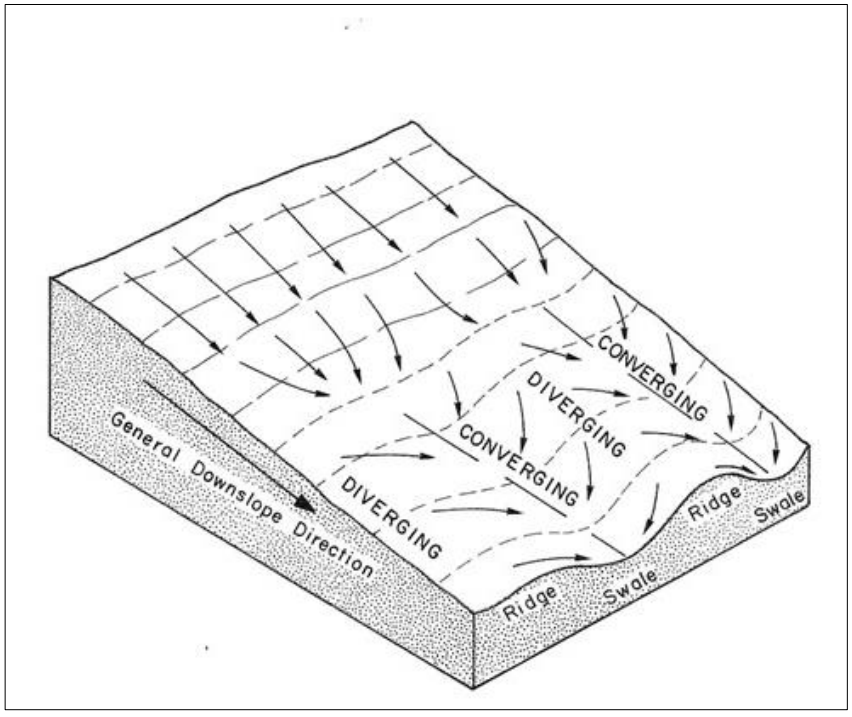

Figure 1.3: Concentration of flow in swales due to topographic control, after Thorne (1984b).

The initiation of a gully further concentrates subsequent overland flows, further increasing stream power per unit width and enlarging the channel – to drive a positive feedback loop. In some cases, this relationship can be highly destructive, with channels rapidly enlarging as greater volumes of runoff are concentrated into

the growing gully. As a result, channel dimensions increase and specific stream power no longer correlates with the initial surface curvature, but with the discharge, slope and width of the gully itself (Conoscenti *et al.*, 2014; Bergonse and Reis, 2016; Bingner *et al.*, 2016; Cappadonia *et al.*, 2016; Xu *et al.*, 2016) (Figure 1.4).

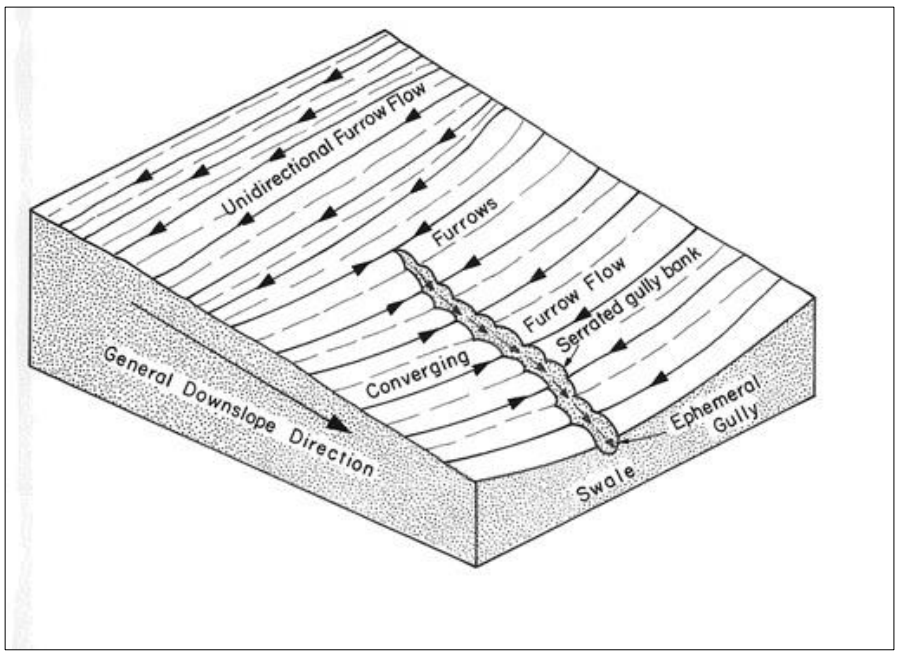

Figure 1.4: Concentrated flow and ephemeral gully caused by converging furrow flows on plowed field after Thorne (1984b).

Gullies initiated by this process differ from classical gullies in that they may be subsequently obliterated by routine land tillage. They are, however, likely to reform after each intense rainfall event (Thorne and Zevenbergen, 1984; Thorne and Zevenbergen, 1990b; Vandaele *et al.*, 1996a; Vandekerckhove *et al.*, 1998; Woodward, 1999; Daggupati *et al.*, 2014; Bingner *et al.*, 2016; Wells *et al.*, 2016). For this reason, such channels are often referred to as ephemeral gullies. When farmers fill in ephemeral gullies by ploughing over them, the unintended impact of this reworking of the land surface is to increase planform curvature in swales, because soil from the side slopes and floor of the swale is mechanically shifted and used to fill the gully. Consequently, the degree to which the flow converges to form concentrated runoff, and its propensity to form a new gully in the loosely

compacted fill along the pathway of the former ephemeral gully, increase year on year (Zevenbergen, 1989). Through time, the depth and convergence in the swale increase, until eventually a classical gully forms: i.e. one that is too large to obliterate through normal tillage.

To measure planform curvature in the field, the ratio of swale width (W) to depth (H) is measured (Figure 1.5), and:

$$PlanC = \frac{200H}{W}$$ Equation 1.2

Different types of cropland erosion have been defined and differentiated according to their character (Laflen *et al.*, 1985). Ephemeral and classical gullies are formed by concentrated flow and, as such, are referred to as outcomes of concentrated flow erosion. In contrast, sheet and rill erosion is usually attributable to unconcentrated, surface wash (

Table 1.2).

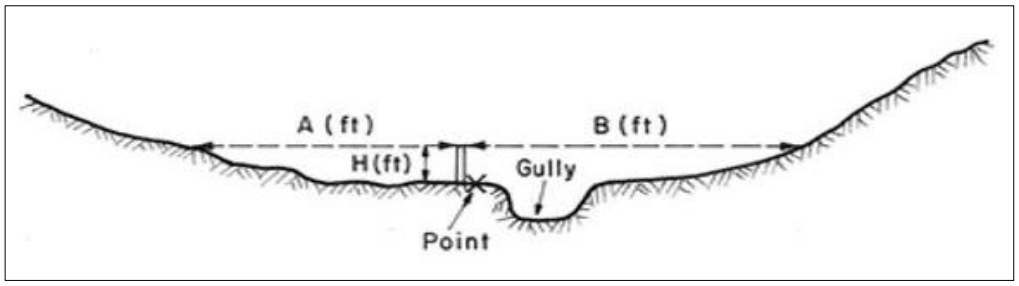

Figure 1.5: Field measurent of PlanC, where W = A + B, and H = swale depth.

Table 1.2: Characteristics of different cropland erosion processes. After Laflen et al. (1985).

S/No	Sheet and rill erosion	Ephemeral gully erosion	Gully erosion
1	Occurs on smooth side slopes above concentrated flow paths.	Occurs along shallow concentrated flow paths upstream from incised channels or gullies.	Generally, occur in well-defined concentrated flow paths.
2	May be of any size but are usually smaller than concentrated flow channels.	Usually larger than rills and smaller than permanent gullies. Agricultural equipment is able to travel across these.	Usually larger than concentrated flow channels and rills. Agricultural equipment is not able to travel across these.
3	Flow pattern develops many small disconnected channels which end at concentrated flow channels, terrace channels or in depositional areas	Usually forms a dendritic pattern along water courses beginning where overland flow, including rills, converges. Flow patterns influenced by tillage, rows, terraces and other man-made features.	Dendritic pattern along natural water courses. May occur in non-dendritic patterns in road ditches, terrace or diversion channels, etc.
4	Rill cross-sections are usually narrow relative to depth.	Cross-sections are usually wide relative to depth. Sidewalls not well defined.	Cross-sections usually narrow relative to depth. Sidewalls are steep. Headcut prominent. Eroding channel advances upstream.
5	Rills normally removed by tillage and usually do not reoccur in the same place.	Temporary feature, usually removed by tillage but reoccur in the same place.	Not removed by tillage.
6	Soil removed in thin layers or shallow channels. Soil profile becomes thinner over entire slope.	Soil removed along narrow flow path to the tillage depth if unfilled layer is resistant to erosion.	Soil may erode to the depth of the soil profile and can erode into soft bedrock.
	Low erosion rates not readily visible.	Area may or may not be visibly eroding.	Erosion readily visible.
	Detachment and transport by raindrops and shallow flow.	Detachment and transport by concentrated flow only.	Detachment by flowing water, slumping of unstable banks and head cut retreat. Transport by flowing water.

1.3.4. **Modelling gullying with topographic data and the Compound Topographic Index (CTI)**

Most works on soil erosion by water are centred on sheet (inter-rill) and rill erosion processes operating at the runoff plot scale. For example, Poesen *et al.* (2011) drew conclusions from numerous run-off plot studies, reporting soil loss rates caused by sheet and rill erosion for a diverse set of climatic and land use circumstances; utilising both experimental and process-based field-scale and catchment-scale erosion models to establish soil erosion risk maps at various scales (Morgan and

Nearing, 2011). However, these results do not account for the process of gullying and so are not applicable herein.

In most cases, gully channels are found on less than 5% of a catchment area, except their contribution to entire catchment sediment yield is much greater than this percentage: usually ranging from 10% to 90% and varies with environmental controls (climate and weather, soil type, topography, land use, gully type) (Poesen *et al.*, 2011). Despite knowing that, where gullying occurs, it represents the dominant contribution to soil loss, soil losses provoked by gully erosion have infrequently been included in soil loss assessment programmes (Poesen *et al.*, 2003). The evolution of gully channels leads to a significant decline in soil quality by very high soil losses, recorded up to 10-100 t ha^{-1} y^{-1} (Poesen *et al.*, 2002). The improved drainage of inter-gully areas can also degrade soils due to desiccation and limited soil water availability.

Slope is an important input in models of water erosion, regardless of whether those models are empirical, conceptual and physics-based (Laflen and Flanagan, 2013). For example, the Universal Soil Loss Equation (USLE) is widely used to model unconcentrated flow erosion (i.e. rill and inter-rill erosion, but not gullying) using the slope length and aspect, with other environmental descriptors used to account for rainfall erosivity, soil erodibility and conservation practices. In the USLE, slope length (L) is the distance from the point of origin of overland flow to the point where the slope decreases sufficiently for deposition to occur, or to the point where surface runoff enters a channel that is part of the permanent drainage network. Slope gradient (S) is the inclination along the direction of the measured length of slope, expressed in percent. The slope length and gradient factors are often combined into a single topographic factor (LS) (Wischmeier and Smith, 1978; Cooke and Doornkamp, 1990; Morgan *et al.*, 1998b; Morgan, 2005; Morgan, 2009; Laflen and Flanagan, 2013; Maxwell *et al.*, 2016). However, in the field, there are often practical difficulties in determining representative values for slope length and gradient. Particularly, the effects of complex slopes, expressed through non-zero values of profile and planform curvature, are not well represented by this simple topographic factor.

In an attempt to incorporate concentrated flow erosion (i.e. gullying) into existing models of soil loss, Thorne (1984b) proposed a pragmatic, reasonable and easy to apply topographic index, which was based on field-measured topography and is known as the Compound Topographic Index (CTI) (Equation 1.3).

$$CTI = A \times S \times PlanC \qquad \text{Equation 1.3}$$

where, A = upstream drainage area (m^2), S = slope ($m\ m^{-1}$), and PlanC = planform curvature in units of 1/100 m.

Calculation of CTI does not require comprehensive, complex data collection over extended periods. Instead, the parameter was intended to be calculated and applied by field personnel with relative accuracy and repeatability (Thorne, 1984b). The CTI takes the upstream drainage area or flow accumulation (A), the local slope (S), and the degree of flow convergence or planform curvature (PlanC), at each point in a matrix of gridded elevation data for the study area as input variables to predict the intensity of concentrated surface runoff at any point in a field. Thorne *et al.* (1986) used the CTI to better represent swales and other topographic features when predicting concentrated flow erosion in croplands. They showed that planform curvature does identify areas prone to concentrated flow erosion and that it can also provide insights into ephemeral gully formation. In some of the subsequent implementations, it is suggested that a log transformation of flow accumulation area will improve the performance of the CTI (Thorne *et al.*, 1987).

Physically, the product of upstream area (A) and local slope (S) can be taken to represent stream power, while planform curvature indicates the degree to which *specific* stream power (stream power per unit flow width) is increased due to planform convergence, or reduced by planform divergence.

When applying CTI to predict the initiation of ephemeral gullying, it is necessary to define a critical or threshold value of CTI at which concentrated flow is sufficiently strong to erode an ephemeral gully, but this critical value cannot be calculated from basic principles. This is because its value varies depending on the complex interaction of multiple variables, including climate, soil type, crop type, and management/conservation practice. Instead, CTI values at the known locations of

critical conditions (i.e. gully heads observed during field observations) are compiled and averaged to calculate the critical threshold value as:

$$CTI_{crit} = \frac{\sum_1^n (CTI_{gh})}{n} \qquad \text{Equation 1.4}$$

where, CTI_{crit} = critical CTI for gully initiation, CTI_{gh} = gully head CTI, and n = number of gully heads.

1.3.5. **Approaches to modelling gullying**

This thesis focuses on the possibility of using globally available, topographic data to identify areas prone to concentrated flow erosion in data-sparse regions, under the influence of different land-uses and other environmental descriptors of interest. The remainder of this initial review of the relevant literature is, therefore, devoted to consideration of historical and recent papers that address soil erosion and sediment transport by overland flow and which include equations or models that can help inform in general terms how it might be possible to achieve the stated aim of this thesis.

Based on evidence from earlier work in the states of Alabama, Georgia and Mississippi, Thorne (1984b) showed that, under adverse conditions, soil loss can be very serious and that predictions based on rill and inter-rill erosion alone may underestimate the actual, total soil loss by 50 to 100%. Thorne (1984b) suggested that ephemeral gullies may have been responsible for erosion being significantly greater than that routinely predicted by the US Soil Conservation Service, because their calculations at that time could not account for soil loss due to ephemeral gullies.

This prompted Thorne (1984b) to review the erosion models(Table 1.3) then currently available, with the intention of investigating the capacity of different erosion models to account for soil loss due to ephemeral gullies. He found that none of the existing process and empirically based models was suitable to predict ephemeral gully erosion because the mechanics of concentrated flow erosion differed radically from those driving rill and sheet erosion. It was clear that a new

model would be needed to meet the need to predict soil loss due to ephemeral gullies. Thorne (1984) proposed the addition of the CTI into a suitable, existing models in this context. It was also clear, however, that to be widely applicable, such a new model must also:

1. Accurately characterise concentrated flow erosion in swales.
2. Avoid the lengthy and complex computations and huge and long-term input data requirements of process and some empirical models.
3. Stand-alone and simulate those aspects of the hydrological and sedimentary system controlling ephemeral gullying, without involving all aspects.
4. Be amenable to analysis on, at most, a small computer - in order to satisfy the requirement for a model usable at the local level.
5. Use data readily available or easily obtained from field observation to make the model usable locally and globally.

These criteria are still applicable in LEDCs and other data-sparse regions today and can be used to evaluate the practical utility of candidate gully erosion or susceptibility models.

Reviews by Merritt *et al.* (2003), and Aksoy and Kavvas (2005) of surface erosion models noted that soil erosion and sediment transport are generally represented as physical processes, either on an empirical or conceptual basis, though most erosion models are empirical rather than conceptual (Table 1.3). Recent approaches to gully erosion models are informed by already existing general Soil Erosion and Sediment Transport models presented in Table 1.3.

Table 1.3: Soil Erosion and Sediment Transport models. After Merritt *et al.* (2003)

Model	Type	Scale	Focus	Authors
AGNPS	Conceptual	Small catchment	Water quality	Young *et al.* (1989)
ANSWERS	Physical	Small catchment	Water quality	Beasley *et al.* (1980)
CASC2D-SED	Physical	catchment	Erosion/Sediment	Johnson *et al.* (2000)
CREAMS	Physical	field 40-100 ha	Water quality	Knisel and Foster (1981)
EMSS	Conceptual	Catchment	Water quality	Vertessy *et al.* (2001); Watson *et al.* (2001)
EUROSEM	Physical	fields and small catchment	Erosion	Morgan *et al.* (1998b); Morgan *et al.* (1998a); Morgan *et al.* (1999)
GUEST	Physical	Plot	Erosion	Yu *et al.* (1997); Coughlan and Rose (1997)
HSPF	Conceptual	Catchment	Water quality	Johanson *et al.* (1980)
IHACRES-WQ	Empirical/Conceptual	Catchment	Water quality	Jakeman *et al.* (1990); Jakeman *et al.* (1994); Dietrich *et al.* (1999)
IQQM	Conceptual	Catchment	Water quality	Simons *et al.* (1996)
KINEROS and KINEROS2	Physical	Catchment	Erosion/deposition	http://www.tucson.ars.ag.gov/kineros/Home.html
LASCAM	Conceptual	Catchment	Water quality	Viney and Sivapalan (1999)
LISEM	Physical	Small catchment	Erosion	De Roo *et al.* (1996); Takken *et al.* (1999); (De Roo and Jetten, 1999)
MIKE-II	Physical	Catchment	In-stream transport	Hanley *et al.* (1998)
MUSLE	Empirical	Plot/ Hillslope	Erosion	Kinnell and Risse (1998)
PERFECT	Physical	Field	Erosion	Littleboy *et al.* (1992b); Littleboy *et al.* (1992a)
RUNOFF	Physical	Hillslope/ catchment	erosion /sediment	Borah (1989)
RUSLE	empirical	Plot/ Hillslope	Erosion	Wischmeier *et al.* (1971); (Foster and Wischmeier, 1974; Wischmeier and Smith, 1978)
SEDD	empirical	Plot	sediment yield	Ferro and Porto (2000); Biesemans *et al.* (2000)
SEDNET	Empirical/Conceptual	Catchment	Erosion	Prosser *et al.* (2001a); Prosser *et al.* (2001b)
SEM	Physical	Catchment	soil erosion	Storm and Jorgensen (1987)
SHESED	Physical	channel	In-stream transport	Wicks (1988); Wicks and Bathurst (1996)
SWRRB	Conceptual	Catchment	Water quality	Arnold *et al.* (1990); Arnold *et al.* (1991)
TOPOG	Physical	Hillslope	Erosion	http://www-data.wron.csiro.au/topog/publications/public.html ,O'loughlin (1986)
USLE	Empirical	Hillslope	Erosion	Wischmeier *et al.* (1971); (Foster and Wischmeier, 1974; Wischmeier and Smith, 1978)
WEPP	Physical	Hillslope/ catchment	Erosion	Nearing *et al.* (1989); Laflen *et al.* (1991b); Laflen *et al.* (1991a); Laflen and Flanagan (2013)
WESP	Physical	Small catchment	Sedimentation	Lopes (1987); Lopes and Lane (1988)

Merritt *et al.* (2003) presented as in Table 1.4 scopes and potential of those models(Table 1.3) to predicting gullying and found that most of the processes being modelled occur at the catchment scale. Unfortunately, many of processes and their models experience problems relating to the high input demands of the model as well as difficulties in the selection of parameter sets that best describe most appropriately the catchment dynamics. Gully erosion for example AGNPS, CREAMS, HSPF and SEDNET have the potential to model gullying, however, they are highly parameterized and may not be applicable in data sparse regions. The CTI by Thorne (1984b) attempted the incorporation of the prediction of concentrated flow erosion (i.e. gullying) into existing models of soil loss, by proposing a pragmatic, reasonable and easy to apply topographic index, which was based on field-measured topography and is known as the Compound Topographic Index (CTI) (Equation 1.3).

Table 1.4: Model scopes and their potential to predict gullying. After Merritt *et al.* (2003)

Model	Rainfall-runoff	Land surface sediment			Gully	In-stream sediment			Sediment-associated water quality	
		G	T	D		G	T	D	Land	In-stream
AGNPS	yes	Yes	no	no[a]	yes	yes	yes	yes	yes	yes
ANSWERS	yes	Yes	yes	yes	no	no	no	no	no	no
CREAMS	yes	Yes	yes	yes	yes	no	no	no	yes	no
EMSS	yes	no[b]	no	no	no	yes	yes	yes	no	no
GUEST	yes	Yes	yes	yes	no	no	no	no	no	no
HSPF	yes	Yes	yes	yes	yes	yes	yes	yes	yes	yes
IHACRES-WQ	yes	No	no	no	no	yes	yes	yes	yes	yes
IQQM	yes	No	no	no	no	no	no	no	no	no
LASCAM	yes	yes	no	no	no	yes	yes	yes	yes	yes
LISEM	yes	yes	no	no	no	yes	yes	yes	no	no
MIKE-11	yes	yes	yes	yes	no	yes	yes	yes	yes	yes
PERFECT	yes	yes	no	no	no	no	no	no	yes	no
SEDNET	yes	yes	no	No[a]	yes	yes	yes	yes	yes	yes
SWRRB	yes	No	no	no	no	yes	yes	yes	yes	yes
TOPOG	yes	yes	yes	yes	no	no	no	no	no	no
USLE	no	yes	no	no	no	no	no	no	no	no
WEPP	yes	yes	yes	yes	no	yes	yes	yes	no	no

G, sediment generation; T, sediment transport; D, deposition.

[a] Requires a sediment delivery ratio (SDR) to compute sediment yield from gross erosion.

[b] Uses prescribed loads for a land use type.

Most of the models of gully erosion over the past 2 decades are based on the aggregation of an array of weighted independent environmental variables to predict the probability of a gully forming or not. For example Capra *et al.* (2005) used the Ephemeral Gully Erosion Model (EGEM) to predict ephemeral gully erosion in Sicily, Italy. However, the EGEM requires 23 separate input parameters, limiting its applicability to data sparse regions (Conoscenti *et al.* (2013). Logistic regression of topographic attributes and environmental variables has also been applied for gully prediction, including the Topographic Wetness Index and Slope-Area parameter (Dewitte *et al.*, 2015). This approach is not process-based, but relies instead on statistical associations between variables, which may or may not represent causality. For this reason, a statistical association approach is not favoured in this research.

Li *et al.* (2016) used a process-based, Annualized Agricultural Non-Point Source Pollution model (AnnAGNPS) to predict ephemeral gully development and topsoil loss due to mechanical in-filling of ephemeral gullies, annually. While the AnnAgnps approach is process-based, it is also highly data-intensive and so does not fulfil the conditions specified above for a gully susceptibility model applicable over large areas and in LEDCs.

Korzeniowska and Korup (2016) and Korzeniowska *et al.* (2018) developed a process-based model using the magnitude and standard deviation of topographic curvature to compute surface roughness. This allowed them to successfully discriminate between gullies and other landforms, such as dunes, in terrain models. However, their approach did not predict gullies or map areas susceptible to gullying and, therefore, is not directly appropriate for the aims of this thesis.

The explosion in remotely sense data over the past 2 decades has led to the increased availability of a wide range of environmental variables and, as a result, further development of erosion modelling approaches. Recent prediction of gully location takes advantage of improved computing power, using machine learning algorithms or classification models to predict landscape geomorphic features such

as gullies (Momm *et al.*, 2011b; Conoscenti *et al.*, 2014; Rahmati *et al.*, 2017; Arabameri *et al.*, 2019a; Avand *et al.*, 2019). For example Yunkai *et al.* (2010) analysed soil erosion characteristics in small watersheds with particle swarm optimization, support vector machine, and artificial neuronal networks. Rahmati *et al.* (2017) evaluated different machine learning models for predicting and mapping the susceptibility of gully erosion. Gayen *et al.* (2019) carried out a gully erosion susceptibility assessment in India using different machine learning algorithms and found that all performed well, with high predictive accuracy, and suggests that they could be used by land managers to initiate remedial measures and hazard mitigation in prioritized areas. Similarly, Garosi *et al.* (2019) assessed the performance of GIS-based, machine learning models with different accuracy measures for determining susceptibility to gully erosion. They found models were highly accurate, with AUC (Area under curve, ROC classifier) values of between 87.2% and 92.4%; however, the area of investigation was only 18.5 km^2 and therefore, did not have the topographic or environmental variability of the regional analysis required here. Arabameri *et al.* (2020) were successfully able to predict gully head-cuts by applying machine learning methods to a study area in north-western Iran but, again, only over small areas or relatively uniform vegetation, geology and topography. Their method could not be applicable in a large-scale, regional application of the type needed for land-use management planning.

Most of the models developed using a machine algorithm approach are powerful predictive tools, but they are still based on a statistical association and the strength of that relationship is dependent on the quality and quantity of input data. Whilst machine learning approaches have been successfully applied to some data sparse regions (e.g. Iran – Arabameri et al. 2020) and have great potential to provide useable predictions of gullying in the future, application of these approaches over large areas and topographically diverse landscapes (i.e. entire countries or regions) still faces challenges.

The above review on approaches (machine learning etc) that are currently used reveals that they are still heavily parameterised, which make them unsuitable to be

applied in data sparse regions. The benefits of the CTI over these approaches is the low computational power required, and the intuitive, process-based approach it represents.

1.3.6. **Gully prediction using topographic data and the future utility of the CTI**

Since pioneering work in the 1980s, researchers have developed process and terrain-based approaches to predict cropland and ephemeral gully erosion (Woodward, 1999; Casalí *et al.*, 1999). For example, Casalí *et al.* (1999) characterised the susceptibility of a catchment to classical and ephemeral gullying using a simple topographic index based on the area-weighted mean slope. This requires the availability of detailed field measurements and a high-resolution DEM. Thresholds for gully initiation and sedimentation in Mediterranean Europe (Vandekerckhove *et al.*, 2000) as well as a review of topographic threshold conditions for gully head development in different environments has been published (Torri and Poesen, 2014).

Most of these are based on the Area-Slope method which is a conceptual step backwards compared to the CTI – which better accounts for terrain complexity (Thorne *et al.*, 1984b; Thorne, 1984b; Thorne and Zevenbergen, 1984; Thorne *et al.*, 1984c; Thorne *et al.*, 1986; Thorne *et al.*, 1987; Zevenbergen and Thorne, 1987; Vendrusculo, 2014).

Parker *et al.* (2007) automated calculation of the CTI and investigated whether it could be applied in data sparse regions using the globally-available, medium to coarse DEMs then readily accessible from the USGS. They found this to be unfeasible with the 10m and 30m resolution DEMs available at that time, and recommended that, to perform satisfactorily, ephemeral gully prediction using the CTI requires a high resolution, good quality DEM.

The most popular topographic indices for estimating the erosive power of concentrated flow have been compared and contrasted in recent research

(Daggupati *et al.*, 2013; Sekaluvu *et al.*, 2015; Sheshukov *et al.*, 2018) and concluded that CTI outperforms other topographic indices. Indices examined included:

CTI (Thorne, 1984a; Thorne and Zevenbergen, 1984; Thorne *et al.*, 1984b) - Equation 1.3;

Topographic Wetness index (TWI) (Moore *et al.*, 1988b; Vandaele *et al.*, 1996b) - Equation 1.5,

$$\mathrm{TWI} = \ln\left(\frac{A}{tanS}\right) \qquad \text{Equation 1.5}$$

where, A = Discharge surrogated by flow accumulation area, S = Local slope.

Slope Area index (SAI) (Moore *et al.*, 1988b; Vandaele *et al.*, 1996a) -Equation 1.6,

$$SAI = A * S \qquad \text{Equation 1.6}$$

where, A = Discharge surrogated by flow accumulation area, S= Local slope.

Slope Area Power Index (SAPI) (Vandaele *et al.*, 1996a; Vandaele *et al.*, 1996b) - Equation 1.7,

$$\mathrm{SAPI} = A * S^2 \qquad \text{Equation 1.7}$$

where, A = Discharge surrogated by flow accumulation area, S= Local slope.

Some confusion may arise when the terms CTI and TWI are considered because in the literature, some authors use these terms interchangeably when, in fact, these indices are not the same. For example Yang *et al.* (2005) and Yang *et al.* (2007) consistently refer to TWI as being the same as CTI. A website that has popularised interchangeable use of TWI and CTI is the GIS 4 Geomorphology website. This is unfortunate as CTI and TWI-based approaches are different and have been developed independently, by different groups of researchers: (Moore *et al.*, 1988b; Moore *et al.*, 1988a; Moore and Nieber, 1989; Moore *et al.*, 1991; Ladson and Moore, 1992; Moore and Thompson, 1996; Murphy *et al.*, 2009) and for CTI

(Thorne, 1984b; Thorne and Zevenbergen, 1984; Thorne *et al.*, 1984b; Thorne *et al.*, 1984c; Thorne *et al.*, 1986; Thorne *et al.*, 1987; Thorne and Zevenbergen, 1990a).

It was established at the beginning of this chapter that the locations of areas of concentrated flow are controlled by field surface topography (Thorne, 1984b), although the presence and subsurface topography of an impermeable layer or plough-pan can also be a factor (Moore *et al.*, 1988a; Moore and Thompson, 1996). The literature review presented above establishes that the CTI (Equation 1:3) outperforms other similar topographic indices (i.e. equations 1:6; 1:7 and 1:8) when it comes to predicting either ephemeral gullying or susceptibility to gullying, and in data sparse regions represents a suitable candidate topographic attribute for potential use in predicting susceptibility to concentrated flow erosion. It must also be concluded, however, that serious issues still remain to be resolved before a CTI-based approach can be used successfully in data-sparse regions and that much research remains to be done, which is the focus of this thesis.

Accurate slope calculation is vital to the computation of reliable values of CTI and in the next chapter, issues concerning the relative accuracy of slope calculations calculated in areas with varying ruggedness of terrain are addressed, and ways to achieve better slope estimates for use in the CTI are addressed. In Chapter 3, the influence of raster cell resolution on slope, ruggedness and, particularly, the CTI is addressed. Validation of the CTI using field and high resolution remotely-sensed topographic data is of paramount importance in this work. When it emerged that calculated values of CTI were not in agreement with observed data for low-resolution grids, a new method of CTI-based analysis using fuzzy logic was developed to address this problem, and this is work is reported in Chapter 4. The potential for additional environmental descriptors (mostly categorical) to further improve and check the predictive performance of the fuzzy CTI-based method in delineating areas susceptible to gullying was investigated next, and this is reported in Chapter 5.

CHAPTER 2: INVESTIGATING VARIATION OF TWO OF THE MOST POPULAR SLOPE DERIVATION METHODS WITH TERRAIN RUGGEDNESS

2.1. Introduction and aim

An essential challenge of creating a predictive model of gully susceptibility that is applicable over large areas is that it must work in both rugged and smooth terrains. However, it is known that the accuracy of calculating slope from DEMs is dependent on the nature of the terrain surface (Tang and Pilesjö, 2011). There are many methods of representing the topographic attributes of DEMs and calculating slope, all of which give slightly different answers, but none of which fully and correctly represent the complexity of the land surface. However, small differences in slope can lead to significant discrepancies in the prediction of sediment transport and gully formation. Imperfections in the representation of a slope may, therefore, lead to over- or underestimation in the prediction of susceptibility to gullying.

Recognising this, Chapter 2 investigates the accuracy of different methods of calculating slope. The aim was to identify the conditions where alternative methods work better. In particular, the suitability of different approaches for smooth and rugged terrain was investigated, providing the basis for exploring the possibility of employing appropriate methods in different sub-areas within a DEM, where the method applied is matched to the nature of the terrain (see Chapter 1, Objective 1).

2.2. Literature Review

2.2.1. Approaches to terrain analysis and slope fitting

The existence of many mathematical options for calculating slope and terrain attributes reflects the inadequacy of any single polynomial to precisely model a natural land surface. Ultimately, it is not possible to represent a natural land surface using any single, simple mathematical model. This explains why the development of computer algorithms for processing and analysing topographic data has continued (Florinsky, 1998a).

Mandelbrot (1982) contemplated the complex nature of the Earth's surface and the inability of Euclidean geometry to represent nature effectively. According to Mandelbrot (1982; page 1) explanation of the limited capacity of Euclidean geometry to represent a natural land surface, "lies in its single inability to describe the shape of a cloud, mountain, a coastline, or a tree. Clouds are not spheres; mountains are not cones, coastlines are not circles." It is also true that floodplains are not flat, and neither are hillslope profiles composed of circular arcs or even logarithmic spirals. Therefore Mandelbrot (1982) began to develop fractal geometry to deal with the fractal dimensions and self-similarity in the Earth's features. After reviewing mathematical and digital models of the land surface, Hengl and Reuter (2009; page 31) concluded that, "Land surface is a unique natural feature that cannot be simulated in any simple way. It needs to be measured, systematised and represented. This is mainly because, landscape-forming processes alternate and interact, resulting in unpredictable features at local, regional, and global scales."

Computer algorithms for processing and analysing topographic data, and the computational power available, are both increasing rapidly (Florinsky and Kuryakova, 1996; Florinsky and Pankratov, 2015).The data required to represent topographic surfaces, coupled with the information generated from their analysis, is substantial and can be challenging to manipulate. However, the availability of ever more powerful computers and the use of global polynomial approximations present promising potential solutions to dealing with land surface complexity (Zhao and Li, 2015).

Approaches to terrain analysis that fit a three-dimensional surface to a grid of surveyed elevations to generate the topographic attributes have been categorised into different groups based on their popularity, usage and the order of the finite difference equations they use by Zhou and Liu (2004), as follows:

- Second-order finite difference (2FD) associated with, for example, Fleming and Hoffer (1979); Zevenbergen and Thorne (1987) and Ritter (1987);

- Third-order finite difference (3FD) (Sharpnack, 1969; Horn, 1981; Wood, 1996);
- Third-order finite difference weighted by reciprocal of squared distance (3FDWRSD)(Horn, 1981)
- Third-order finite difference weighted by reciprocal of distance(3FDWRD) (Unwin, 1981);
- Frame finite difference (FFD) (Chu and Tsai, 1995);
- The simple difference (SimpleD) (Jones, 1998b).

Most slope algorithms (e.g. 2FD, 3FDWRD, 3FD, 3FDWRSD FFD and Simple-D), are based on similar theories for calculating partial derivatives of Z = F(x, y) by differentiating partial the function to solve for x and y, respectively. Despite this similarity, Tang and Pilesjö (2011) found that 2FD and the Simple-D methods yield higher slope values than other methods, due to less sampled grids when estimating slope. Their results demonstrate that there can be significant differences between the eight slope algorithms they tested Tang and Pilesjö (2011). Jones (1998b) ranked the performance of eight slope algorithms by comparing calculated slopes to the actual slope for an artificial surface (Table 2.1).

Table 2.1. Eight slope algorithms investigated by Jones (1998b).

Rank	Slope algorithm
1	Zevenbergen and Thorne (1987)
2	Horn (1981)
3	one over distance weighting (Unwin, 1981)
4	Third-order finite-difference method of Sharpnack (1969)
5	constrained quadratic method(Wood, 1996)
6	diagonal Ritter's Method – modified from method of Fleming and Hoffer (1979)
7	simple method - similar to that of Fleming and Hoffer (1979)
8	maximum downward gradient method(Travis *et al.*, 1975; EPPL, 1987; Onorati and Poscolieri, 1988)

While it is acknowledged that methods for estimating raster-based slope and references associated with them are dated (Table 2.1), they are still relevant in that many of them are implemented in contemporary GIS software platforms (Table 2.2) and are still used when performing terrain analysis for decision making of all kinds. The issue that remains is of identifying the slope algorithm most suitable for each

type of terrain (Skidmore, 1989). For example, considering the slope algorithms of Horn (1981) and Zevenbergen and Thorne (1987) (which were ranked the highest by Jones (1998b)) a decision has to be made on which to use - based on the complexity or ruggedness of the terrain. Hodgson (1995) demonstrated that Horn's method captures more variance when applied to more complex surfaces. Lecours *et al.* (2017) support the earlier finding of Hodgson (1995) and also argue that the

Zevenbergen and Thorne (1987) method works best on smooth surfaces, while Horn (1981) works best on rough surfaces. However, neither Hodgson (1995) or Lecours *et al.* (2017) actually define how a surface is designated as being 'rough' or 'smooth'.

Many of the methods listed above are implemented in contemporary GIS software platforms (Table 2.2) and are still used when performing terrain analysis for decision making of all kinds. Table 2.2 lists slope algorithms currently in use in Quantum GIS (QGIS), SAGA (System for Automated Geoscientific Analyses) GIS, GRASS and Whitebox GIS. Jenness (2013) develop an extension to be used in ArcGIS and contains methods by Sharpnack (1969), Horn (1981), and Zevenbergen and Thorne (1987)

Table 2.2. Slope calculation methods implemented in GIS platforms.

Method	Associated Authors	Year	Available in
Maximum slope	(Travis *et al*. 1975)	1975	QGIS, SAGA, GRASS
6 parameter 2nd order polynomial	(Evans 1979)	1979	ARCGIS extension (Jenness, 2013), GIS, SAGA, GRASS
Least squares fitted plane	(Horn 1981, Costa-Cabral & Burgess 1996)	1981	QGIS, SAGA, GRASS, Whitebox
6 parameter 2nd order polynomial	(Heerdegen and Beran 1982)(Heerdegen and Beran, 1982)	1982	QGIS, SAGA, GRASS
10 parameter 3rd order polynomial	(Haralick 1983)(Haralick, 1983.)	1983	QGIS,SAGA,GRASS
6 parameter 2nd order polynomial	(Bauer *et al*. 1985)	1985	QGIS, SAGA, GRASS
9 parameter 2nd order polynomial	(Zevenbergen and Thorne 1987)	1987	ARCGIS extension (Jenness, 2013), QGIS, SAGA, GRASS
Maximum triangle slope	(Tarboton 1997)	1997	QGIS, SAGA, GRASS

Jones (1998a) comparison of the Horn (H) and Zevenbergen and Thorne (Z&T) methods reached a significant conclusion, which is pivotal to the philosophy underpinning this chapter: that knowledge of the amount of observational noise present in a DEM at the sub-matrix, 3 x 3 grid, kernel scale is of vital significance when deciding the best slope algorithm for a given application. Jones (1998a) recommended further investigation into the spatial correlation structure of DEM noise concerning the slope estimating intricacy. A single RMS error value is taken to represent most DEM surface variability, which implies that variability is constant over the whole DEM surface with no spatial correlation structure. For DEMs of real, naturally-varying landscapes, this is a gross oversimplification. Real terrain surfaces usually have components that are significantly rougher than others; areas where the roughness is patchy or some other degree of spatial organisation. Thus, a slope algorithm that performs best for the smoothest part of a DEM might not be the best performing algorithm for another, rougher part of the same DEM (Jones, 1998a pp.250-250). These findings regarding slope method suitability with respect to roughness or smoothness of the terrain are consistent and reasonable. However, what constitutes 'roughness' or 'ruggedness' in a real terrain surface, and an appropriate metric to quantify this, remain to be clarified. A later section of this chapter considers the methods available to quantify topographic ruggedness.

The Horn (1981), Evans (1972), Zevenbergen and Thorne (1987), Shary (1995) and Modified Evans-Young (Young, 1978; Evans, 1980) methods are most frequently referred to in the literature (Shary *et al.*, 2002); Hengl and Evans (2009)). Cadell (2002) noted that the only difference between them is in the number of grid cells they use to calculate slope, and the weightings applied to each cell. Jones (1998) considered the second-order, finite-difference algorithm (e.g. Zevenbergen and Thorne, 1987) to be the best method and the third order, finite-difference method (e.g. Horn, 1981) to be the second best.

Therefore, in this chapter, the Horn (1981) and Zevenbergen and Thorne (1987) methods have been selected for further investigation because they represent two different methods that are widely considered to be the best options and are two of

the most commonly applied slope algorithms. For example, QGIS currently supports the use of the Zevenbergen and Thorne (1987) algorithm to calculate slope, aspect and planform curvature, whereas the ArcGIS 10.3 Spatial Analyst extension uses the Horn (1981) method. However an extension developed by Jenness (2013) can be used in ArcGIS to compute slope based Sharpnack (1969), Horn (1981) and Zevenbergen and Thorne (1987) methods.

However, also as reported above, the literature suggests that these methods do not work uniformly well across varied terrain ruggedness. The Horn (1981) method is thought to be most suitable for rough or rugged terrains whereas the Zevenbergen and Thorne (1987) method is preferred on smoother, flatter terrain (Jones, 1998b; Cadell, 2002; Jenness, 2004; Jenness, 2013). Therefore, these two methods also represent a useful case study to compare slope algorithms when generating topographic indices over different levels of ruggedness.

2.2.2. **Zevenbergen and Thorne method**

Evans (1980) computed four topographic attributes (slope, aspect, profile curvature and planform curvature) from a full quadratic surface. In this approach, an altitude sub-matrix of 3 x 3 nodes (Figure 2.1) is analysed repetitively throughout a square altitude matrix of evenly spaced point elevations covering the entire area in question. Values of the topographic attributes for the central point of each 3 x 3 submatrix are determined. The nine elevations of the 3 x 3 sub-matrix are used to determine the six parameters, A . . . F, in Equation 2.1:

$$Z = Ax^2 + By^2 + Cxy + Dx + Ey + F \qquad \text{Equation 2.1}$$

The Evans-Young algorithm (Evans, 1972; Young, 1978; Pennock et al., 1987) fits a second-order polynomial to the 3 x 3 neighbourhood filters. This (e.g. equation 2.1) has six coefficients and passes close to all of the points in the 3 x 3 sub-matrix but does not necessarily pass through any of the nine original elevations. Therefore, it is questionable whether Evans' equation can be said to represent the topography of

the land surface accurately. For this reason, Zevenbergen and Thorne (1987) modified Evans' equation.

The first modification Zevenbergen and Thorne (1987) made was to ensure that their surface does pass precisely through the nine sub-matrix elevations, using a partial quartic equation (Equation 2.2, Figure 2.1):

$$Z = Ax^2y^2 + Bx^2y + Cxy^2 + Dx^2 + Ey^2 + Fxy + Gx + Hy + I \qquad \text{Equation 2.2.}$$

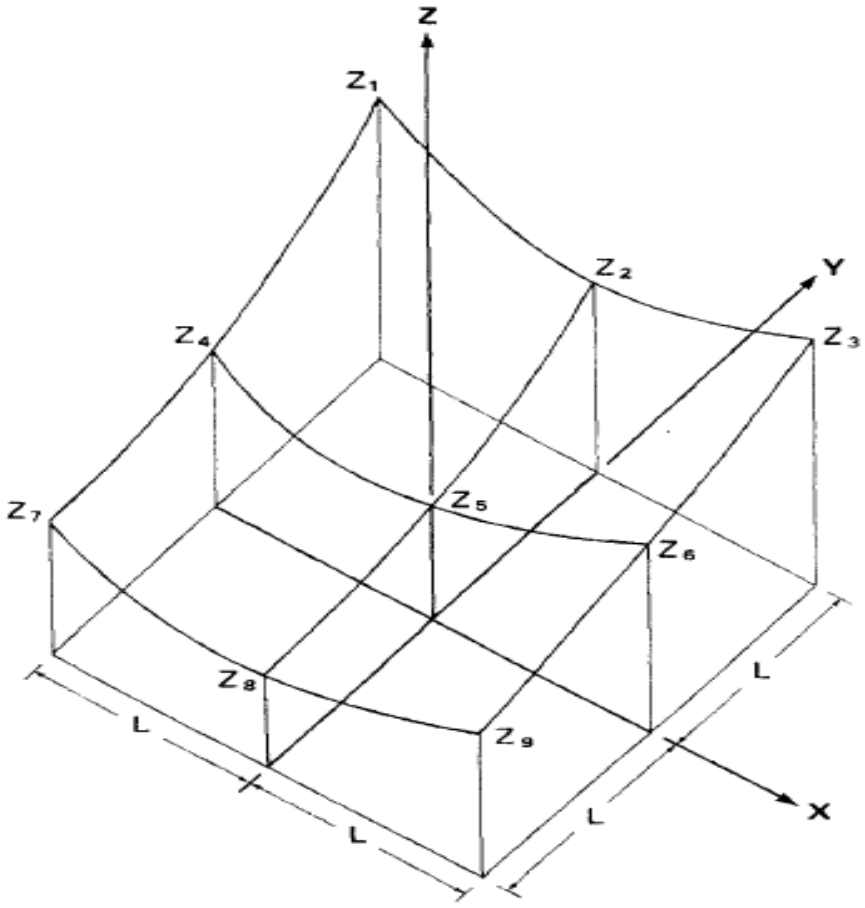

Figure 2.1: 3 x 3 elevation sub-matrix, adapted from Zevenbergen and Thorne (1987)

Table 2.3: Coordinates in the 3 x 3 elevation sub-matrix

Elevation(Z)	Easting(X)	Northing(Y)
Z_1	-L	L
Z_2	0	L
Z_3	L	L
Z_4	-L	0
Z_5	0	0
Z_6	L	0
Z_7	-L	-L
Z_8	0	-L
Z_9	L	-L

The coordinates (L_x, L_y and Z) of the nine points in Figure 2.1 are in units of length and L_x and L_y equal in the quantity: that is L = Z = 1. All the coordinates of the nine points of elevation in the regular elevation grid in Figure 2.1 are presented in Table 2.3.

The coefficients A, B, C, D, E, F, G, H and I in Equation 2.2.2 were algebraically determined by Zevenbergen and Thorne (1987) and are shown in Equation 2.2 to Equation 2.11:

$$A = \frac{\left[\frac{Z_1 + Z_3 + Z_7 + Z_9}{4} - \frac{Z_2 + Z_4 + Z_6 + Z_8}{2} + Z_5\right]}{L^4} \quad \text{Equation 2.3}$$

$$B = \frac{\left[\frac{Z_1 + Z_3 - Z_7 - Z_9}{4} - \frac{Z_2 - Z_8}{2}\right]}{L3} \quad \text{Equation 2.4}$$

$$C = \frac{\left[\frac{-Z_1 + Z_3 - Z_7 + Z_9}{4} + \frac{Z_4 - Z_6}{2}\right]}{L^3} \quad \text{Equation 2.5}$$

$$D = \frac{\left[\frac{Z_4 + Z_6}{2} - Z_5\right]}{L^2} \quad \text{Equation 2.6}$$

$$E = \frac{\left[\frac{Z_2 + Z_8}{2} - Z_5\right]}{L^2}$$ Equation 2.7

$$F = \frac{-Z_1 + Z_3 + Z_1 - Z_9}{4l^2}$$ Equation 2.8

$$G = \frac{-Z_4 + Z_6}{2L}$$ Equation 2.9

$$H = \frac{Z_2 - Z_8}{2L}$$ Equation 2.10

$$I = Z_5$$ Equation 2.11

A 3 x 3 sub-matrix or window within the regular DEM grid moves over the surface, and the target is always to solve the equations defining the topographic attributes for the centre cell. Any of the interior cells in the DEM can be the centre cell for which the solution is sought. The centre cell (Z_5) will always have coordinates x = 0 and y = 0 and can be solved. Differentiating Equation 2.2 concerning x and concerning y, respectively, so Z = Z_5, x = 0 and y = 0 yields:

$$\frac{\partial z_5}{\partial x_5} = G$$ Equation 2.12

and

$$\frac{\partial z_5}{\partial y_5} = H$$ Equation 2.13

Slope at Z_5 is then obtained as:

$$\text{Slope } = (G^2 + H^2)^{\frac{1}{2}} = \left(\left(\frac{\partial z_5}{\partial x_5}\right)^2 + \left(\frac{\partial z_5}{\partial x_5}\right)^2\right)^{\frac{1}{2}}$$ Equation 2.14

We know from Equation 2.9 that, $G = \frac{-Z_4 + Z_6}{2L}$ and from Equation 2.10 that, $H = \frac{Z_2 - Z_8}{2L}$ so:

$$\text{Slope } = -(G^2 + H^2)^{\frac{1}{2}} = \left(\left(\frac{\partial z_5}{\partial x_5}\right)^2 + \left(\frac{\partial z_5}{\partial x_5}\right)^2\right)^{\frac{1}{2}} = \left(\left(\frac{-Z_4 + Z_6}{2L}\right)^2 + \left(\frac{Z_2 - Z_8}{2L}\right)^2\right)^{\frac{1}{2}}$$ Equation 2.15

The aspect, profile curvature and planform curvature can also be computed from the sub-matrix, through differentiation of Equation 2:2, as:

$$\text{Aspect} = \tan^{-1}\left(\frac{-H}{-G}\right) = \tan^{-1}\left(-\frac{\frac{Z_2 - Z_8}{2L}}{-\frac{-Z_4 + Z_6}{2L}}\right)$$ Equation 2.16

$$\text{Profile curvature } = -\frac{2(DG^2 + EH^2 + FGH)}{G^2 + H^2}$$ Equation 2.17

$$\text{Planform curvature } = \frac{2(DH^2 + EG^2 - FGH)}{G^2 + H^2}$$ Equation 2.18

Zevenbergen and Thorne (1987) consider Equation 2.2 to be more general and better able to fit the measured points because it is more 'flexible' than Equation 2.1, arguing that if the surface indicated by the nine sub-matrix elevations is of a lower order than Equation 2.2 the appropriate coefficients will equal zero and not affect the equation. For example, if the best-fit surface is quadratic, A, B and C will all equal zero, and if the surface is a planar, coefficients A to F will all equal zero.

However, it cannot be guaranteed that either Equation 2.1 or Equation 2.2 will fully replicate the actual land surface topography between the measured grid points and so an appropriate grid mesh size is required to optimise the match between actual and modelled topography.

2.2.3. **Horn (1981) method**

The equations used in Horn's method are categorised as third-order finite difference equations (Sharpnack and Akin, 1969; Horn, 1981; Wood, 1996). The method of Horn (1981) is a modified version of the technique of Sharpnack and Akin (1969), using unequal weighting coefficients for the nearer elevation values. These weightings are proportional to the reciprocal of the square of the distance from the kernel centre. Horn's method is implemented in the "SLOPE" function of the ArcInfo GRID software package (ESRI, 1995). This method uses eight grid points to calculate each gradient and aspect value.

Both the Horn (1981) (Figure 2.2) and Zevenbergen and Thorne (1987) (Figure 2.1, above) methods use elevations in a 3 x 3 neighbourhood or sub-matrix. Consequently, the notation of Horn can be replaced with that of Zevenbergen and Thorne (1987) for ease of understanding, as shown in equation 2.19 to 2.25. The distance between cells representing elevation remains L.

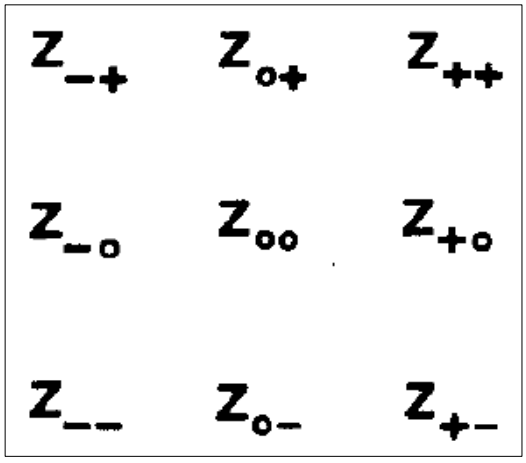

Figure 2.2. Horn's 3 × 3 neighbourhood matrix notation.

$$Z_1 = Z_{\mp} \quad \text{Equation 2.19}$$

$$Z_2 = Z_{0+} \quad \text{Equation 2.20}$$

$$Z_3 = Z_{++} \quad \text{Equation 2.21}$$

$$Z_5 = Z_{00} \quad \text{Equation 2.22}$$

$$Z_7 = Z_{--} \quad \text{Equation 2.23}$$

$$Z_8 = Z_{0-} \quad \text{Equation 2.24}$$

$$Z_9 = Z_{0\pm} \quad \text{Equation 2.25}$$

The Horn (1981) slope method considers the gradient in both West-East and North-South directions, with the north-south gradient based on the cells immediately north and south of the central cell, and the east-west gradient calculated from the cells immediately east and west of the central cell. This differs from the method used by Zevenbergen and Thorne (1987), in which the north-south and east-west gradients are each calculated from all three columns in the 3 x 3 array, but with the central column double-weighted compared to the two outer columns.

$$\frac{\partial z}{\partial x} = \frac{[(Z_3 + 2Z_6 + Z_9) - (Z_1 + 2Z_4 + Z_7)]}{8L} \quad \text{Equation 2.26}$$

$$\frac{\partial z}{\partial y} = \frac{[(Z_1 + 2Z_2 + Z_3) - (Z_7 + 2Z_8 + Z_9)]}{8L} \quad \text{Equation 2.27}$$

$$Slope = \left[\left(\frac{\partial z}{\partial x}\right)^2 + \left(\frac{\partial z}{\partial y}\right)^2\right]^{\frac{1}{2}} \quad \text{Equation 2.28}$$

$$\text{Aspect} = \text{Tan}^{\wedge}(-1)\ ((\partial \text{z}/\ \partial \text{x})/(\partial \text{z}/\ \partial \text{y})) \quad \text{Equation 2.29}$$

To aid understanding of differences between the ways in which slope is calculated in the Zevenbergen and Thorne (1987) and Horn (1981) methods, Jenness (2013) provided the illustrations depicted in Figure 2.3.

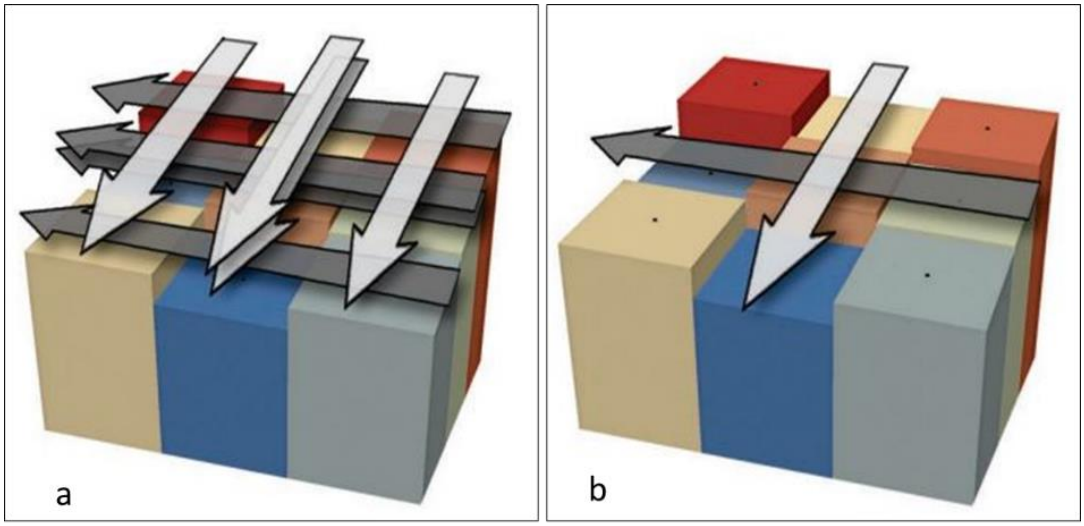

Figure 2.3: (a) Zevenbergen and Thorne (1987) and (b) Horn (1981) slope calcualtion methods as illustrated by Jenness (2013).

2.2.4. **Quantifying topographic ruggedness**

The assertion that the Zevenbergen and Thorne (1987) method is more suitable for smooth terrain, while Horn (1981) method is better suited for rugged terrain is widely acknowledged, but no relationship between performance and values of ruggedness has been sought. For example, Tang and Pilesjö (2011) investigated the influence of terrain on different slope algorithms. They calculated slope values using eight different algorithms and found the resulting slopes differed depending on whether terrain ruggedness was 'flat', 'undulating' or 'steep'. However, they neither indicated how ruggedness was defined, or quantified the levels of ruggedness to which these categories relate.

It would therefore be preferable to relate calculated slopes to ruggedness using a selected metric, and several candidates are available for attempting this. The more widely used indices are the Terrain Ruggedness Index (TRI) (Riley, 1999), the Land Surface Ruggedness Index (LSRI) (Beasom *et al.*, 1983), and the Vector Ruggedness Measure (VRM) (Sappington *et al.*, 2007). LSRI is based on the assumption that ruggedness is a function of the total length of topographic contour lines in a given area. TRI involves quantifying the total elevation change across a given area. VRM measures the dispersion of vectors orthogonal to the terrain surface (Figure 2.4).

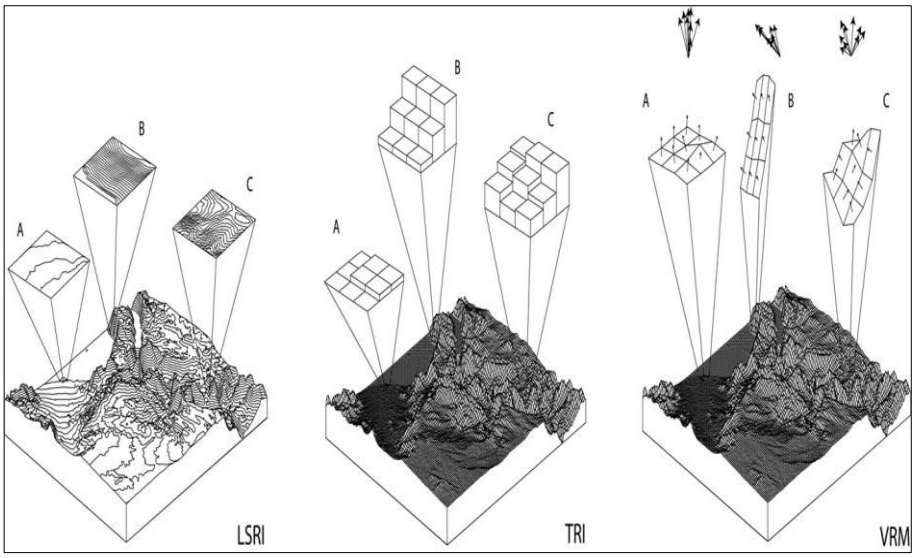

Figure 2.4: Visual representation of the three most common terrain ruggedness calculation methods. After Sappington et al. (2007).

Sappington *et al.* (2007) pointed out that neither the LSRI nor the TRI directly measures variability in topographic aspect and gradient, and both appeared to be strongly correlated with slope (Figure 2.5). Consequently, LSRI and TRI cannot distinguish between high slope plus low ruggedness (i.e. steep and even terrain), and high slope plus high ruggedness areas (i.e. steep, uneven and broken terrain) (Sappington *et al.* 2007). They further argued that a ruggedness measure that incorporates variability in *both* the aspect and gradient components of slope, and which contributes to a multivariate representation of topography, has much greater utility. Quantifying ruggedness independently of the slope is clearly important, and this led Sappington *et al.* (2007), building on work by Hobson (1972), to develop the VRM, an index that incorporates the heterogeneity of both slope and aspect.

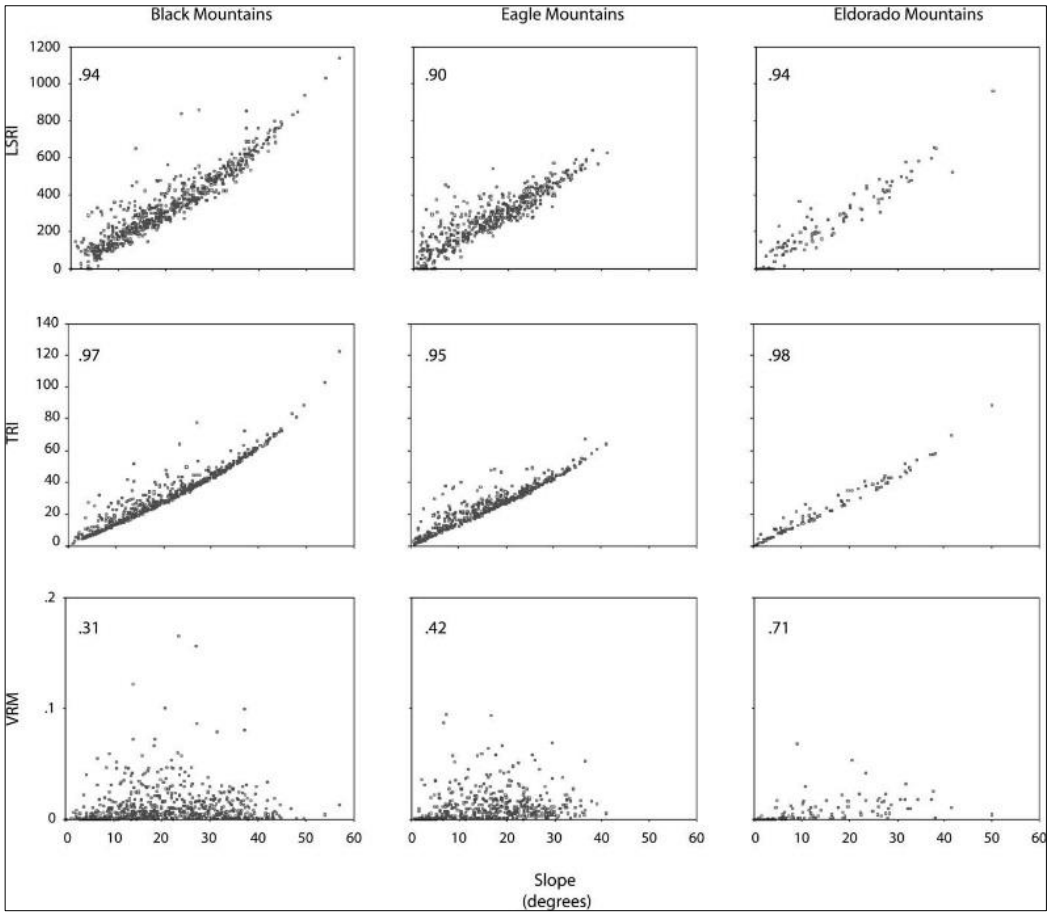

Figure 2.5: Correlations of slope to ruggedness parameterised using the LSRI, TRI and VRM. After Sappington et al. (2007).

The method by which VRM is calculated is explained by (Sappington *et al.*, 2007)) as the projection of a unit vector orthogonal to each grid cell in the DEM. The vectors are then decomposed into their x, y, and z components. The slope (α) and aspect (β) of the cells are computed. A 3 x 3 moving-window is used to calculate the magnitude of the resultant vector (|r|) centred on each interior grid cell (Figure 2.6).

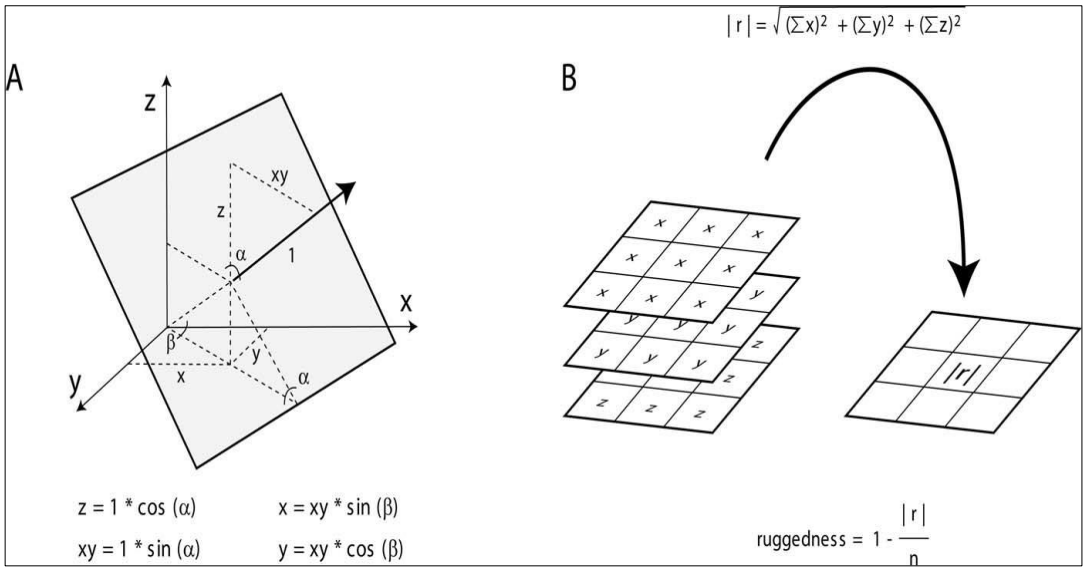

Figure 2.6: Diagrammatic representation of how to compute VRM (Sappington *et al.*, 2007).

VRM measures terrain ruggedness as the variation in the three-dimensional orientation of grid cells within each window, using vector analysis to calculate the dispersion of vectors normal (orthogonal) to grid cells within the specified window. VRM is dimensionless and values in the output raster range from 0 (no terrain variation) to 1 (complete terrain variation). Values of 0.4 and less are typical for natural, rolling terrain (Sappington *et al.*, 2007). The method effectively combines variability in slope and aspect into a single index of ruggedness, and (Sappington *et al.*, 2007) found that values are only weakly correlated with slope (Figure 2.5). These attributes make VRM more attractive than alternative ruggedness indices when studying slope variability In DEMs with different levels ruggedness, avoiding circularity and auto-correlations in the computations.

2.3. **Chapter objectives**

Tang and Pilesjö (2011) recommended that for real-world applications, a combination of slope calculation methods is needed, so an appropriate method can be used to estimate slope based on the terrain. They also recommend that field work and appropriate ground truth data need to be integrated, in order to inform

the best slope estimation algorithm. This is particularly significant when estimating slope over large areas where terrain ruggedness could vary greatly.

As stated in Section 2.1, the aim of this chapter is to identify which of the two leading methods of slope calculation is most accurate, and identify the conditions where alternative methods of slope calculation work better, with particular reference to the suitability of the two different approaches for smooth and rugged terrain. Having reviewed the available literature in Section 2.2, it is now possible to explore the possibility of analysing terrain in a DEM that covers a varied landscape for which field data (ground truth) are available and which comprises of both rugged and smooth terrains without compromising the relative accuracy of the method selected to compute slopes. This exploration requires achievement of the following objectives:

2.1. Compare the Horn (1981) and Zevenbergen and Thorne (1987) methods of computing slope to determine whether they would be likely to produce significantly different slopes when applied in the context of predicting susceptibility of an area to concentrated flow and erosion, leading to gullying: *i.e. do the methods generate significantly different slopes?*

2.2. Determine which slope calculation method works better through comparison with slope values measured in the field: i.e. *if they do generate significantly different slopes, which method is closer to the 'true' slope – as measured on the ground?*

2.3. Investigate whether the accuracy in slope prediction for each method is related to terrain ruggedness: i.e. *is it true that Horn is more applicable to "rough" terrain and Zevenbergen and Thorne is more applicable to "smooth" terrain?*

2.4. Investigate how slope accuracy and the influence of terrain ruggedness change with data resolution: *i.e. do the findings of objectives 1 – 3 apply only to DEMs with small grid sizes?*

2.4. **Methodology**

2.4.1. **Introduction to the methods**

Elevation data in the form of DEMs were used to compute topographic attributes including aspect, slope, and profile and plan curvature. Although this thesis focuses on globally available data and DEM spatial resolution is relatively low for much of the World's land surface (e.g. ~ 30 m pixel size), the area used in these exploratory investigations was required to have a high spatial density of terrain information and accurate field measurements of slope for comparison and validation purposes. This was necessary so that accuracy in estimating slope magnitude using a topographic analysis could be assessed relative to 'ground truth' data obtained by detailed surveying for a range of DEM resolutions, by progressively coarsening that resolution in a DEM with a small grid size. The site chosen for analysis also needed a range of landforms, including smooth and highly rugged terrains. Based on these considerations, the site selected was the North Fork Toutle River basin at Mount St. Helens, USA. This area comprises of very varied landscapes and landforms, and repeated, high-resolution DEMs that can be coarsened. It has also been subject to repeated cross-sectional surveys tied to fixed monuments, which can supply 'ground truth' data needed for exploring the accuracy of slopes derived from DEM-based, topographic analyses.

2.4.2. **Mount St Helens**

Following the eruption of Mount St. Helens, Washington State, USA, on the 18th May 1980, a substantial volume of material was deposited over the surrounding landscape, including in the basin of the Toutle River. Taking the opportunity for fundamental research, shortly after the eruption, the United States Geological Survey (USGS) embarked on a campaign of repeat, regular monitoring of the topography of the area which still continues. In parallel, the U.S. Army Corps of Engineers (USACE) addressed concerns that material deposited by the eruption would be washed downstream, reducing river channel capacity, and substantially

increasing flood risk in towns downstream. In this context, the USACE has been monitoring sediment erosion and downstream deposition since the eruption. The USACE have made use of airborne LiDAR practically since its inception (Table 2.4). For example, high-resolution LiDAR was obtained between 16th and 20th September 2009, for a 214 km^2 area along the North Fork Toutle River, including and immediately downstream of, the volcano. This data was used by the USGS to produce a 1 m grid size DEM, with 10 cm vertical accuracy and 95% confidence interval on bare road surfaces, taken as the average of five laser last-return points per square metre (Figure 2.7). In this study, DEMs based on LiDAR imagery were sourced from the USGS for surveys 2003 and 2013 (Table 2.4). In all cases, the DEMs were resampled at 5 m resolution and then at progressively coarser resolutions up to 30 m, which is representative of globally available data.

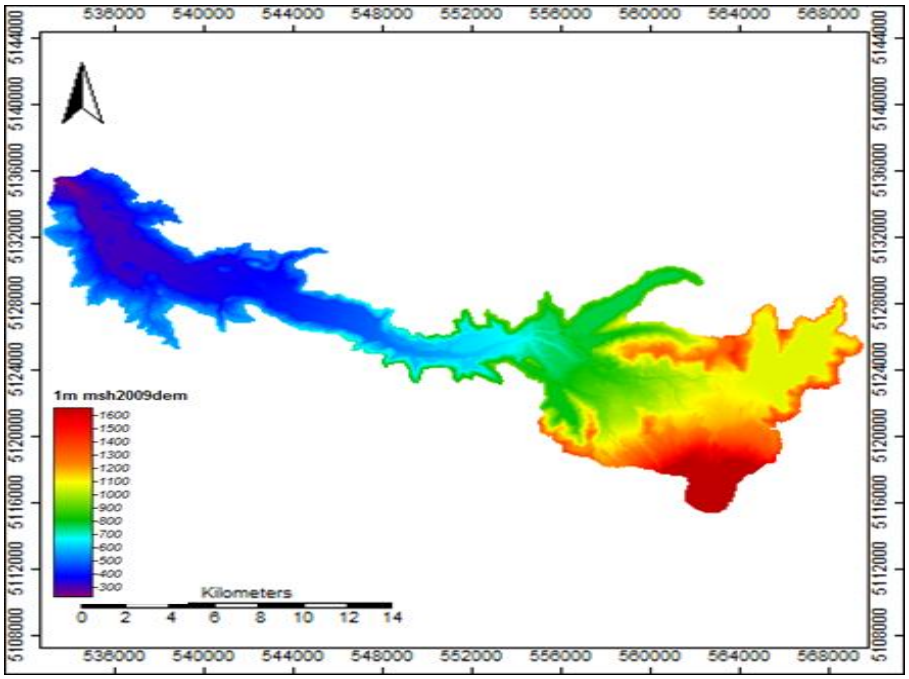

Figure 2.7: LiDAR-derived DEM of the Upper North Fork Toutle River (UNFTR) basin, downstream from Mount St Helens. Spatial resolution = 1 m. Data acquired in 2009 and provided by the USGS.

Table 2.4: LiDAR-based DEMs available for the UNFTR basin at Mount Saint Helens, USA.

DEMS		Resampled Resolutions (m)					
	Original Resolution (m)	5	10	15	20	25	30
DEM_2003_MSNB	5.00	-	✓	✓	✓	✓	✓
DEM_2005_MSNB	10.00	-	-	✓	✓	✓	✓
DEM_2006_MSNB	0.91	✓	✓	✓	✓	✓	✓
DEM_2007_MSNB	1.00	✓	✓	✓	✓	✓	✓
DEM_2009_MSNB	1.00	✓	✓	✓	✓	✓	✓
DEM_2010_MSNB	1.00	✓	✓	✓	✓	✓	✓
DEM_2011_MSNB	1.00	✓	✓	✓	✓	✓	✓
DEM_2012_MSNB	1.00	✓	✓	✓	✓	✓	✓
DEM_2013_MSNB	8.63	-	✓	✓	✓	✓	✓

2.4.3. **Comparing the Horn and Zevenbergen and Thorne slope calculation methods (Objective** 2.1**)**

The DEM shown in Figure 2.7 was resampled into 1, 5, 10, 15, 20, 25, and 30 m resolutions and the Horn (H) and Zevenbergen and Thorne (Z&T) terrain analysis methods were applied to each of the resampled resolutions. Due to the large file size of the 1 m resolution DEM, an area close to the crater of Mount St Helens that included highly varied terrain was clipped out and used for the exploratory analysis. This was important because slope and other topographic attributes vary with resolution. Particularly, land surface features in a DEM are progressively under-represented as DEM resolution coarsens. Metrics of terrain ruggedness will also vary with DEM resolution, leading to further issues with what are designated as 'rough' or 'smooth' surfaces. To explore these issues, both slope methods and the VRM ruggedness index calculations were performed at selected, coarser resolutions. The extent to which the calculated slopes differ was examined and the way in which ruggedness of the surface could inform which slope algorithm should be preferred was considered. Comparisons were undertaken using four measures of difference, as described in A to D, below.

A. **Simple subtraction**

Differences between slopes computed using the H and Z&T methods were computed using the spatial analyst extension tools in ArcGIS 10.4. Both slopes were

rounded up before finding the difference between them. In ArcGIS10.4, the roundup tool takes positive or negative input values and assigns the next higher integer according to the input number (which has values to the right of its decimal point). The output is a floating-point number without any decimal part (Table 2.5)

Table 2.5: An example of the input and output values when using the round up tool in ArcGIS10.4.

Input	5.3	4.9	3	6.5	-0.2	-2.8
Output	6	5	3	7	0	-2

The outputs for all grid resolutions were classified as: (1) slopes for which the H and Z&T methods were the same, (2) slopes where the H slope was less than that calculated using Z&T, and (3) slopes where the H slope was the higher of the two. Cell count, Area covered, Minimum difference, Maximum difference, Range of difference, mean of difference, and Standard deviation of difference for each class of difference was computed using the 'zonal statistics as a table' tool in the zonal toolbox of the ArcGIS 10.4 spatial analyst extension.

B. **Linear regression and correlation**

H and Z&T slopes for grid cells across the DEM were also compared by plotting their values against each other, such that exact agreement would plot on the 1:1 line of perfect agreement. The distribution of points around the 1:1 line reveals whether the slope is consistently under- or over-predicted by one method compared to the other. The best-fit regression line was fitted to the data and correlation coefficient (r) and coefficient of determination (r^2) values were calculated to test the degree to which values of slope calculated using the H and Z&T methods are related to one another.

C. **Paired sample t-tests**

Paired sample t-tests were used to test the null hypothesis that there is no significant difference between sample means for distributions of slopes generated using H and Z&T. A tool implemented in White Box GIS (Lindsay, 2009; Lindsay, 2014) executes a paired-sample t-test between two images, in this case the Horn slope raster and the Z&T slope raster. A caveat, however, is that given a sufficiently large sample, minimal and non-notable differences can be found to be statistically significant. Also, statistical significance says nothing about the cause of a difference, or whether either parameter is better than the other. Reducing the points or sample size (N) is essential and fortunately SAGA GIS can do this. The GIS does this by constructing a scatter plot between the two rasters and using it to extract the data to table that can be used for plotting, correlation and paired-sample t-testing. The points are sampled such that all data cells (pixels) participate, but if the number of points is too large, the SAGA system selects only points essential for the analyses. In this study, the SAGA GIS tools were used to generate points for the paired sample t-test, which were transferred to an excel spreadsheet. The numbers of data points were much lower following extraction of the essential points from Raster-based scatterplot by SAGA GIS and were suitable to conduct a paired t-test using White box GIS.

D. **Geomorphological Slope Classification**

Geomorphological classes of slopes defined by (Young and Clayton, 1972) were used and are described below and listed in Table 2.6:

1. Slopes in the range of 0° - 2° are described as *Level to very gentle.* These are considered as 'flat' areas in representative, erosional landscapes with erosion surface remnants commonly including the land of up to 1.5°. This is a ‘no-limitation’ category when evaluating land for capability and it is usually considered acceptable for agriculture and most other practical land-use purposes. Within this same class, sub-classes are:

a. Level: slopes in range 0°- 0.5° are termed “Level”, and their direction often cannot be determined.
b. Almost level: Those in the range of 0.5° - 1° are termed “Almost level”, and the slope is sufficient to discern slope direction.
c. Slopes in the range 1°- 2° are considered “Very gently sloping”. Although they appear nearly level in a normal land-form context, in some erosional plains the maximum segments of valley sides may fall within this class.

2. Slopes in the range of 2°- 5° are termed *Gentle.* On most peneplains, 5° is the steepest acceptable slope with most pediments included. Its practical limitations in terms of land capability are relatively slight.
3. Slopes in the range of 5°- 10° are termed *Moderate*, and in many regions, angle frequency declines steeply in this range.
4. Slopes in the range of 10°- 18° are *Moderately steep* and are reflective of landscapes that are neither plains nor steeply dissected. Although their practical limitations are tangible, they can still be utilised to derive moderate economic value.
5. Slopes in the range of 18°- 30° are *Steep.* Above l8° arable cultivation requires special measures, and many forms of land use become uneconomic.
6. Slopes in the range of 30°- 40° are *Very steep* with the upper and lower limits close to the limiting angles for a regolith cover and a smooth and continuous regolith cover respectively. Such land has little economic value.
7. Slopes > 45° are classified *Precipitous to vertical and typical of* cliffs. There are two sub-classes:
    a. Those within the range of 45°- 70° are *Precipitous* and are *u*sually irregular or stepped cliffs.
    b. Sheer rock faces share slopes in the range of 70°- 90° termed *almost vertical.*
8. Slopes steeper than 90° are usually considered overhanging.

Table 2.6. Classification of slope angles proposed by (Young and Clayton, 1972).

Slope class name	Slope range (deg)	General class	Class number
Level	0° - 0.5°		1
Almost level	0.5° -1°	Level to Very gentle	2
Very gently sloping	1° -2°		3
Gentle	2.00-5°		4
Moderate	5° -10°		5
Moderately steep	10° -18°	Gentle to Very steep	6
Steep	18° -30°		7
Very steep	30° -40°		8
Almost Precipitous	40° -45°		9
Precipitous	45° -70°	Precipitous to vertical	10
Almost vertical	70° - 90°		11
Overhanging	>90°		12

Slopes calculated by the H and Z&T methods were subjected to this geomorphological classification. Total numbers of the cells for each geomorphological class were obtained and plotted against the geomorphological slope class to reveal trends for each grid resolution. The percentage difference between the H and Z&T methods in each geomorphological slope class was calculated for each resolution:

$$\text{Percentage difference} = \left| \frac{Z\&Tslope - Hslope}{(Z\&Tslope - Hslope)/_2} \right| \times 100 \qquad \text{Equation 2.30}$$

2.4.4. **Comparison of calculated slopes with field measurements** (Objective 2.2)

Comparisons between the slopes calculated from the DEMs using the two methods indicate where differences occur but do not establish which method is more accurate. Assessment of accuracy requires knowledge of the 'true' slope. However, this type of slope validation is notoriously challenging to achieve because field data is seldom available and, in any case, is unlikely to have been measured at the same spatial scale as that used in the DEMs. Field data is also likely to be patchy and is usually expressed through a 2-dimensional measurement, in contrast to the 3-dimensional surfaces making up the DEMs.

To attempt to validate slopes calculated in the research reported here, cross-sectional transects surveyed across the valley of the UNFTR were accessed (Mosbrucker *et al.* (2015). The data come from the same years as the LiDAR-derived DEMs and allowed comparisons to be made between four measures of slope, as follows:

- Horn (1981) algorithm,
- Zevenbergen and Thorne (1987) algorithm,
- 2-dimensional field surveyed slope, and
- 2-dimensional slope represented in the DEM.

The 2-dimensional slope from the DEM was calculated along the same transect line as the field survey, as the elevation drop between consecutive cells divided by cell distance (in this case, the grid size).

The field-surveyed cross-sections were inputted to ArcGIS as polylines so that information could be extracted along exactly the same transects as those established in field surveys. The spatial analyst tool was used to extract cell values along these transect lines, which were then compared to field slope values. Because H and Z&T measure slope using a 3-dimensional surface, with the value indicating the maximum slope in the 3 x 3 window regardless of direction, not all values are directly comparable to field surveyed slopes, which only measure the slope along the direction of the transect. Therefore, before comparison, all slope values that did not have the same aspect as the transect line were removed from analyses. The resultant dataset, consisting of four comparable measures of slope along the transects, was analysed using linear regression and correlation.

Over 100 transects were used in this study, selected from over 300 available cross-sections (Mosbrucker *et al.* (2015). The surveyed data was collected with Leica total stations, with surveyed points occurring at every break of slope and multiple benchmarks, called ‘monuments’ located along each transect to ensure the same transect is resurveyed through time.

As a check on the compatibility of the surveyed cross-sections and the DEMs and their suitability to allow comparison between rasterised slope methods and slopes measured in the field, absolute elevation points were extracted along the cross-sections, compared directly to data extracted from the DEMs.

Elevations surveyed in the field can be used to estimate the average slope of the land surface using Pythagoras theorem and trigonometry whereby knowing two sides of a right-angle triangle its third face or side can be computed (Figure 2.8). In the field, the elevation, also known as the rise (Z) and slope distance (L), (i.e. the hypotenuse in Figure 2.8) were measured. The horizontal distance and the slope are calculated using Pythagoras theorem and trigonometrical ratios.

The slope distances (L) is computed as:

$$|AC|^2 = |AB|^2 + |BC|^2 \qquad \text{Equation 2.31}$$

Thus,

$$|AC| = \sqrt{(AB)^2 + (BC)^2} = L \qquad \text{Equation 2.32}$$

Also, given coordinates (longitude(x) and latitude(y)):

$$|AC| = \sqrt{(\Delta X)^2 + (\Delta Y)^2} = L \qquad \text{Equation 2.33}$$

The horizontal distance is also is known as the run (HD) is computed as:

$$|AB|^2 = |AC|^2 - |BC|^2 \qquad \text{Equation 2.34}$$

Therefore,

$$\mathrm{HD} = |\mathrm{AB}| = \sqrt{|AC|^2 - |BC|^2} \qquad \text{Equation 2.35}$$

and,

$$\sqrt{\left|\sqrt{(\Delta X)^2 + (\Delta Y)^2}\right|^2 - |\Delta Z|^2} \qquad \text{Equation 2.36}$$

where y = Northing, x = Easting, Z = Elevation, and Δ = change.

The slope is then computed by traditional slope formula:

$$\text{The slope in percent} = \left(\frac{\text{BC}}{\text{AB}}\right) * 100 \qquad \text{Equation 2.37}$$

$$Slope\ in\ degree = Tan^{-1}\left(\frac{AB}{BC}\right) \qquad \text{Equation 2.38}$$

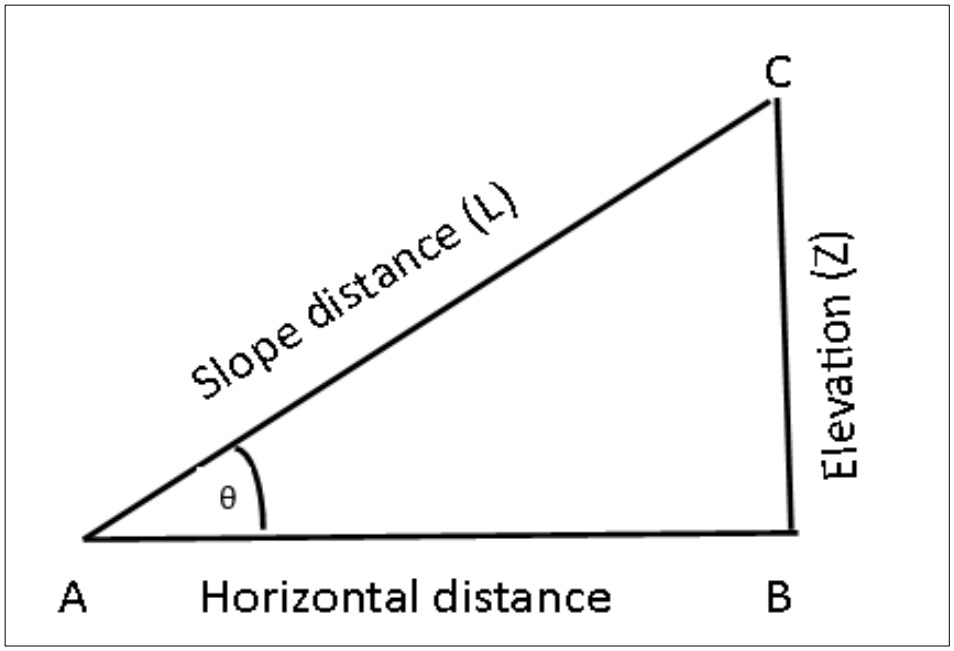

Figure 2.8: Trigonometric and Pythagoras approach to derivation of the field surveyed slopes.

2.4.5. **Investigation of whether slope accuracy is related to terrain ruggedness based on cross-sectional data (Objective** 3**)**

VRM was used to parameterise ruggedness at Mount St Helens. It was calculated in ArcGIS 10.3 using the benthic terrain tool extension (Wright *et al.*, 2005) based on a moving 3 x 3 interrogation window that matched that used to calculate H and Z&T slopes. Ruggedness level was initially calculated for the cross-sections selected from within the area covered by the 2009 Lidar-based, 1 m DEM. This layer was used to partition slope values into ruggedness categories, to allow investigation of whether differences between the slopes calculated using the H and Z&T methods are related to ruggedness.

Overall, the range of VRM values was lower than expected, remaining below 0.4 in all cases despite the varied terrain (Table 2.7). Even so, coefficients of variation (CV) along the cross-sections were high, indicating that all the cross-sections have a range of ruggedness levels.

Table 2.7. USGS cross-section names and ruggedness statistics for the 2009 LiDAR DEM (1 m).

Name	No. of points	MEAN of VRM	MAX_of VRM	STD of VRM	CV of VRM
CA200	401	0.0019	0.0144	0.0023	119.3064
CA205	143	0.0032	0.0202	0.0036	110.6700
CA210	339	0.0020	0.0260	0.0027	133.3832
CA215	375	0.0027	0.0260	0.0043	156.8282
CA220	449	0.0042	0.0639	0.0075	178.0128
CA225	508	0.0041	0.0381	0.0051	124.7859
CA230	392	0.0044	0.0737	0.0066	149.6007
CS075	117	0.0044	0.0371	0.0062	142.8670
CS080	458	0.0031	0.0346	0.0041	133.2576
CS085	358	0.0029	0.0272	0.0040	138.8276
CW240	339	0.0032	0.0353	0.0048	150.8555
CW245	309	0.0037	0.0416	0.0055	147.1850
CW250	271	0.0019	0.0141	0.0026	133.1102
CW255	260	0.0041	0.1610	0.0126	305.0449
CW260	669	0.0039	0.0906	0.0078	200.3839
CW265	360	0.0050	0.0315	0.0054	107.0130
CW270	686	0.0036	0.0496	0.0048	130.7164
CW275	130	0.0021	0.0116	0.0022	107.9396
CW280	247	0.0068	0.0829	0.0102	148.5008
LO010	228	0.0292	0.2146	0.0366	125.3994
LO020A	735	0.0240	0.3669	0.0434	181.1077
LO020B	139	0.0047	0.0609	0.0085	181.8104
LO030	929	0.0038	0.1303	0.0095	247.4669
LO031	2094	0.0027	0.0840	0.0061	226.9202
LO032	712	0.0036	0.0922	0.0092	253.6276
LO033	212	0.0073	0.2154	0.0205	279.3861
LO040	300	0.0043	0.0614	0.0081	189.4835
MR290	382	0.0030	0.0277	0.0038	124.7125
NF100	125	0.0025	0.0262	0.0054	219.7637
NF105	105	0.0046	0.0343	0.0066	145.0504
NF110	456	0.0035	0.0488	0.0049	141.2154
NF113	618	0.0017	0.0192	0.0024	144.4378
NF117	713	0.0039	0.0424	0.0061	154.9671
NF120	1165	0.0026	0.0623	0.0053	199.3955
NF125	281	0.0016	0.0421	0.0039	251.4801
NF130	232	0.0069	0.0904	0.0123	179.6129
NF135	180	0.0077	0.0800	0.0126	163.8135
NF295	166	0.0048	0.0321	0.0047	97.9267
NF300	138	0.0041	0.0620	0.0080	195.0828
NF310	934	0.0040	0.0712	0.0075	186.8014

NF320	501	0.0043	0.0476	0.0061	141.9422
NF321	537	0.0038	0.0641	0.0074	195.2154
NF325	146	0.0048	0.0599	0.0091	189.1779
NF327	491	0.0026	0.0843	0.0060	232.8571
NF330	303	0.0034	0.0456	0.0056	164.0315
NF335	432	0.0027	0.0338	0.0044	162.0486
NF340	461	0.0036	0.0882	0.0068	188.1477
NF345	766	0.0017	0.0172	0.0025	143.9209
NF350	167	0.0022	0.0351	0.0042	189.0380
NF360	1374	0.0020	0.0536	0.0041	204.9352
NF365	973	0.0013	0.0244	0.0024	181.8736
NF370	522	0.0008	0.0083	0.0010	124.7585
NF375	1137	0.0022	0.0336	0.0037	165.3829
NF390	1126	0.0008	0.0099	0.0011	131.2500
NF395	243	0.0008	0.0079	0.0012	149.9383
NF400	222	0.0013	0.0092	0.0017	135.3736
NF405	1031	0.0008	0.0190	0.0014	177.5841
NF410	1033	0.0007	0.0079	0.0011	154.4669
NF415	436	0.0004	0.0045	0.0005	146.2567
NF420	1411	0.0005	0.0132	0.0010	199.1984
NF425	661	0.0003	0.0086	0.0007	240.1961
NF430	452	0.0003	0.0048	0.0005	185.7143
NF435	358	0.0001	0.0017	0.0002	143.6508
NF440	406	0.0001	0.0009	0.0001	92.1053
SC230	262	0.0026	0.0286	0.0043	167.2875
SC231	203	0.0009	0.0075	0.0014	156.5976
SC232	201	0.0037	0.0343	0.0053	141.9839
SC234	114	0.0027	0.0198	0.0030	108.6733
SC235	131	0.0042	0.0258	0.0058	139.3627
SC236	230	0.0035	0.0323	0.0056	161.3042
SC237	286	0.0018	0.0209	0.0028	161.2094
SC238	327	0.0013	0.0144	0.0022	166.4409
SC239	126	0.0010	0.0056	0.0012	122.5074
ST025	193	0.0048	0.0366	0.0073	153.6483
ST027	290	0.0045	0.0659	0.0081	182.3596
TR050	836	0.0034	0.0487	0.0060	175.2638
TR055	1201	0.0059	0.0988	0.0098	166.3262
TR060A	881	0.0043	0.0594	0.0063	144.5314
TR060B	139	0.0053	0.0240	0.0054	100.8626
TR065	432	0.0046	0.0864	0.0077	168.0088
TR070	548	0.0031	0.0470	0.0062	199.9040

While the VRM values are lower than was expected for the heavily dissected terrain around the UNFTR, they do accord with the general finding noted earlier, that natural landscapes rarely have VRM values higher than 0.4. Probably, the low range of VRM values reflects the fact that being averages for transects across the North Fork Toutle River and its tributaries, the data do not fully capture the landforms close to the crater. The implication of this is that it will make it challenging to

examine the effect of ruggedness on the two slope calculation methods applied to those cross sections and ascertain which of the slope method better approximates field slope, because none of the transects crosses terrain that would be considered highly rugged. For this reason, while correlations between the 2-D expression of slope in the DEM, the slope calculated using the Horn and Z&T methods, and the field slope measured along the cross-section were performed, it was decided not to analyse the cross-sectional data by ruggedness class. Instead, analysis of ruggedness as it affects slope calculations using the H and Z&T methods focused on the raster sets for the selected study area as a whole and were dealt within analysis of the influence of DEM grid size.

2.4.6. **Investigation of how calculated slopes are affected by ruggedness and grid resolution (Objectives** 3 **and** 4**)**

VRM was computed across the DEMs for each grid resolution and the actual values for all cells were reclassified into classes of ruggedness (Table 2.8).

Table 2.8. Reclassification of VRM values

VRM Class	VRM range
VRM1	0-0.1
VRM2	0.1-0.2
VRM3	0.2-0.3
VRM4	0.3-0.4
VRM5	0.4-0.5
VRM6	0.5-0.6
VRM7	0.6-0.7
VRM8	0.7-0.8
VRM9	0.8-0.9
VRM10	0.9- 1.0

A variety of statistical parameters were generated for differences between slopes computed using the Horn and Z&T methods (in raw and rounded up forms), with

the results grouped according to the VRM class of the relevant cell. These statistical parameters were then tabulated and plotted in a variety of graphs to identify trends of change with VRM class and DEM grid resolution.

2.5. **Results**

2.5.1. **Comparison of slopes calculated using the Horn and Z&T methods (Objective 1)**

A. **Simple subtraction**

Subtracting the raw, unrounded slopes revealed differences between ~93% of slopes calculated using the H and Z&T methods (Figure 2.9). ~53% of Horn slopes were lower than the equivalent Z&T slope, while ~40% were steeper. These simple differences were similar at all DEM resolutions. The differences and zonal statistics of differences between raw H and Z&T slopes is also in terms of the proportion of cells where raw slopes are computed using Horn are the same, less and more than those computed using Z&T is clearly indicated in both Figure 2.9 and Table 2.9 below.

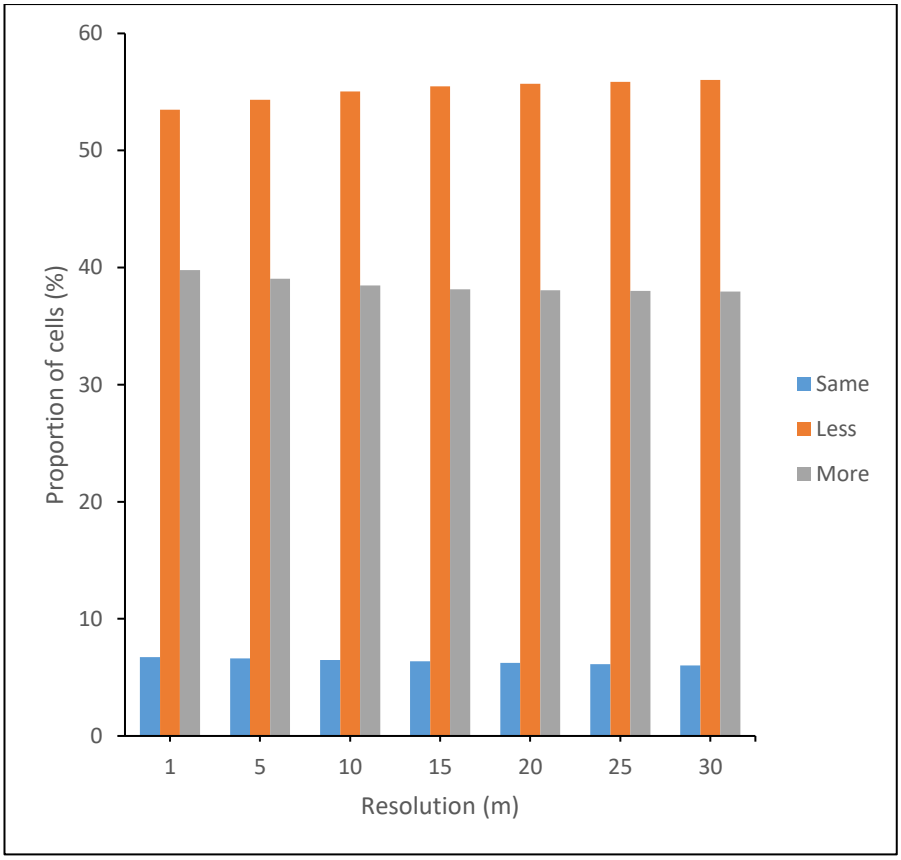

Figure 2.9: Proportion of cells where raw slopes computed using Horn are the same, less or more than those computed using Z&T.

Table 2.9. Differences and zonal statistics of differences between raw H and Z&T slopes

Change*	COUNT	Count (%)	AREA	MIN	MAX	RANGE	MEAN	STD	Resolution (M)
1	14356695	6.73	14356695	0.00	0.00	0.00	0.00	0.00	1
2	114105042	53.47	114105042	-671.33	0.00	671.33	-1.03	1.82	1
3	84923159	39.80	84923159	0.00	462.66	462.66	0.83	1.37	1
1	565275	6.62	14131875	0.00	0.00	0.00	0.00	0.00	5
2	4642908	54.34	116072700	-455.51	0.00	455.51	-2.05	3.16	5
3	3335910	39.04	83397750	0.00	154.96	154.96	1.57	2.29	5
1	138676	6.50	13867600	-24.36	0.00	24.36	0.00	0.07	10
2	1174759	55.04	117475900	-438.11	117.41	555.51	-1.04	3.60	10
3	821013	38.46	82101300	-342.48	104.09	446.57	0.19	2.76	10
1	60429	6.37	13596525	-5.60	0.00	5.60	0.00	0.03	15
2	526120	55.49	118377000	-455.51	125.30	580.81	-0.76	3.62	15
3	361572	38.14	81353700	-108.06	86.61	194.66	-0.20	2.80	15
1	33340	6.24	13336000	0.00	0.00	0.00	0.00	0.00	20
2	297418	55.70	118967200	-70.68	0.00	70.68	-2.46	3.18	20
3	203228	38.06	81291200	0.00	62.95	62.95	1.75	2.34	20
1	20940	6.13	13087500	0.00	0.00	0.00	0.00	0.00	25
2	190928	55.86	119330000	-58.30	0.00	58.30	-2.54	3.18	25
3	129901	38.01	81188125	0.00	56.85	56.85	1.81	2.31	25
1	14284	6.02	12855600	0.00	0.00	0.00	0.00	0.00	30
2	132925	56.01	119632500	-89.67	0.00	89.67	-2.60	3.22	30
3	90097	37.97	81087300	0.00	58.80	58.80	1.85	2.31	30

* 1 = no difference, 2 = Horn < Z&T, and 3 = Horn > Z& T

Maximum, variance, mean, and standard deviation of the distributions of the raw Horn and Z&T slopes are plotted against DEM resolution in Figure 2.10. However, using the raw values tends to exaggerate differences between the H and Z&T methods. When the figures in the slope rasters are rounded up (as described above), minor differences are eliminated and similarity is much higher, as expected. The proportion of cases where both methods produce the same slope rises from ~7% to ~47%. In ~32% of cases, Horn slopes are less than Z&T values, and ~21% they are steeper (Figure 2.11). For rounded up values, the percentage of cells where slope estimates are the same decreases as resolution coarsens from 1 m to 30 m.

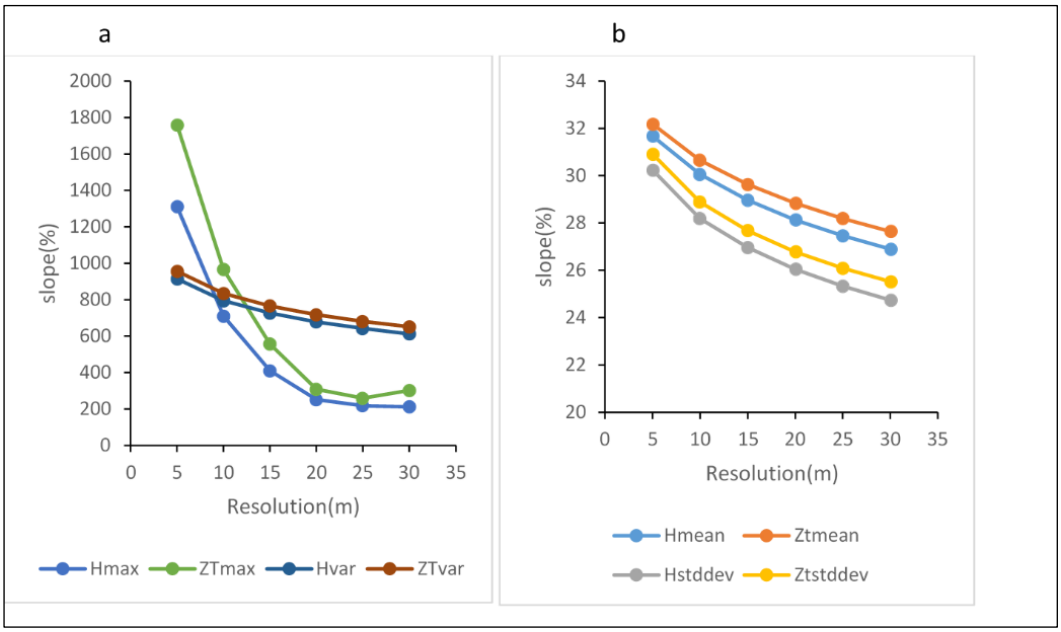

Figure 2.10: (a) maximum and variance and b) mean and standard deviation of raw Horn and Zevenbergen and Thorne slopes, as a function of DEM resolution.

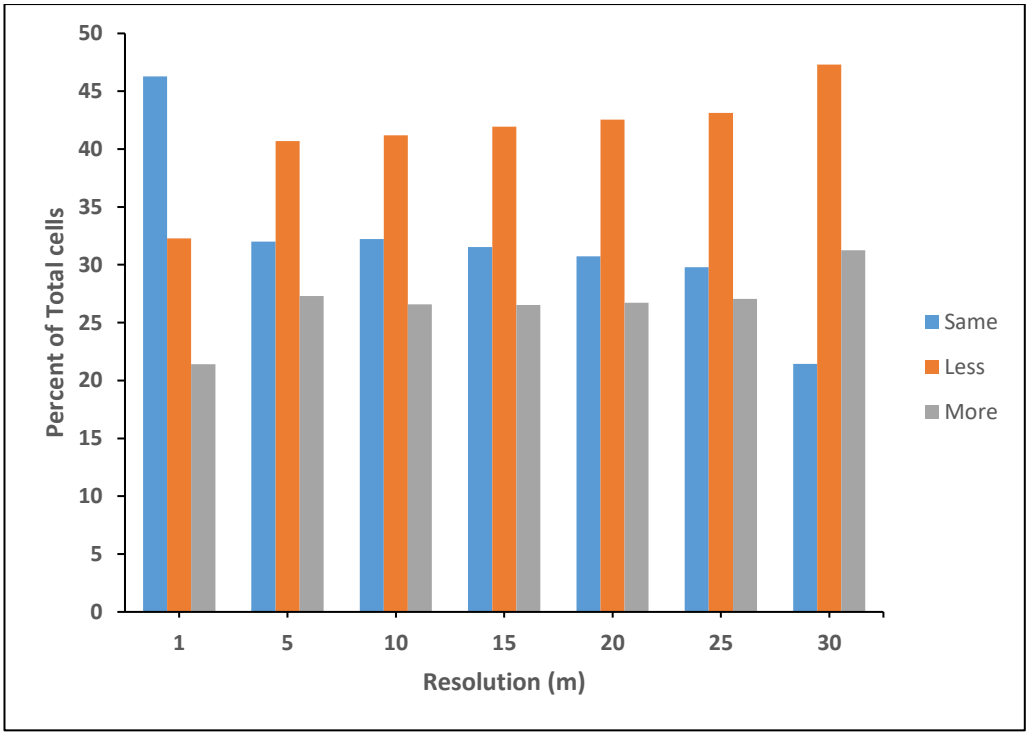

Figure 2.11: Proportions of cells where rounded up slopes computed using Horn are the same as, less than, and more than those computed using Z&T.

Simple differencing of the rounded up (integer) values, indicates that the Horn and Z&T methods produce similar slopes for about half of the cells when a high resolution (1 m) DEM is available, falling to around a third for grid sizes between 5m and 25 m. However, agreement falls to only a fifth for the low-resolution DEM (30 m). Where the methods differ, there is a systematic tendency for Horn's method to compute lower slopes than Z&T.

Table 2.10: Differences and zonal statistics of differences between rounded up Horn and Z&T slopes

VALUE	COUNT	Per cent count	AREA	MIN	MAX	RANGE	MEAN	STD	Resolution
1	98783799	46.29	98783799	0.00	0.00	0.00	0.00	0.00	1
2	68897781	32.29	68897781	-672.00	-1.00	671.00	-1.70	2.15	1
3	45703316	21.42	45703316	1.00	463.00	462.00	1.54	1.64	1
1	2734867	32.01	68371675	0.00	0.00	0.00	0.00	0.00	5
2	3476648	40.69	86916200	-455.00	-1.00	454.00	-2.73	3.41	5
3	2332578	27.30	58314450	1.00	155.00	154.00	2.24	2.50	5
1	688222	32.22	68822200	0.00	0.00	0.00	0.00	0.00	10
2	879981	41.20	87998100	-256.00	-1.00	255.00	-2.98	3.37	10
3	567789	26.58	56778900	1.00	77.00	76.00	2.35	2.51	10
1	299300	31.53	67342500	0.00	0.00	0.00	0.00	0.00	15
2	398187	41.94	89592075	-147.00	-1.00	146.00	-3.12	3.35	15
3	251890	26.53	56675250	1.00	70.00	69.00	2.43	2.48	15
1	164088	30.73	65635200	0.00	0.00	0.00	0.00	0.00	20
2	227227	42.55	90890800	-71.00	-1.00	70.00	-3.22	3.32	20
3	142671	26.72	57068400	1.00	63.00	62.00	2.49	2.49	20
1	101867	29.81	63666875	0.00	0.00	0.00	0.00	0.00	25
2	147400	43.13	92125000	-58.00	-1.00	57.00	-3.28	3.29	25
3	92502	27.07	57813750	1.00	57.00	56.00	2.54	2.43	25
1	50746	21.43	45671400	0.00	0.00	0.00	0.00	0.00	30
2	112013	47.31	100811700	-100.00	-1.00	99.00	-5.50	5.90	30
3	73986	31.25	66587400	1.00	84.00	83.00	4.19	4.47	30

B. **Correlation**

The results of correlation analyses indicate that slopes calculated using the Horn and Z&T methods are very strongly related (*r-vales* > 0.99) across all DEM resolutions (Figure 2.12) despite the differences when the slopes for individual cells are differenced, as noted above. Given the strong correlation between methods, it is clear that fundamentally they are producing very similar distributions of slope across the DEM.

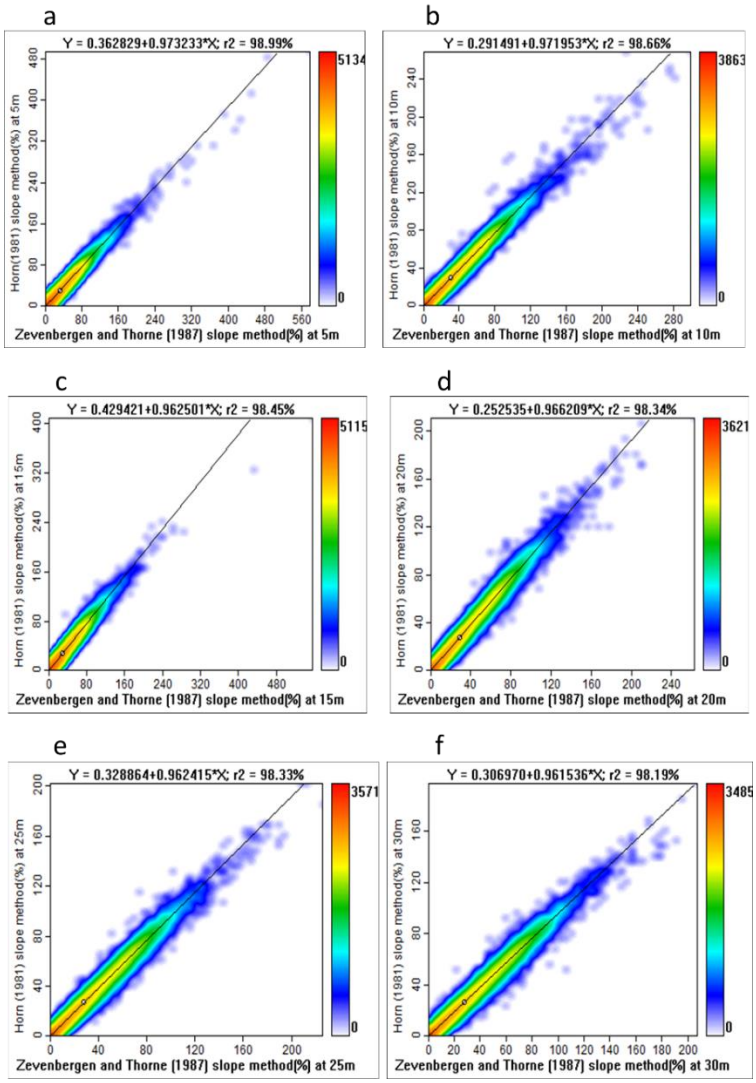

Figure 2.12: Correlation between slopes calculated using the Horn and Z&T methods at grid resolutions of (a) 5m, (b) 10m, (c) 15m, (d) 20m, (e) 25m, and (f) 30m.

C. **Paired t-test**

The t-tests for all DEM resolutions produced p-values < 0.001, as detailed in Table 2.11. These results indicate that the null hypothesis should be rejected and that there are differences in the slope calculated using differing methods. However, inspection of the mean slopes for the Horn and Z&T indicate that these are usually within a degree of each other. Hence, while differences between mean slopes calculated using the two methods are statistically different, they are also very small in absolute terms.

Table 2.11: Results of paired-sample t-tests on slopes calculated using the Horn and Z&T methods

Resolution	Horn Mean	Horn SD	Z&T Mean	Z&T SD	N	t	p-value
1	82.873	69.375	83.783	71.662	3,496,322	-237.172	<0.001
5	31.674	30.231	32.175	30.911	8,544,093	-453.294	<0.001
10	30.053	28.188	30.656	28.889	2,135,992	-266.201	<0.001
15	28.965	26.961	29.63	27.68	949,377	-191.925	<0.001
20	28.13	26.046	28.833	26.777	533,986	-149.822	<0.001
25	27.461	25.332	28.191	26.084	341,769	-123.297	<0.001
30	26.89	24.738	27.645	25.518	237,306	-104.582	<0.001

D. **Geomorphological classification of slope**

The Horn and Z&T slope values for each DEM resolution were put into geomorphological classes as listed in Table 2.12.

Histograms of the cell frequencies for the geomorphological slope classes reveals that, at all resolutions, slopes in the ‘steep’ class had the highest frequency and that the shapes of the histograms are practically identical for the Horn and Z&T methods of slope computation (Figure 2.13).

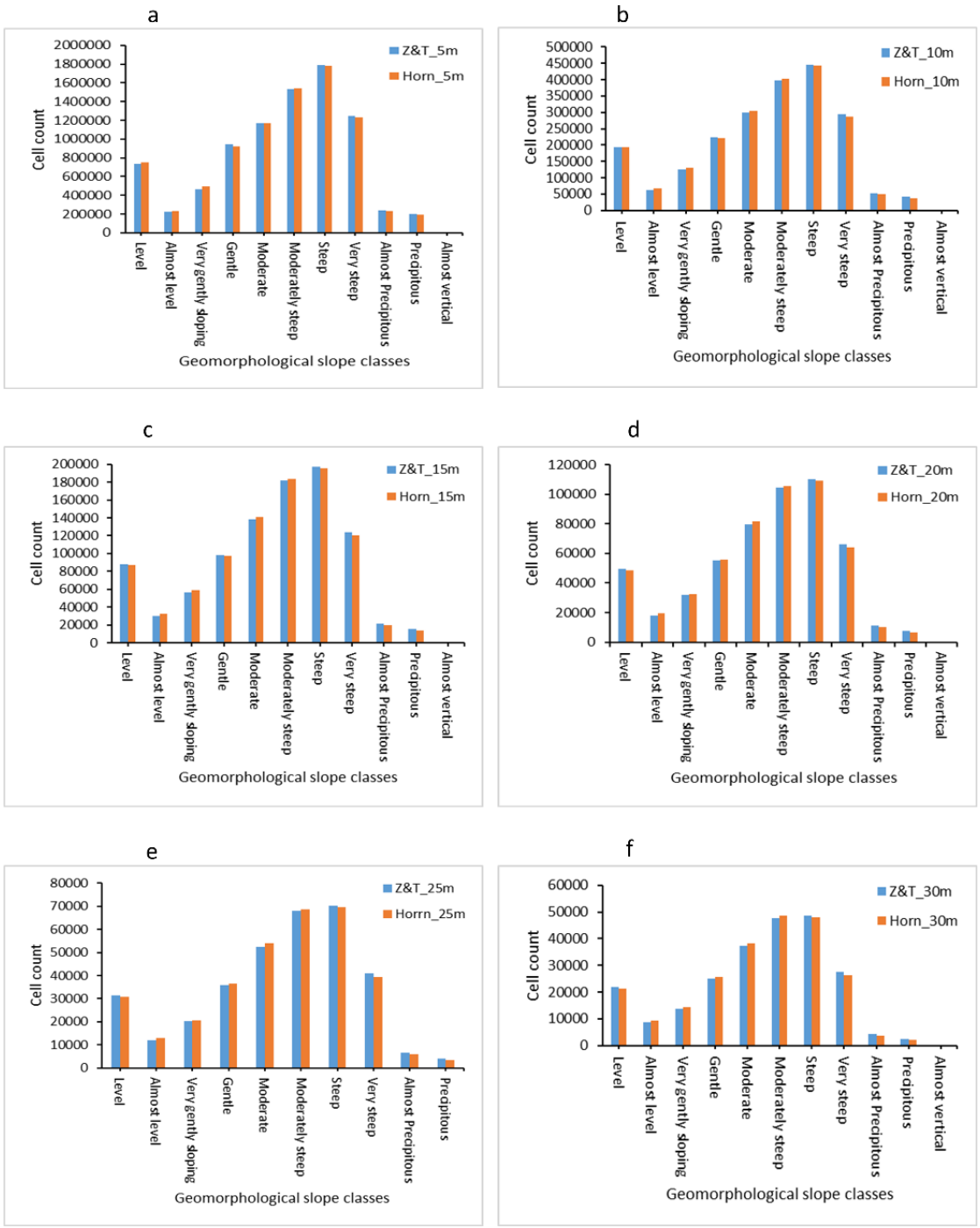

Figure 2.13: Frequencies of cell for each geomorphological slope class and DEM grid resolutions of (a) 5m, (b) 10m, (c) 15m, (d) 20m, (e) 25m and (f) 30m.

Table 2.12: Geomorphological classification of slopes at various resolutions

	Geomorphological slope class*										
Slope/Resolution	1	2	3	4	5	6	7	8	9	10	11
Horn at 1m	16321505	4206899	9801575	24779041	29457193	37067681	45463410	32816727	6808887	6389718	272260
Z&T at 1m	16049936	3864543	9576120	24946774	29675935	37098062	45599463	32860849	6893548	6532383	287283
Horn at 5m	751596	233009	493842	917881	1169915	1543307	1781365	1233605	227495	188666	3412
Z&T at 5m	735956	222907	464997	942672	1165947	1530250	1789505	1249399	236270	201609	4581
Horn at 10m	194567	67773	129566	220754	304601	402994	441854	286558	49830	37322	173
Z&T at 10m	194079	62523	124675	224763	299536	398616	444508	293303	52436	41194	359
Horn at 15m	87048	32417	58536	97575	141123	183833	195161	120104	20104	13462	14
Z&T at 15m	87743	30085	56547	97800	138293	181665	196813	123421	21607	15363	40
Horn at 20m	48646	19454	32595	55895	81859	105562	109171	64358	10090	6356	
Z&T at 20m	49459	17973	31720	55377	79916	104344	110175	66436	11119	7463	4
Horn at 25m	30943	12869	20679	36443	53842	68764	69437	39436	5927	3429	
Z&T at 25m	31571	12066	20191	35791	52363	67937	70174	40963	6601	4112	
Horn at 30m	21189	9209	14341	25618	38415	48517	47998	26227	3732	2060	
Z&T at 30m	21824	8729	13856	25016	37410	47740	48525	27409	4270	2526	1

*Level = 1, Almost level = 2, Very gently sloping = 3, Gentle = 4, Moderate = 5, Moderately steep = 6, Steep = 7, Very steep = 8, Almost Precipitous = 9, Precipitous = 10, Almost vertical = 11

Plotting pooled percentage differences between H and Z&T slopes for all DEM resolutions as a function of geomorphological slope class revealed that these differ by less than ~5% for most slope classes (Figure 2.14. Percentage differences between Z&T and Horn slopes according to geomorphological slope class). However, differences between the two slopes are more noticeable for Almost level and Very gentle sloping classes and they increase markedly for the steepest slope classes (Almost precipitous and Precipitous). The data plotted in

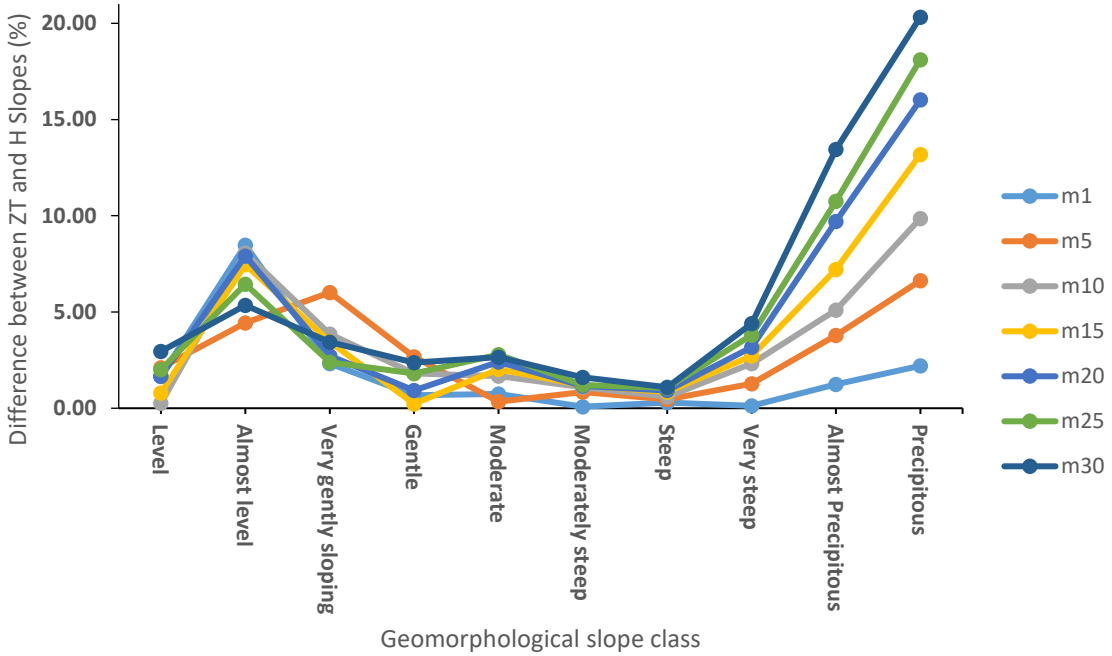

Figure 2.14. Percentage differences between Z&T and Horn slopes according to geomorphological slope class

Table 2.13. Breaking down the data by DEM resolution shows that the shapes of the histograms are similar for all grid sizes (Figure 2.15).

	Level	Almost level	Very gently sloping	Gentle	Moderate	Moderately steep	Steep	Very steep	Almost Precipitous	Precipitous	Almost vertical
H at 1m	53.80	29.09	17.96	10.03	5.51	3.32	2.14	1.57	1.75	2.38	4.18
ZT at 1m	51.18	29.22	18.78	10.52	5.67	3.37	2.17	1.58	1.77	2.40	4.32
H at 5m	49.17	33.78	24.77	17.87	11.42	7.18	4.60	3.25	3.93	5.66	8.63
ZT at 5m	51.36	32.99	24.41	18.66	11.38	7.17	4.75	3.42	4.16	5.84	9.68
H at 10m	43.47	31.91	24.26	19.57	12.62	7.94	5.15	3.65	4.59	6.47	10.07
ZT at 10m	48.09	30.17	23.73	19.72	12.25	7.99	5.41	3.93	4.92	6.73	12.72
H at 15m	40.14	29.76	24.21	21.09	13.46	8.55	5.61	4.01	4.97	6.90	13.23
ZT at 15m	46.58	28.28	23.30	20.42	13.04	8.66	5.93	4.37	5.37	7.28	14.69
H at 20m	37.39	28.58	24.42	22.11	14.08	9.02	6.03	4.34	5.36	6.98	
ZT at 20m	45.64	26.46	23.49	20.93	13.63	9.15	6.40	4.74	5.77	7.61	21.33
H at 25m	37.06	27.45	24.95	23.20	14.71	9.38	6.38	4.61	5.57	7.01	
ZT at 25m	47.16	25.98	23.71	21.45	14.06	9.56	6.81	5.04	6.16	7.82	
H at 30m	35.24	26.78	25.59	24.13	15.03	9.77	6.69	4.78	5.72	7.16	
ZT at 30m	47.48	25.38	23.47	21.92	14.43	9.99	7.12	5.34	6.32	8.06	34.86

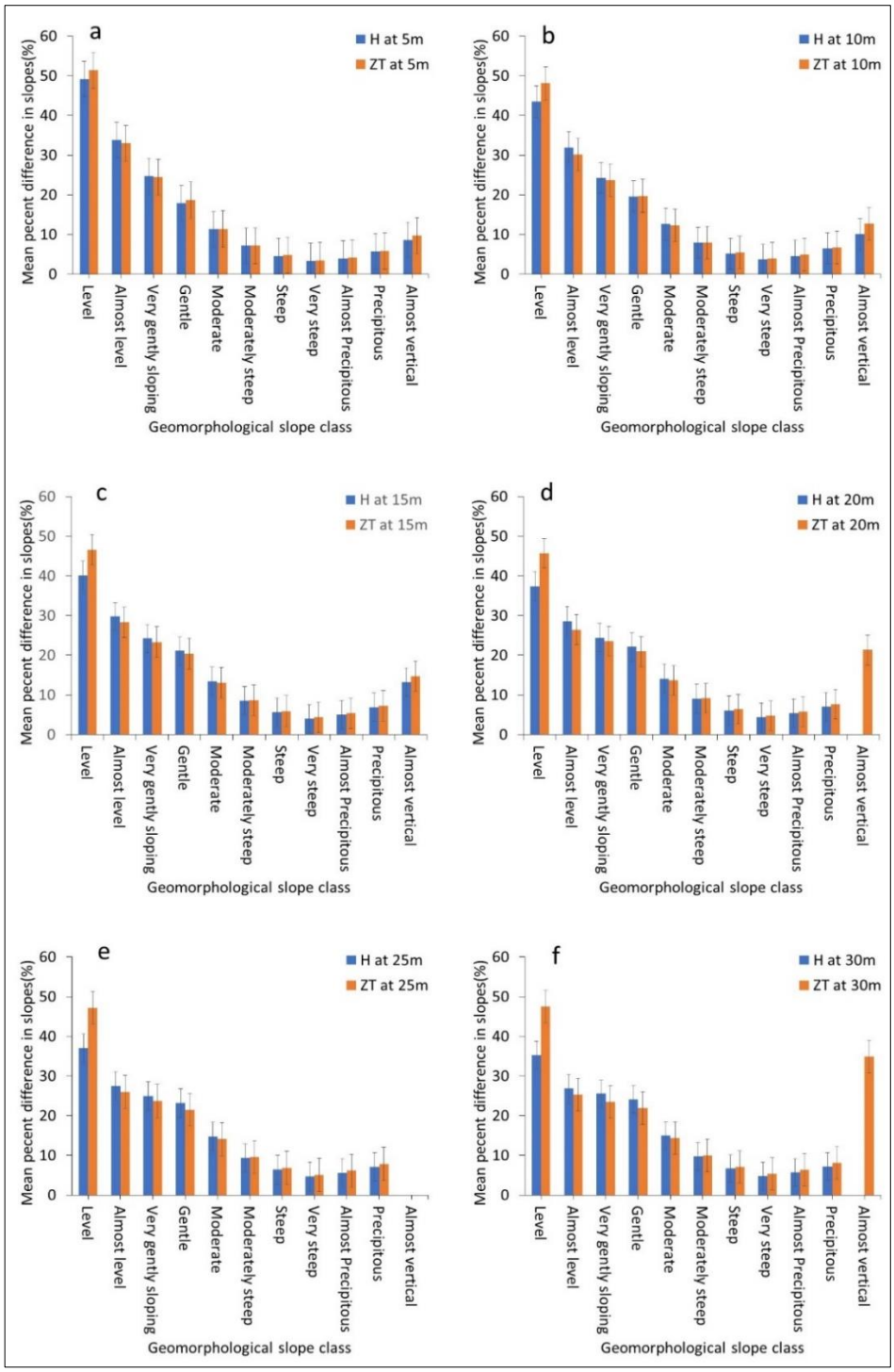

Figure 2.15: Mean percentage differences between Z&T and Horn slopes in each geomorphological slope class at DEM resolutions of: (a) 5m, (b) 10m, (c) 15m, (d) 20m, (e) 25m, and (f) 30m.

Taking these findings together, it may be concluded that selection of either the Horn or Z&T methods of computing slopes would make no material difference to

the spatial distribution or proportions of land falling into different geomorphological classes of slope.

2.5.2. **Comparison of calculated slopes with field measurements (Objective 2)**

To check the comparability of field surveyed transects with those extracted from the DEMs, data from four, selected cross-sections were compared to data extracted from the 1m resolution, LiDAR-generated DEM (Figure 2.16).

There is a strong similarity between the data, with the resultant cross-sections appearing almost identical. However, there is some variation, for example, at NF300 where a relatively consistent offset of approximately 1 m is apparent. While this would affect absolute elevations, it would not affect changes in elevation, and hence the slopes calculated, between adjacent points in the transect.

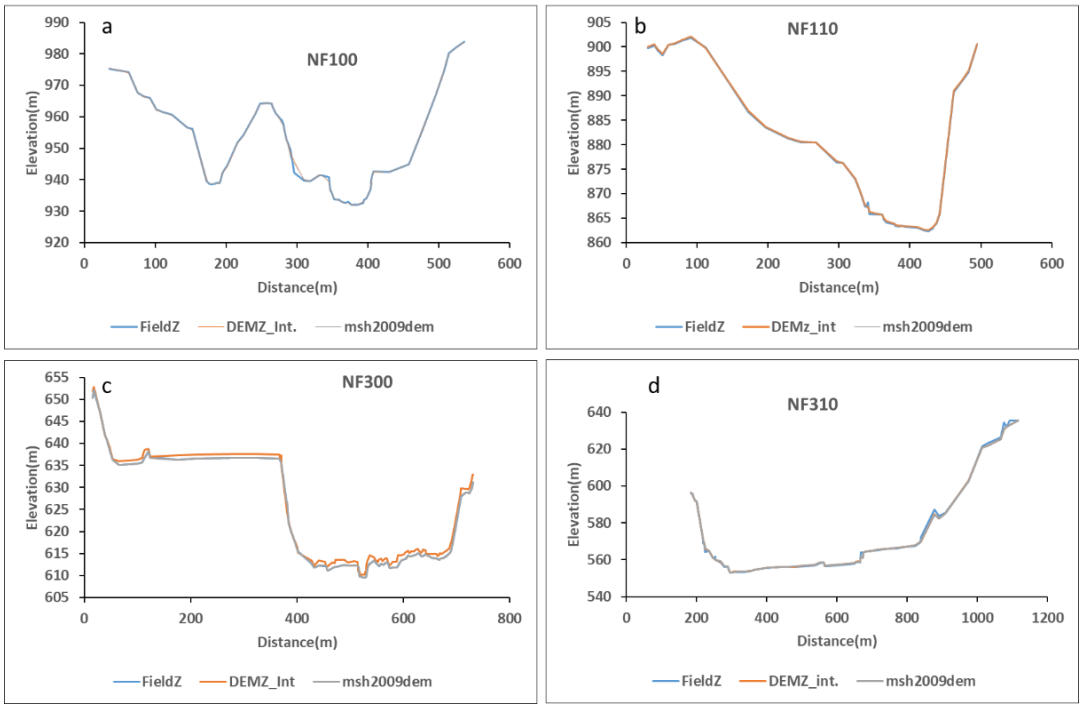

Figure 2.16. Field surveyed and DEM-based elevations along cross-sections (a) NF100, (b) NF110, (c) NF300, and (d) NF310.

Taking cross-section NF100 and the 1 m DEM as an example, the distributions of slopes along the line of the cross-section that were computed directly from the DEM (2D-slopes), calculated using the Horn and Z&T methods, and actually surveyed in the field (Field slope) are compared in Figure 2.17.

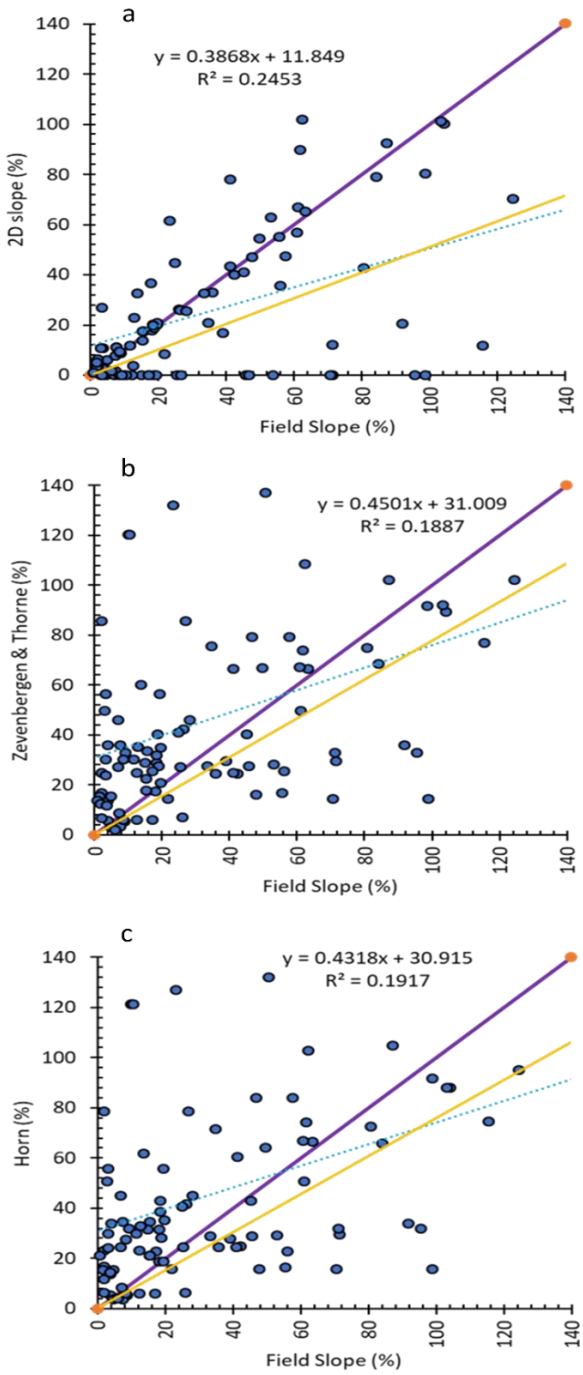

Figure 2.17. Comparisons of field and computed slopes along cross-section NF100 at 1m resolution. (a)2D Slope vs field slope, (b)Zevenbergen & Thorne vs field slope and (c) Horn vs Field slope. Purple line = 1:1 line of perfect agreement, Yellow line = the regression line passing through the origin, light blue line = the regression line pass through the y- intercept.

The first point to note is that 2-dimensional slopes measured along the cross-section calculated directly from the DEM are relatively weakly correlated with the slopes measured in the field survey (r^2 = 0.24, Figure 2.17a). This establishes that only a quarter of the variance in slopes derived directly from the DEM can be explained by variation in the slopes actually surveyed in the field. This effectively sets a low bar for what can be expected of the H and Z&T methods, which, being computed using data extracted from the DEM, would not be expected to correlate better with the field slopes than the 2D slopes derived directly from the DEM.

Bearing this in mind, for the 1m grid resolution DEM, both the Horn and Z&T methods correlated to the field slope nearly as well as the 2-D DEM-derived slope, though their r^2 values (0.193 and 0.190, respectively) are somewhat lower. Inspection of Figure 2.17b and c suggests that both Horn (1981) and Zevenbergen and Thorne (1987) tend to over-predict somewhat, when compared to the slopes surveyed in the field. Comparing goodness of fit between slopes computed using Horn and Z&T and those surveyed in the field reveals that the r^2 values are practically identical.

Similar comparisons for coarser grid resolutions produced steadily declining r^2 values for 2D, H and Z&T slopes when the results were regressed against the slopes surveyed in the field (Appendix B below).

The regression analyses performed here demonstrate the challenge posed by trying to match slopes calculated using a DEM to slopes surveyed in the field. The coefficients of determination are low for all the slopes derived from the DEM and trying to resolve the reasons for these weak correlations is beyond the scope of the research performed in these doctoral studies, which are focused developing a method to use low grid-resolution DEMs to identify gully-prone areas in developing nations.

With specific reference to whether slopes computed using the Horn method or Z&T method are closer to 'ground truth' slopes surveyed in the field, regression coefficients for H and Z&T slopes were almost identical at all grid resolutions. While

the r^2 for Z&T was slightly higher than that for Horn at some grid-scales and Horn was very slightly higher at others, no systematic pattern emerged. Consequently, despite exhaustive testing, it has not been possible to recommend one method over the other on the basis of their performance when applied to cross-sections surveyed across the UNFTR at Mount St Helens.

2.5.3. **Investigation of whether slope accuracy is related to terrain ruggedness and grid resolution (Objectives 3 and 4)**

Having established that there were differences between the Horn and Z&T slopes, the next step was to investigate whether these differences relate to ruggedness. Absolute and percentage differences between the slope values are plotted as a function of ruggedness (VRM) in Figure 2.18 and 2.19, respectively. In these graphs, most data plot very close to the origin and, as noted previously, VRM values are lower than expected, which limits the potential for establishing trends in the data.

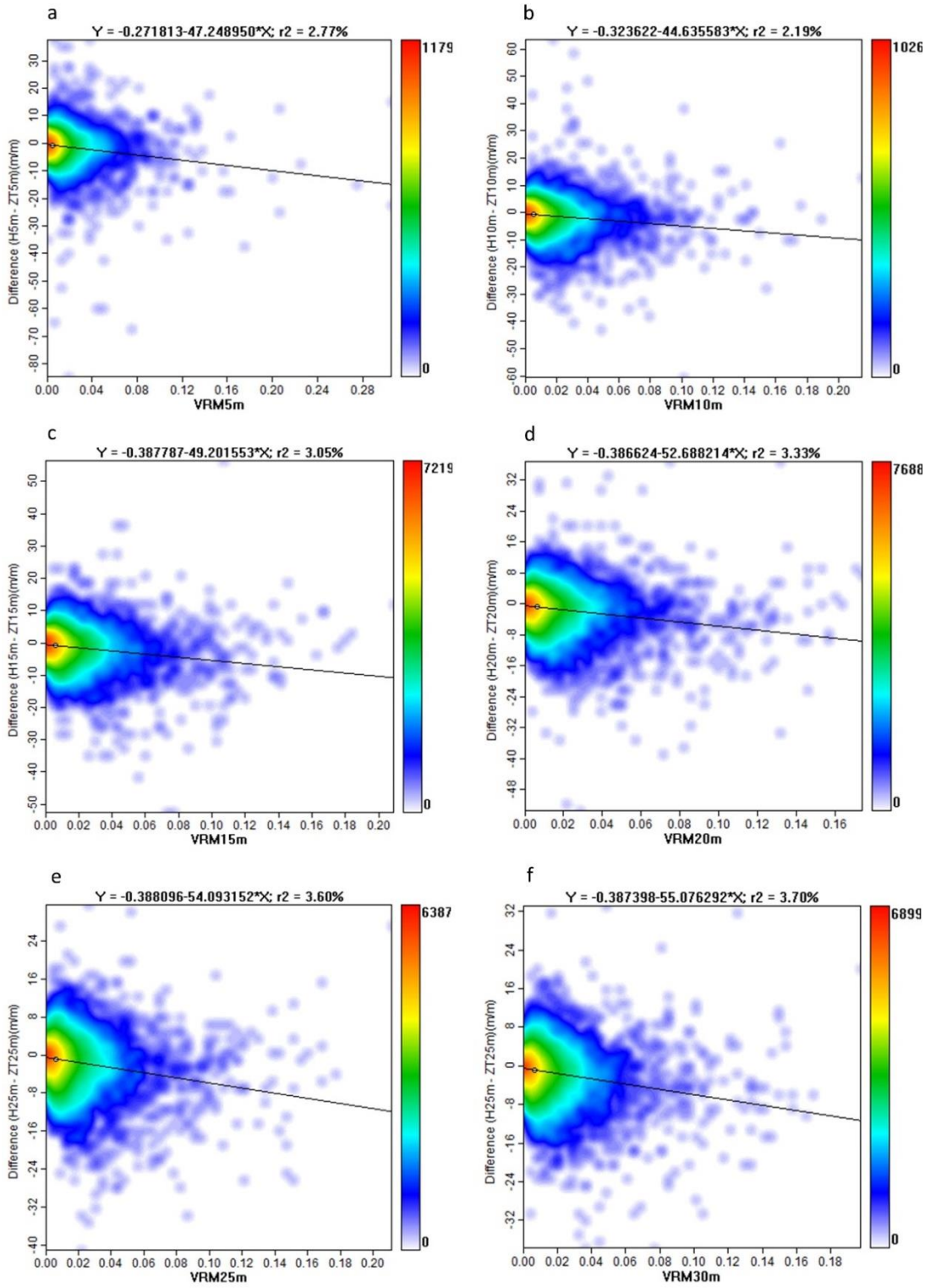

Figure 2.18. Absolute differences between slopes computed using the Horn and Z&T methods plotted as a function of VRM for DEM resolutions of (a) 5m, (b) 10m, (c) 15m, (d) 20m, (e) 25m, and (f) 30m. Note: while indicative trend lines are fitted to the data, all the r2 values are very small.

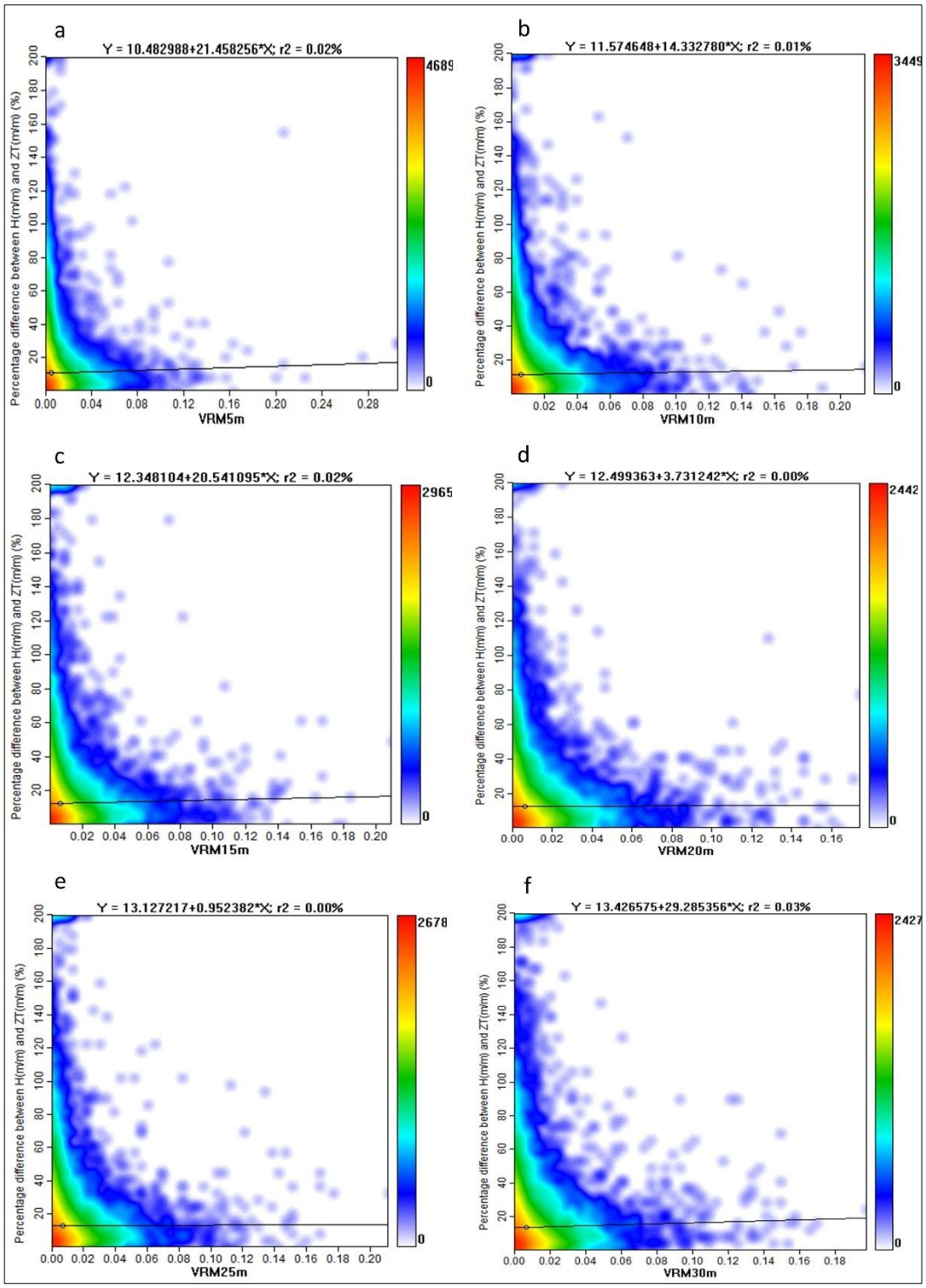

Figure 2.19. Percentage differences between raw slopes computed using the Horn and Z&T methods plotted as a function of VRM for DEM resolutions of (a) 5m, (b) 10m, (c) 15m, (d) 20m, (e) 25m, and (f) 30m.

When percentage differences between H and Z&T slopes for the 1m grid resolution DEM are grouped by VRM class and plotted as a function of the VRM class, it is clear that these differences increase with increased ruggedness (Figure 2.20a). The trend is similar at the other resolutions (Figure 2.20b,c). However, the number of VRM classes decreases from 8 to 3 as resolution coarsens, because (as expected for any topographic attribute) the spatial detail in the DEM is reduced and the way the landscape is represented becomes increasingly generalised.

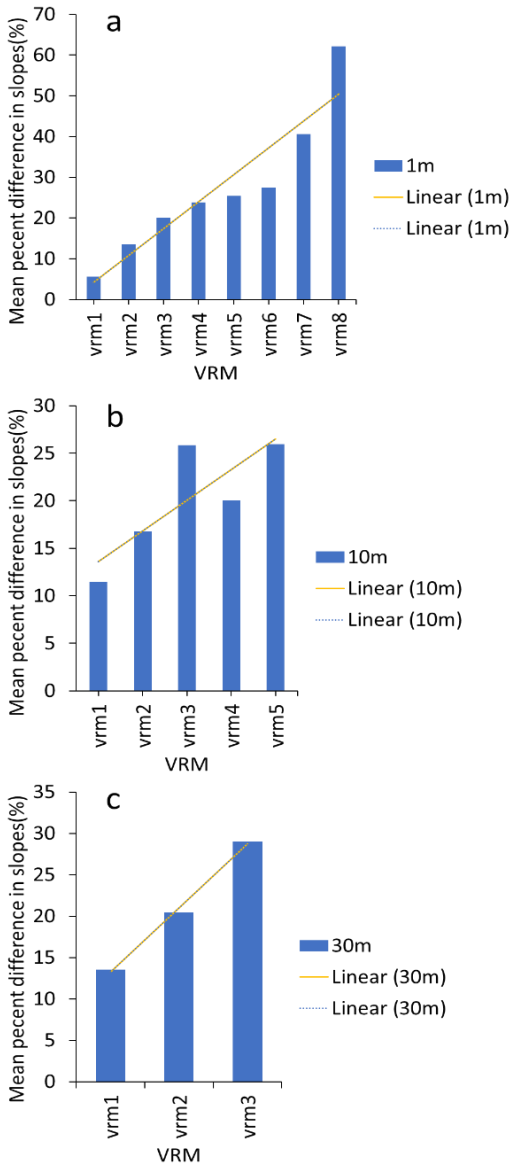

Figure 2.20. Percentage differences between slopes calculated using the H and Z&T methods grouped by VRM class for the (a) 1m ,(b) 10m, and (c) 30m grids.

The influence of ruggedness on estimates of the slope was further investigated using the full DEMs. Correlations between slopes calculated using the Horn and Z&T methods for each ruggedness category indicated that differences increased with increasing ruggedness (2.51).

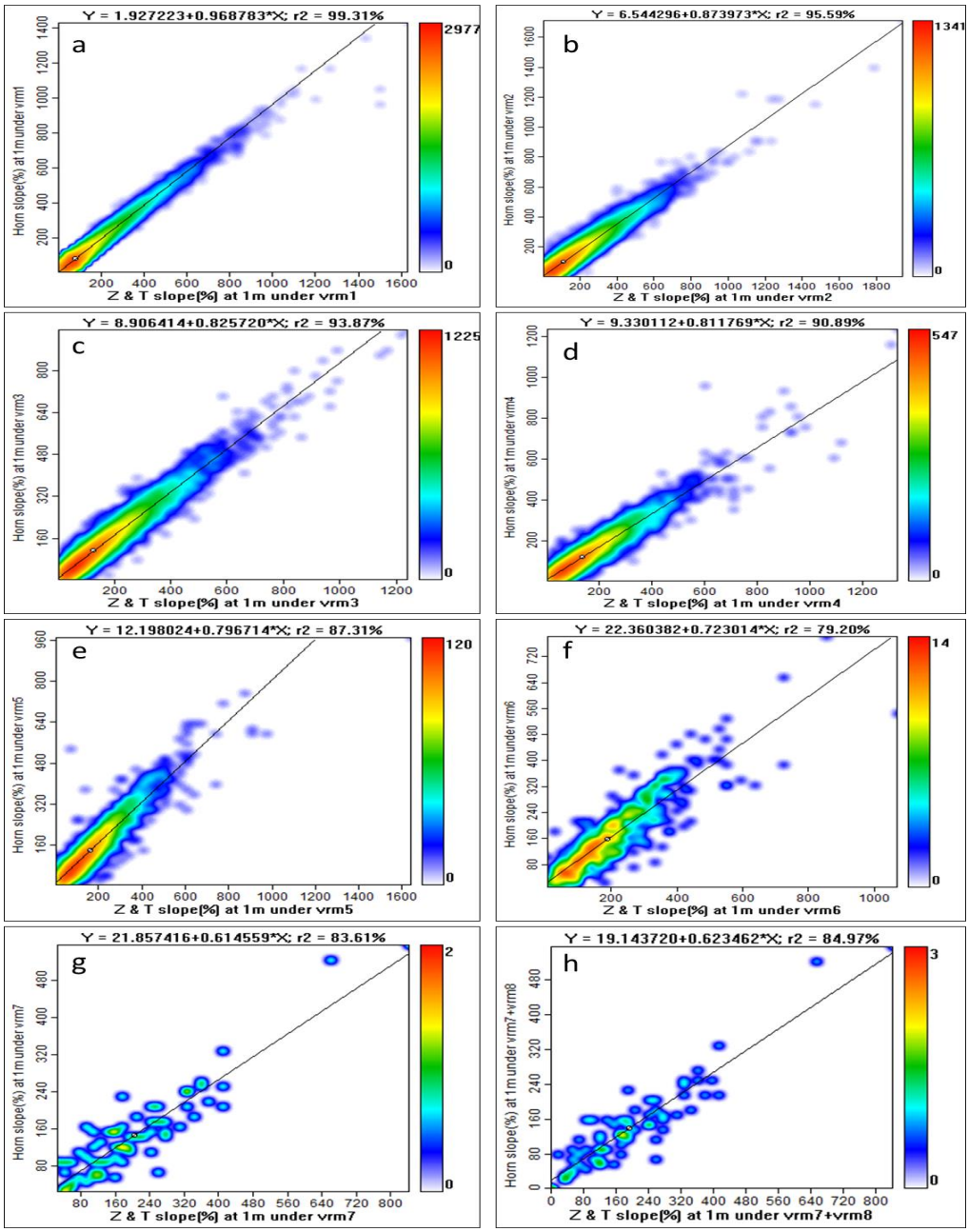

Figure 2.21.Graphs of slopes calculated using the Horn method plotted against Z&T slopes for ruggedness categories of: (a) VRM = 1, (b) VRM = 2, (c) VRM = 3, (d) VRM = 4, (e) VRM = 5, (f) VRM = 6, (g) VRM = 7, and (8) VRM = 8.

At the highest ruggedness levels, the r^2 value falls to 0.65 in comparison to 0.996 at the lowest ruggedness category, although it should be noted that the number of points also decreases with ruggedness. The gradient of the best fit line between the H and Z&T methods consistently drops from just over 1 at the lowest ruggedness to just 0.73 at the highest ruggedness. This indicates that, as ruggedness level increases, the H method consistently predicts lower slopes than Z&T.

The difference between H and Z&T methods is, therefore, most significant at the highest VRM levels due to this systematic difference between the regression line and the 1:1 line of perfect agreement. However, scatter around the best-fit line is greatest for low slopes in the rugged terrains – possibly because there are far more data points for low slopes and VRM values. The most significant divergence between the two methods occurs on relatively low slopes within rugged terrains.

The correlation data for slopes calculated by applying the H and Z&T methods to the 1m grid resolution DEM, at various classes of VRM were collected together, and plotted with VRM class on the x-axis in Figure 2.22. The strength of the correlation between the two slope measures gradually declines as ruggedness increases, with a notable drop occurring at VRM 6 (Figure 2.22).

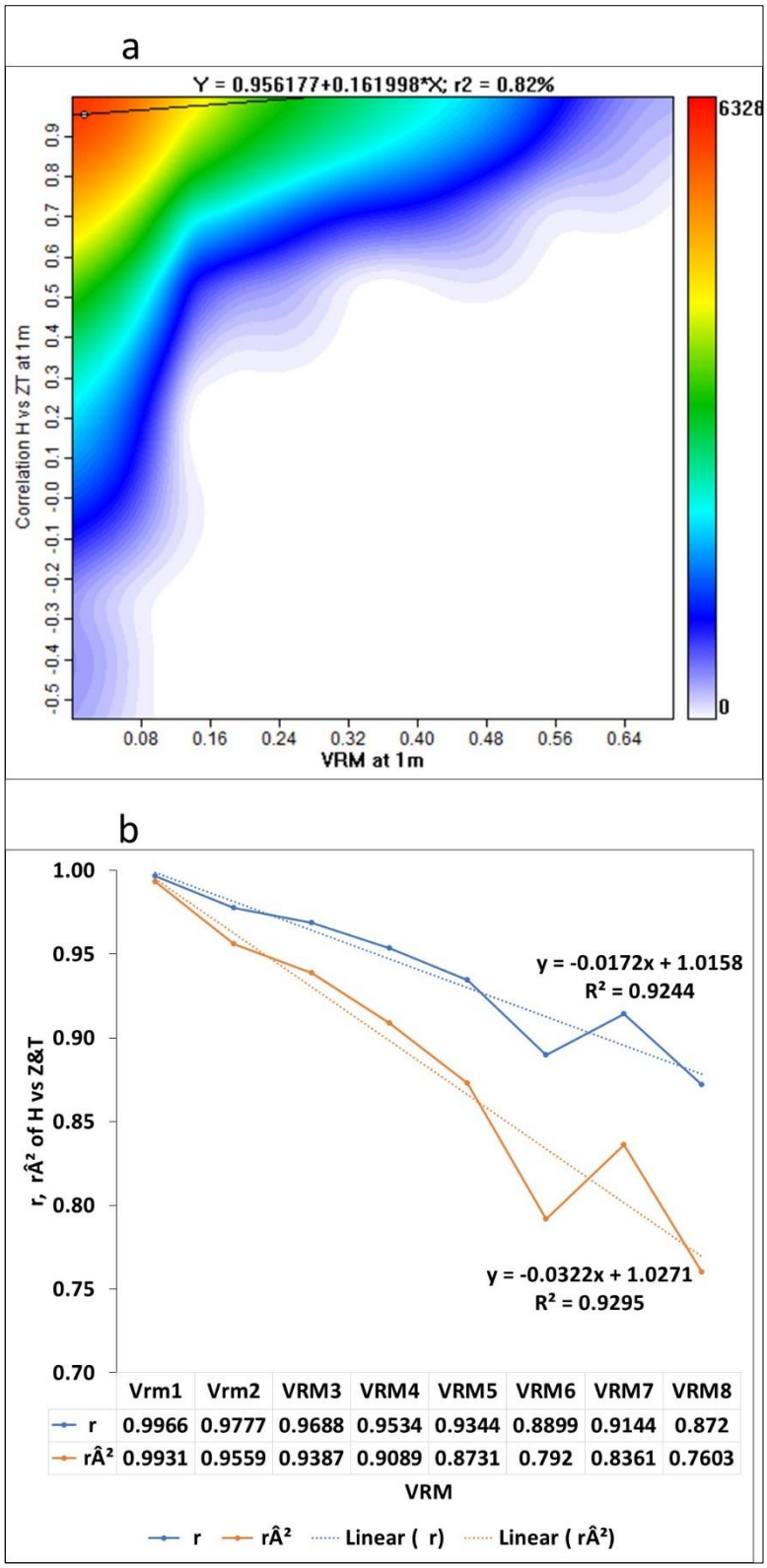

	Vrm1	Vrm2	VRM3	VRM4	VRM5	VRM6	VRM7	VRM8
r	0.9966	0.9777	0.9688	0.9534	0.9344	0.8899	0.9144	0.872
rÂ²	0.9931	0.9559	0.9387	0.9089	0.8731	0.792	0.8361	0.7603

Figure 2.22: Correlation coefficients and Coefficients of determination between Horn and Z&T slopes (a) for VRM dervied from 1m grid resolution DEM, and (b) grouped by VRM class.

Similar patterns were observed for the other DEM grid resolutions, with differences being greater in more rugged terrain and divergence between methods being greatest at the lowest slopes. The two slope calculation methods produce more similar results as spatial resolution coarsens, probably because of the reduction in overall ruggedness of the terrain (Figure 2.23). However, it must be noted that the coefficients of determination are all less than 0.05, indicating that across the range of grid resolutions, <5% of variance in Horn slope values can be explained by change in the Z&T slope.

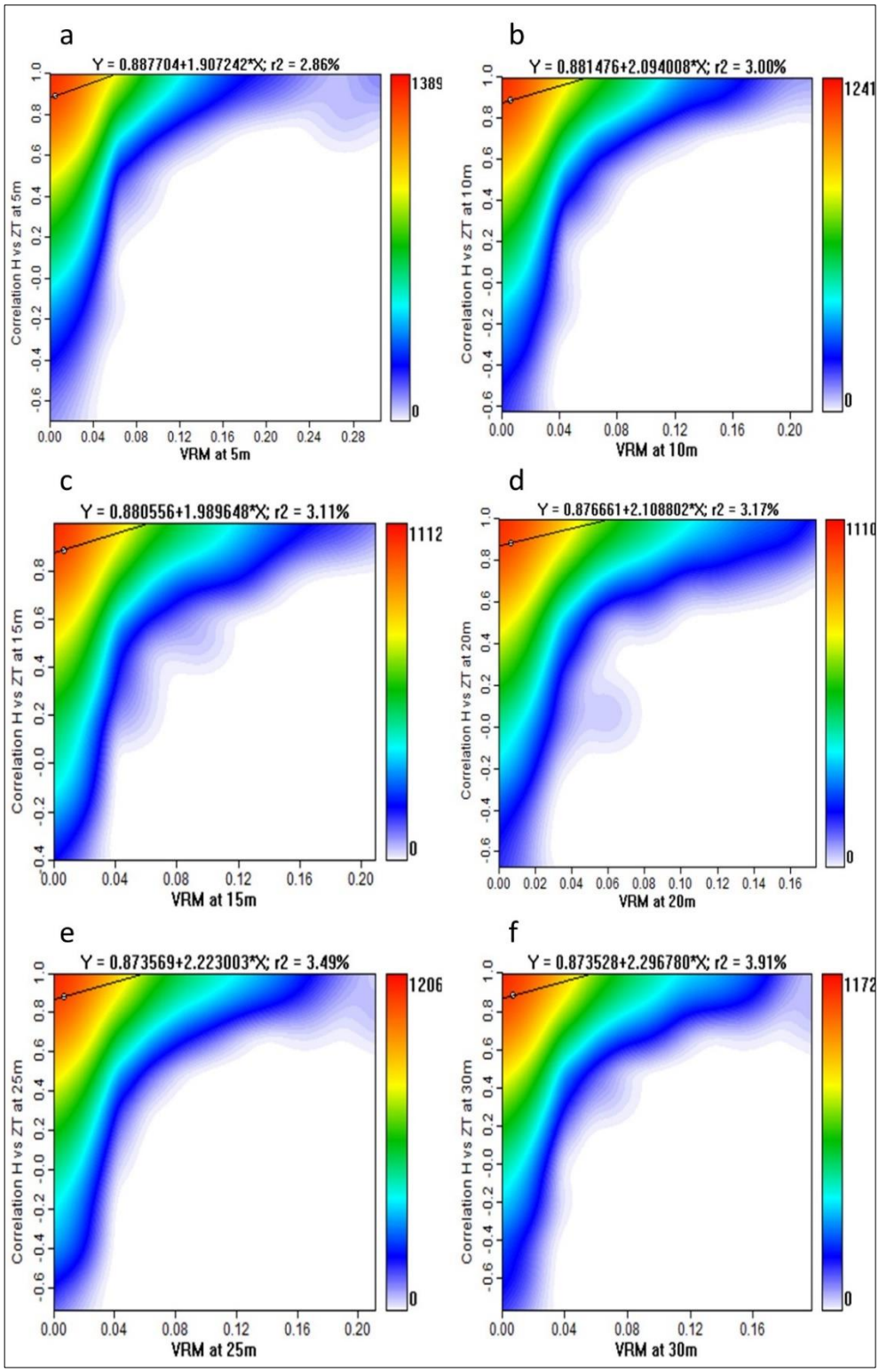

Figure 2.23**:** Plots of correlations between slopes calculated using Horn and Z&T plotted as a function of VRM at the DEM resolutions indicated on the VRM axis. Note: while indicative regression lines are fitted to the data, all the r^2 values are very small.

These results reveal that the H and Z&T only produce identical raw slopes values for areas in the lowest VRM class i.e. the smoothest terrain. The balance between cases where H produces a lower or higher raw slope than Z&T is also affected by VRM class. For the highest resolution grid (1m), the balance changes progressively from 53:40 to 100:0 between VRM classes 1 and 8. It must, however, be borne in mind that the number of cells in each class decreases as VRM increases, with only 64 cells in VRM class 7 and 3 cells in VRM class 8. Recognising this, firm conclusions should not be drawn for VRM classes with low cell counts. Table 2.14 lists summary statistics of differences in raw slopes calculated using Horn and Z&T for each VRM class.

Table 2.14. Statistics for raw differences between H and Z&T grouped by VRM class

VRM	COUNT	AREA	MIN	MAX	RANGE	MEAN	STD	Resolution
1	213239410	213239410	-526.25	269.40	795.65	-0.22	1.72	1
2	113617	113617	-368.06	224.72	592.77	-4.43	17.69	1
3	21785	21785	-312.93	252.60	565.53	-10.83	27.89	1
4	7057	7057	-501.75	357.37	859.11	-15.46	35.15	1
5	2384	2384	-671.33	462.66	1134.00	-20.15	43.48	1
6	576	576	-525.45	165.42	690.88	-30.00	58.06	1
7	64	64	-287.26	75.40	362.66	-56.77	67.65	1
8	3	3	-181.41	-56.44	124.96	-114.92	51.33	1
1	8487113	212177825	-148.99	154.96	303.95	-0.49	3.07	5
2	13824	345600	-104.52	132.60	237.12	-4.56	15.53	5
3	1058	26450	-105.61	144.53	250.14	-7.02	22.01	5
4	97	2425	-107.23	126.33	233.56	-9.98	30.87	5
5	15	375	-40.17	23.04	63.21	-5.35	17.85	5
1	2111263	211126300	-95.60	70.38	165.97	-0.60	3.20	10
2	4063	406300	-81.23	77.35	158.58	-4.30	12.50	10
3	179	17900	-80.80	52.13	132.93	-5.49	19.49	10
4	5	500	4.99	17.53	12.54	12.43	5.19	10
5	1	100	-24.32	-24.32	0.00	-24.32	0.00	10
1	933916	210131100	-91.79	64.78	156.57	-0.66	3.25	15
2	1925	433125	-70.98	61.81	132.80	-4.21	11.92	15
3	50	11250	-49.55	46.29	95.84	-5.08	19.13	15
4	4	900	-26.92	1.49	28.41	-8.72	11.32	15
1	522844	209137600	-70.68	57.99	128.67	-0.70	3.29	20
2	1108	443200	-52.41	47.64	100.04	-4.39	11.10	20
3	14	5600	-37.43	15.28	52.71	-1.78	14.43	20
1	333120	208200000	-58.30	48.21	106.50	-0.72	3.32	25
2	709	443125	-43.02	49.43	92.45	-4.60	10.53	25
3	11	6875	-25.73	26.55	52.28	-6.11	16.21	25
1	231307	144566875	-47.05	52.31	99.36	-0.74	3.36	30
2	511	319375	-37.36	32.13	69.50	-4.41	9.73	30
3	9	5625	-18.65	20.34	38.98	-1.71	13.50	30

The mean difference between the raw slopes computed by the H and Z&T methods is negative and its value decreases with ruggedness, while the standard deviation increases with ruggedness. The negative mean indicates that on average the H method computes lower slopes Z&T and the trend shows that the negative difference grows as ruggedness increases. The increasing standard deviation reveals that as ruggedness increases so does variability in the degree to which H raw slopes are lower than those computed by Z&T. On this basis, the investigations performed here provide no evidence from which to identify either the H or Z&T algorithm as being more accurate than the other.

The effect of decreasing DEM resolution on mean VRM values for the study area is depicted in Figure 2.24. There is a strong negative trend in the plot, with VRM decreasing as DEM grid size increases. This again reflects the inevitable loss of topographic fidelity that accompanies an increase in DEM grid size. Based on this finding, the conclusion must be that a fine grid size is essential to capturing the full degree of ruggedness in a study area.

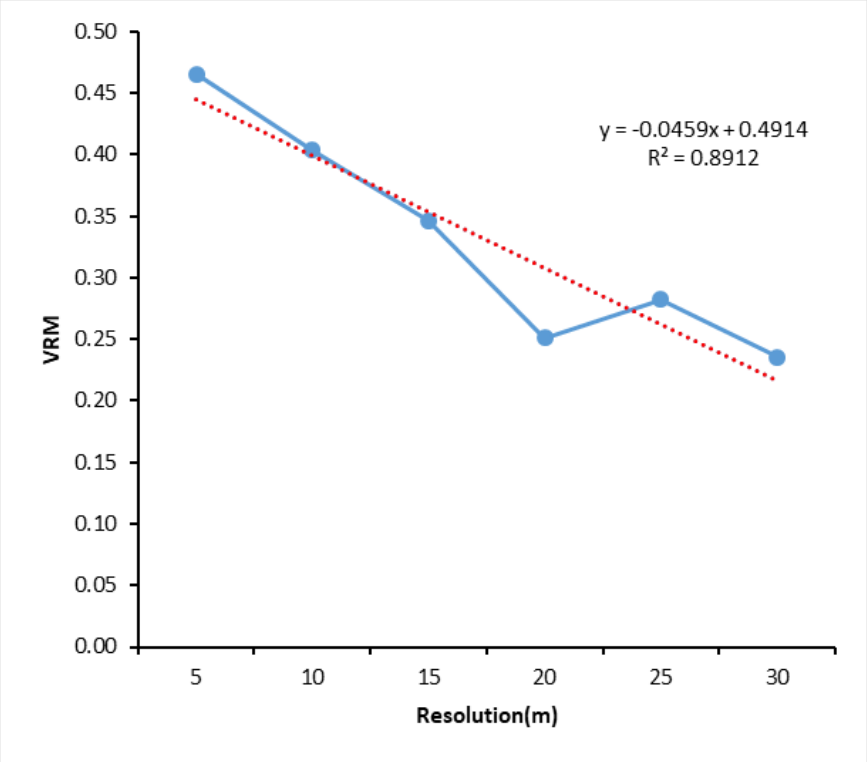

Figure 2.24: Plot of overall mean VRM values as a function of DEM grid size.

2.6. **Discussion**

Taking the results of the research reported in this chapter as a whole, they indicate that the Horn (1981) and Zevenbergen and Thorne (1987) methods yield similar slope values across DEMs with varied resolutions. However, small deviations between methods do occur at low slopes and for smooth terrain, and these differences grow as ruggedness increases and resolution coarsens, leading to statistically significant differences between methods.

Most differences between the methods had minimal impact on the spatial distributions of slopes in raster maps, but it proved challenging to identify which method was more accurate using slopes surveyed in the field (i.e. 'ground truth'). The reasons for this are not associated with the underlying elevation data because cross-sections extracted from the DEMs and field surveyed cross-sections were shown to match very well. The difficulty, therefore, is more likely to be associated with the aspect (i.e. slope direction) and the fact that slopes surveyed along a transect (i.e. USGS cross-section) all had precisely the same aspect, whereas the H and Z&T slopes represent the steepest slope in a 3-dimensional surface fitted to a 3 x 3 sub-matrix of elevations, which is not necessarily oriented along the direction of the transect. Attempts were made to account for this by only using slopes oriented with the same aspect as the transect, but even very small differences in aspect could have had led to substantial differences in the calculated slope. For this reason, an additional slope was computed from the DEM, the two dimensional slope (2D slope) actually along the transect extracted from the DEM. Surprisingly, correlations between 2D slopes and those surveyed in the field for the finest resolution DEM (1m grid size) were only a little higher than those for the H and Z&T methods and for coarser grids, the correlation for the 2D slope was actually weaker than that for the terrain analysis algorithms. For these reasons, validation of the DEM-derived slopes was inconclusive, and it was not possible to identify which slope method is the more accurate.

Based on inspection of the results, it appears that slopes computed using the Z&T method are more consistent over the range of slopes encountered in the study area

at Mount St Helens, which varied from level to almost vertical. The impression is that the Horn method tends to underestimate the maximum slope in a 3 x 3 window because it averages over the three-dimensional surface. With regard to ruggedness, the exploratory research performed here provides no basis on which to question expert recommendations in the literature that the Z&T method is more suitable in areas of smooth terrain while the Horn method is preferred for rugged terrains. What this research adds to that position is the suggestion that the VRM be adopted to quantify ruggedness and that, at least as a default value (when no better data are available and pending further study); the threshold value of VRM should be set at 0.4.

In conventional analyses, the elevations of points around abrupt edges are adjusted so that they are slightly lower or higher than the top of the bank. In that way, the occurrence of extremely high values of slope and sudden changes of aspect can be avoided. However, if the grid spacing in the DEM is greater than the width of the gully or stream, and no or only a few x, y, z points are located between the banks, this can lead to a glaring hole in the land surface. In that circumstance the algorithm for the drainage area and drainage distance fails and terrain analysis can no longer be used to identify areas at risk of concentrated flow erosion (Zevenbergen and Thorne, 1987).

Further, previous research has established that other topographic attributes, including profile and plan curvatures, are also sensitive to terrain ruggedness and that there is an optimum grid mesh from which those are more accurately predicted or estimated from a DEM (Gerrard and Robinson, 1971; Goodchild, 1980; Goodchild and Mark, 1987; Zevenbergen and Thorne, 1987; Zevenbergen, 1989; Hengl and Reuter, 2009). This is highly relevant to identification of areas prone to concentrated overland flow and gullying because the sense and degree of planform convergence was found by Zevenbergen (1989) to be an important component of the CTI used to predict gully location.

The choice of an appropriate spatial resolution or optimum grid mesh is, therefore, an important consideration in terrain analysis using DEMs (Zevenbergen, 1989). This is because, a too coarse resolution will miss important topographic features, while too fine resolution will increase data with serious implications for the computational power needed to processes large, high resolution DEMs (Gerrard and Robinson, 1971), and the risk of producing unrealistic wide variations in local slopes and aspects. Also, too fine a grid spacing may result in a level of precision that limits the analysis to locating only small, localised features of the land surface. In the context of identifying areas that already have deep gullies, particular care must be taken to select the appropriate resolution for the DEM.

Although the mathematical complexity of deriving the optimum grid mesh from which to compute slope and its derivatives (i.e. profile and planform curvatures) can be computed from a DEM - as proposed by Zevenbergen (1989) - is yet to be fully addressed, the practical problem of selecting a grid size is encountered by every terrain analyst, every time. In this context the results of investigations reported here may be of some assistance. Specifically, outcomes for a 1m grid were consistently different to those for coarser grids, suggesting that such a grid size is picking up local features and is probably sub-optimal for landform/landscape scale terrain analysis. In any case, it proved impossible to analyse the entire experimental DEM simply due to the large size of the 1m DEM. Outcomes for grid sizes between 5m and 25m were much more consistent, indicating that in this range, computed slopes and slope distributions do not change radically as a function of grid size and so the choice of DEM resolution may not be critical. In many of the Figures and Tables, a drop in the strength of correlations between slopes and other attributes (such as VRM) for the 30m grid size may indicate a significant loss of fidelity in the way terrain, in general, and slopes, in particular, are represented. This suggests that a 30m grid size is probably too coarse.

As ruggedness increased, divergence between slopes computed using Horn and Z&T also increased. For low ruggedness classes, differences between the methods were minimal and, when predicting gullying in smooth landscapes, the choice of slope

algorithm is not as important. However, where the VRM exceeded 0.4, correlation coefficients between the two slopes declined substantially and the 1:1 relationship broke down, with the Z&T method consistently over-predicting relative to H. In the context of identifying gully prone areas, discrepancies between the slopes computed using the two methods become problematic because such large differences in slope are likely to affect the potential for concentrated overland flow and/or the probability that a gully may form. This suggests that in very rugged terrain (VRM >0.4), an informed choice must be made regarding which slope computation method to apply.

As DEM spatial resolution coarsens (i.e. the grid cell size gets larger), ruggedness decreases because small topographic features and sharp edges are lost from the DEM. At 1 m resolution, the Mount St Helen's DEM featured cells in all 8 classes of VRM, including the most rugged. However, at the lower resolutions of practical interest for terrain analysis of large DEMs, no cells had a VRM of 0.4 or greater. Given that Mount St Helens represents one of the most rugged landscapes on Earth, it is unlikely that VRM will exceed 0.4 except in high resolution DEMs for the most rugged of landscapes. Therefore, for a globally applicable gully susceptibility model like that being developed here, it is less important to differentiate between the slope methods, and terrain attributes are likely to be similar regardless of whether the Horn or Z&T method is used.

Though there is consensus in the literature on the assertion that the Zevenbergen and Thorne (1987) method performs better in smooth landscapes with low ruggedness, this research could not validate empirically the accuracy between the two method with respect to ruggedness. Therefore, the outcomes of the exploratory research reported in this chapter, did not lead to implementation of the T-STAM. The Zevenbergen and Thorne (1987) method is retained in the use of CTI. Even if T-STAM were to be implemented in the case of this research, The Zevenbergen and Thorne (1987) would still be more important since ruggedness will be low (VRM <0.4) in DEMs with relatively coarse grid sizes that are globally-available, in the remainder of the research analyses.

CHAPTER 3: PREDICTING CONCENTRATED OVERLAND FLOW AND GULLYING

3.1. Introduction

Remotely sensed data with a resolution that surpasses that available from traditional topographic maps is now readily available, primarily due to advances in geospatial technology and increased computing power. However, access to such high-resolution data is limited in many less economically developed countries (LEDCs) due to lack of in-country capacity to remotely sense the land surface using LiDAR, lack of computer processing power needed to handle very large data arrays, and the high acquisition cost of obtaining high-resolution datasets from out-of-country providers. In such areas it is likely that the topographic data available is of relatively coarse spatial resolution, having been obtained from earth-orbiting satellites. While these sparse data regions may have only relatively limited spatial information available to them they face multiple, severe environmental challenges, including problems arising from inappropriate land-use or poor soil conservation. At least potentially, relatively coarse resolution data can still be useful in guiding scientists and planners towards finding solutions to these problems. It is therefore important to establish the extent to which it is possible to detect, predict and solve environmental and land-use related problems using coarse resolution, remotely-sensed data.

Concentrated overland flow erosion, leading to gullying, is a primary environmental threat in many countries, but prediction of this hazard typically requires high-resolution data. This is because many predictive methods function at the scale of the individual field and attempt to predict the exact paths of concentrated flow and associated gully formation. However, as explained in the preceding chapters of this thesis, the aim of the research reported here is not to attempt to predict the exact location of gullies, but instead to identify areas within whole catchments that are more susceptible to gullying because of topographic concentration of overland flow. It is hypothesised here that the requirement for high-resolution data will be

reduced when predicting susceptibility to gullying rather than specific gully locations.

The particular issue at hand is that, to be applicable in data sparse regions, a gully susceptibility model for concentrated flow erosion will have to produce reliable predictions using DEMs of 30 m resolution or coarser. Many gullying models are known to work well when applied using high-resolution DEMs (Santisteban *et al.*, 2005; Valentin *et al.*, 2005; Casalí *et al.*, 2006; Parker *et al.*, 2007; Marzolff and Poesen, 2009; Taguas *et al.*, 2010; Hofle *et al.*, 2013; Momm *et al.*, 2013; d'Oleire-Oltmanns *et al.*, 2014; Korzeniowska *et al.*, 2018) but these models have not been fully tested for low resolution DEMs.

3.2. **Literature review**

3.2.1. **Influence of data resolution on terrain analyses for gully prediction**

As outlined in Chapter 1.4, there is extensive literature on gullying and its prediction using numerical methods. Most rely on high resolution data and require data inputs that are highly site specific, requiring local knowledge and field measurements. For the purpose of this study, these models are over-parameterized and such locally-sourced information is not available. In addition, variability and error is incorporated within each additional parameter, which will cumulatively affect prediction accuracy, especially where field measurements are impractical and observations are either extrapolated over large spatial areas, or not well constrained. As detailed in Chapter 2, considerations such as the specific algorithm used to calculate topographic indices, including slope, can also be highly significant to output accuracy and cause substantial deviations in results between methods.

There is a broad assumption that higher resolution data lead to more accurate topographic analysis but, the optimum mesh size when performing landscape analysis is not necessarily the highest possible resolution, leading to a debate about optimum grid sizes in spatial analysis (Gerrard and Robinson, 1971; Zevenbergen and Thorne, 1987; Zevenbergen, 1989). According to Gerrard and Robinson (1971),

the effects of different recording intervals are evident in the field measurement of slopes. An optimum recording interval is dependent on aims and requires a scale coarse enough that inaccuracy and variability introduced by surface micro-relief is minimal but, high enough that features of interest are suitably documented (Gerrard and Robinson 1971).

Unlike surveying and other field-based measurement options, remotely-sensed elevation data from which a rasterised slope is estimated, is obtained at a specific resolution and cannot be dramatically improved-upon after collection (Wong *et al.*, 2014; Grohmann, 2015; Yan *et al.*, 2015; Florinsky and Pankratov, 2016). Therefore, understanding the error and variability introduced by using spatial data of specific resolution is significant. Some researchers have attempted to improve DEM resolution through interpolation and extrapolation, and this can work well in some circumstances (Dillard *et al.*, 1992; Mitášová and Hofierka, 1993; Wood and Fisher, 1993; Robinson, 1994; Wood, 1994; Desmet, 1997; Wise, 1998; Aguilar *et al.*, 2006; Hofierka and Cebecauer, 2007; Arun, 2013; Godone and Garnero, 2013; Wong *et al.*, 2014; Florinsky and Pankratov, 2015, 2016). However, the interpolation remains an approximation and will itself introduce error, and is dependent on the nature of the underlying DEM.

There is also a balance between data resolution and processing time, with very high data resolution unlikely to yield substantial improvements in efficiency but substantially increasing both processing time and effort (Zevenbergen and Thorne, 1987; Zevenbergen, 1989; Florinsky, 1998b, a; Florinsky and Pankratov, 2015, 2016). This is particularly important if prediction is going to take place over large spatial areas. For example, high-resolution data may be necessary and feasible at the field-scale, but different requirements will be optimal at a catchment or national scale, both in terms of accuracy and logistics.

Very high-resolution data can also have other significant implications. Evans (Evans, 1979; Evans, 1998) noted that slope statistics derived from different data resolutions vary considerably but, many still believe that one grid mesh is more

suitable than the others, since errors related to slope and curvature do vary with the DEM grid size (Zevenbergen and Thorne, 1987; Zevenbergen, 1989). A mathematical determination of an optimum grid mesh for topographic analysis was proposed by Zevenbergen (1989) to that effect, but the type of depth of technical and analytical steps involved fall outside the scope of this thesis, which concerns gully prediction in data-sparse areas.

3.2.2. **Threshold CTI values for gully initiation**

The CTI is one of the widely used topographic attributes in modelling concentrated overland flow erosion, at least partially because it is intuitive to use and one of the least data-intensive methods (Thorne *et al.*, 1984b; Thorne, 1984a; Thorne *et al.*, 1984c; Thorne and Zevenbergen, 1984). Parker *et al.* (2007) showed that the CTI is able to predict the location of ephemeral gullies when applied using high-resolution topographic data obtained using LiDAR, AutoTopo and traditional surveys. On the other hand, they found that CTI did not perform well when applied using USGS 10 m and 30 m resolution DEMs.

Thorne and Zevenbergen (1990) suggested that there is a threshold value of CTI which must be exceeded in order for concentrated overland flow to have sufficient stream power per unit width to initiate gully incision. Parker *et al.* (2007) experimented with three methods of finding the threshold CTI value at selected sites in the USA:

1. Calculate CTI values for grid cells at the start and end points of each gully in a field and then average these values for that field. This is a GIS-based adaptation of the field technique suggested initially by Thorne and Zevenbergen (1990).
2. Calculate CTI values for every pixel in a grid that coincides with the known location of a gully. Then rank these values in order from lowest to highest to find the base value that results in formation of a gully.

3. Set a threshold CTI for gully formation and adjust it until a value is found which best distinguishes between a gully being present or not. This value is adopted as the critical CTI.

Parker *et al.* (2007) found the first and second methods to be impractical for the following reasons:

- in the first method, it was impracticable to obtain typical values for the start and end points of each of the gullies in the field;
- in the second method, the distribution of CTI values was so extensive that no precise breakpoint could be defined upon plotting CTI values of the known gully course.

The third method involved repetitive adjustment of the CTI's symbology until the one that best represented the locations of known gullies was found, and that became the CTI threshold value for locating other gullies at that field site. Threshold CTIs for Parker et al.'s (2007) 10 study sites determined using the iterative technique display a wide range of threshold values, varying from 5 to 62 (Table 3.1). Variations in threshold CTI values would be expected as the site characteristics differ. However, there was no apparent trend between threshold CTI values and crop/soil characteristics for the study sites.

Table 3.1: Critical CTI values and available information on crop and soil type for sites in the Parker *et al.* (2007) study. After Parker *et al.* (2007).

Site	Land Use	Soil Type	Critical CTI
1. Melton Farm		Alligator - Sharkey - Dundee	36
2. Ellis Site A	Broadcast Soybeans	Loring	62
3. Ellis Site B	Corn	Loring	32
4. Flannigan	Milo	Loring	35
5. Henson	Corn	Loring	12
6. New Hampshire Site	-	-	9
7. Herbert Downey A	Soybeans	Memphis	8
8. Herbert Downey B	Soybeans	Memphis	7
9. Bobbie Mellon	Corn	Loring	5
10. James Goodlow	Soybeans	Providence	30

It is important to recall that CTI is a numerical representation of the intensity of concentrated flow at each point in the landscape. In principle, any positive CTI indicates a degree of land surface convergence that generates concentrated flow and hence the *potential* for concentrated flow erosion. As such, the threshold CTI was solely intended to identify whether that concentrated flow was sufficiently intense to initiate a gully and its value was calibrated based on locations along a concentrated flow path where a gully was actually observed. This is important because, in this research, the aim is to predict susceptibility to gullying, rather than whether a gully has actually been initiated (and observed) at any specific location, either in the landscape, or along a known concentrated flow path. The intention is to map susceptibility to gullies rather than trying to predict the existence and precise locations gullies. Consequently, the approach adopted in interpreting CTI values and thresholds will vary from that used by Parker *et al.* (2007). Particularly, it is the degree of susceptibility of the land surface to concentrated flow erosion that is of most interest, with the likelihood of gullies being observed being addressed using other environmental parameters (i.e. land-use, soil structural strength).

3.2.3. **Specific and relative values of threshold CTIs in the USA**

Application of the CTI to predict the specific locations of gullies using very high resolution DEMs can produce very good agreement with the digitised courses of gullies observed in the field (Parker *et al.*, 2007; Daggupati *et al.*, 2013; Daggupati *et al.*, 2014; Sekaluvu *et al.*, 2015; Sheshukov, 2015; Sheshukov *et al.*, 2018). For instance, at Melton farm calculation of CTI using a LiDAR-derived DEM with a 1m grid-size and 1m resolution AutoTopo elevation data, reliably predicted the formation of ephemeral gullies at observed locations (Parker *et al.*, 2007). The threshold or critical CTI for gully initiation at Melton farm was 36. This implies that a value of CTI ≥ 36 was necessary for gullies to begin to form at this site, as validated by observed and digitized field gullies.

At Ellis farm site 2A, Parker *et al.* (2007) calculated CTI values from a field survey-based DEM with 6.1m grid size. They also produced CTIs using a USGS-sourced, 10m DEM. Subsequently, the USGS-sourced 10m DEM was resampled to 6.1m, and CTIs were produced from it for comparison with the CTIs produced from a field survey-based DEM of 6.1m. Finally, the field survey-based, 6.1m DEM was resampled to 10m, and the CTIs produced from it were compared with those produced from the USGS-sourced 10m DEM.

The results indicated that CTIs produced from the 6.1m DEM derived from the field survey, and its 10m resampled copy were successful in predicting the locations of observed ephemeral gullies (Figure 3.1 a and c), with the critical CTI being 62. This value was very close to that reported earlier by Zevenbergen (1989). In contrast, CTIs produced from 10m DEM derived from the USGS data failed to reliably predict the locations of known ephemeral gullies, although the version resampled to 6.1m did somewhat better than the original 10m version (Figure 3.1 b and d).

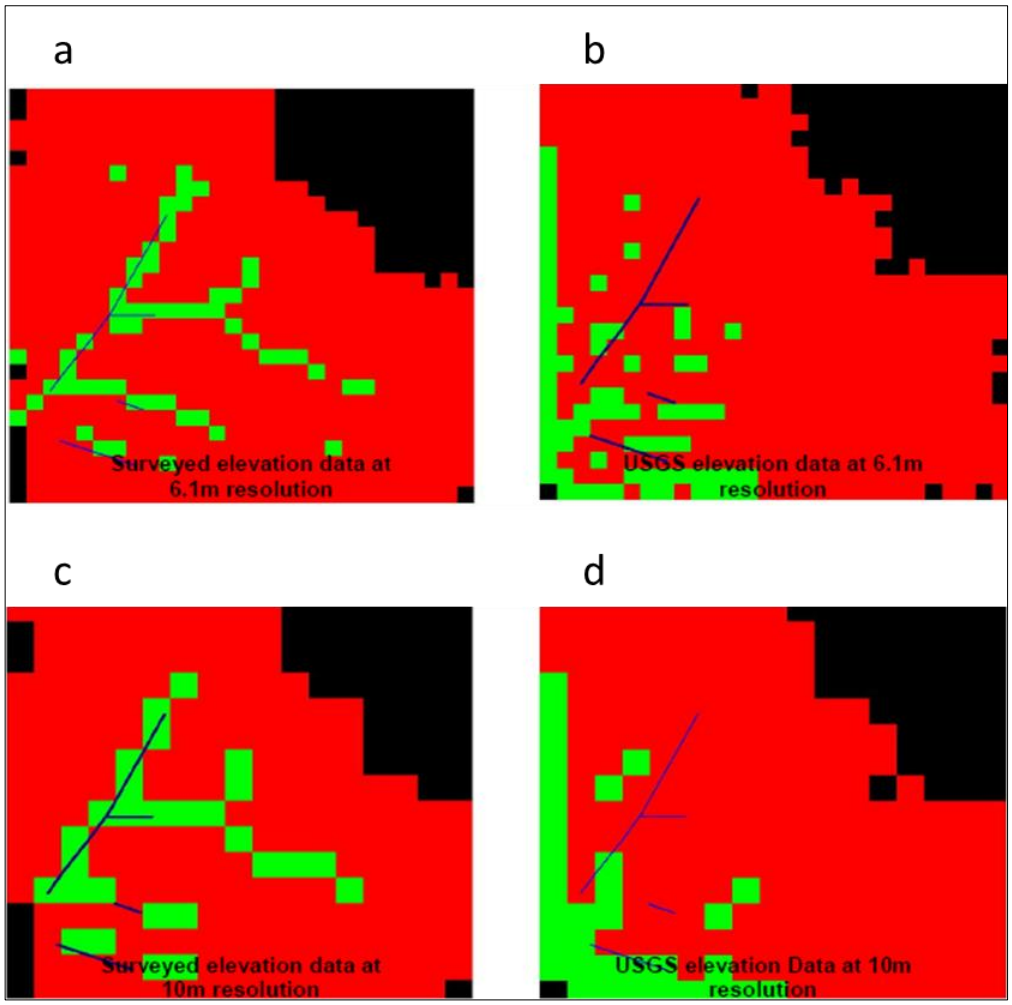

Figure 3.1: Maps showing CTI values greater than 10 (green) and known gullies (blue) at Ellis Farm, Site 2A. (a) Field surveyed data at 6.1m resolution (b), USGS elevation date resampled to 6.1m (c), Field surveyed data at 10m resolution and (d) USGS elevation date to 10m. After Parker *et al.* (2007).

Parker *et al.* (2007) noted that the threshold CTI had wide range of values, suggesting that it may, in practice, be challenging to use a fixed threshold CTI over large areas or at multiple, different sites. However, while CTI threshold values varied between ~10 and ~100, the spatial trend of gullies predicted using the CTI did not change with changing thresholds for CTI, only for their extent (Figure 3.1). They found a relatively strong correlation between the locations of ephemeral gullies and areas with the highest positive differences between the USGS DEM and the DEM based on Zevenbergen's field-based survey (Figure 3.3). This was strong evidence that the USGS DEM had failed to accurately represent the topographic

depressions (swales) responsible for generating the concentrated overland flow responsible for forming the ephemeral gullies. Hence, failure to identify swales explained the poor performance of CTIs produced from the USGS DEM.

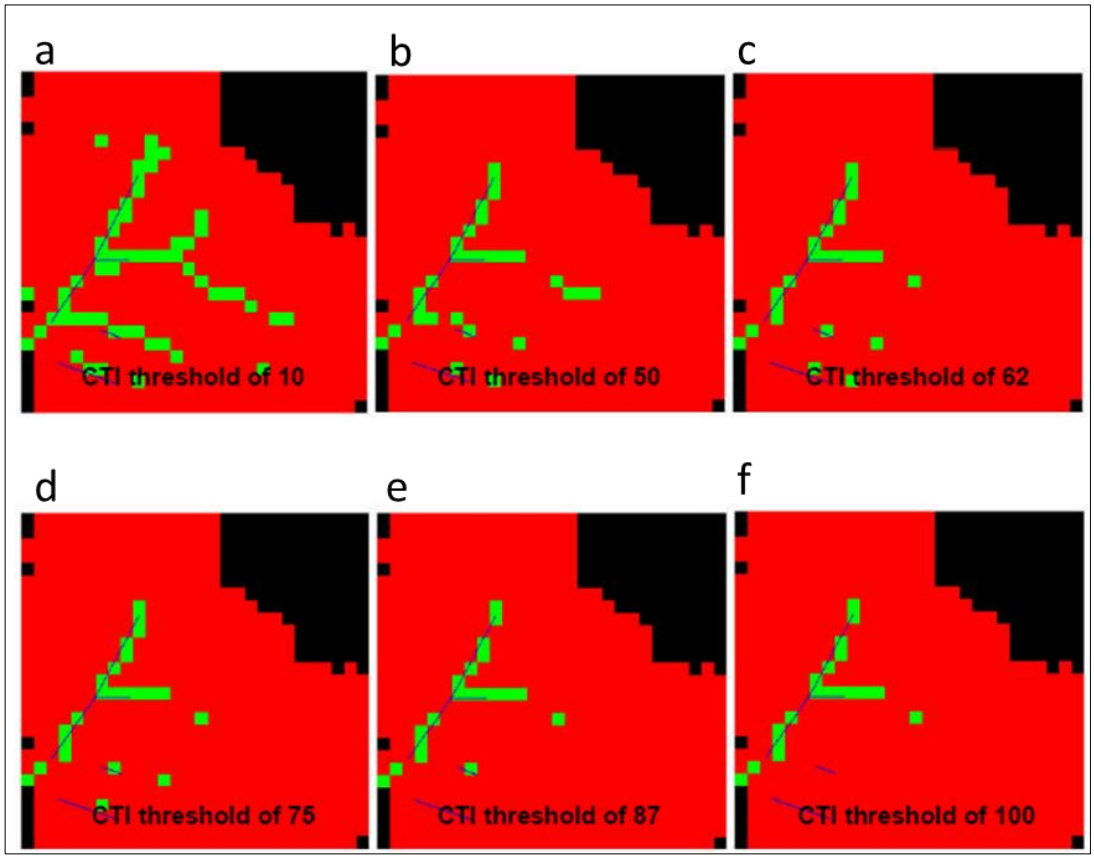

Figure 3.2: The CTI gully threshold set at (a) 10 m, (b) 50 m, (c) 62m, (d) 75m, (e) 87 m and (f) 100 m. After Parker *et al.* (2007).

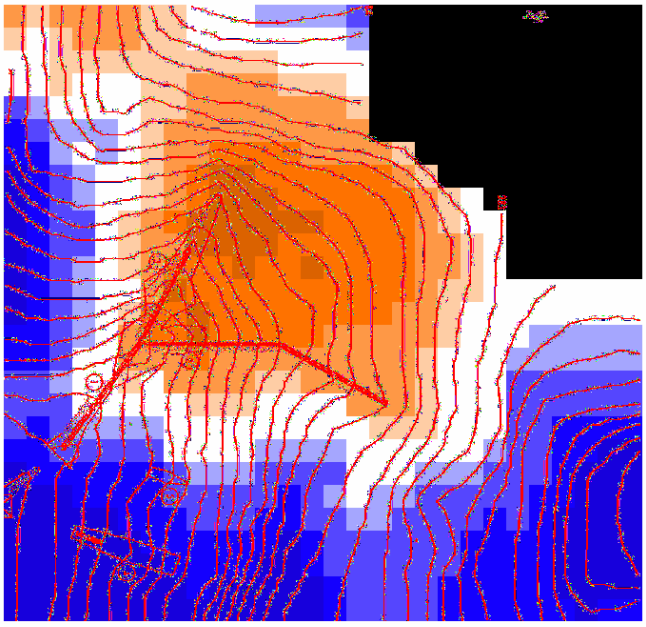

Figure 3.3: Map of height differences between Zevenbergen's field-surveyed DEM and the USGS 10m DEM for Ellis Site2 A. Cells in which the field-surveyed DEM is lower than in the USGS DEM are orange, while those in which the field-surveyed DEM is higher than the USGS DEM are blue. After Parker *et al.* (2007).

Parker *et al.* (2007) warned that though a global threshold CTI value could be used to highlight areas of potential ephemeral gulling, it must be acknowledged the extent of the predicted gully network may not be accurate. It follows that, if the purpose of using the CTI approach is to predict the actual locations of known gullies (as was the case when the CTI was first formulated), a reliable threshold value is absolutely essential, and deriving that threshold value accurately demands very high-resolution terrain data.

In the context of extending the use of the CTI approach to data sparse regions where, for example, the best available DEMs have grid sizes ≥30m, one must certainly heed Parker *et al.* (2007) warning that using a fixed, global value for the critical CTI may lead to inaccuracy in the extent of the gully network being predicted. Indeed, in addition to problems with the extent of gullies, the coarse resolution of the grid alone means that many of the small swales likely to host the ephemeral and/or classical gullies that are of interest, are not even represented in the DEM. Further, setting a high value for the threshold CTI means that the

upstream contributing area tends to be large. Unavoidably, a high threshold CTI will mean that the analysis will miss gullies that initiate in small sub-catchments but then gradually grow downstream in extent until they either disappear due to flow divergence or confluence with the main drainage network.

In this study, all these issues were contemplated and taken into account during an attempt to arrive at a well-founded method for setting the threshold CTI. The possibility of developing an automated procedure for deriving a suitable threshold CTI for a given location (i.e. one that could be validated using 'ground truthing' or comparison to gully head locations observed from RS) was also considered. Parker *et al.* (2007) used a reasonable but subjective approach to validating the CTI's performance (Figure 3.4). However, early in this research project, the need for a more objective (i.e. quantitative) validation of CTI performance was identified. Consequently, in the research reported later in this thesis, a quantitative validation has been developed. This is essential if the approach is to be suitable for global applications that take up and use multiple sources of data and varying grid resolutions.

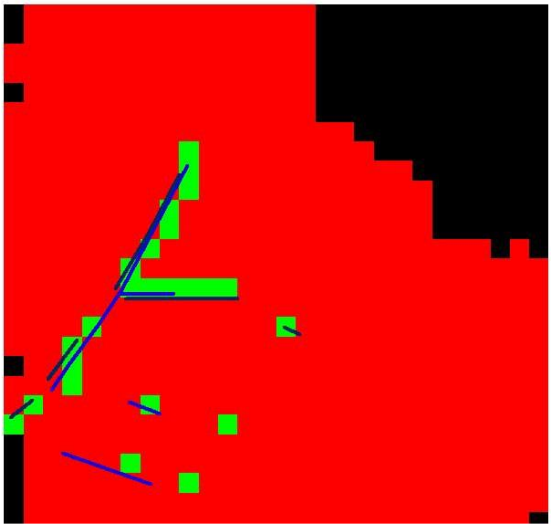

Figure 3.4: Map showing observed and predicted gully locations at the Ellis Farm Site2A. Cells with CTI values ≥62 (green) are predicted to contain a gully according to a GIS-based application of the CTI method. These cells match well to known field gully locations (blue polyline) and original predictions made by Zevenbergen (purple polyline). After Parker *et al.* (2007).

3.2.4. **DEM of difference (DoD) concept and technique**

Terrain changes can be detected using a DEM of Difference (DoD), computed by subtracting the elevations in one DEM from another, later one (Wheaton 2012, Figure 3.5). In the output surface, negative values represent ground lowering (erosion), and positive values represent ground raising (deposition). DoDs have been widely used to investigate the morphological impacts of geomorphological processes (Wheaton, 2008; Williams, 2012; Cucchiaro *et al.*, 2019; Grams *et al.*, 2019; Guisado-Pintado *et al.*, 2019; Leduc *et al.*, 2019; Morino *et al.*, 2019; Schwindt *et al.*, 2019; Watson *et al.*, 2019). Williams (2012) compiled a list of DoD applications (Table 3.1) and the list has continued to grow since then. DoDs have the potential to detect gully initiation and erosion based on remotely-sensed terrain data, and so the method could prove useful in validating gully predictions. However, very high resolution DEMs are needed to detect gullies and changes in gullies due to the small widths and depths of these features. Nonetheless, gullies detected using DoDs could serve as a viable alternative to using ground truth for method validation.

Table 3.2. Examples of investigations that have applied DEM differencing in a range of geomorphological settings (Williams (2012).

Geomorphological field	Application	Geomatics technology	Monitoring duration	Survey frequency	Approximate spatial extent	Reference
Coasts	Estuary change	Bathymetric charts (lead lines and echo sounding)	150 years	Half-century	217 km^2	van der Wal *et al.* (2002)
	Estuary change induced by earthquakes	Airborne LiDAR	Five months	Start and end of the monitoring	5 km^2	Measures *et al.* (2011)
	Beach changes after a hurricane	Airborne LiDAR	Event	Pre- and post-event	40 km long coastline	Zhang *et al.* (2005)
	Cliff and gully erosion	Airborne LiDAR	Six years	Start and end of the monitoring	77 km long coastline	Young and Ashford (2006)
	Cliff erosion	TLS	16 months	Monthly	0.1 km^2	Rosser *et al.* (2005)
	Cliff erosion	TLS	One year	Start and end of the monitoring	0.005 km^2	Hobbs *et al.* (2010)
	Cliff erosion	Oblique terrestrial imagery: SfM and MultiView Stereo	One year	Seven surveys during one year	0.05 km long coastline	James *et al.* (2012)
Fluvial reworking of sediment stores	Talus cone erosion	TLS	Three months	Start and end of the monitoring	0.009 km^2	Morche *et al.* (2008)
	Cut / fill of gully and alluvial fan	Kinematic GPS	32 months	3 - 5 months	0.5 km^2	Fuller and Marden (2010)
Glaciology	Glacier surface elevation change	Aerial photogrammetry	One year	Start and end of the monitoring	6.3 km^2	Hubbard *et al.* (2000)
	Glacier surface elevation change	Aerial photogrammetry and cartographic data	18 years	Start and end of the monitoring	5.5 km^2	Rippin *et al.* (2003)
	Rock glacier movement	TLS	Eight years	One month - 3 years	0.04 km^2	Avian *et al.* (2009)
	Glacier surface elevation change	Aerial photogrammetry and airborne LiDAR	Two years	Start and end of the monitoring	6 km^2	Barrand *et al.* (2009)
	Debris covered glacier margins	Airborne LiDAR	Four years	Start and end of the monitoring	0.5 km^2	Abermann *et al.* (2010)
	Permafrost affected bedrock and glacier ice	Aerial photogrammetry and airborne LiDAR	51 years	2 - 22 years	6.5 km^2	Fischer *et al.* (2011)
	Forefield sediment redistribution	Airborne LiDAR	Two years	Start and end of the monitoring	2 km^2	Irvine-Fynn *et al.* (2011)
	Proglacial and braidplain change	Airborne LiDAR and TLS	Two years	One day - 1 year	1.5 km^2	Carrivick *et al.* (2012)
	Glacier surface elevation change	TLS	Five days	Daily	0.05 km^2	Nield *et al.* (2012)
Mass movements	Mudflow	Cartographic data	45 years	1 - 16 years	1.2 km^2	van Westen and

						Lulie Getahun (2003)
	Landslide	Kinematic GPS	18 months	7 - 11 months	0.04 km^2	Mora *et al.* (2003)
	The earthquake triggered landslide and river erosion of deposit	Aerial photogrammetry and airborne LiDAR	14 years	1 - 11 years	6 km^2	Chen *et al.* (2006)
	Rockfall and slope failure (coast)	TLS	32 months	Monthly	0.1 km^2	Rosser *et al.* (2007)
	Rockfall and slope failure (deglaciated terrain)	TLS	One year	One day - 6 months	0.06 km^2	Oppikofer *et al.* (2008)
	Landslide (deep-seated, Tertiary sediments)	Aerial photogrammetry and airborne LiDAR	50 years	6 - 21 years	0.8 km^2	Dewitte *et al.* (2008)
	Rockslide (fjord)	TLS	Two years	Annual	0.6 km^2	Oppikofer *et al.* (2009)
	Landslide (slope undercut by a river)	TLS	18 months	2 - 6 months	0.01 km^2	Prokop and Panholzer (2009)
	Rockfall from landslide scar	TLS	Ten months	2 - 8 months	0.004 km^2	Abellán *et al.* (2010)
	Debris flow and flood	Airborne LiDAR	Event	Pre- and post-event	0.4 km^2	Bull *et al.* (2010)
	Earthflow (soil and weathered bedrock)	Airborne LiDAR	Four years	Start and end of the monitoring	0.06 km^2	DeLong *et al.* (2012)
Seismology	Deformation due to surface rupture	Airborne LiDAR	Event	Pre- and post-event	50 km long multi-fault	
Volcanology	Landslide	Aerial photogrammetry	18 years	3 - 10 years	7 km^2	Fabris and Pesci (2005)
	Slope evolution during an eruption	Aerial photogrammetry	Four years	Eight days 14 months	1 km^2	Baldi *et al.* (2008)
	Summit morphological change due to eruptive processes and deformation	Airborne LiDAR and aerial photogrammetry	21 years	2 – 12 years	7 km^2	Neri *et al.* (2008)
	Lava dome growth	Oblique terrestrial imagery	17 months	24-48 hours	1 km^2	Major *et al.* (2009)
	Lava flow dynamics	Airborne LiDAR	Two days	15-minute intervals	28 km^2	Favalli *et al.* (2010)
	Growth and deformation of a scoria cones	Airborne LiDAR	Four years	Annual	2 km^2	Fornaciai *et al.* (2010)
	Lahar	Airborne LiDAR	Event	Pre- and post-event	62 km long river	Procter *et al.* (2010)
	Crater wall collapse	TLS	Four years	17 – 32 months	9 km^2	Pesci *et al.* (2011)

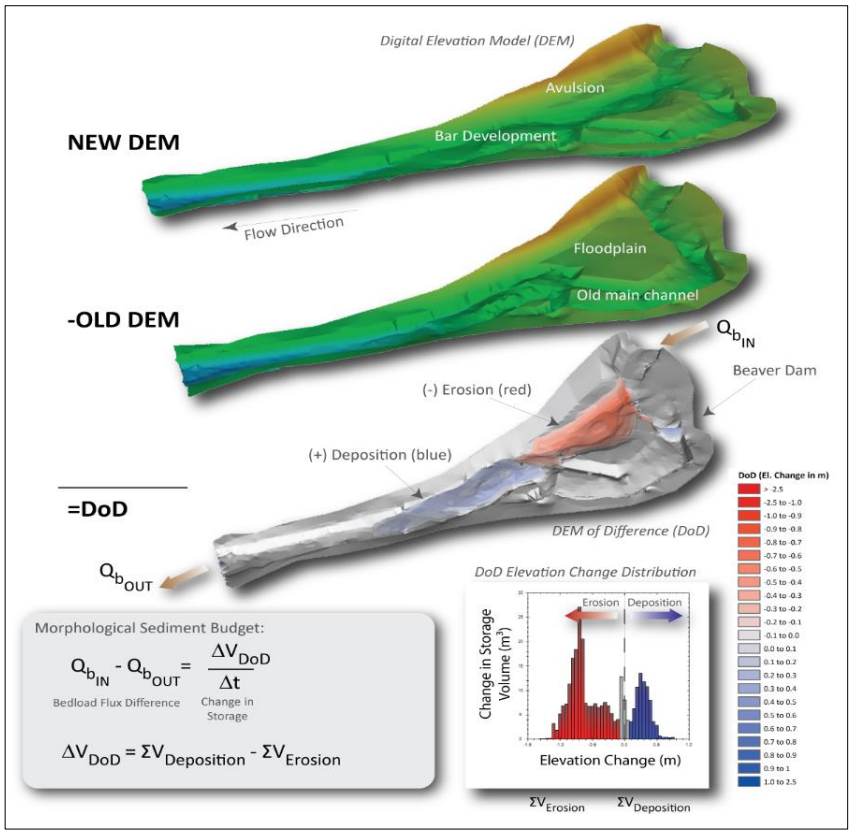

Figure 3.5: The principles underpinning the concept of a DEM of Difference. After Wheaton (2012).

3.3. **Chapter Objective**

Globally available terrain data typically has a resolution of between 12 m and 30 m and this limits the utility of the CTI method across much of the World. Parker *et al.* (2007) believed that CTI applications could be extended to the catchment scale and incorporated into models like the ARS AnnAGNPS, which were not at the time capable of locating potential ephemeral gullies but instead relied on extensive and rigorous, process-based data to predict soil erosion. Indeed, gully information is itself among the inputs required to run ARS AnnAGNPS. In that context, the CTI approach could obviate the need to input gully information into AnnAGNPS and other similar models.

The CTI's applicability in data-sparse regions has been framed as being dependent on increasing the availability of high quality and high-resolution topographic data.

No doubt higher resolution data will eventually become accessible in the future, but that may not be achieved for decades. Recognising this, this thesis explores the possibility of employing the CTI to predict not the precise locations of observed or future gullies, but the susceptibility of land to concentrated overland flow, concentrated flow erosion and gullying, over wide areas and in data-sparse regions. It is hypothesised that it may be possible to predict topographic-susceptibility to gullying using the DEMs with ~30 m grid sizes that are currently available in data-sparse regions. In exploring this issue, it was envisaged from the outset that the approach to would initially be informed through application of CTI methods using data from the data-rich regions.

Therefore, this chapter's objective is "to determine the effect of a Digital Elevation Model's (DEM) spatial resolution when calculating the Compound Topographic Index (CTI), which models concentrated overland flows" (see Chapter 1, Objective 2).

The steps necessary to achieve this objective are to:

3.1. compute CTIs using a 2003 DEM available for Mount St. Helens that has a 5m grid size, and use the CTIs to predict areas of concentrated overland flow and erosion (i.e. gullying);

3.2. subtract elevations in the 2003 DEM from those for a 2009 DEM of the same area, to generate a DoD with 5m resolution, and interpret the DoD to map actual gully erosion;

3.3. validate CTI-based predictions in 1. using the gullies observed in 2. above, and extend the validation to some of the applications reported by Parker *et al.* (2007) using a quantitative and objective approach, namely the Receiver Operator Characteristics (ROC);

3.4. repeat steps 1. and 2. with the 2003 and 2009 DEMs degraded to resolutions of 10, 15, 20, 25 and 30m, and then validate the performance of the CTI using step 3.

3.4. **Methodology**

3.4.1. **Historical DEMs at Mount Saint Helens**

The reasons for selecting Mount St. Helens, Washington State as the study site for initial elements of the research were explained in Chapter 2. The primary drivers were the availability of repeat, high resolution DEMs and the highly dynamic nature of the landscape, which means that erosion and deposition can be detected reliably over short timespans (Mosbrucker, 2014). Details of the DEMs obtained in the area have already been presented, in section 2.4.2.

The area selected for this study features extensive gullying due to concentrated overland flow erosion. On braid plain and terrace surfaces along the North Fork Toutle River, the land is still being regularly reworked by the river. While gullies form frequently, they are rapidly destroyed by migration of the river channel. Also, the extremely low slopes on the braid plain and lack of soil mean gullying processes are unlikely to be analogous to those on agricultural soils, which the focus of this study. Therefore, these areas were excluded from analysis and only gullies in the valley sides were used. The valley sides are readily gullied because of unconsolidated nature of underlying deposits (i.e. ash and landslide debris) and the poorly developed vegetation, which is mostly composed of mosses, lichens and small flowering plants. The south side of the North Fork Toutle River valley in a reach around Bear Creek was selected for this use in chapter because gully development was clearly visible in hill shades of the high-resolution, LiDAR-based DEMS of the area (Figure 3.6 and Figure 3.7). DoDs were generated using 2003 and 2009 at 5, 10, 15, 20, 25, and 30m resolutions (Table 3.2).

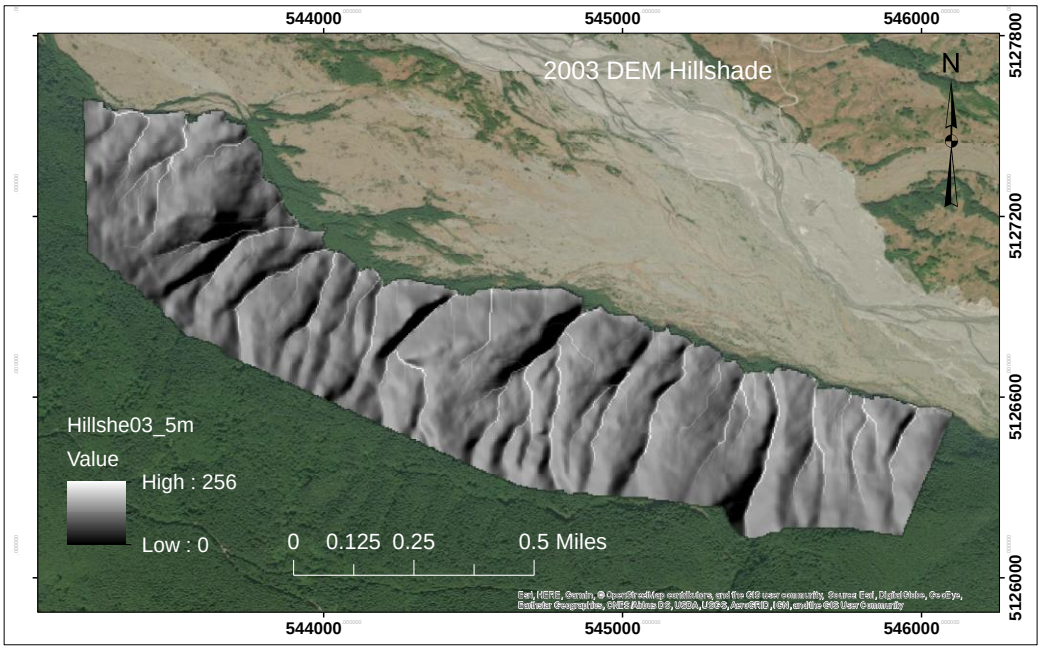

Figure 3.6. Hillshade of the 2003, 5m DEM of the south valley side of the North Fork Toutle River at Mount St. Helens near Bear Creek.

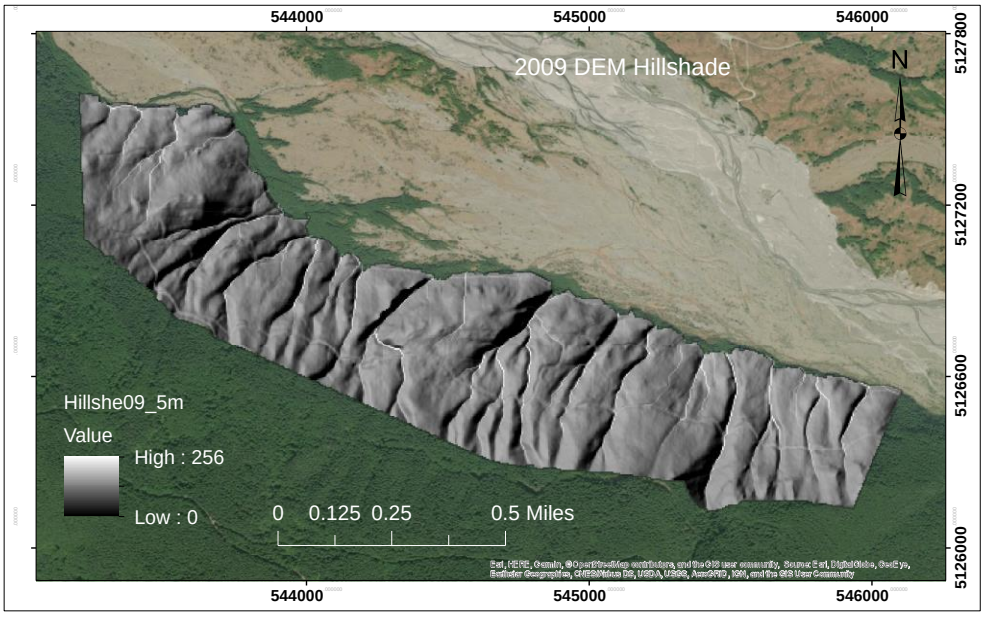

Figure 3.7: Hillshade of the 2009, 5m DEM of the south valley side of the North Fork Toutle River at Mount St. Helens near Bear Creek.

Table 3.2: DEMs of Difference (DoD) generated for the study site at Mount St. Helens.

Resolution	DEM2003	DEM2009	DoD
5	DEM	DEM	DEM2009 - DEM2003
10	DEM	DEM	DEM2009 - DEM2003
15	DEM	DEM	DEM2009 - DEM2003
20	DEM	DEM	DEM2009 - DEM2003
25	DEM	DEM	DEM2009 - DEM2003
30	DEM	DEM	DEM2009 - DEM2003

3.4.2. **Field mapped gullies, CTI threshold gullies and gullies extracted from DoDs as ground truth**

In the studies performed by Parker *et al.* (2007) at the Melton site (Figure 3.8), gullies either mapped in the field or digitised from aerial photographs were used as 'ground truth' in validating the CTI approach to predicting gully locations.

Areas outside the gullies were coded 1 = no gully, while areas within the gully and were coded 2 = gully. The areas predicted for gullying based on their having CTI values higher than the threshold value of 36 (based on DEMs with 10m and 30m resolutions), were coded as 2 = gully erosion, in ArcGIS.

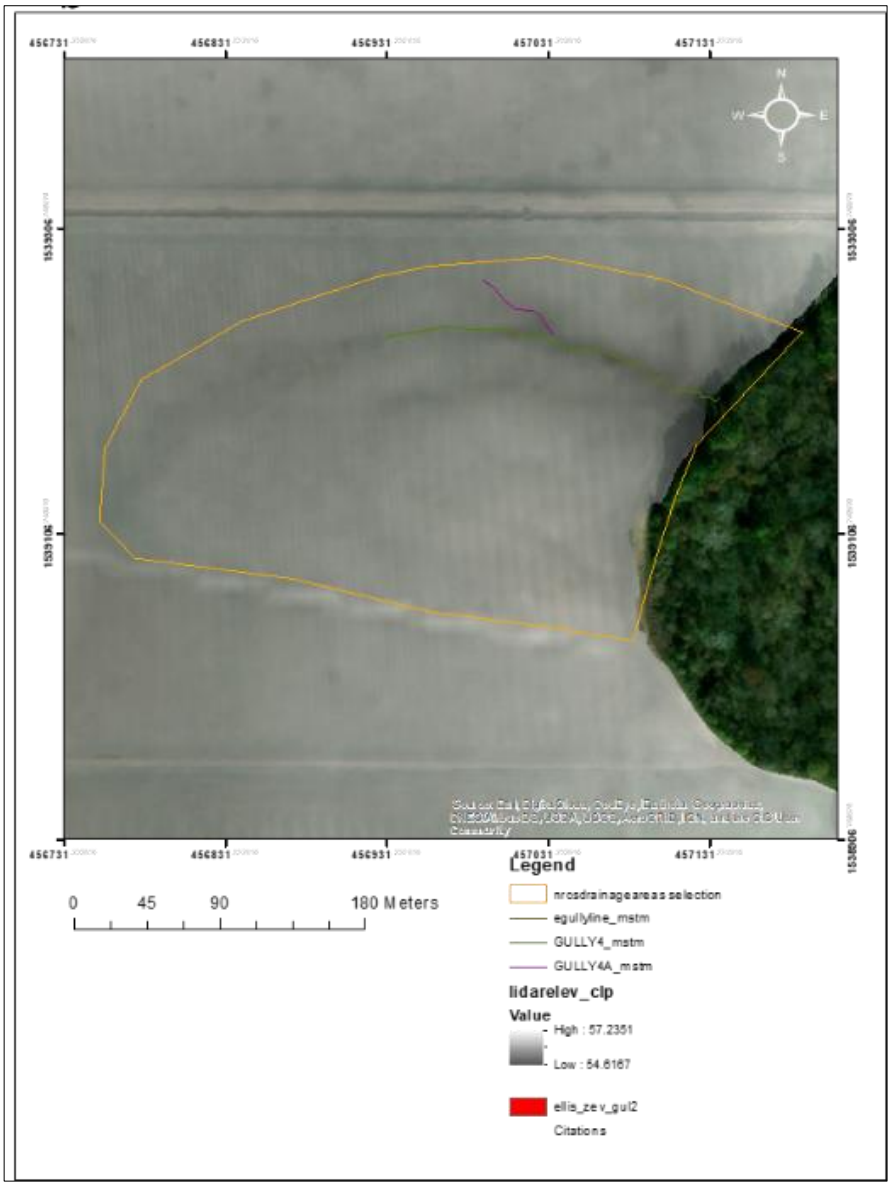

Figure 3.8. An image of gullies from a DEM of Melton farm

At Mount St Helens, gullies identified and extracted from 5m DoD served as the 'ground truth' in place of field surveyed gullies or digitised gully lines. Areas in the DoD raster representing concentrated flow erosion (gullying) were reclassified as 2 = gully, while areas outside the gullies were reclassified as 1 = no gully, in ArcGIS.

3.4.3. **Using the DEM of Difference (DOD) to detect areas of gully erosion**

A DoD was created to detect areas of erosion within the selected area at Mount St Helens. It is important to account for error when interpreting a DoD because the vertical accuracy of DEMs is never perfect. For example, the DEMs differenced to create the DoD, achieved and target errors were approximately 0.032m and 0.13m, respectively (Mosbrucker, 2014). Errors in the DEMs mean that in the DoD, there are values clustered around zero that cannot be differentiated from 'no change' because they are within the margin for error in differences between the DEMs.

Also, and more significantly, in addition to differences resulting from actual gully erosion, land lowering may arise due to other geomorphic processes, such as weathering and trampling by elk. Hence, there is a risk that areas of weathering or trampling could be mistaken for gullying. However, weathering and trampling does not lower the ground surface as rapidly or severely as gullying. Recognising this, and to reduce the risk of interpreting no significant lowering or minor lowering by weathering or trampling as evidence of gullying, an error band was introduced and reductions in elevation in the 2003-2009 DEM that were <1.5m were excluded from further analysis. This was achieved as follows: Erosion threshold in the DoD was set based on the command, Con (("DoD" > 1.5) | ("DoD" < - 1.5), 2, 1), where 1 represents no erosion and 2 represents erosion and can be translated through the "if-then" statement; IF DoD> 1.5m, there is no gully erosion, whereas if DoD < - 1.5, there is gully erosion.

While misinterpretation of areas eroded by weathering and trampling as being gullied can be avoided by ignoring land lowering by <1.5m, there are other processes with the capacity to erode land as fast as gullying; for example, landslides. However, while concentrated flow erosion is associated with elongated swales that accumulate surface runoff, landslides occur in isolation, on steep slopes, and they create irregularly-shaped depressions. Based on these differences, it was recognised that the flow accumulation tool in ArcGIS could be used to identify and exclude areas lowered by landslides. This tool determines the upstream contributing area for a pixel, taking account of the fact that overland flow

will only become sufficient to initiate a channel when the upstream contributing area is sufficient to supply enough water, generating the necessary stream power to erode. In trials, it was discovered that a flow accumulation critical value of 80 was effective in removing many erosion features in the DoD that were unrelated to gullying. It was decided to investigate whether ≥80 could be used as a minimum (i.e. critical) flow accumulation for classifying lowered areas in the DoD as having definitely been subject to concentrated flow erosion.

Consequently, the CTI model was applied and validated in four versions representing a combination of 2 versions of the CTI (CT1 and CTI2) and 2 versions of ground-truth, validation data-sets (G1 and G2). CTI1 had no critical value for flow accumulation, so any accumulation of water was hypothesised as potentially initiating a gully, whereas CTI2 had a critical flow accumulation value of 80, with the hypothesis that values less than this would not instigate gully erosion. G1 was DoD data where any decline in cell elevation was considered erosion, with no critical flow accumulation value in the DoD. In contrast, G2 had a critical flow accumulation value of 80, consistent with the CTI2, and DoD vertical changes had to be greater than -1.5 m, to indicate gullying and excluding smaller amounts of erosion and inherent error in DEMs. More detail on these four approaches is presented in Table 3.3. All four approaches were applied to 5, 10, 15, 20, 25, and 30 m resolution datasets.

The modelling steps in ArcGIS are presented in Figure 3.9.

Table 3.3. Matrix for the validation runs of CTI1 and CTI2, by G1 and G2.

S/no	Code	PREDICTOR (CTI VERSIONS)	Ground Truth (Observed gully)	Interpretation
1	CTI1_G1	**CTI 1** Concentrated flow erosion was predicted by the CTI based on the intersection (multiplication or conditional) in the 2003 DEM (i.e. the old DEM) of planform curvature less than zero (with convergence expressed as a negative number); slope greater than zero, and; flow accumulation greater than zero. If conditional output is desired, when the intersection condition is met, then 2 is returned to mean concentrated flow erosion is predicted, or else 1 for no concentrated flow being predicted. The conditional statement that expresses this concentrated flow erosion prediction condition is expressed as: Con (("Old plan concavity"< 0) & ("Old slopes"> 0) & ("Fac2003" > 0),2,1).	**G1** cells with erosion (i.e. changes in elevation in the DoD are less than zero) and flow accumulation values (in the 2009 DEM) greater than zero were treated as having experienced true concentrated flow erosion (gullying). Where this intersection condition was true, 2 was returned, to mean concentrated flow erosion, or else 1 was returned, meaning no concentrated flow erosion. This was captured in the conditional statement: Con (("DoD"< 0) & ("Fac2009" > 0),2,1).	Prediction by CTI1 and validation by G1.

2	CTI2_G1	**CTI2** Concentrated flow erosion was predicted by the CTI based on the intersection (multiplication or conditional) of planform curvature in the 2003 DEM (i.e. Old plan concavity) being less than zero (with concavity generating negative planform curvature values), slope in the 2003 DEM ((Old slope)) being greater than zero and flow accumulation in the 2003 DEM (Fac2003) being greater than 80. If a conditional output is desired, when the intersection condition is met, then 2 is returned to mean that concentrated flow erosion is predicted, or else 1 for no concentrated flow erosion being predicted. The conditional statement that expresses this-concentrated flow erosion prediction is: Con (("Old plan concavity"< 0) & ("Old slopes"> 0) & ("Fac2003" ≥80),2,1).	**G1** cells with erosion (i.e. changes in elevation in the DoD are less than zero) and flow accumulation values (in the 2009 DEM) greater than zero were treated as having experienced true concentrated flow erosion (gullying). Where this intersection condition was true, 2 was returned, to mean concentrated flow erosion, or else 1 was returned, meaning no concentrated flow erosion. This was captured in the conditional statement: Con (("DoD"< 0) & ("Fac2009" > 0),2,1).	prediction by CTI2 and validation by G1
3	CTI2_G2	**CTI2** Concentrated flow erosion was predicted by the CTI based on the intersection (multiplication or conditional) of planform curvature in the 2003 DEM (i.e. Old plan concavity) being less than zero (with concavity generating negative planform curvature values), slope in the 2003 DEM ((Old slope)) being greater than zero and flow accumulation in the 2003 DEM (Fac2003) being greater than 80. If a conditional output is desired, when the intersection condition is met, then 2 is returned to mean that concentrated flow erosion is predicted, or else 1 for no concentrated flow erosion being predicted. The conditional statement that expresses this CTI concentrated flow erosion prediction is: Con (("Old plan concavity"< 0) & ("Old slopes"> 0) & ("Fac2003" ≥80),2,1).	**G2** thresholds values for contributing area in CTI and DoD erosion), thresholds were used for both true and predicted concentrated flow erosion. The intersection of change in the DoD less than -1.5 m and flow accumulation (Fac2009) in the 2009 DEM greater than 80 (Fac2009≥80) was taken to indicate areas of true concentrated flow erosion (i.e. gullying). Where this intersection condition is true, 2 is returned to mean concentrated flow erosion, or else 1 is returned to mean no concentrated flow erosion. This is captured in conditional statement: Con (("DoD"< -1.5) & ("Fac2009" ≥80),2, 1).	prediction by CTI2 and validation by G2

4	CTI1_G2	**CTI1** Concentrated flow erosion was predicted by the CTI based on the intersection (multiplication or conditional) in the 2003 DEM (i.e. the old DEM) of planform curvature less than zero (with convergence expressed as a negative number); slope greater than zero, and; flow accumulation greater than zero. If conditional output is desired, when the intersection condition is met, then 2 is returned to mean concentrated flow erosion is predicted, or else 1 for no concentrated flow being predicted. The conditional statement that expresses this concentrated flow erosion prediction condition is expressed as: Con (("Old plan concavity"< 0) & ("Old slopes"> 0) & ("Fac2003" > 0),2,1).	**G2** In the fourth version (Version 4, CTI1 = no threshold value for flow accumulation in CTI and G2, threshold value for flow accumulation in DoD erosion), there was no threshold for contributing area in the CTI, but there was a threshold for erosion in the DoD. The intersection of change in the DoD less than -1.5 m and flow accumulation (Fac2009) in the 2009 DEM greater than 80 (Fac2009≥80) was taken to indicate areas of true concentrated flow erosion (i.e. gullying). Where this intersection condition is true, 2 is returned to mean concentrated flow erosion, or else 1 is returned to mean no concentrated flow erosion. This is captured in conditional statement: Con (("DoD"< -1.5) & ("Fac2009" ≥80),2, 1).	prediction by CTI1 and validation by G2

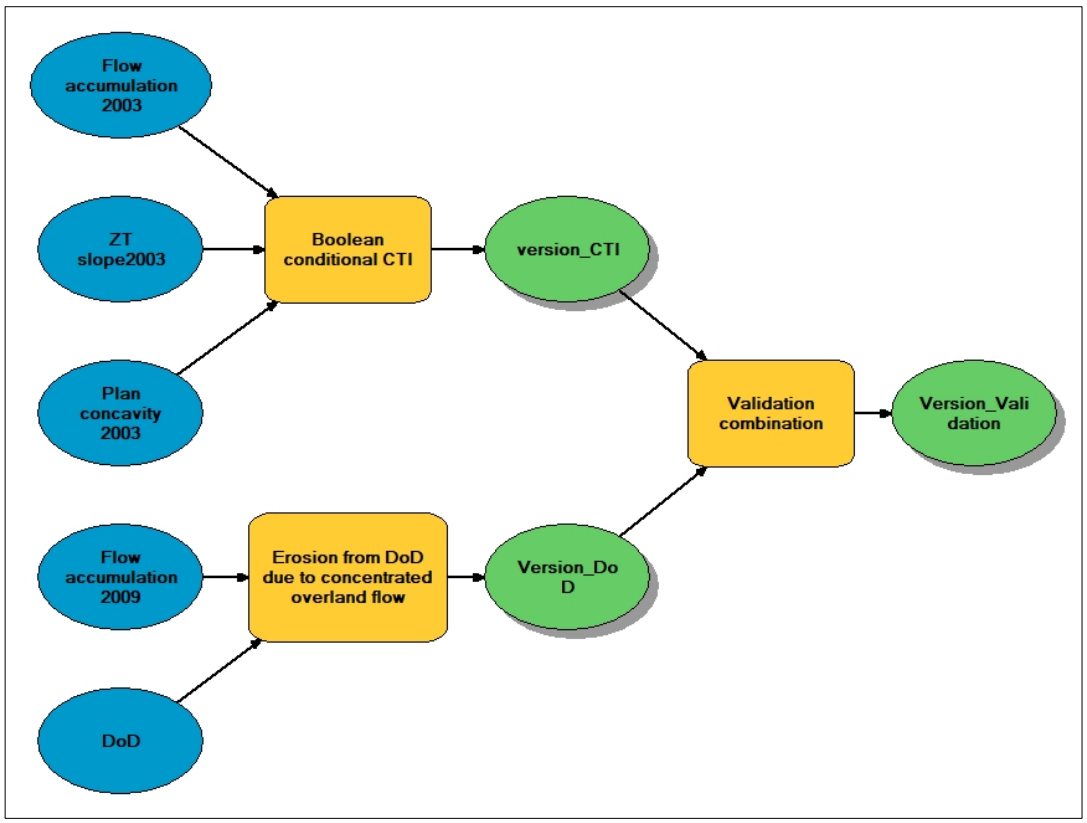

Figure 3.9: The model built in ArcGIS model builder to evaluate the models and the validations respectively.

3.4.4. **Principle behind validating a model using the Receiver Operator Characteristics (ROC)**

To validate the CTI models, the Receiver Operator Characteristics (ROC) method (Hanley and McNeil, 1982; Zweig and Campbell, 1993) was used, as is typical for models and algorithms and in many machine learning classifier algorithms. The ROC approach has been adopted in this study to validate the CTI model against the reality of gullies or no gullies (ground-truth) as captured from high resolution remotely sensed data.

Four conditions are possible when making predictions: True Positives (TP) and True Negatives (TN) indicate correct predictions, and False Positives (FP) and False Negatives (FN) indicate incorrect predictions. The CTI calculation in ArcGIS 10.4 was

reclassified so there were two conditions, indicating a prediction of gullying and a prediction of no gullying. Similarly, the DoD layer was reclassified into areas of gullying and no gullying. The CTI and DoD layers were then combined, using the combine tool in ArcGIS, to assign to each cell the appropriate one of the four possible conditions i.e. TP, TN, FP, FN (Table 3.4).

Table 3.4. Receiver operator characteristics matrix or cross-tabulation

		Confirmation from the DoD		
		No gully erosion	Gully erosion	Total
Predicted by CTI	No gully erosion	True Negative (TN): DoD show there are no gullies and the CTI truly predicted no presence of gullies	False negative (FN): DoD show there are gullies, CTI predicted no existence of gullies	TN+FN
	Gully erosion	False positive (FP): DoD show there are gullies, but the C predicted no presence of gullies	True positive (TP): DoD show there are gullies and the CTI truly predicted presence of gullies	FP+TP
Total		TN+FP	FN+TP	TN+FP+FN+TP

Cross-tabulation of the diagnostic test against ground-truth allows the Sensitivity, Specificity, Accuracy and Prevalence to be computed, as well as the overall probabilities of making TP and TN predictions (PPV and NPV). These fundamental parameters are defined below and are calculated to validate the model, based on how it performs in terms of (a) discriminating between TP and TN and (b) identifying them correctly, by avoiding FP and FN.

The first parameter represents how often the CTI model predicts gully erosion observed in the DoD correctly (TP). This is the *Sensitivity* of the model. It is calculated as:

$$\text{Sensitivity} = \left(\frac{TP}{TP + FN}\right) \times 100 \qquad \text{Equation 3.1}$$

The second parameter represents how often the CTI model correctly predicts that there is no gully erosion in the DoD (TN). This is the *Specificity* of the model, calculated as:

$$\text{Specificity} = \left(\frac{TN}{TN + FP}\right) \times 100 \qquad \text{Equation 3.2}$$

The third parameter represents the overall performance of CTI in terms of the proportion of correct predictions (TP and TN) it makes when compared to cells in the DoD coded as experiencing, or not experiencing, gully erosion. This is the *Accuracy* of the model, computed as:

$$\text{Accuracy } = \left(\frac{TP+TN}{TP+TN+FP+FN}\right) \times 100 \qquad \text{Equation 3.3}$$

The fourth parameter represents the percentage of cells in the DoD that actually have gullies, which indicates the *Prevalence* of the modelled feature, and is calculated as:

$$\text{Prevalence} = \left(\frac{TP + FN}{TP + TN + FP + FN}\right) \times 100 \qquad \text{Equation 3.4}$$

The fifth parameter represents the probability that in areas where the CTI model predicts gullying in the landscape, there is actually gully erosion in the DoD. This is the *Positive Predictive Value* (PPV), which is calculated as:

$$\text{PPV} = \left(\frac{TP}{TP + FP}\right) \times 100 \qquad \text{Equation 3.5}$$

The sixth parameter represents the probability that in areas where the CTI model predicts no gullying there is actually no gully erosion in the DoD. This is *Negative Predictive Value* (NPV), which is calculated as:

$$\text{NPV} = \left(\frac{TN}{TN + FN}\right) \times 100 \qquad \text{Equation 3.6}$$

These parameters are not all mutually independent. For example, NPV is inversely related to *Prevalence*, while the PPV is directly related to *Prevalence* in a positive way. Conversely, S*ensitivity* and *Prevalence* are not directly related.

The words “accuracy”, “sensitivity”, “specificity” and “prevalence” are common words but, they are also ROC parameters as presented above. Therefore, throughout this thesis where these words are used as descriptors of ROC parameter, they are capitalised with italics (i.e. *Accuracy*, *Sensitivity*, *Specificity* and *Prevalence).*

Plotting the true positive rate (*Sensitivity*) against the false positive rate (i.e. 1 – *Specificity*) yields the ROC curve. The more the ROC curve trends towards the *Sensitivity* axis, the better the performance of the model in correctly predicting areas in the landscape that, according to interpretation of the DoD, did or did not experience gully erosion between 2003 and 2009. The area under the curve measures the *Accuracy* of the CTI in terms of how well it correctly predicts the observed gully or no gully condition. This area is often expressed as a percentage. The greater the area under the curve, the better is its *Accuracy*. A curve that precisely follows 45 degrees in the Cartesian plane in the plot has an area under the curve of 0.5 (50%).

For a predictive model to be considered accurate as a predictor of observed conditions, the area under its ROC curve should be greater than 50%, and the difference between the area under the curve and an area of 50% should be statistically significant (IBM SPSS Statistics, 25). ROC analysis and area under the ROC curve can be used to identify small differences performance between models (and applications of the same model using different resolution input data), and they and support objective, quantitative assessment of predicative capacity. It is the area under the curve (AUC) that is used here to evaluate the predictive performances of the four modelling approaches (i.e. CTI1_G1; CTI1_G2; CTI2_G1, CT2_G2).

3.5. **Results**

3.5.1. **Melton Farm**

ROC curves for prediction of gullies surveyed in the field at the Melton Site and applying CTI at grid resolutions of 1, 5 and 30 m are plotted in Figure 3.10 (a). The areas under the ROC curves are plotted in Figure 3.10 (b) and the relevant significance test statistics are listed in Table 3.5.

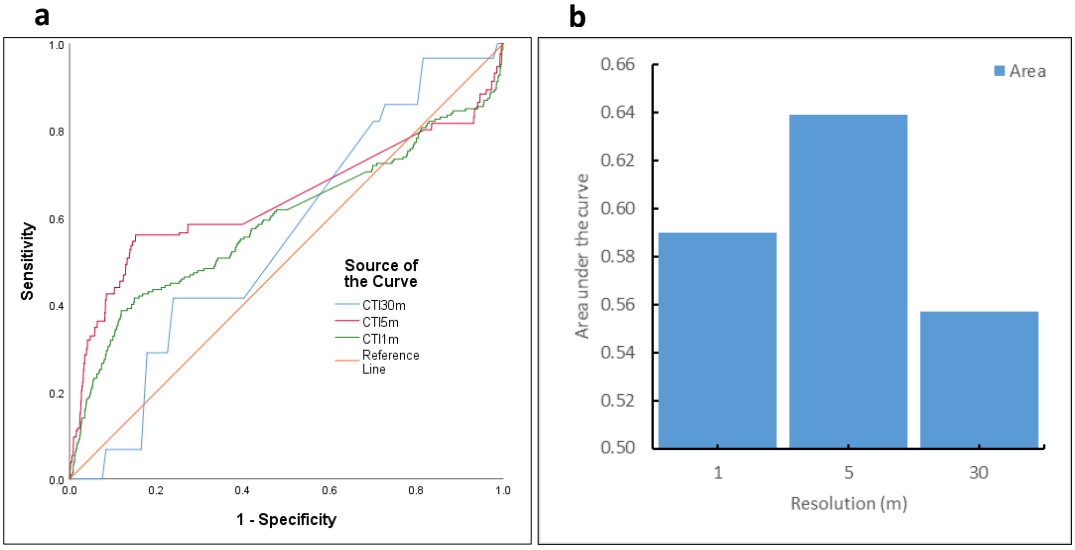

Figure 3.10. (a) ROC curves for CTI predictions of gullying at Melton Farm, with grid resolutions of 1, 5 & 30m. (b) Areas under ROC curves (i.e. Accuracy values) for the CTI model at Melton, using the 1m, 5m & 30m DEMs.

Table 3.5: Test statistics for areas under the ROC curves at different grid resolutions.

Test Result Variable(s)	Area	Std. Error[a]	Asymptotic Sig.[b]	Asymptotic 95% Confidence Interval	
				Lower Bound	Upper Bound
CTI30m	0.557	0.019	0.007	0.520	0.594
CTI5m	0.639	0.026	0.000	0.588	0.691
CTI1m	0.590	0.025	0.000	0.541	0.640

a. Under the nonparametric assumption
b. Null hypothesis: true area = 0.5

Areas under the curves are all greater than 50%. Interestingly, the area is largest for the 5m DEM (64%). The smaller area under the curve for the 1m DEM (59%) indicates that the CTI did not perform as well as for a 5 m grid. The poorer

performance of CTI at 1 m compared to that at 5 m is consistent with the idea that the finest resolution is not necessarily the optimum resolution, as suggested by (Zevenbergen, 1987). As would be expected based on Parker et al.'s (2007) analysis, the area under the ROC curve for a 30m grid (56%) is lower again, though it is still above 50%.

Statistical testing was performed to determine whether areas under the curves listed in Table 3.5 differed significantly from 50%. Values of the test statistic listed in Table 3.5 indicate that the null hypothesis should be rejected and that, at the 95% level of confidence, the areas under all three CTI curves are significantly different from 50%.

The finding that CTI alone can perform to this standard based on a 30m DEM suggests that it may be capable of identifying areas that are likely to be subject to concentrated flow that has at least the potential to cause concentrated flow erosion. To an extent, whether that concentrated flow does or does not lead to gullying depends on the influence of the other factors mentioned above. It follows that the CTI could be used to alert landowners and developers regarding areas at risk of gullying by concentrated flow in data sparse regions where readily available DEM resolution is 30m.

In an attempt to isolate and better understand the influence of grid resolution on CTI performance, the centrelines of gullies predicted using the CTI model were extracted from the 1m DEM and used to represent 'ground truth' with respect to the presence of gullies at the Melton site. Then, noting that CTI actually performed better for the 5 m DEM (see Table 3.2), the centrelines of gullies predicted using CTI for that DEM resolution were also extracted and used as an alternative 'ground truth'. The CTI model was then applied at 1 m, 5 m and 30 m grid resolutions. First, a threshold CTI value for gully formation of 36 was used, based on the results of earlier research at the Melton site Parker *et al.* (2007). To evaluate whether use of a threshold CTI improves the performance of the CTI model, applications at 1 m, 5 m and 30 m grid resolutions were then repeated, but with the threshold CTI set to

zero. In Figure 3.10 and Table 3.6, areas under the ROC curve are 100% for CTI with and without a threshold value. This is because gullies predicted using the 1m DEM were used as a 'ground truth'. This step was taken so that the CTI's performance using the 1 m DEM could act as a base case against which to compare performance of the CTI model at coarser grid resolutions. The area under the curve for application to the 5 m DEM of the CTI with a threshold value for gully initiation is 82%. This indicates that the performance of the model was not badly impacted by coarsening of the grid resolution from 1 m to 5 m. However, when the grid was further coarsened to 30 m, the area under the ROC curve fell to 48%, indicating that the CTI model was ineffective at this coarse resolution. For 5 m grid resolution, the area under the ROC curve for CTI without a threshold is 61%, indicating that omitting the threshold reduced model performance compared to that with a threshold. Interestingly, for the 30m DEM, the CTI model without a threshold performed slightly better than that with a threshold. However, with an area under the ROC curve of just 50%, the CTI without a threshold did not provide any significant predictive performance.

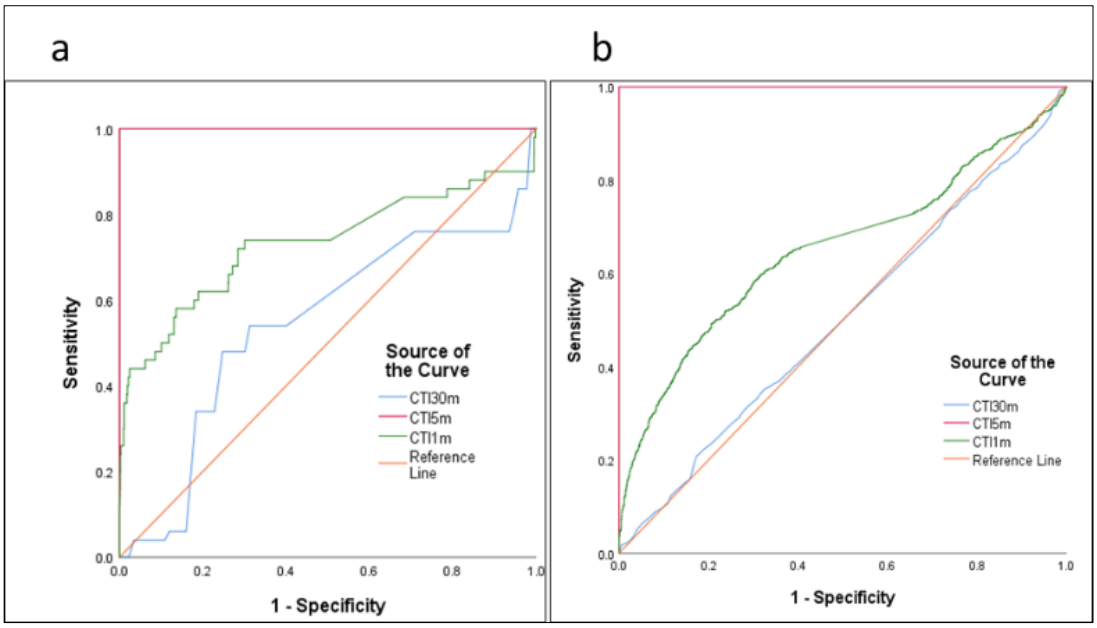

Figure 3.11. ROC curves for CTI predictions of gullying (a) with a threshold CTI = 36 and (b) with the threshold set to zero, for DEM resolutions of 1m, 5m and 30m. Note that the curve for 5m must be ignored as, for the purpose of revealing the influence of grid resolution, gullies predicted using this grid resolution were used as 'ground truth' for the presence of gullies at the Melton site, ensuring perfect agreement between predicted and observed gullying.

Table 3.6. Test statistics for areas under ROC curves in Figure 3.11.

Threshold	CTI	Area	Std. Error[a]	Asymptotic Sig.[b]	Asymptotic 95% Confidence Interval	
					Lower Bound	Upper Bound
With threshold	CTI30m	0.543	0.047	0.302	0.451	0.634
	CTI1m	0.732	0.049	0.000	0.637	0.827
Without threshold	CTI30m	0.500	0.011	0.964	0.479	0.522
	CTI1m	0.651	0.011	0.000	0.630	0.673

a. Under the nonparametric assumption
b. Null hypothesis: true area = 0.5

In summary, investigation of the impact of changing grid resolution relative to a base case under which the CTI was set-up to generate perfect performance, confirms that the ideal grid resolution may not be the finest grid resolution and establishes that the method performs poorly at 30m grid resolution. Performance was better when a site-specific threshold CTI for gully initiation was used on 1 m

and 5 m resolution data. However, at 30 m areas under the ROC curve were not statistically different from 50% regardless of whether or not a CTI threshold was used. This confirms the earlier conclusion of Parker *et al.* (2007) that the original CTI model cannot be used to predict the centrelines of known gullies at Melton Farm when it is applied using a 30m DEM, whether a threshold CTI is used or not.

3.5.2. **Symbology and visualisation of the CTI at Mount Saint Helens**

To test the CTI in a rugged environment, it was applied to a DEM of Mount St Helens. The four CTI modelling set-ups were used (i.e. with and without critical flow accumulation values and with and without critical DoD ground-truth values – CTI1_G1, CT1_G2, CTI2_G1, CTI2_G2) The first step in the investigation and validation study at Mount St Helens was to identify gullies already present in 2003, using the 5m DEM for that year. Both swales providing preferred flow paths and ridges between those swales are clearly visible in the hillshade of the DEM (Figure 3.12).

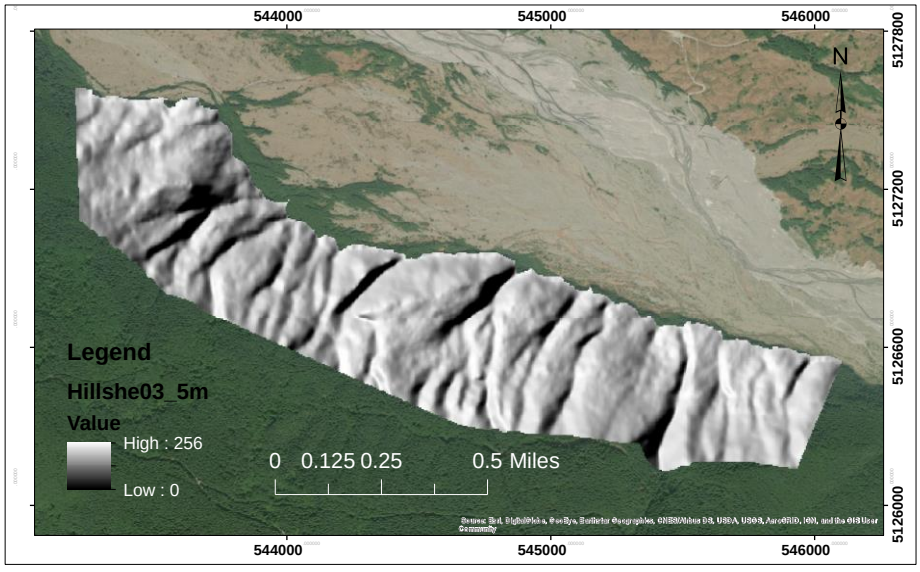

Figure 3.12. Hillshade of the study area at Mount St Helens based on the 2003 DEM at a grid resolution of 5m. The drainage pathways for concentrated overland flow (swales) and drainage divides (ridges) existing in 2003 are clearly visible.

The next step was to apply the CTI with no threshold (i.e. CTI1) to the 2003 DEM, at the 5m resolution. Gullies predicted using CTI1 are mapped over the DEM itself and the hillshade rendition, in Figure 3.13(a) and (b), respectively.

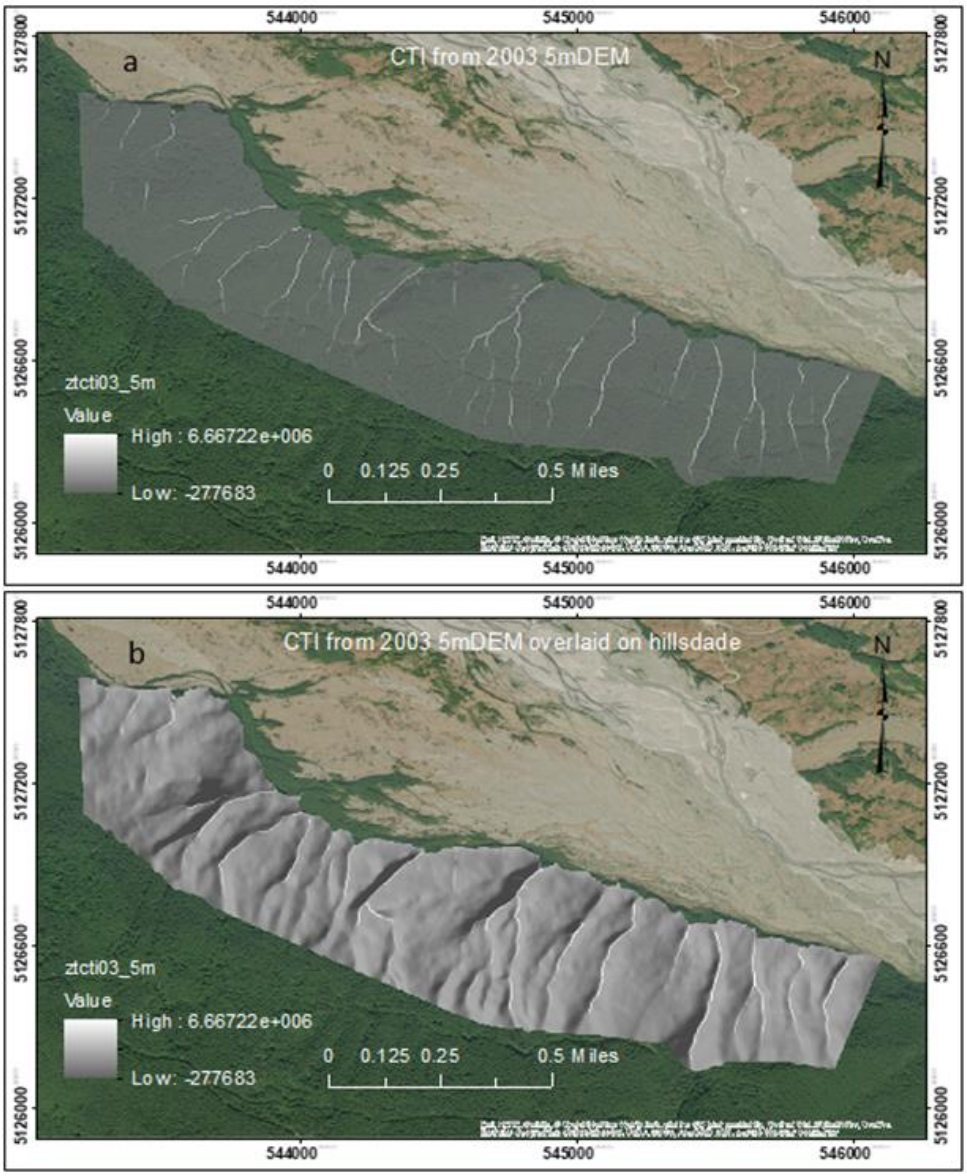

Figure 3.13: Gullies predicted using CTI1 values calculated using the 2003, 5m DEM and plotted as white lines added to (a) the DEM and (b) the hillshade.

It was apparent that the way that the CTI values are mapped makes a big difference to how well they visualise the presence and alignment of gullies predicted using the CTI model. This is because the appearance of the any derived parameter displayed in a GIS-generated map is controlled by symbology, rendering or classification,

which are collectively described as the data or image ‘stretch’. Multiple types of ‘stretch’ are available in the symbology for ArcGIS 10.4 and several alternatives were tested to address issues with the way the results appeared, cartographically.

To illustrate the effects of using different symbologies to better visualise gullies predicted using the CTI, maps with the following types of ‘stretch’ were generated: per cent clip, standard deviation, custom, minimum-maximum, and histogram equalise (Figure 3.14 to 3.18, respectively).

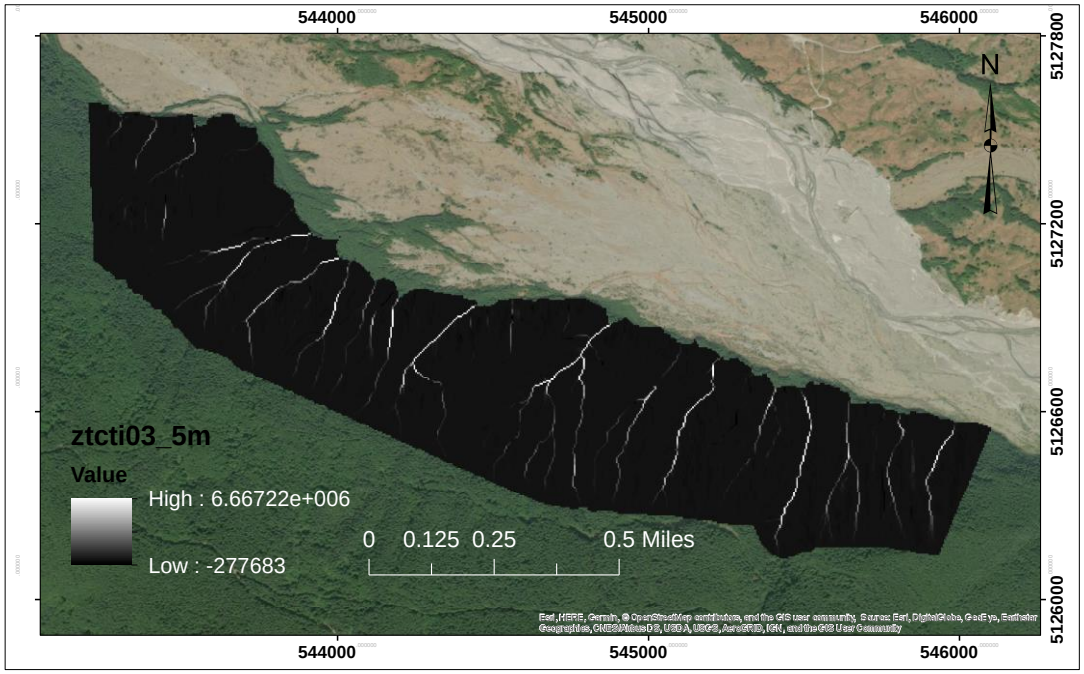

Figure 3.14: CTI values calculated using the 2003, 5m DEM displayed using ‘per cent clip’ stretch.

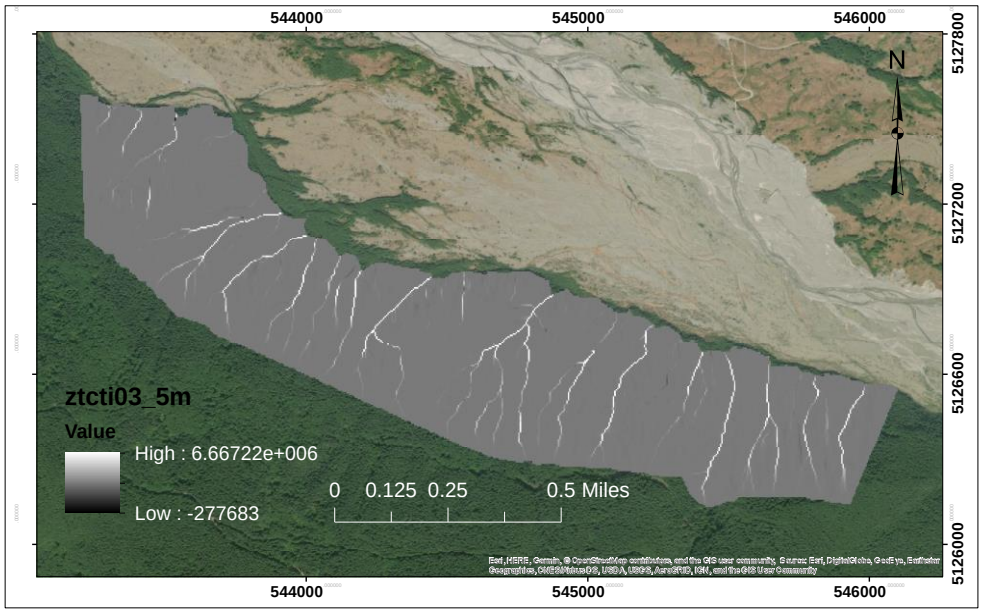

Figure 3.15: CTI values calculated using the 2003, 5m DEM displayed using 'standard deviation'.

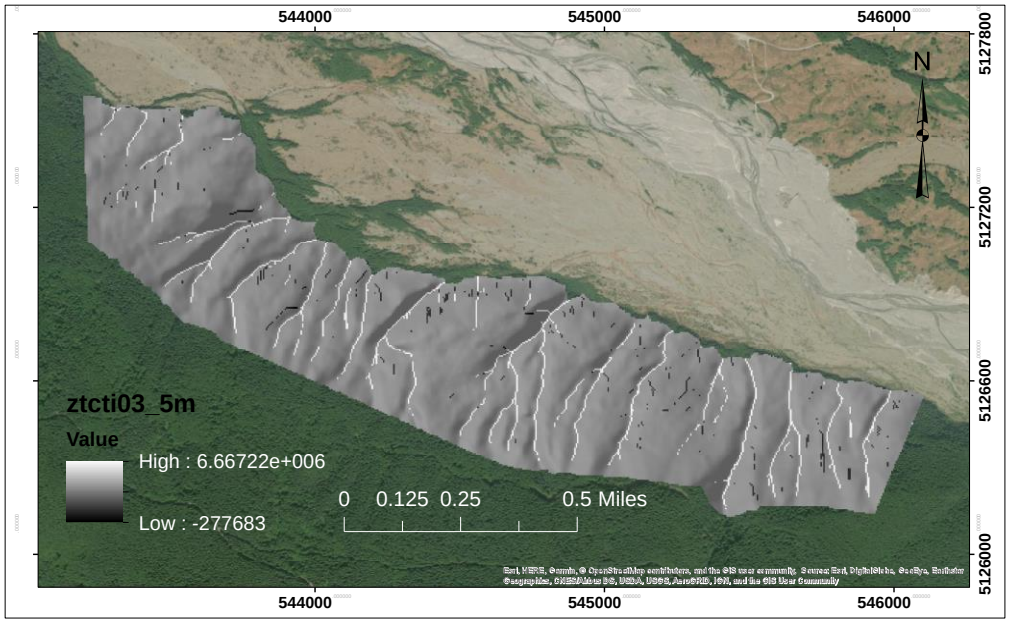

Figure 3.16: CTI values calculated using the 2003, 5m DEM displayed using 'custom stretch'.

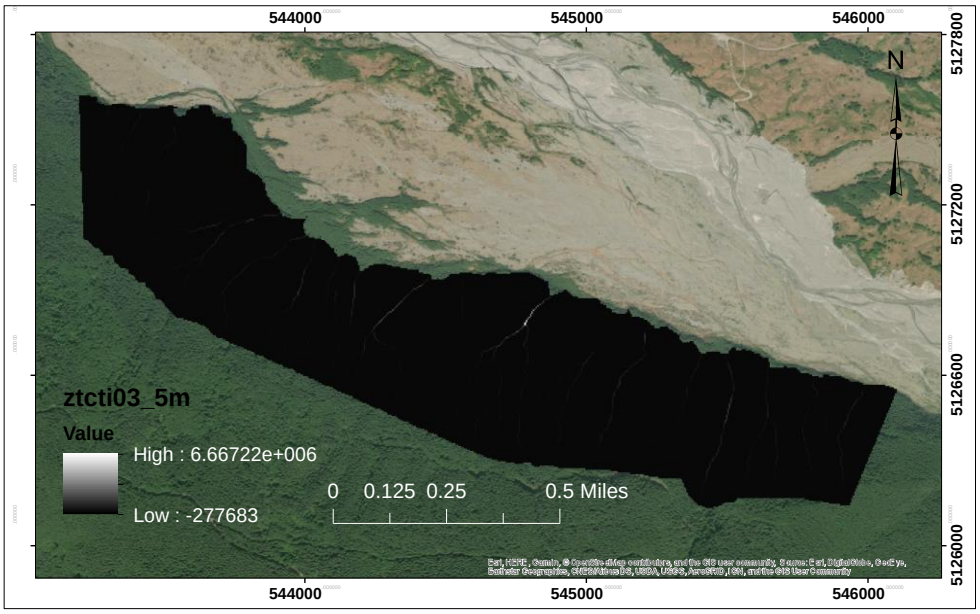

Figure 3.17: CTI values calculated using the 2003, 5m DEM displayed using 'minimum-maximum'.

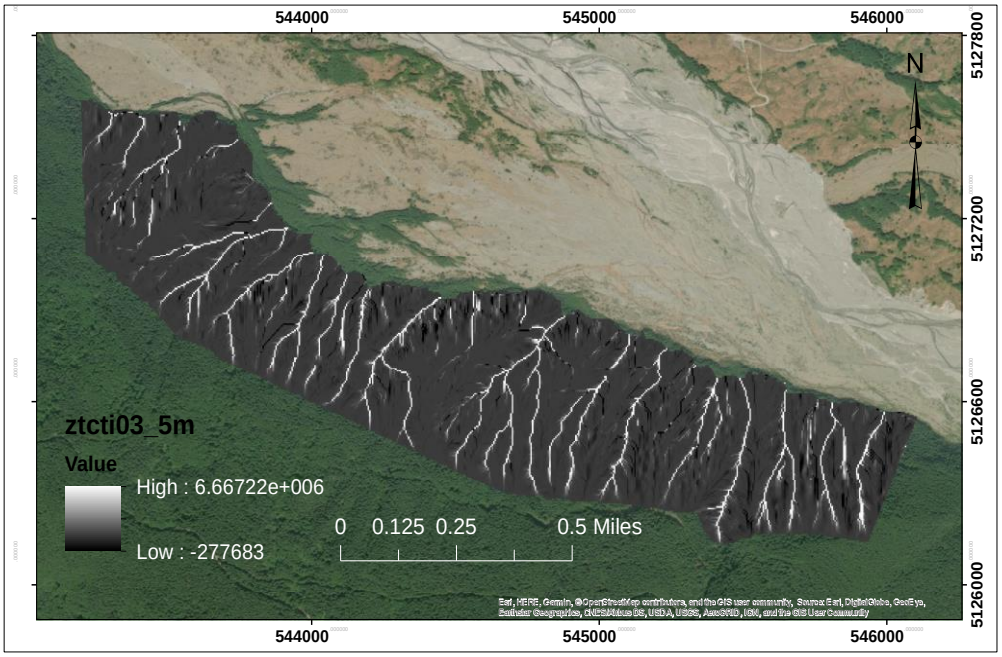

Figure 3.18: CTI values calculated using the 2003, 5m DEM displayed using 'histogram equalize '.

Examining Figure 3.14 to 3.18, it emerges that the clarity with which predicted gully lines are visualised can be significantly enhanced by selection of the appropriate

'stretch'. In my opinion, the best visualisation of results obtained using the CTI1 (with no thresholds) is given by the 'histogram equalise' stretch in Figure 3.18. Based on these findings, it is recommended that either the 'histogram equalise' or 'standard deviation' stretches are used to display CTI values when assessing how well they represent predicted gully lines and whether they concur with 'ground truth' in the form of gullies observed in the field, in aerial images or in DEMs.

3.5.3. **Prediction performance evaluation of CTI using observed gullies at Mt St Helens**

A CTI1_G1

The performance of CTI1_G1 (no critical flow accumulation on the CTI, and no minimum difference for DoD), parameterised using the ROC approach, are presented in Table 3.7

Table 3.7**.** CTI1_G1 of prediction performance evaluation at Mount St Helens.

model	Grid	TN	TP	FN	FP	TPR	TNR	FPR	PPV	NPV	AC	Prevalence
CTI1_G1	5	435	3273	727	725	81.83	37.50	62.50	81.87	37.44	71.86	63.43
	10	430	3231	769	730	80.78	37.07	62.93	81.57	35.86	70.95	62.62
	15	485	3241	759	675	81.03	41.81	58.19	82.76	38.99	72.21	62.81
	20	460	3093	907	700	77.33	39.66	60.34	81.54	33.65	68.86	59.94
	25	470	3079	921	690	76.98	40.52	59.48	81.69	33.79	68.78	59.67
	30	538	2935	1065	622	73.38	46.38	53.62	82.51	33.56	67.31	56.88

At the Mount St Helens study area, areas of gullying could easily be identified in the hill shaded DEMs and this was consistent with the finding that the area of concentrated flow erosion in the DoD was extensive. In the ROC analysis, this is manifest in the values for *Prevalence*, which is the proportion of cells where gully erosion was observed, which ranged from 63.43% to 56.88% (Table 3.8).

CTI1_G1 has very high *Sensitivity* (TPR values) at all grid resolutions. It is interesting is that *Prevalence* decreased little with coarsening grid resolution, remaining within the range 63.43% at 5m to 56.88% at 30 m. The *Accuracy* (AUC) of CTI1_G1 is well above 50% in all cases, ranging from 71.86% at 5 m to 67.31% at 30 m.

High values of TPR, PPV and *Accuracy*, coupled with a relatively high *Prevalence* indicate that when validated against G1, CTI1 has performed well. However, relatively high values of FPR across all resolutions show that many cells which did not have gullies according to the G1 raster were in incorrectly predicted by CTI1 to be experience concentrated flow erosion. This is reflected in relatively low *Specificity* and NPV values. However, overall the model performed well as reflected in the area under the ROC curve (AUC), which was statistically significant at all grid resolutions (Figure 3.19, Table 3.8).

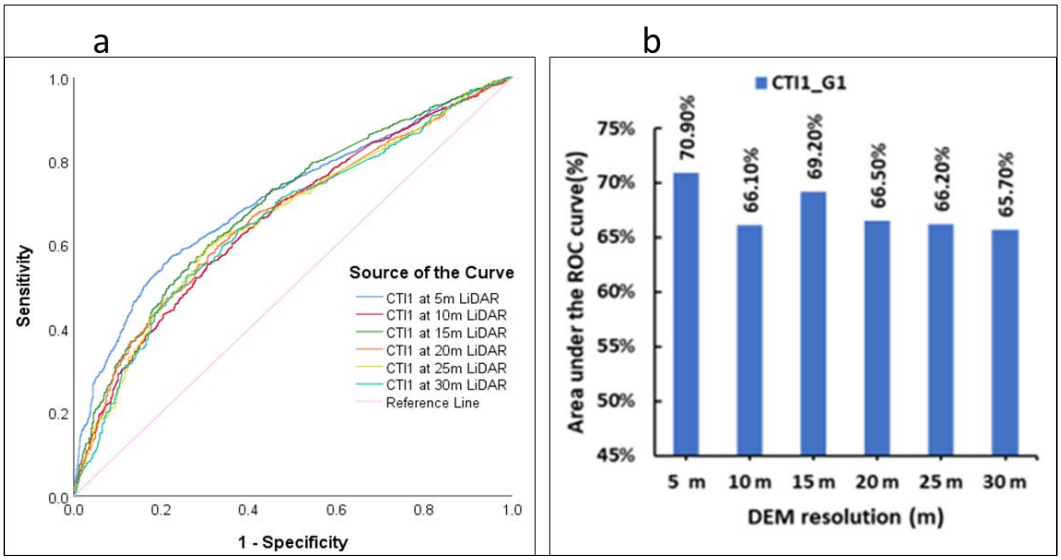

Figure 3.19: (a) ROC curve for predictions based on CTI1 and validation by G1 at 5, 10, 15, 20, 25 and 30 m resolution, (b) AUC values for prediction by CTI1 and validation by G1 at 5, 10, 15, 20, 25 and 30 m resolution.

Table 3.8: Test statistics for Areas Under the ROC Curves for CTI1_G1 presented in Figure 3.19

Test Result Variable(s) i.e CTI1 at various DEM resolution	Area under the curve	Std. Error[a]	Asymptotic Sig.[b]	Asymptotic 95% Confidence Interval	
				Lower Bound	Upper Bound
5m	0.709	0.008	0.000	0.693	0.724
10m	0.661	0.009	0.000	0.644	0.678
15m	0.692	0.008	0.000	0.675	0.708
20m	0.665	0.009	0.000	0.648	0.682
25m	0.662	0.009	0.000	0.645	0.679
30m	0.657	0.009	0.000	0.639	0.674

has at least one tie between the positive actual state group and the negative actual state group. Statistics may be biased. a. Under the nonparametric assumption. b. Null hypothesis: true area = 0.5

For resolutions of 20 m and coarser, AUC decreased as expected, but even at the coarsest resolution a value of 67% was achieved. The AUC for the 10 m DEM is lower than would be expected given the overall, decreasing trend with increasing grid size, without any obvious reason for this anomalously poor performance. This finding further hints the finest grid resolution may not necessarily be optimal for gully prediction for a given terrain, as has been suggested previously by others (Gerrard and Robinson, 1971; Zevenbergen and Thorne, 1987; Zevenbergen, 1989).

B CTI2_G1

ROC characteristics for CTI2_G2 are listed in Table 3.10 and plotted in Figure 3.20. The results reveal that when CTI2 (with a threshold flow accumulation of 80) is validated using G1 (no threshold), TPR is moderately high at 5 m but collapses to very low values at all coarser resolutions. Conversely, high TNR and PPV values at all resolutions suggest that a high percentage of cells that did not actually have gullies were predicted to not be susceptible to gullying.

Specificity appears not only to be relatively high, but increases with coarsening resolution, suggesting that, as the resolution coarsened, the ability of CTI2 to correctly classify cells with no gullies increased, even as its ability to correctly classify cell with gullies declined. This performance may result from the use of a uniform threshold for flow accumulation in CTI2 that does not vary with grid resolution. It appears that this reduced the model's ability to capture gullies present in the G1-defined, 5 m DoD. This is evidenced by the very low *Prevalence* values at 10, 15, 20, 25 and 30m.

Table 3.9: Prediction performance using CTI2 (with critical flow accumulation value) and G1 (without a minimum difference in the DoD).

model	Grid	TN	TP	FN	FP	TPR	TNR	FPR	PPV	NPV	AC	P
CTI2_G1	5	643	2642	1358	517	66.05	55.43	44.57	83.63	32.13	63.66	51.20
	10	1068	672	3328	92	16.80	92.07	7.93	87.96	24.29	33.72	13.02
	15	1071	717	3283	89	17.93	92.33	7.67	88.96	24.60	34.65	13.90
	20	1100	477	3523	60	11.93	94.83	5.17	88.83	23.79	30.56	9.24
	25	1132	250	3750	28	6.25	97.59	2.41	89.93	23.19	26.78	4.84
	30	1146	128	3872	14	3.20	98.79	1.21	90.14	22.84	24.69	2.48

The overall *Accuracy* of the CTI2 model at all but 5 m resolution is poor and, in practice, has little predictive ability. This conclusion is reinforced by the ROC AUC (Figure 3.20 and Table 3.10).

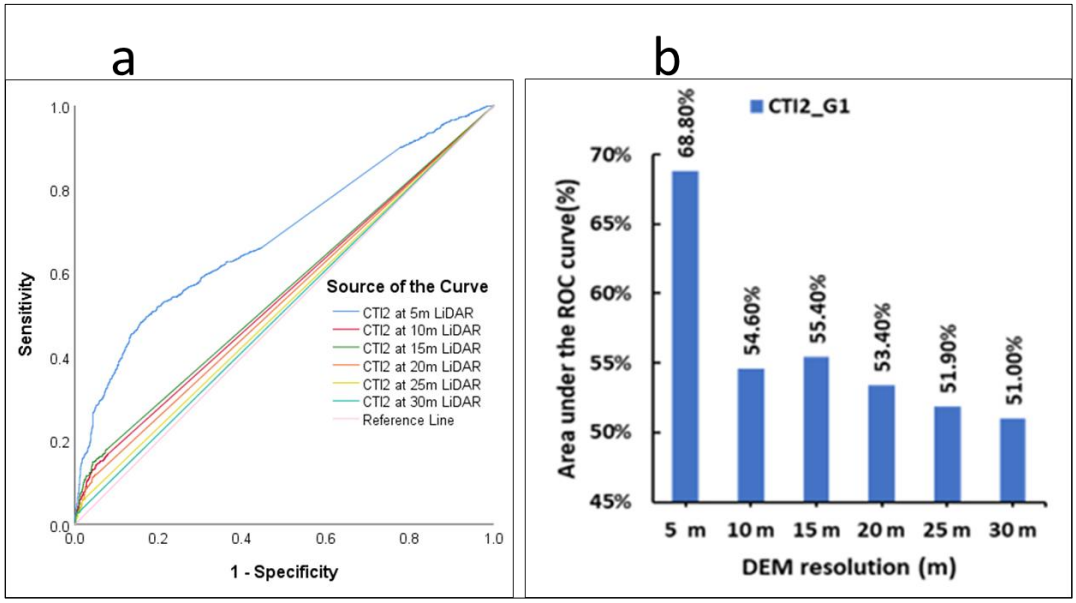

Figure 3.20**.** (a) ROC curve for CTI2 and validation by G1 at 5, 10, 15, 20, 25 and 30 m resolution, (b) ROC AUC values for CTI2 and validation by G1 at 5, 10, 15, 20, 25 and 30 m resolution.

Table 3.10. Areas Under the ROC Curves for CTI2_G1 presented in Figure 3.20.

Test Result Variable(s)	Area	Std. Error[a]	Asymptotic Sig.[b]	Asymptotic 95% Confidence Interval	
				Lower Bound	Upper Bound
5m	0.688	0.008	0.000	0.672	0.704
10	0.546	0.009	0.000	0.528	0.564
15	0.554	0.009	0.000	0.536	0.571
20	0.534	0.009	0.000	0.516	0.553
25	0.519	0.009	0.045	0.501	0.538
30	0.510	0.010	0.296	0.491	0.529

The test result variable(s): has at least one tie between the positive actual state group and the negative actual state group. Statistics may be biased. a. Under the nonparametric assumption. b. Null hypothesis: true area = 0.5

C CTI2_G2

ROC characteristics for CTI2_G2 are listed in Table 3.11. Application of the CTI2 variant, validated using the G2 DoD, resulted in a very high *Sensitivity* when a 5 m resolution grid was used, but it collapsed when the DEM was coarsened to 10 m and then it remained low to extremely low at all other resolutions, decreasing markedly with coarsening resolution above 20 m. *Specificity* was relatively high at all but the highest resolution, and it increased with coarsening resolution, suggesting that, as grid resolution coarsened ability of CTI2 to correctly classify cells without gullies increased even as its ability to correctly classify cell with gullies declined. NPV was very high at 5 m resolution (99%), but it decreased for all other resolutions, to around 80%. Hence, the CTI2, G2 combination did quite well in predicting non-gullied cells where gullies were truly absent from the observed landscape of Mount St Helens.

For grids coarser than 5 m, *Accuracy* is also impressively high and it increases with coarsening grid size. Conversely, Prevalence starts low and becomes vanishingly small with further coarsening of DEM resolution. Basically, the Sensitivity (TPR or ability to correctly predict cells which actually have gullies as defined in G2) is so poor at all the but finest grid sizes that, in practice, it has no utility in trying predict susceptibility to concentrated flow erosion using coarse resolution in data sparse regions. This conclusion is reinforced by the ROC AUC results and statistical test outcomes (Figure 3.21 and Table 3.11).

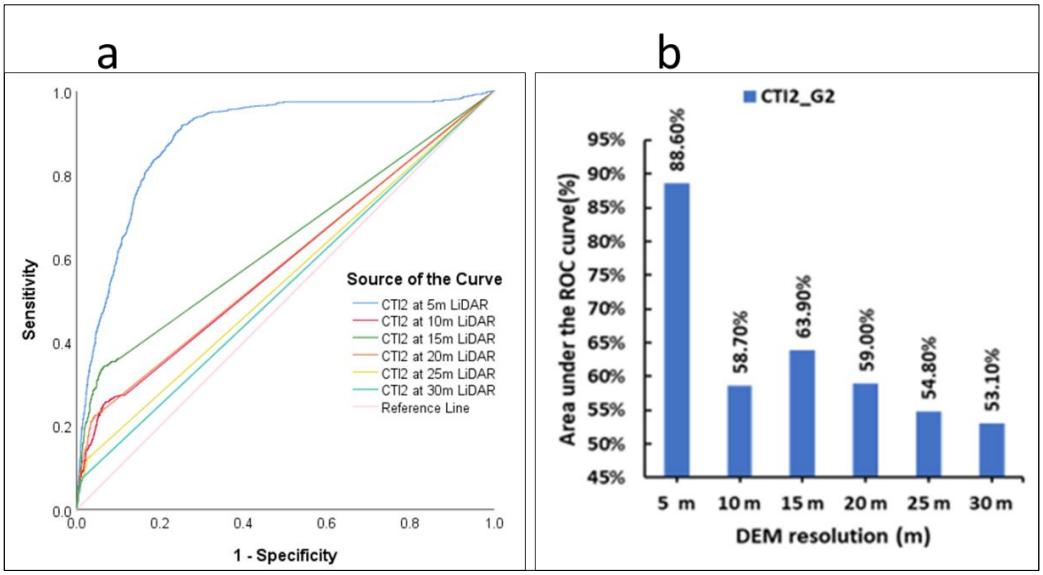

Figure **3.21**: (a) ROC curve for predictions using CTI2 and validation using G2 at 5, 10, 15, 20, 25 and 30 m grid resolutio. (b) ROC AUC results for CTI2 as validated using G2 at 5, 10, 15, 20, 25 and 30 m grid resolutions.

Table 3.11. Areas Under the ROC Curves for CTI2_G2 presented in Figure 3.21.

Test Result Variable(s)	Area	Std. Error[a]	Asymptotic Sig.[b]	Asymptotic 95% Confidence Interval	
				Lower Bound	Upper Bound
5m	0.886	0.006	0.000	0.875	0.897
10m	0.587	0.010	0.000	0.567	0.608
15m	0.639	0.010	0.000	0.618	0.659
20m	0.590	0.010	0.000	0.570	0.611
25m	0.548	0.010	0.000	0.528	0.568
30m	0.531	0.010	0.002	0.511	0.551

The test result variable(s): has at least one tie between the positive actual state group and the negative actual state group. Statistics may be biased. a. Under the nonparametric assumption. b. Null hypothesis: true area = 0.5

D CTI1_G2

ROC characteristics for CTI1_G2 are listed in Table 3.12. When predicted using CTI1 and validated using G2, *Sensitivity* is very high across all grid resolutions although there is a slight decrease at the coarsest resolutions (i.e. 25 and 30 m). *Prevalence* of observed gullies in the study area as defined by G2 remains steady at about 20% for all grid resolutions. Though CTI1 has a very high TPR (i.e. it is highly Sensitive in correctly identifying areas with gullies), the positive predictive value (PPV) indicates

that out of the cells predicted as positive, only 25 to 30% actually featured gullies, according to G2.

This outcome occurs because False Positive Rates (FPRs) are also high for all grid sizes, albeit they are not as high as the True Positive Rates (TPR). The overall *Accuracy* (i.e. capacity to discriminate both TP and TN correctly) is low at all grid sizes, varying between ~42% at 5m, 50% at 30 m, respectively). PPV is dependent on Prevalence, and so the low prevalence of ~20%, is matched by the PPV remaining down at between 25 to 27% throughout the grid resolutions. Prevalence is a function of the number of observed gullies (i.e. gullies represented by G2 in the 5m DoD. G2 has critical values for both vertical erosion (DoD < -1.5) and flow accumulation (flow accumulation ≥ 80). The implication is that imposition of these thresholds may have excluded too many real gullies from the 'ground truth' against which CTI1 predictions are validated. This is possible because CTI1 (which uses no critical value for minimum flow accumulation) is very sensitive to detecting concentrated flow, meaning it picks up larger areas where concentrated overland flow occurs, but from which G2 eliminates the possibility of gullies being recorded in the 'ground truth' due to their small contributing drainage areas.

Table 3.12**:** Prediction performance of the CTI2_G1 model at Mount St Helens through ROC.

model	Grid	TN	TP	FN	FP	TPR	TNR	FPR	PPV	NPV	AC	P
CT1_G2	5	1134	1063	28	2935	97.43	27.87	72.13	26.59	97.59	42.58	20.60
	10	1158	1050	41	2911	96.24	28.46	71.54	26.51	96.58	42.79	20.35
	15	1217	1064	27	2852	97.53	29.91	70.09	27.17	97.83	44.21	20.62
	20	1335	1059	32	2734	97.07	32.81	67.19	27.92	97.66	46.40	20.52
	25	1337	1037	54	2732	95.05	32.86	67.14	27.51	96.12	46.01	20.10
	30	1545	1033	58	2524	94.68	37.97	62.03	29.04	96.38	49.96	20.02

In summary, CTI1_G2 Sensitivity is very high, but its PPV is very low (Table 3.12). AUCs are impressively high (compared to the base value of 50%) at all grid resolutions (Figure 3.22;Table 3.12). For coarser resolutions of 20, 25 and 30 m, *Accuracy* decreased as expected, but a value of 81% was recorded even at the coarsest resolution. Again, *Accuracy* for the 10m DEM is lower than would be expected. Therefore, it is concluded that further investigation in this thesis is

necessary to establish whether using CTI1 (that is a CTI computed with no critical value for flow accumulation) and validation using G2 (that is 'ground truth' based on excluding nodes in the DoD with elevation changes < -1.5 m and flow accumulation values smaller than 80) can lead to better capability to predict susceptibility to gully erosion when using coarse resolution DEMs in data sparse regions.

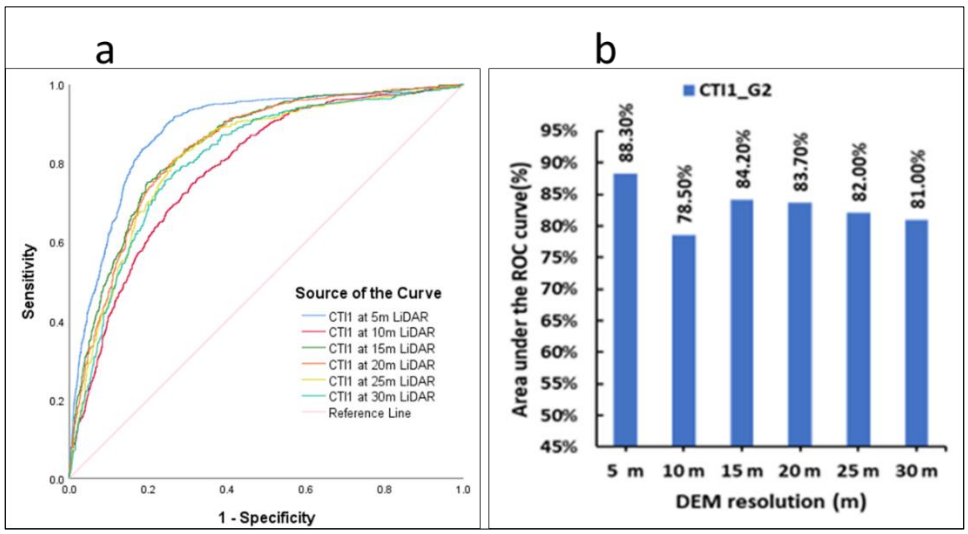

Figure 3.22**:** (a) ROC curves for prediction of gullies using CTI and validation using G2 at 5, 10, 15, 20, 25 and 30 m resolutions. (b) AUCs for CTI1 and validation using G2 at 5, 10, 15, 20, 25 and 30 m resolutions.

Table 3.13**.** Areas Under the Curves for CTI1_G2 presented in Figure 3.30.

Test Result Variable(s)	Area	Std. Error[a]	Asymptotic Sig.[b]	Asymptotic 95% Confidence Interval	
				Lower Bound	Upper Bound
5 m	0.883	0.006	0.000	0.871	0.894
10 m	0.785	0.007	0.000	0.770	0.800
15 m	0.842	0.006	0.000	0.830	0.855
20 m	0.837	0.006	0.000	0.824	0.849
25 m	0.820	0.007	0.000	0.806	0.834
30 m	0.810	0.007	0.000	0.796	0.824

The test result variable(s): has at least one tie between the positive actual state group and the negative actual state group. Statistics may be biased. a. Under the nonparametric assumption. b. Null hypothesis: true area = 0.5

3.5.4. **Comparing and Ranking the predictive abilities based on their Accuracies**

The predictive accuracies of the four CTI+G model and ground truth combinations at each resolution are presented in Figure 3.23, with CTI1_G2 performing the best at all resolutions.

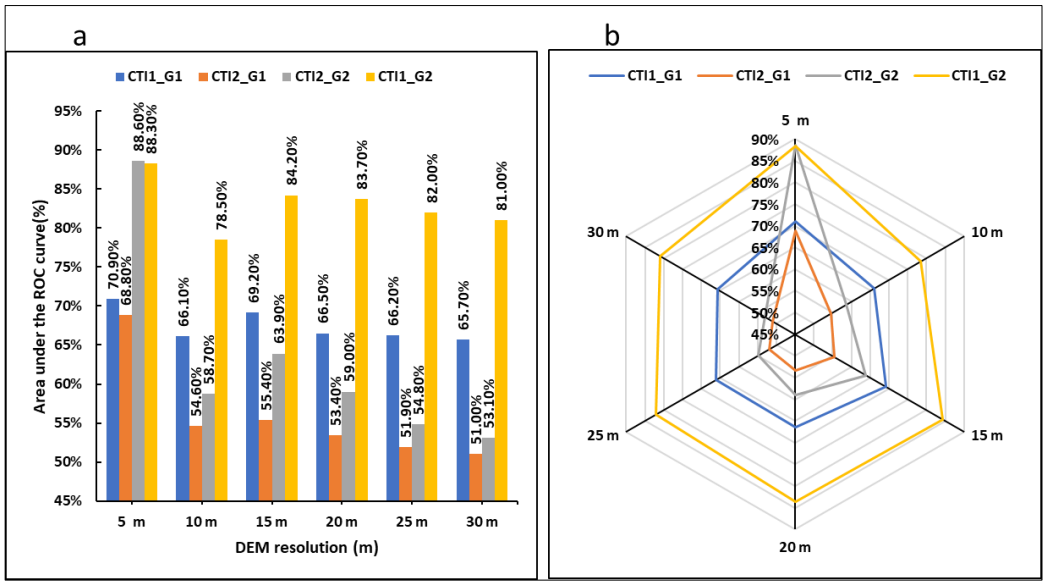

Figure 3.23**.** Areas under the ROC curves for prediction of gully suceptibility based on validation Versions 1 to 4 at Mount St Helens, under a range of grid resolutions.

3.6. **Discussion and conclusion**

At Melton Farm, the CTI model based on a 5m DEM performed well and this confirms the validity of using the CTI with a field-calibrated threshold CTI of 36, as concluded by previous research at that study site. However, in this investigation, CTI based on a 30m DEM performed weakly. It may be the case that when other factors influencing susceptibility to erosion are put together with the 30 m resolution CTI, its predictive performance may improve. The way to go about doing so must be carefully considered, bearing in mind that the CTI is not an empirical regression fit and so, as Parker *et al.* (2007) observed, its validity does not depend on independence of the input variables.

At Mount St Helens, the highest prediction *Accuracy* was achieved using the CTI1_G2 combination. The accuracy for this model (i.e. no critical flow accumulation value in calculating the CTI, and in the DoD, a minimum (critical) flow accumulation

value of 80 and only vertical elevation changes <-1.5) was 88% at a 5 m grid size, and only decreased to 81% at a 30 m grid size. Set against this excellent performance in terms of Accuracy is CTI1_G2's high FPR, which ranged between 72 and 62% for DEM resolutions of 5 and 30 m, respectively.

Second to CTI1_G2 in overall predictive performance was CTI1_G1. Omitting a minimum flow accumulation area gives CTI1_G1 an advantage with respect to validation in many data spare regions, where it may be difficult or even impractical to select a suitable critical flow accumulation area value for use in either calculating CTI values or 'ground truthing' gullies, or both. Even if field-mapped gullies exist for validation of the selected CTI model, their extents and characteristics may be poorly defined, complicating the setting of a reliable minimum flow accumulation area at which they exist.

On the other hand, when reliable field observations or remotely-sensed data defining 'ground truth' gullies does exist, CTI1_G2 can adopt the approach developed by previous researchers (Parker *et al.*, 2007; Daggupati *et al.*, 2009; Daggupati *et al.*, 2013; Daggupati *et al.*, 2014; Sekaluvu *et al.*, 2015; Sheshukov, 2015; Sheshukov *et al.*, 2018) in which, when validating predictions against known gullies, the optimum critical value for concentrated flow erosion to be considered as having formed a true gully is determined by matching the field data with model prediction through iterative manipulation of the symbology.

Despite its strengths in some performance measures, CTI1_G2 has a high FPR and lacks the ability to correctly predict true gullies even though its PPV is good. CTI1_G2 limitations mean it can only be used under a restricted range of special cases, as mentioned in the paragraphs above.

Given the restricted applicability of CTI1_G2, the recommendation that emerges from the validations reported in this chapter is to adopt the next best version, which is CTI1_G1 when predicting susceptibility to concentrated flow erosion in data sparse regions with coarse DEMs and potentially unreliable ground truth data. Given that CTI1_G1 is not based on critical (minimum) values for flow accumulation

or differences in the DoD, it provides a more pragmatic option which, despite having lower accuracy, is more widely applicable, globally.

In conclusion, based on the validations described in this chapter, it is possible to use a 30 m DEM to identify areas topographically-susceptible to gullying. The question of whether the CTI model can actually be further modified and developed to improve its performance in predicting areas susceptible to gullying at 30 m resolution is addressed in Chapter 4. More specifically, as the research has sharpened the focus on identifying the degree of susceptibility to concentrated flow (rather than the specific locations of gullies), the possibility arises that techniques of fuzzy logic (which is known for its ability to deal with degrees of membership rather than ambivalent classification) may further improve the candidate CTI model (CTI1 with no critical value for flow accumulation) to better predict topographic-susceptibility to concentrated flow erosion in data sparse regions. These and other issues are explored in the next chapter. The question of whether taking other environmental factors aside from topography into account can make it possible to use a 30 m DEM to predict where in a landscape concentrated flow is likely to be sufficiently strong to initiate and maintain a gully, is addressed in Chapter 5.

CHAPTER 4: NEW VERSION OF THE CTI MODEL, BASED ON FUZZY LOGIC

4.1. Introduction

The aim of this chapter was to 'fuzzify' the CTI and assess its performance relative to the original CTI, creating a new version that offers an outcome representing the confidence placed in predictions of topographic-susceptibility to concentrated flow erosion, rather than the binary outcome (concentrated flow erosion, or no concentrated flow erosion). 'Fuzzification' was achieved by modifying the three inputs to the CTI (local slope, flow accumulation and planform curvature) using a fuzzy logic approach. It was hypothesised that the resultant, fuzzy CTI model should offer improved performance over the original, binary CTI model, when applied using DEMs with 30 m grid resolutions and low-quality data to predict areas susceptible to concentrated flow erosion.

4.2. Chapter Objectives

The specific objectives of this chapter were to:

4.1. develop a fuzzy logic-based version of the CTI, hereafter called fuzzy CTI, using the 2003, 30m DEM of the study area at Mount St Helens that was previously used in Chapter 3;

4.2. validate the fuzzy CTI using the 2003-2009 DoD and evaluate the predictive performance using analysis of the Receiver Operator Characteristics (ROC);

4.3. compare the predictive performance of the fuzzy CTI with that of the original CTI when applied to the same area, using the same DEM (as reported in Chapter 3);

4.4. produce original and fuzzy CTI using a 30 m, USGS-sourced, Shuttle-based DEM at Mount St Helens and compare the results with those produced from the USACE, airborne LiDAR-based, 30 m DEM.

4.3. Literature review

4.3.1. Topographic modelling with continuous variables

DEMs and many of their topographic derivatives (e.g. slope, flow accumulation and planform curvature) are expressed as continuous variables. This means that

coarsening resolution inevitably leads to a loss of detail and precision in topographic attributes. This poses a problem when attempting to categorise topographic data or determine critical values, because it is unlikely that a specific threshold value represents a true Boolean case. This is because a Boolean classifier assumes exactness in the description and also precision in the measurement of natural phenomena. Neither assumption is likely to be met in practice.

Raster and vector map data categorise continuous data and this accentuates interpolation errors as well as introducing additional errors. When topographic data are used in modelling, these errors are passed onto the results of the model, especially when boundaries are modelled using Boolean classes (Heuvelink, 1998, 2002).

The alternative of modelling a continuum, in which boundaries are vague or imprecise, has resonated with human thinking from time immemorial. In attempting to solve mathematical problems with such data, Zadeh (1965) considered the development of human-like logic and instigated a branch of mathematics called 'fuzzy logic', which simply infers 'fuzzy thinking', and this was subsequently popularised by Zadeh and his followers (Kosko and Toms, 1993). According to Zadeh (1965) as quoted by Negnevitsky (2005, pp.89),

"fuzzy logic is determined as a set of mathematical principles for knowledge representation based on degrees of membership rather than on the crisp membership of classical binary logic. Unlike two-valued Boolean logic, fuzzy logic is multi-valued. It deals with degrees of membership and degrees of truth. Fuzzy logic uses the continuum of logical values between 0 (completely false) and 1 (completely true). Instead of just black and white, it employs the spectrum of colours, accepting that things can be partly true and partly false at the same time".

Negnevitsky (2005, pp.89) distinguished classical binary logic from fuzzy logic, which extends the range of logical values from Boolean logic, using Figure 4.1.

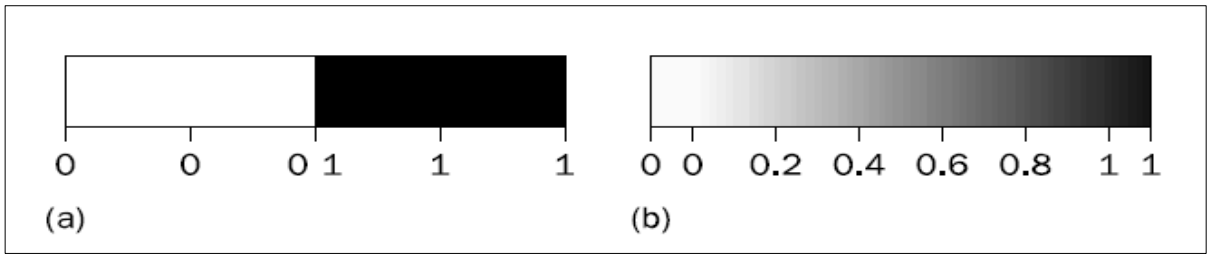

Figure 4.1: Visualisation of (a) classical binary logic and (b) fuzzy logic. Reproduced from Negnevitsky (2005).

Comparison of error propagation by Boolean and fuzzy logic-based classifications has demonstrated that the latter is far less sensitive to small errors in data, under circumstances where values are close to thresholds or class boundaries (Heuvelink and Burrough, 1993). A discussion of modelling the location of landform features in geomorphometry (specifically, Helvellen Mountain) using a fuzzy logic approach in a GIS substantially increased the uptake of fuzzy approaches in geoscience (Fisher *et al.*, 2004; Arrell *et al.*, 2007). Partially as a result of these papers, the application of fuzzy logic to solve problems in the environmental, earth and geosciences has increased over the last two decades.

4.3.2. **Using fuzzy logic in topographic analysis**

Using conventional or classical mathematics to combine topographic attributes such as slope, contributing area, and planform curvature, which are by their nature fuzzy, to develop topographic indices with which to predict phenomena such as variable or partial source areas and erosion is not unusual in geomorphology and other sciences (Yang, 1979; Thorne *et al.*, 1988; Mitasova *et al.*, 1996; Vandaele *et al.*, 1996a; Knighton, 1999; Kakembo *et al.*, 2009; Parker *et al.*, 2011; Torri *et al.*, 2012; Aiello *et al.*, 2015; Zakerinejad and Maerker, 2015; Dumitriu, 2016; Lin *et al.*, 2016; Angileri *et al.*, 2016; Wells *et al.*, 2016; Zheng *et al.*, 2017; Kornejady *et al.*, 2017; Mararakanye and Sumner, 2017). The CTI is just one such model (Parker *et al.*, 2007), which is evaluated using a mathematically simple product of flow accumulation (upslope contributing area), local slope and planform curvature.

However, if boundary conditions are to be more realistically modelled, use of fuzzy logic rather than Boolean logic, may have an advantage.

Another compelling reason to deploy fuzzy logic in modelling landforms is due to errors inherent in globally available data (e.g. USGS 30 m DEMs). In this context, Parker *et al.* (2007) opined that these coarse DEMs were unsuitable for predicting the locations of gullies using the CTI. They supported their opinion by citing the work of Wolock and Price (1994), who identified errors in using original source data (contour maps) to create DEMs, and the effects of the map scale in producing DEMs. The process of interpolating DEMs from contour lines (McCullagh, 1998) and projection issues due to the study site situation can also introduce errors into DEMs. Studies have shown that systematic errors within the USGS 10 m and 30 m DEM are often compounded in calculated terrain attributes such as the slope, curvature and upstream area (Bolstad and Stowe, 1994; McKenzie et al., 2000).

Heuvelink and Burrough (1993) hypothesised that transforming topographic attributes calculated from DEMs using fuzzy logic could help improve predictive models, especially where the interest is in modelling the susceptibility of areas to surface processes, rather than attempting to predict the specific locations of local features produced by those processes.

Zhu *et al.* (2001) mapped soils in a GIS based on expert knowledge and fuzzy logic. In fact, there is a catalogue of applications of fuzzy logic in soil science (McBratney *et al.*, 2003; Antoniol *et al.*, 2003; Bui, 2004; Shi *et al.*, 2004; Qi *et al.*, 2006).

In landform mapping, Schmidt and Hewitt (2004) undertook a fuzzy land element classification from Digital Terrain Models (DTMs) based on terrain geometry and position. Fisher *et al.* (2004) explored the location of landforms through fuzziness of multi-scale landscape morphometry and Arrell *et al.* (2007) carried out a fuzzy classification of elevation derivatives to extract the morphometric classification of landforms in Snowdonia, Wales. Summerell *et al.* (2005) used the Fuzzy Landscape Analysis Geographic Information System (FLAG) model to delineate the major landforms of catchments in a hydrological terrain analysis.

In summary, there are numerous applications of fuzzy logic in the geosciences literature (Frank, 2011; Evans, 2012; Saleh and Belal, 2014; Haider *et al.*, 2015; Bigdeli *et al.*, 2015; Vanegas *et al.*, 2016; Veitinger *et al.*, 2016; Viloria and Pineda, 2016; Noto *et al.*, 2017).

4.3.3. **Fuzzy logic and land surface erosion modelling**

Guesgen *et al.* (2000) applied fuzzy values of slope, annual precipitation, soil, vegetation and geology when using a raster-based GIS to predict and map the degree of erosion. Indeed, during the twenty first century, prediction of soil erosion has benefited from multiple, fuzzy logic approaches (Burrough *et al.*, 2000; MacMillan *et al.*, 2000; Antoniol *et al.*, 2003; Summerell *et al.*, 2005; Sriti *et al.*, 2005; Dragut and Blaschke, 2006; Arrell *et al.*, 2007; Minar and Evans, 2008; Bock, 2010; Svidzinska, 2011; Evans, 2012). Even before 2000, Mitra *et al.* (1998) applied fuzzy logic to predict soil erosion in a large watershed. More recently, Noto *et al.* (2017) used an integration of fuzzy logic and image analysis from airborne LiDAR to detect gullies in the Calhoun Critical Zone Observatory. This study used a very high-resolution LiDAR DEM and the approach differs from the CTI model in terms of the rationale used to select and combine topographic attributes to detect gullies. In their test area, Noto *et al.* (2017) used LiDAR-derived DEMs with grid resolutions of 10, 20 and 30m to compute normalised Topographic Position Indices (nTPIs), which were fuzzified and combined into a single gamma distribution for gully bottom delineation. They then used the 10m DEM alone to compute two further topographic indices (maximum curvature (Cmax), MinMax), which were fuzzified and combined into another gamma distribution. That gamma distribution was combined with the Vosselman index for gully edge delineation. They then combined the fuzzy bottom and edge delineations with an arbitrary threshold value for maximum depth, to detect fuzzy gullies (Figure 4.2). Noto *et al.* (2017) validated the model using a kappa index (K), achieving a very high degree of agreement (k = 0.876). It is however worth noting that generating this agreement required use of a high resolution (10m) DEM. It also used a threshold value of maximum depth to

identify when concentrated flow erosion was sufficiently deep to constitute a gully. Hence, validation of the approach proposed by Noto *et al.* (2017) was dependent on both the availability of a high resolution DEM and selection of a threshold depth for gully identification.

While the research reported by Noto *et al.* (2017) provides useful insights regarding the potential utility of fuzzy logic in prediction of susceptibility to concentrated flow erosion and gully formation, in its published form it cannot be applied to data sparse regions and it remains dependent on a user-selected or field-calibrated threshold value. In these respects, the research reported later in this chapter goes beyond the method proposed by Noto *et al.* (2017).

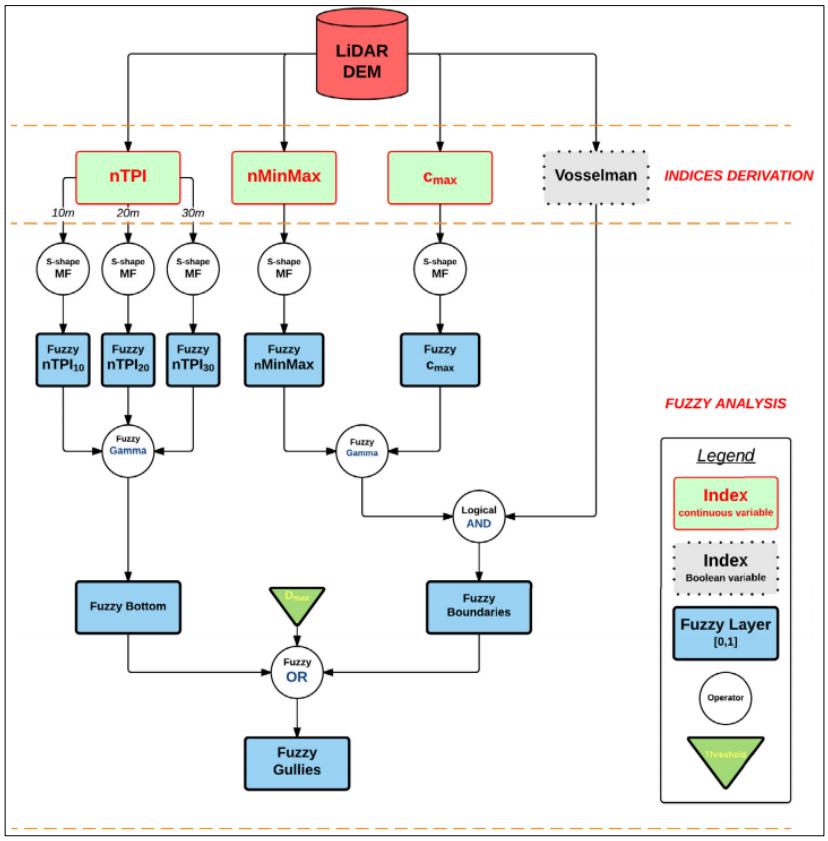

Figure 4.2: Flow chart of gully detection algorithm proposed by Noto *et al.* (2017). This is part II, which supports identification of the gully boundary through image analysis.

Recognising the benefits that fuzzy logic can provide in modelling environmental processes and features, and its wide use in academia and beyond, it was decided to investigate how fuzzy logic could be used in further developing the CTI model. To ensure that the resulting fuzzy CTI model would be accessible to users in LEDCs, it was decided to use only open source and easily available software, including MATLAB, Python, R, SAGA, ArcGIS, QGIS and Grass GIS. The rationale behind the CTI equation is scientifically sound and pragmatic, and its capability to detect and predict concentrated flow erosion leading to gullying on arable and disturbed lands has been proven both in past research and that reported in Chapter 3. However, as already note in Chapters 1 and 3, the applicability of the current CTI model is restricted to data rich regions. This review of the literature on fuzzy logic suggests that fuzzifying the CTI model might allow its applicability to be extended to data sparse regions. This would open up the possibility of using the new Fuzzy CTI to predict susceptibility to concentrated flow erosion and gullying in areas of data sparse regions where it is has become a menace, such as Nigeria (see for example: https://www.bbc.com/news/av/world-africa-48463191/our-village-is-disappearing-due-to-erosion (BBCNews, 2019)

and:

http://www.theguardian.com/world/2018/apr/01/argentina-new-river-soya-beans (Goñi, 2015).

4.4. **Methodology**

4.4.1. **Expert-based knowledge concerning topographic parameters**

The first step in creating a fuzzy logic model (which is a form of expert system), is acquiring expert-based knowledge. In this study, I drew on existing work by experts that demonstrates that where accumulating flow is concentrated due to planform concavity on hillslopes, the initiation of concentrated flow erosion becomes possible (Thorne *et al.*, 1984b; Thorne, 1984a; Thorne *et al.*, 1984c; Thorne and Zevenbergen, 1984; Thorne *et al.*, 1986; Thorne *et al.*, 1987). If such conditions

persist downstream, a gully can be initiated. First, an ephemeral gully forms, but this can develop into a classical gully that extends the drainage network headward. Factors influencing ephemeral gully formation, as outlined by Zevenbergen (1989) include:

1. overland flow discharge and duration, without which ephemeral gullies could not exist;
2. slope and flow depth, which determine the magnitude of the flow's downslope component of weight and, therefore, the boundary shear stress exerted by the flowing water on the soil;
3. planform curvature, which determines the local flow convergence and, therefore, the concentration of stress along a flow path or swale;

This knowledge is captured by the CTI mathematically, as described in previous chapters and has already been automated in a GIS. Experts have also led us to understand that when the performance of CTI a model for predicting concentrated flow is compared with other models doing the same thing, based on a high resolution and good quality DEM, the CTI out-performs the alternative approaches (Momm *et al.*, 2011a; Daggupati *et al.*, 2013; Daggupati *et al.*, 2014; Sekaluvu *et al.*, 2015; Sheshukov *et al.*, 2018; Ruiz *et al.*, 2007). The understanding that slope, flow accumulation and planform convergence are measured on interval and ratio scales and are thus essentially continuous variables has also become commonplace. It is universally accepted that, given the unavoidable errors and uncertainties with measuring topographic attributes, these parameters are, by their nature, fuzzy variables.

4.4.2. **Expert knowledge-based rules and knowledge-based systems.**

The second step in creating a fuzzy logic model is the development of knowledge-based rules for the fuzzy expert systems, based on knowledge acquired from human experts. The heuristic conditional knowledge representation for CTI would be translated in IF-THEN statements as:

IF slope > a given threshold AND flow accumulation > a given threshold AND given planform concavity > threshold,

THEN concentrated flow is initiated.

The given threshold in each case could be a value >0, which would mean that if all 3 conditions are positive, there is a possibility of concentrated flow erosion although, if all 3 values are relatively small then the probability of concentrated flow erosion is low, while if all 3 values are relatively great then the probability of concentrated flow erosion is high.

It is in this context that fuzzy logic becomes useful. Slope, flow accumulation and planform concavity are linguistic or 'fuzzy' variables. For example, slope may be defined using linguistic values such as 'level', 'almost level', 'very gently sloping', 'gentle slope', 'moderate slope', 'moderately steep slope', 'steep slope', 'very steep slope', 'almost precipitous slope', 'precipitous slope', and 'almost vertical slope'. Similar adverbs and adjectives (linguistic values) can be used to qualify flow accumulation and planform curvature. The expert knowledge-based rules for a fuzzy expert system will then mainly convey a linguistic value. For example:

IF slope is increasing AND flow accumulation is more AND plan concavity is increasing

THEN increasing concentrated flow

What the linguistic values are doing to the fuzzy variables is annotating their fuzziness. This prompts the modeller to consider all variables on a scale of 'degree of truth' (or degree of membership). In fuzzy logic, the highest and lowest values of the fuzzy variable are represented by 0 and 1, respectively. A value of 1 means 'full membership of the variable' and a value of 0 means 'not a member of the variable'. Values between these extremes represent varying degrees of membership (or truth).

4.4.3. **Fuzzification**

The third step in creating a fuzzy logic model (or an expert system) is to convert the variables that are considered to be fuzzy in nature into actual fuzzy variables, using their linguistic values. Membership functions handle the linguistic transformation. Several types of membership functions are used in fuzzy expert systems, and these are catalogued in the literature relating to fuzzy logic (Bellman and Zadeh, 1970; Mamdani, 1974; Mamdani and Assilian, 1975; Zadeh, 1976; Zadeh, 1983; Takagi and Sugeno, 1985; Burrough, 1989; Salski, 1992; McNeill and Freiberger, 1994; Zadeh, 1996a; Zadeh, 1996b; Zadeh, 1997; Schmidt and Hewitt, 2004; Negnevitsky, 2005). These membership functions have been used in a wide variety of ways by geographers (Irvin *et al.*, 1997; Nisar Ahamed *et al.*, 2000; Carre and Girard, 2002; Drăguţ and Blaschke, 2006; Qi *et al.*, 2006; Evans, 2012; Gorsevski *et al.*, 2012; Pu and Bell, 2013; Silvan-Cardenas and Wang, 2014; Pipaud and Lehmkuhl, 2017).

In this research, fuzzy logic has been implemented in ArcGIS. The fuzzy overlay tool in ArcG10.4 was used to create a fuzzy version of the CTI model, using an existing, linear membership function that transforms linguistic values of the fuzzy variable into the corresponding number equivalences of their linguistic values. The linear function assigns a membership value of 0 at the minimum and a membership of 1 at the maximum. Fuzzy set qualifiers or 'hedges' are used to modify the shape of fuzzy sets by using adverbs such as "very", "somewhat", "quite", "more or less" and "slightly" via mathematical operations as follows:

SOMEWHAT: when applied, the SOMEWHAT hedge increases the fuzzy membership function. It is a dilation function to the fuzzy membership function. A typical dilation function takes the square root of the fuzzy membership function, as in Equation 4.1.

$$\sqrt{[\mu_A(x_i)]} \qquad \text{Equation 4.1}$$

VERY: when applied, VERY decreases the fuzzy membership functions. It is obtained by taking the square of the fuzzy membership function. It is a concentration

function, narrowing a set and thus, reducing the degree of membership of fuzzy elements. This operation is given as a mathematical square (Equation 4.1)

$$[\mu_A(x_i)]^2 \qquad \text{Equation 4.2}$$

EXTREMELY: Extremely serves the same purpose as VERY, but does it to a greater extent. This operation can be performed by raising membership to the third power, as in Equation 4.3:

$$[\mu_A(x_i)]^3 \qquad \text{Equation 4.3}$$

VERY VERY: VERY VERY is a further extension of concentration. It can be given as raising membership by the power of four, as in Equation 4.4:

$$[\mu_A(x_i)]^4 \qquad \text{Equation 4.4}$$

Shapes associated with the mathematical operation of the hedges are illustrated in Figure 4.4. Hedges for fuzzy membership function are used optionally. Hedges when applied increase or decrease the fuzzy membership thus modifying the meaning of a fuzzy set but basically assigns a membership value of 0 at the minimum and a membership of 1 at the maximum based on a membership function.

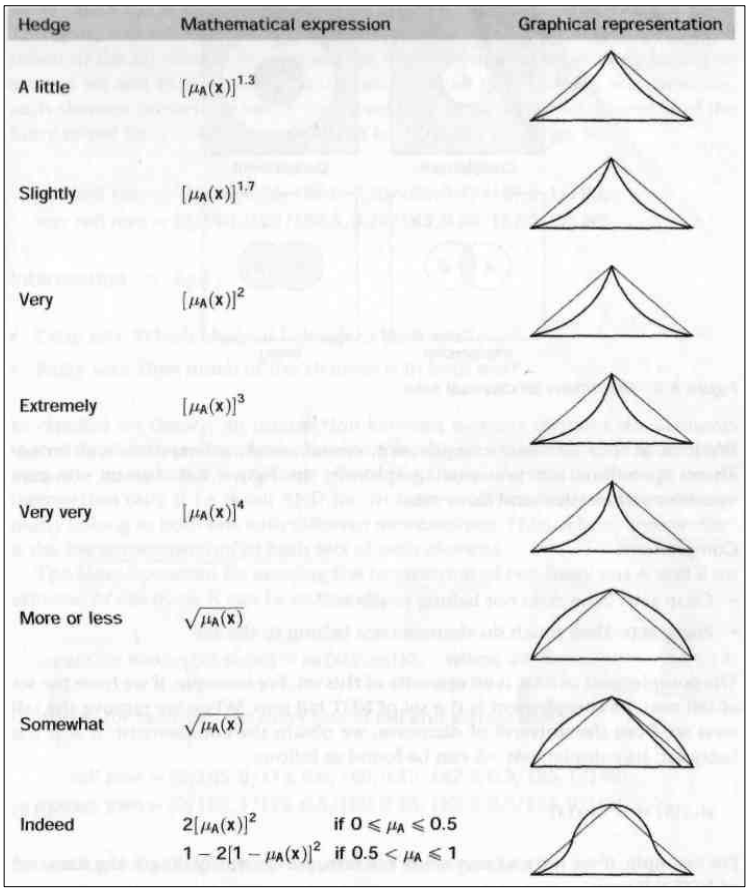

Figure 4.3: Hedge expressions and their graphical representations. After Negnevitsky (2005)

MORE OR LESS: More Or Less, the operation of dilation, expands a set and thus increases the degree of membership of fuzzy elements. It is very similar to the somewhat hedge and shares the same mathematical formula (Equation 4.1), but it differs slightly in its diagrammatic representation as shown in Figure 4.3.

INDEED: Indeed intensifies the meaning of the whole sentence. It can be used by increasing the degree of membership above 0.5 and decreasing those below 0.5. The hedge "indeed" is given as Equation 4.5 and illustrated in Figure 4.3:

$$2[\mu_A(x_i)]^2 \qquad \text{Equation 4.5}$$

In this study, The SOMEWHAT hedge was applied because the intention is to increase the fuzzy membership functions of flow accumulation, slope and planform curvature using a dilation function (Figure 4.4).

Mathematically, fuzzy membership is denoted by; $\mu_A(x_I)$, and it is translated using the fuzzy membership function in ArcG10.4, as shown in Figure 4.4

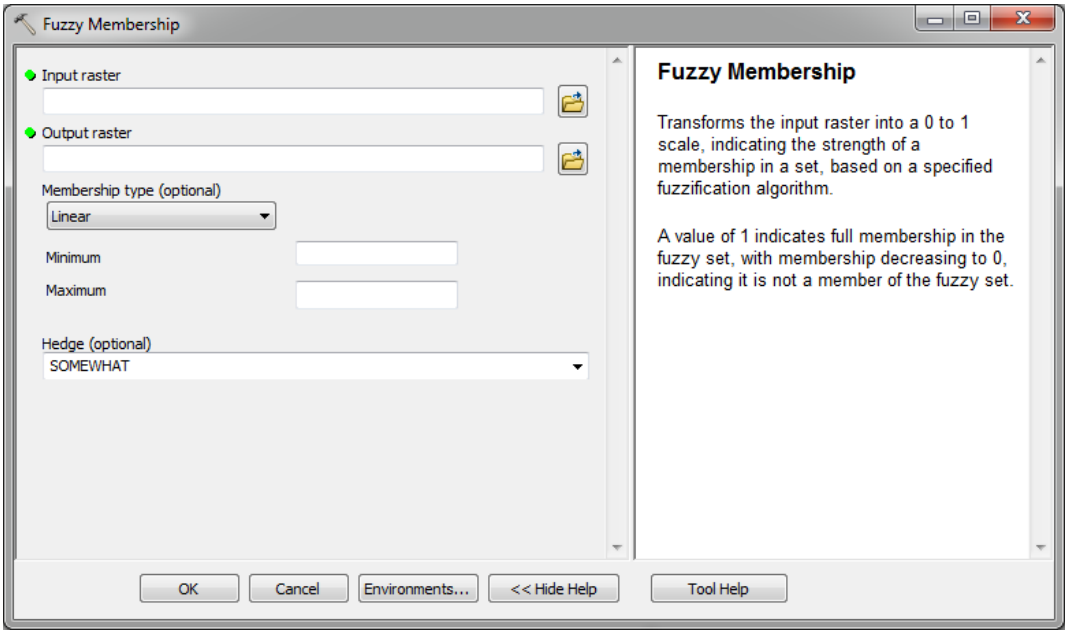

Figure 4.4: Fuzzy Membership type and Hedges in ArcGIS 10.4.

4.4.4. **Fuzzy Rule evaluation**

The development of the fuzzy CTI through a fuzzy overlay of variable membership requires fuzzy evaluation rules. The product of flow accumulation, planform concavity and slope indicate where these three conditions are met, which can also be thought of as the intersection of these three variables. In fuzzy logic, the AND operator enables calculation of the intersection of variables in the same way, and allows the user to extract the values that are common to all sets (Figure 4.5). The AND operator can be distinguished from the OR operator in that when the fuzzy AND overlay type (Equation 4.6) is used to combine fuzzy memberships, the intersection is evaluated and the minimum value from all of the fuzzy input

memberships (evidence) is outputted. In contrast, the Fuzzy OR operator (Equation 4.7) outputs the maximum value from all of the input fuzzy membership:

$$\mu_{A\cap B}(x_i) = \min\left[\mu_A(x_1), \mu_A(x_2), \mu_A(x_3), \ldots\ldots \mu_n(x_n)\right] \quad \text{Equation 4.6}$$

$$\mu_{A\cup B}(x_i) = \max\left[\mu_A(x_1), \mu_A(x_2), \mu_A(x_3), \ldots\ldots \mu_n(x_n)\right] \quad \text{Equation 4.7}$$

where, $\mu_A(x_I)$ refers to the various input fuzzy membership of fuzzy sets in both Equation 4.6 and Equation 4.7.

Equation 4.6 and Equation 4.7 are based on Mamdani fuzzy AND overlay approach (Mamdani, 1974; Mamdani and Assilian, 1975). This differs from the Takagi and Sugeno (1985) approach, which is adopted in Equation 4.8:

$$\mu_{A\cap B}(x_i) = \mu_A(x_1) * \mu_A(x_2) * \mu_A(x_3) *, \ldots\ldots \mu_n(x_n)] \quad \text{Equation 4.8}$$

In ArcGIS, the notation: $fuzzyAndValue = \min(\mu_{x1}, \ldots. \mu_{xn})$ corresponds to Equation 4.6, both being based on the Mamdani fuzzy overlay approach. In the research reported here, the fuzzy CTI model was evaluated using both the Mamdani and Assilian (1975) and Takagi and Sugeno (1985) approaches.

With the Mamdani approach, the original CTI is modified by fuzzy logic into a fuzzy CTI using the fuzzy AND operator, which is fuzzy overlay tool. It is the intersection of the fuzzy membership of the flow accumulation (A_S), planform concavity (PlanC) and slope (S). The fuzzy memberships of A_S, PlanC and S are denoted by: $\mu_A(A_s)$, $\mu_A(PanC)$, and $\mu_A(S)$, respectively and the fuzzy AND overlay are applied to produce the fuzzy CTI (Equation 4.9) from a DEM in ArcGIS, based on Equation 4.8. This would be expressed mathematically as;

$$\text{Mamdani Fuzzy CTI} = \min\left[\mu_A(A), \mu_A(S), \mu_A(\text{PlanC})\right] \quad \text{Equation 4.9}$$

Fuzzy overlay types are illustrated graphically in Figure 4.5.

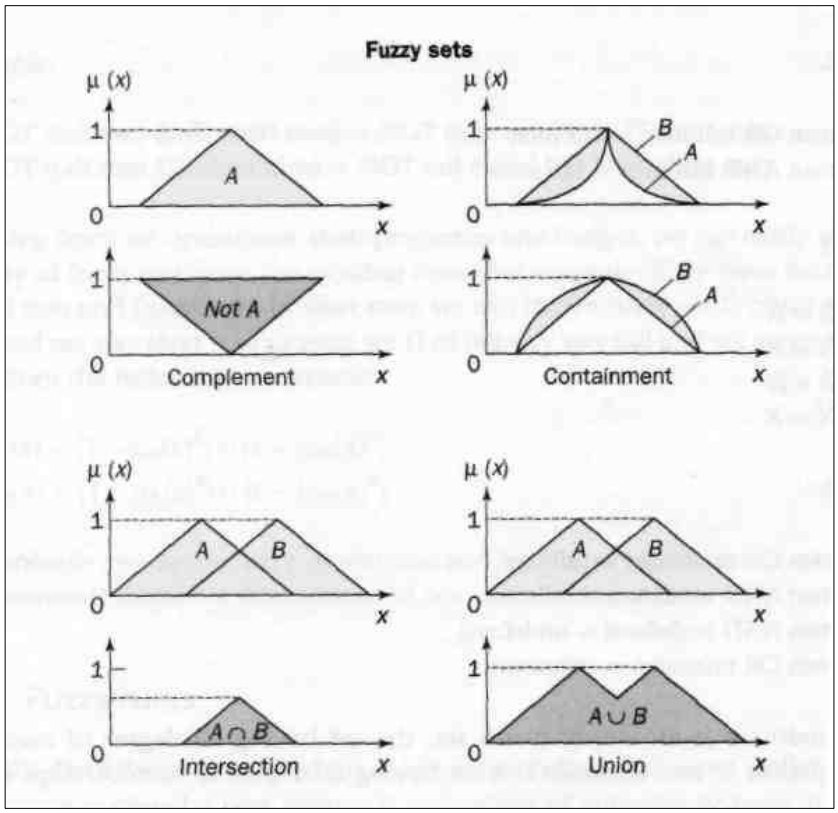

Figure 4.5: Graphical representation of fuzzy overlay types. After Negnevitsky (2005)

4.4.5. **Validation of fuzzy CTI, comparison with the original CTI and effect of DEM quality at Mount Saint Helens and Eastern Cape Province of South Africa.**

Fuzzy CTI (Equation 4.9) raster values were computed at 5, 10, 15, 20, 25 and 30 m grid resolutions at Mount St Helens and their performances in predicting areas in the landscape susceptible to concentrated flow were validated and evaluated using the G1 and G2 DoDs that were described in Chapter 3, section 3.2.4 above. The full validation matrix is set out in Table 3.8.

Table 4.1. Validation matrix for applications of original and fuzzy CTIs and validation using G1 and G2 DoDs.

Code	Predictor and DEM resolution	DEM source
CTI1_G1	CTI 1 at 5 m , 10 m, 15 m, 20 m, 25 m and 30 m	LIDAR DEM
fuzzy CTI1_G1	Fuzzy CTI at 5 m, 10 m, 15 m, 20 m, 25 m and 30 m	LIDAR DEM
CTI1_G1	CTI at 30 m	USGS SRTM
fuzzy CTI1_G1	fuzzy CTI at 30 m	USGS SRTM

As listed in Table 3.8, predictions and validations were performed at all grid resolutions, although it is the predictive performance of the original and fuzzy CTI variants at 30 m DEM resolution that is most important to the aim and objectives of this study. This is because, the results for 30 m DEMs will indicate whether fuzzy-fying CTI can improve its ability to predict susceptibility to concentrated flow erosion in data sparse regions with coarse resolution DEMs. Also, selection of the preferred prediction and validation approaches depends on the availability of good validation data such as high-resolution satellite images, DoDs with small grid sizes, reliable data from field-mapped gullies and/or pre-existing knowledge of threshold values for an area. For most the data sparse regions, there are no high-resolution DoDs. Even where there are field-mapped gullies, knowledge of threshold values is lacking.

The other important factor to examine is the impact on performance of the source and quality of DEM used to compute CTI (i.e. The USACE, airborne LiDAR at 30 m or the USGS, SRTM at 30 m). So, the comparison of fuzzy CTI and original CTI produced from LIDAR 30 m DEM and USGS Sourced 30 m DEM respectively validated by G1 was also of paramount importance in this chapter.

4.4.6. **Field gullies in South Africa and data availability**

Soil erosion has been identified as an important form of land degradation in South Africa and a critical environmental issue in the country (Hoffman and Todd, 2000; Mararakanye and Le Roux, 2012). Given the significance of soil erosion, particularly as a result of gullying, there has been considerable effort in South Africa to map its

spatial extent. This has been largely done by, and in collaboration with, the South African Department of Agriculture, Forestry and Fisheries. This has mostly used SPOT 5 satellite imagery at a scale of 1:10,000 (Mararakanye and Le Roux, 2012; Mararakanye, 2015) (Figure 4.7). Mararakanye and Le Roux (2012) mapped gully location at a national scale for South Africa (Table 4.2). The spatial resolution of the SPOT 5 imagery is 2.5 m panchromatic sharpened images and 10 m resolution multispectral bands. The two different resolutions are merged to produce 5 m resolution images. The temporal resolution is a composite of various acquisition dates between 2006 and 2008. The delineation of the outer boundaries of gullies has been carried out in ArcMap and relies on the tone, shape, drainage pattern and association observed from the SPOT 5 imagery. The data layers indicating the location of gullies in South Africa are freely available online (http://www.sasdi.net/metaview.aspx?uuid=d883e90c22bc468ee7cf25a3f53c0a4a#).

The data was downloaded as an ESRI shapefile (polygon) format. This information is useful to establish the extents of real gullies, against which to validate gully predictions, but in the current research it is also necessary to validate predictions of areas with no gullies. To identify areas with no gullies, the first step was to create an administrative shapefile over the gullied area. The gully polygon and the administrative boundary were both made in the same projection in ArcGIS, and the gullied area was used to erase the administrative boundary map. The resultant polygon shapefile represented areas without gullies. The actual gully area polygon shapefile was resampled and given an arbitrary value of 2, while areas without gullies were given a value of 1. The two layers were then merged and rasterised. The raster has the same projection and cell size as the rasters for DEM, slope, flow accumulation and planform convergence data, and any subsequent raster that was created in this research. Hence, this raster represented the field reality of areas with gullies and without gullies, respectively.

The study area is the Eastern Cape Province of South Africa (Table 4.2). It has an area of 167,845.67 km^2. It is divided into 77 local government areas (Figure 4.6).

Table 4.2: Gullies observed Provinces of South Africa

Province Names	Province Abbreviation	Area of province(ha)	Gullies observed	Gullies correctly captured	Accuracy (%)
Gauteng	GP	110	21	15	71
North West	NW	10,782	26	21	81
Mpumalanga	MP	17,420	41	36	88
Western Cape	WC	25,403	68	63	93
Limpopo	LP	58,669	133	125	94
KwaZulu-Natal	KZN	92,543	137	132	96
Eastern Cape*	EC	161,517	191	175	92
Free State	FS	64,674	193	176	91
Northern Cape	NC	160,885	209	172	82
Total accuracy:		592,003	1019	915	90

* The study area for this current thesis

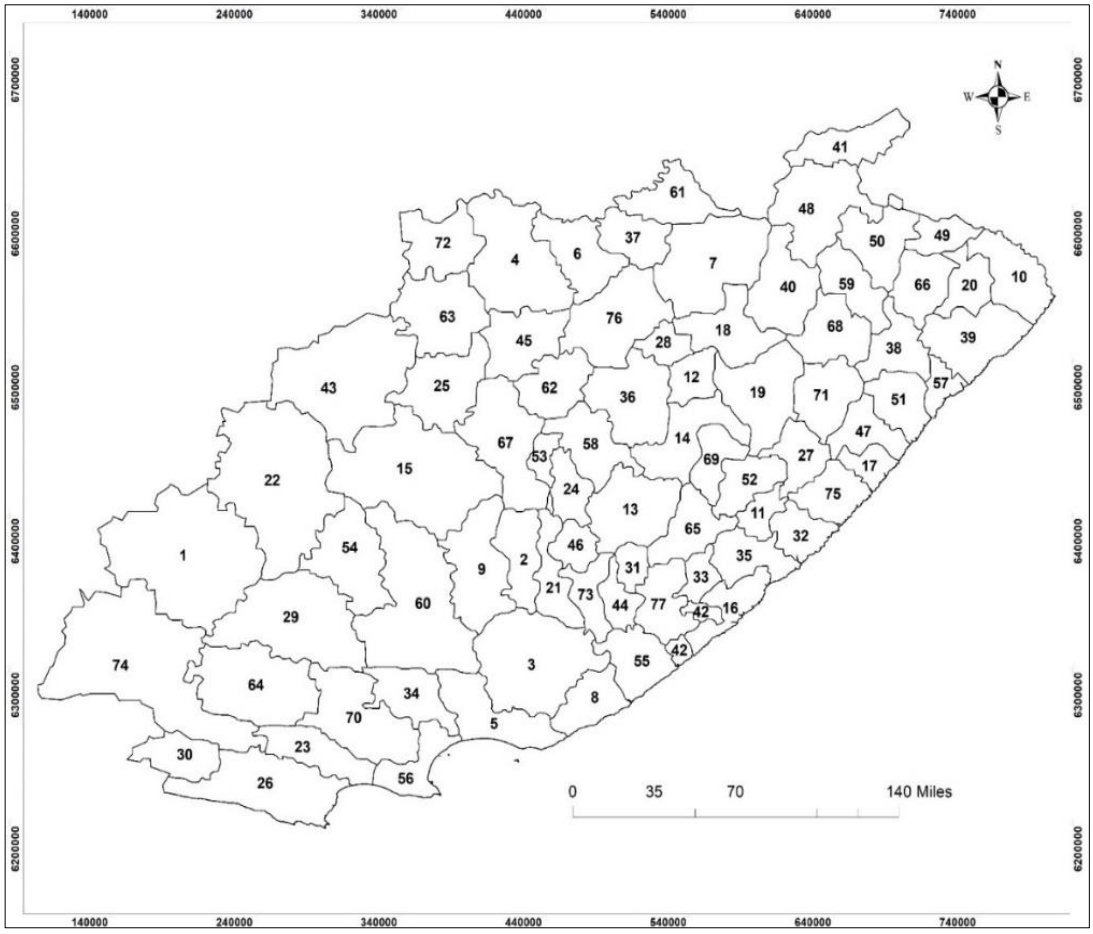

Figure 4.6: Study Area of the Eastern Cape province, showing LGAs.

Figure 4.7: A gully example in the South African study site. After Kakembo *et al.* (2009)

The CTI was applied to a freely-available, USGS-sourced, 30m DEM. Where CTI was > 0, values were reclassified 2, indicating gully presence, and where CTI = 0 values were reclassified 1, indicating no gullies. This was also performed for the fuzzy CTI, using the same study area and DEM resolution. The combine tool in ArcGIS 10.4 was used to combine the real gully raster with the rasters for gully-susceptible areas predicted using CTI and fuzzy CTI. The resultant raster allowed cell counts for False Negatives (FN), False Positives (FP), True Negatives (TN) and True Positives (TP).

Validation was then performed using the ROC, in just the same way as reported in chapters 3 and 4. Interest here is primarily on model sensitivity, since the focus of this Chapter is on the correct prediction of areas with gullies, rather than on correct prediction of areas without gullies. The combined rasters (the real gully raster and the CTI and fuzzy CTI predicted gully rasters) were converted to a Points shapefile. The 'extract multi raster values to point(s) tool' was used to extract values of CTI,

fuzzy CTI, geology, soil, land cover, slope and hillslope form elements within the study area, for consideration following analysis in either SPSS or excel.

The study area is very large and it includes several large rivers, which have fuzzy CTI values close to unity. However, the gullies of interest here have fuzzy CTI values closer to zero because they have contributing areas that are small compared to those of main streams and rivers. To properly differentiate between these small, but important fuzzy CTI vales, they are reported to four decimal places. This is necessary to help identify the relative strength of membership of small values within the range 0 to 1, when the data include a few high fuzzy CTI values, close to 1. Therefore, while a precision of 4 decimal places is used in this thesis, this should not be taken to infer very high accuracy in the specification of fuzzy CTI values.

4.5. **Results**

4.5.1. **Visual comparison of original CTI and fuzzy CTI predictions based on the 5m, LiDAR-based DEM**

Maps of areas predicted to be susceptible to concentrated flow erosion according to the original CTI and fuzzy CTI were generated to allow visual comparison of their outcomes. CTI1 was selected to represent the original CTI. The fuzzy CTI was the fuzzified version of CTI1. Based on experience reported in Chapter 3, symbology for both the original CTI and fuzzy CTI maps in ArcGIS was adjusted to the ‘standard deviation’ and ‘histogram equalise’ stretch types, and the resulting maps are juxtaposed in Figure 4.8.

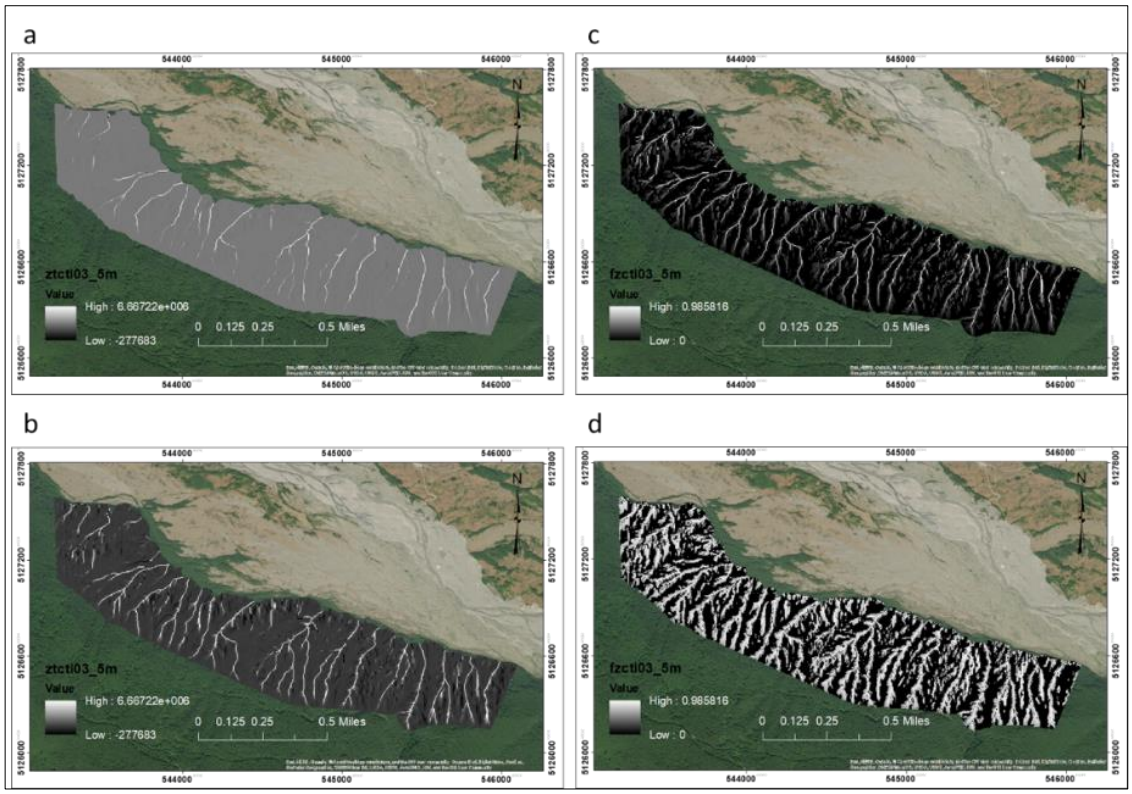

Figure 4.8**.** Areas predicted to be susceptible to concentrated flow erosion (gullying) using (a, b) the original and (c, d) fuzzy CTIs. Maps (a, c) use the 'standard deviation' stretch while (b, d) use 'histogram equalize' stretch.

Maps of concentrated flow erosion predicted using the CTI (Figure 4.8(a)) and fuzzy CTI (Figure 4.8 (c)) that employ the 'standard deviation' stretch are similar in appearance, though the gully channels are more clearly represented and appear to be somewhat more extensive in Figure 4.8 (c). This is because the map based on fuzzy CTI provides more detail and contrast, providing additional information beyond that output using the traditional CTI. The equivalent maps generated using the 'histogram equalized' stretch (Figure 4.8 (b, d) illustrate that the fuzzy_CTI1 is less discriminatory than the original CTI1. The original CTI1 better highlights the actual lines of probable gully channels. It is important to remember that changing the visualization symbology does not change the values predicted by the model, it simply alters their appearance. Nevertheless, the contrasting maps using the 'histogram equalize' stretch symbology (Figure 4.8 (b) and (d)) illustrate how choosing different symbology settings iteratively can enhance visualisation and,

more importantly, help in interpreting the outputs of different versions of CTI or setting appropriate threshold values for flow accumulation (in the 2003 DEM), as Parker *et al.* (2007) noted and used. Most of the times in GIS mapping, the standard deviation is used for raster visualisation and the practical application of that symbology to clearly visualise predictions made using original and fuzzy CTIs is further demonstrated in Figure 4.9.

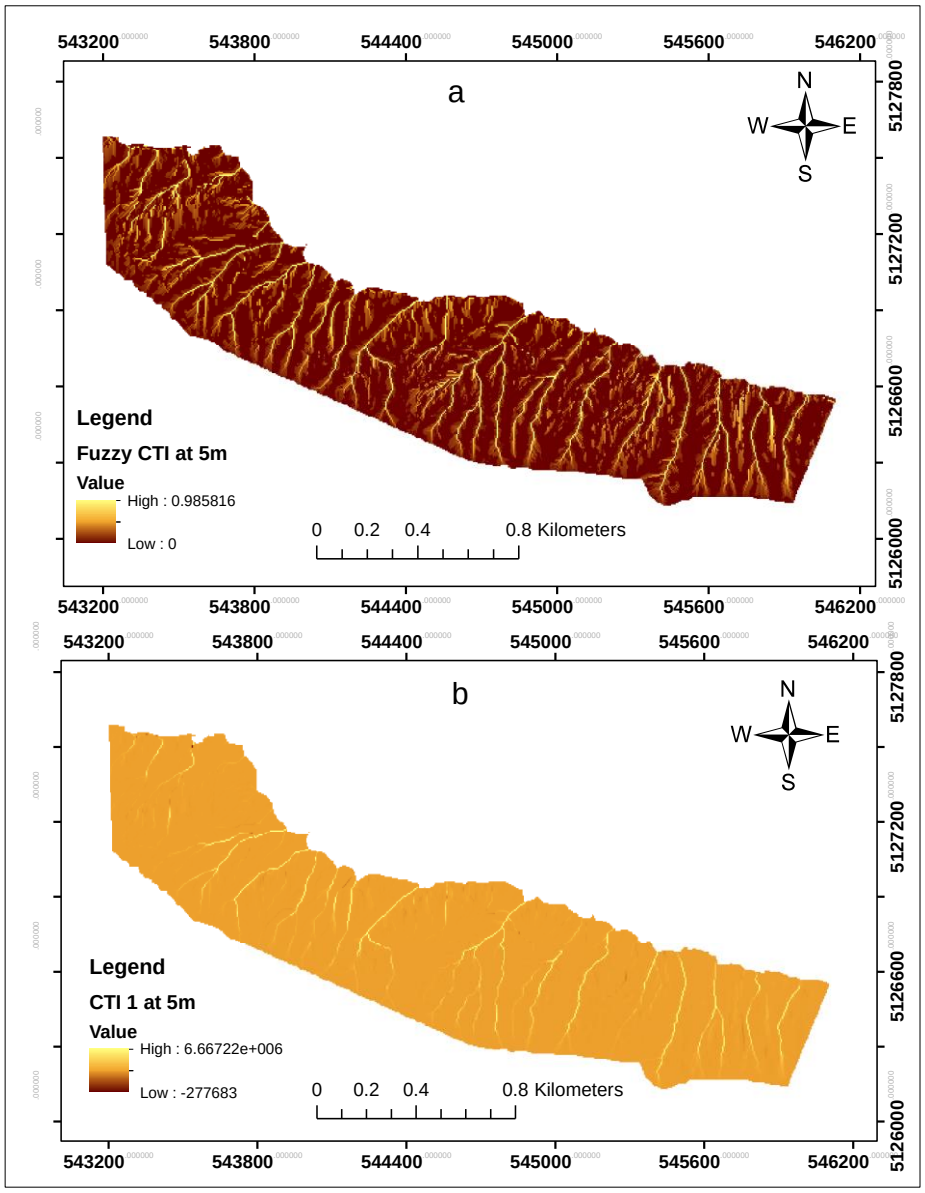

Figure 4.9. Visulization of (a) fuzzy CTI and (b) original CTI using the 'standard deviation' stretch symbology.

4.5.2. **Selected comparisons of ROC performance parameters and curves**

ROC performance evaluation parameters for validation of Fuzzy_CTI1_G1 and Fuzzy_CTI1_G2 are listed in Table 4.3.

Table 4.3: ROC performance Parameter of versions 5 and 6 (which both use fuzzy CTI)

mode	Grid	TN	TP	FN	FP	TPR	TNR	FPR	PPV	NPV	AC	P
FuzzyCT_G1	5	435	3273	727	725	81.83	37.50	62.50	81.87	37.44	71.86	63.43
	10	430	3229	771	730	80.73	37.07	62.93	81.56	35.80	70.91	62.58
	15	485	3239	761	675	80.98	41.81	58.19	82.75	38.92	72.17	62.77
	20	460	3089	911	700	77.23	39.66	60.34	81.53	33.55	68.78	59.86
	25	470	3079	921	690	76.98	40.52	59.48	81.69	33.79	68.78	59.67
	30	550	2935	1065	610	73.38	47.41	52.59	82.79	34.06	67.54	56.88
FuzzyCT_G2	5	1134	1063	28	2935	97.43	27.87	72.13	26.59	97.59	42.58	20.60
	10	1160	1050	41	2909	96.24	28.51	71.49	26.52	96.59	42.83	20.35
	15	1219	1064	27	2850	97.53	29.96	70.04	27.18	97.83	44.24	20.62
	20	1338	1058	33	2731	96.98	32.88	67.12	27.92	97.59	46.43	20.50
	25	1337	1037	54	2732	95.05	32.86	67.14	27.51	96.12	46.01	20.10
	30	1557	1033	58	2512	94.68	38.26	61.74	29.14	96.41	50.19	20.02

Predictions made using Fuzzy_CTI_G1 and Fuzzy_CTI_G2 have high values for TPR (Sensitivity), with the latter being consistently slightly higher at all DEM resolutions. Conversely, PPV values for the Fuzzy CTI_G2 validation are much lower than those for the Fuzzy CTI_G1 validation version. Taken together, TPR, PPV, general Accuracy (AC), FPR and Prevalence parameters indicate that Fuzzy_CTI_G1 is better than Fuzzy_CTI1_G2 for predicting susceptibility to concentrated flow erosion.

ROC curves for prediction-validation approaches that used the original CTI1_G1 and fuzzy_CTI1_G1 are presented in Figure 4.9. Statistical analyses of the Areas under the ROC curves for the curves shown in Figure 4.9 listed in Table 4.4.

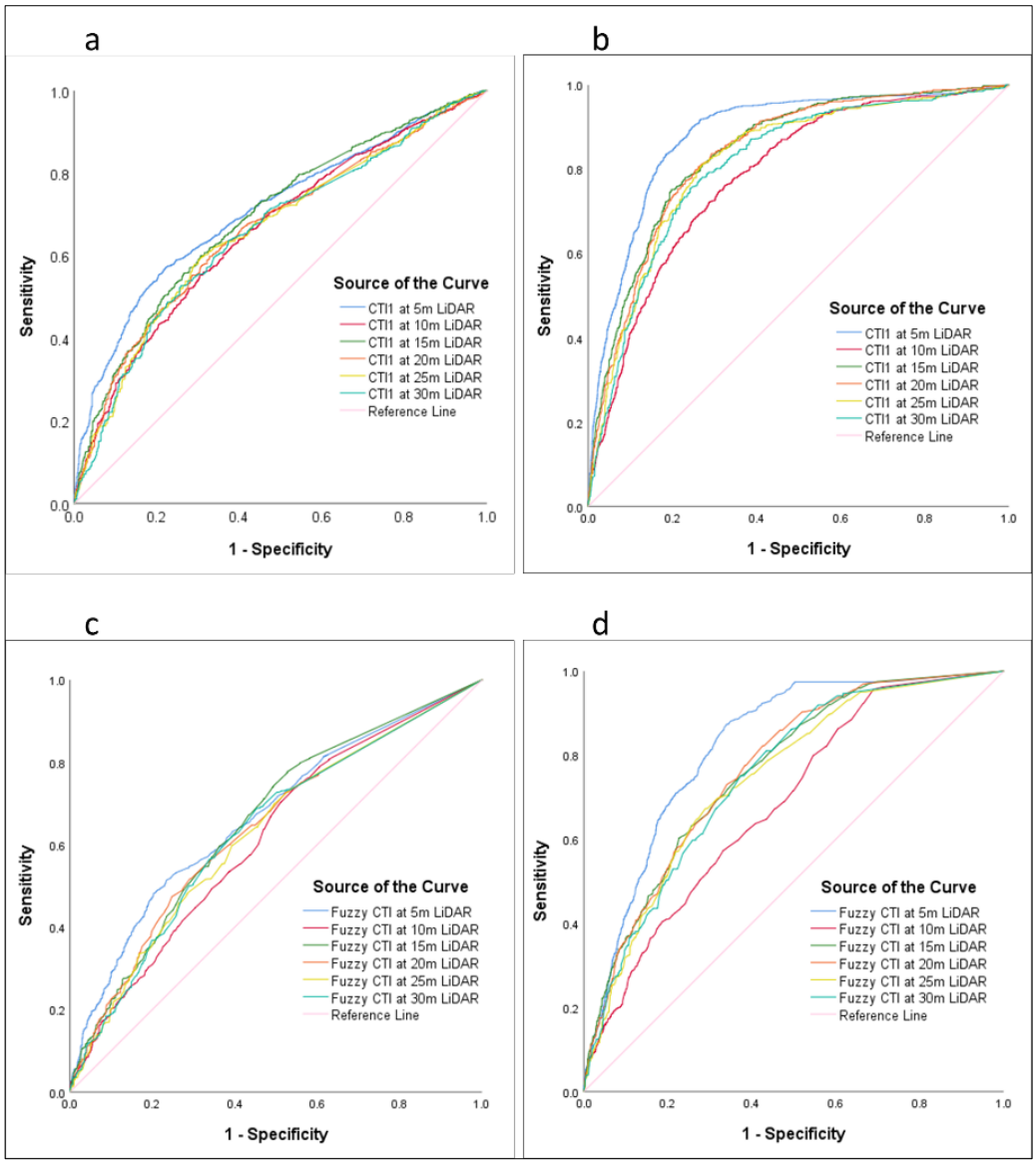

Figure 4.9: Comparison of ROC curves for predictions of concentrated flow erosion at various DEM resolutions using (a) the original CTI(CTI1) validated using DoD G1, (b) CTI1 validated using G2, (c) Fuzzy CTI validated using G1 and (d) fuzzy CTI validated using G2.

Table 4.4: Areas Under the ROC Curves for validation of fuzzy and original CTI methods.

Test Result Variable(s)	Area	Std. Error[a]	Asymptotic Sig.[b]	Asymptotic 95% Confidence Interval	
				Lower Bound	Upper Bound
CTI1_G1					
CTI1 at 5m LiDAR	0.709	0.008	0.000	0.693	0.724
CTI1 at 10m LiDAR	0.661	0.009	0.000	0.644	0.678
CTI1 at 15m LiDAR	0.692	0.008	0.000	0.675	0.708
CTI1 at 20m LiDAR	0.665	0.009	0.000	0.648	0.682
CTI1 at 25m LiDAR	0.662	0.009	0.000	0.645	0.679
CTI1 at 30m LiDAR	0.657	0.009	0.000	0.639	0.674
CTI1 G2					
CTI1 at 5m LiDAR	0.883	0.006	0.000	0.871	0.894
CTI1 at 10m LiDAR	0.785	0.007	0.000	0.770	0.800
CTI1 at 15m LiDAR	0.842	0.006	0.000	0.830	0.855
CTI1 at 20m LiDAR	0.837	0.006	0.000	0.824	0.849
CTI1 at 25m LiDAR	0.820	0.007	0.000	0.806	0.834
CTI1 at 30m LiDAR	0.810	0.007	0.000	0.796	0.824
Fuzzy CTI_G1					
Fuzzy CTI at 5m LiDAR	0.669	0.009	0.000	0.652	0.686
Fuzzy CTI at 10m LiDAR	0.616	0.009	0.000	0.598	0.635
Fuzzy CTI at 15m LiDAR	0.655	0.009	0.000	0.637	0.673
Fuzzy CTI at 20m LiDAR	0.639	0.009	0.000	0.621	0.656
Fuzzy CTI at 25m LiDAR	0.629	0.009	0.000	0.611	0.647
Fuzzy CTI at 30m LiDAR	0.634	0.009	0.000	0.616	0.652
Fuzzy CTI_G2					
Fuzzy CTI at 5m LiDAR	0.823	0.006	0.000	0.811	0.836
Fuzzy CTI at 10m LiDAR	0.684	0.009	0.000	0.667	0.701
Fuzzy CTI at 15m LiDAR	0.763	0.008	0.000	0.748	0.778
Fuzzy CTI at 20m LiDAR	0.766	0.007	0.000	0.752	0.781
Fuzzy CTI at 25m LiDAR	0.746	0.008	0.000	0.730	0.761
Fuzzy CTI at 30m LiDAR	0.751	0.008	0.000	0.736	0.766

a. Under the nonparametric assumption
b. Null hypothesis: true area = 0.5

The areas under the ROC curves (AUC) are found to be statistically significant for all versions and at all grid resolutions, as indicated by Asymptotic Sig. values < 0.05 at the 95% level of confidence. The results also indicate that the original CTI1 'without a minimum flow accumulation' and validated by G2 provides consistently higher in performance when compared to the other versions, at all grid resolutions.

The next best version in terms of overall performance is the fuzzy CTI (without a minimum flow accumulation) validated using G2 (which has a minimum flow accumulation of 80), and this is also consistently the case at all grid resolutions. CTI1 validated using G1 (which does not have a minimum flow accumulation) is

consistently the third best in performance at all resolutions. Fuzzy CTI validated using G1 consistently comes fourth.

Therefore, in terms of AUC, adding thresholds for flow accumulation in identifying areas of true concentrated flow erosion does improve predictive performance. The degree of performance improvement gained by adding a minimum flow accumulation to the original CTI was greater than that for the fuzzy CTI. For both the fuzzy and original CTIs, predictive performance declines gradually as DEM resolution coarsens.

4.5.3. **Fuzzy CTI versus original CTI based on the 30 m LiDAR DEM and USGS SRTM 30 m DEM at Mount St Helens**

Performance comparisons have so far used the LiDAR-based DEM for the Mount St Helens study area, with it in its original form (5 m resolution) and various degrees of grid degradation, up to 30 m. The main aim of this chapter is, however, to explore whether fuzzifying the CTI can enhance its utility at 30 m grid resolution, especially if a globally-accessible USGS 30 m DEM is used (as may be the only option in many LEDCs and other data sparse regions). If that is the case, it may at least be used for predicting susceptibility to concentrated flow erosion.

Therefore, in this sub-section, the fuzzy CTI and original CTI are compared based on applications using the LiDAR-based and STRM-based, 30 m DEMs. The resulting ROC curves are plotted in Figure 4.10 and the base data are listed in Table 4.5. AUC values are summarised and displayed in Figure 4.11.

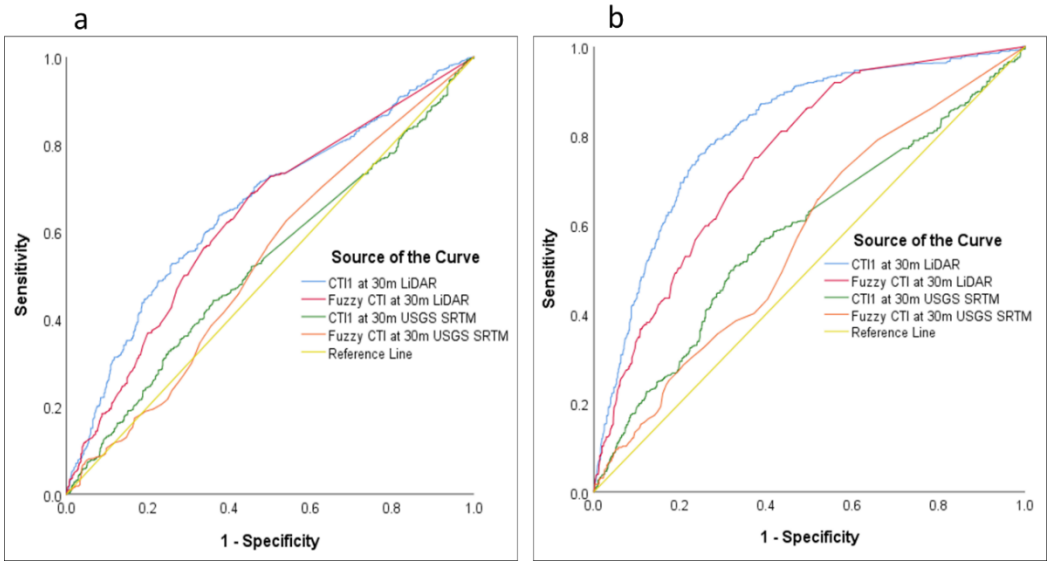

Figure 4.10. Comparison of ROC curves for the fuzzy CTI (Fuzzy CTI at 30m LiDAR and Fuzzy CTI at 30m USGS SRTM) and the original CTI(CTI1 at 30m LiDAR and CTI1 at 30m USGS SRTM) validated by DoD gully (a) without threshold(CTI1_G1) and (b) with threshold(CTI1_G2)

Table 4.5. Predictive Accuracy of fuzzy CTI and original CTI models when applied to LiDAR-based and STRM-based DEMs, both with 30 m grid sizes, and validated using G1 and G2

DEM Source for the CTI	Area Under the curve	Std. Error[a]	Asymptotic Sig.[b]	Asymptotic 95% Confidence Interval	
				Lower Bound	Upper Bound
CTI1_G1					
CTI1 at 30m LiDAR	0.657	0.009	0.000	0.639	0.674
Fuzzy CTI at 30m LiDAR	0.634	0.009	0.000	0.616	0.652
CTI1 at 30m USGS SRTM	0.528	0.009	0.004	0.509	0.546
Fuzzy CTI at 30m USGS SRTM	0.531	0.010	0.002	0.511	0.550
CTI1_G2					
CTI1 at 30m LiDAR	0.810	0.007	0.000	0.796	0.824
Fuzzy CTI at 30m LiDAR	0.751	0.008	0.000	0.736	0.766
CTI1 at 30m USGS SRTM	0.582	0.010	0.000	0.562	0.602
Fuzzy CTI at 30m USGS SRTM	0.570	0.010	0.000	0.552	0.589

The test result variable(s): CTI1 at 30m LiDAR, Fuzzy CTI at 30m LiDAR, CTI1 at 30m USGS SRTM, Fuzzy CTI at 30m USGS SRTM has at least one tie between the positive actual state group and the negative actual state group. Statistics may be biased.
a. Under the nonparametric assumption
b. Null hypothesis: true area = 0.5

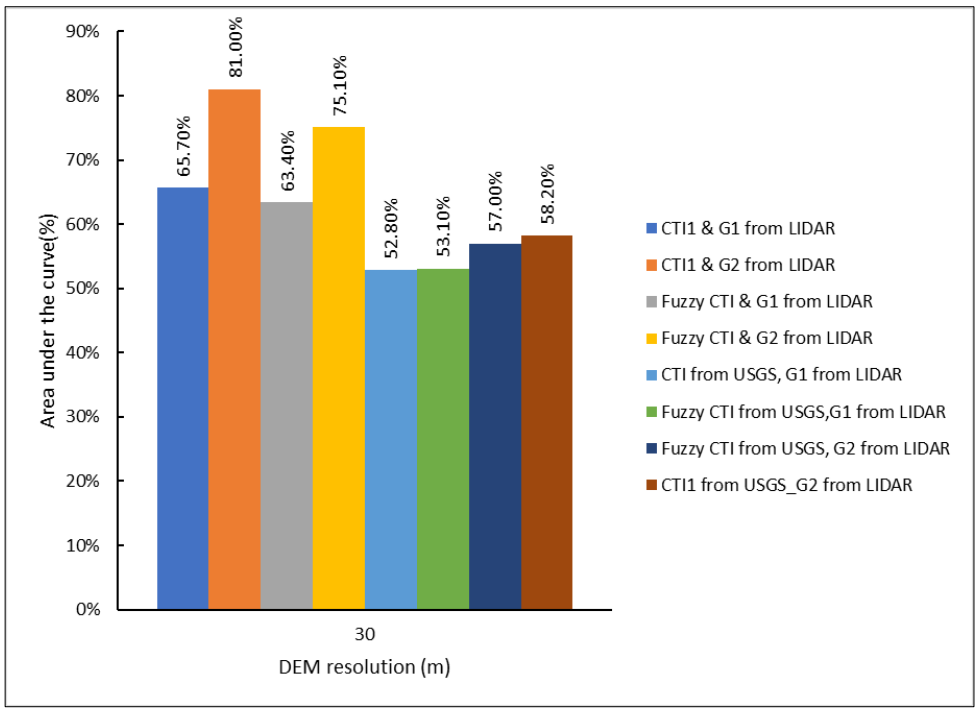

Figure 4.11: AUC values for the original and fuzzy CTI models when applied using 30 m LiDAR and SRTM-based DEMs, respectively.

Using the USGS SRTM-based DEM, AUC for the fuzzy CTI1 with validation using G1 is very slightly higher (53.1%) than that for the original CTI1 and validation using G1 (52.8%). However, neither model can be said to perform well. When the same versions are validated using G2, the original CTI (58.2%) slightly outperforms the fuzzy CTI (57%). These findings support the implication elucidated earlier that, when it is possible to set a threshold flow accumulation for 'ground truth' gullies (either based on gullies observed in the field or discerned in high-resolution satellite images), the CTI performs slightly better than the fuzzy version. In fact, the results throughout this chapter show that, when using a LiDAR-based DEM and validating predictions using G2, AUCs for the original CTI are consistently higher than those obtained using the fuzzy CTI at all grid resolutions. However, when the lower quality SRTM-based 30 m DEM is used, and when no minimum flow accumulation or erosion values for 'ground truth' gullies can be set in validating

predictions, the fuzzy CTI can deliver a very slight improvement over the original CTI.

These results support those presented earlier, that when used with good quality, LiDAR-based DEMs the original CTI can support accurate predictions even at 30 m grid resolution. It does seem then, that if a high quality, 30 m DEM is available, fuzzy logic does not lead to improvement in the predictive performance of the CTI, but rather a slight reduction, at least in terms of the area under the ROC curve for gully prediction. However, this conclusion also hints that, in places where no obvious gullies exist to support robust validation using G2 and only a low quality, SRTM-based, 30 m DEM is available, use of the fuzzy CTI would be preferred.

Finally, while the differences between the curves and the areas under them are very small, these results indicate that, with a threshold value for flow accumulation and when using a coarse resolution (30m) DEM, the predictive performance of the original CTI in predicting actual gullies is slightly better than that of the fuzzy CTI. I hypothesise that this is at least partially because the fuzzy CTI is not predicting gully locations, but is predicting areas that experience concentrated flow (i.e. coarse-scale topography with the potential for concentrating flow), and which are, therefore topographically-susceptible to concentrated flow erosion. Fuzzy CTI is not predicting the initiation of a gully channel, which occurs only once either a critical flow accumulation area or a user-designated threshold CTI is exceeded. Therefore, the lack of strong predictive performance is likely related to the fact that gullying is not only a function of topography but, also relates to environment characteristics such as vegetation cover and soil strength. It also means that model prediction validation using the locations of observed gullies may not truly indicate predictive success because an area without gullies may still be topographically-susceptible to gullying although no erosion has occurred, perhaps because of dense vegetative cover, strong soils or anthropogenic stabilisation of the land surface.

4.5.4. **Predicting and validating gullying in Eastern Cape Province of South Africa.**

Analysis using the ROC indicates an area under the curve of 55.4% for prediction of gullying over the Eastern Cape Province as a whole when using the CTI with no threshold value. The area under the curve using fuzzy CTI (also with no threshold value) was slightly higher, at 56.1% (Figure 4.11). These results confirm that, overall and when applied using a 30m grid and with no supplemental information or analysis to select a threshold value, the fuzzy CTI does out-perform the original CTI, albeit only by a small margin.

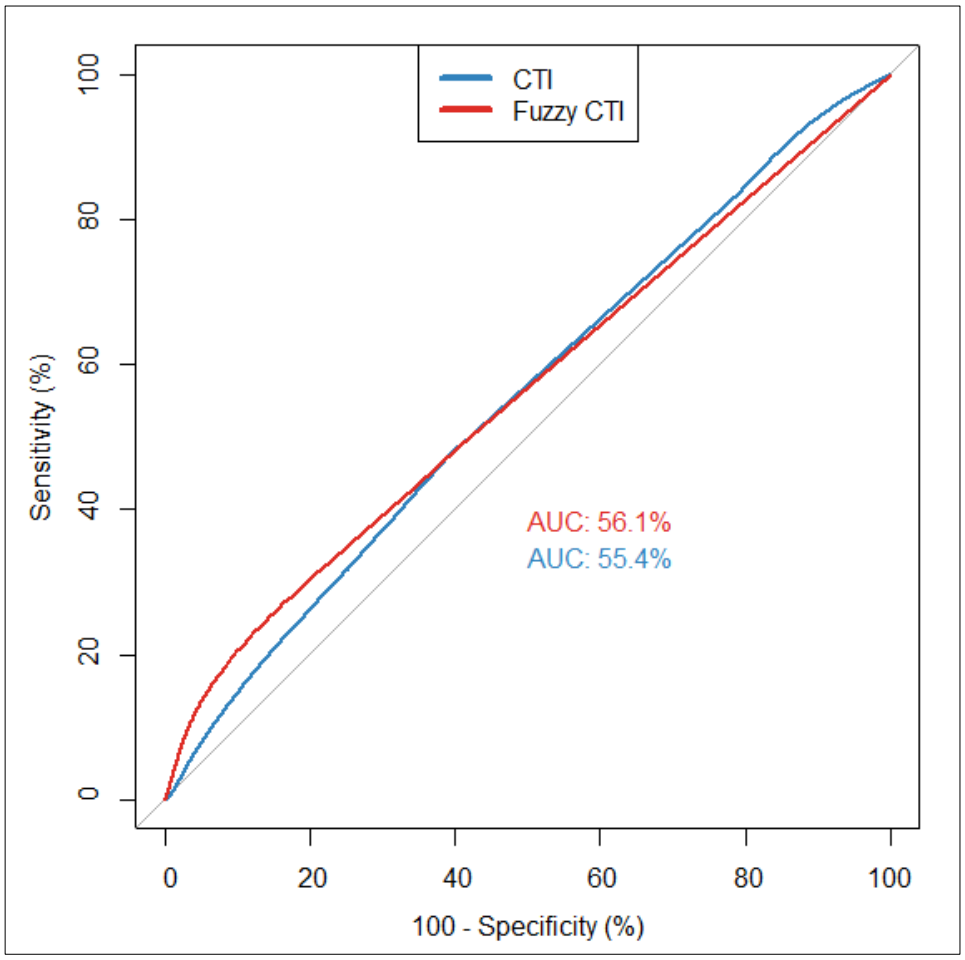

Figure 4.11. ROC curves for prediction of gullying over the whole of the Eastern Cape Province of South Africa using the original and fuzzy CTIs.

It was recognised that including a threshold value for the fuzzy CTI, at which the concentrated overland flow is sufficiently intense to initiate gullying would improve

its performance with respect to predicting gullying actually observed in the high-resolution satellite images. However, without field observations of fuzzy CTI values at gully heads (like that available for the intensively studied sites in the USA) there is no way to determine the threshold, or cutoff value, below which, although concentrated overland flow occurs, it is too weak to erode a gully. Hence, a range of possible cut-off values of CTI was investigated, with the value selected being the one for which the True Positive (TP) rate or *Sensitivity* is at its highest and the False Positive rate (i.e. 100 - *Specificity*) is at its lowest.

To identify threshold or cutoff values of the fuzzy CTI, the Area under the Curve (AUC) for the fuzzy CTI applied to the entire Eastern Cape Province was replotted, with a second y-axis added on the right of the graph and coloured to indicate a range of possible cut-off values for the fuzzy CTI (Figure 4.12(a)). The second graph, in Figure 4.12(b), indicates how the corresponding *Sensitivity* changes as a function of this cutoff value.

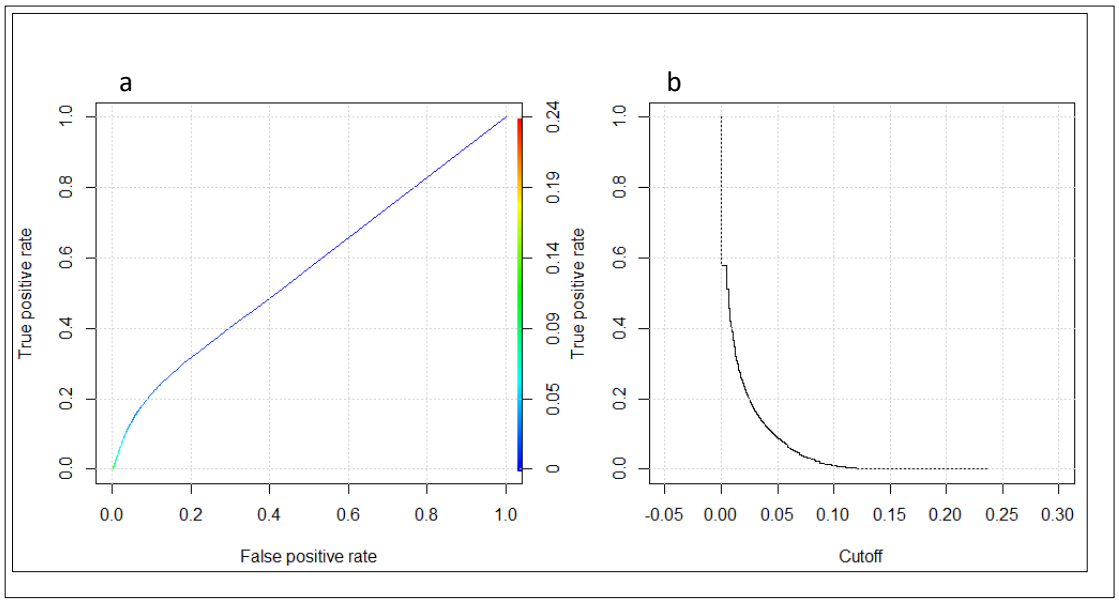

Figure 4.12. Fuzzy CTI prediction performance and possible threshold values. (a) ROC curve for the fuzzy CTI (with a cutoff) and (b) True Positive rate (Sensitivity) as a function of fuzzy CTI cutoff (%).

The data underpinning Figure 4.12 are listed in Table 4.6, in the form of a 'confusion matrix'.

Table 4.6. Confusion matrix for TPs, FPs and TPR as a function of the value selected for the threshold fuzzy CTI.

Threshold fuzzy CTI		TRUTHS		TPR
	PREDICTION	FALSE	TRUE	
fuzzyCTI > 0.0	FALSE	32024	33075	54.91%
	TRUE	29373	40273	
fuzzyCTI > 0.01	FALSE	46477	18622	59.34%
	TRUE	42469	27177	
fuzzyCTI > 0.02	FALSE	57186	7913	67.79%
	TRUE	52990	16656	
fuzzyCTI > 0.03	FALSE	60743	4356	72.62%
	TRUE	58094	11552	
fuzzyCTI > 0.04	FALSE	62318	2781	75.14%
	TRUE	61242	8404	
fuzzyCTI > 0.05	FALSE	63111	1988	75.96%
	TRUE	63364	6282	
fuzzyCTI > 0.06	FALSE	63759	1340	76.08%
	TRUE	65383	4263	
fuzzyCTI > 0.07	FALSE	64140	959	74.97%
	TRUE	66773	2873	
fuzzyCTI > 0.08	FALSE	64383	716	74.13%
	TRUE	67594	2052	
fuzzyCTI > 0.09	FALSE	64637	462	70.55%
	TRUE	68539	1107	
fuzzyCTI > 0.10	FALSE	64749	350	67.41%
	TRUE	68922	724	
fuzzyCTI > 0.11	FALSE	64860	239	63.06%
	TRUE	69238	408	
fuzzyCTI > 0.12	FALSE	64939	160	54.67%
	TRUE	69453	193	
fuzzyCTI > 0.13	FALSE	64989	110	49.54%
	TRUE	69538	108	
fuzzyCTI > 0.14	FALSE	65021	78	35.54%
	TRUE	69603	43	
fuzzyCTI > 0.15	FALSE	65051	48	28.36%
	TRUE	69627	19	

Figure 4.13 uses the data in Table 4.6 to illustrate how *Sensitivity* (TPR) varies as a function of the threshold value selected for the fuzzy CTI in the Eastern Cape Province of South Africa, with the trend indicated using both linear and 2nd polynomial curves fitted to the data.

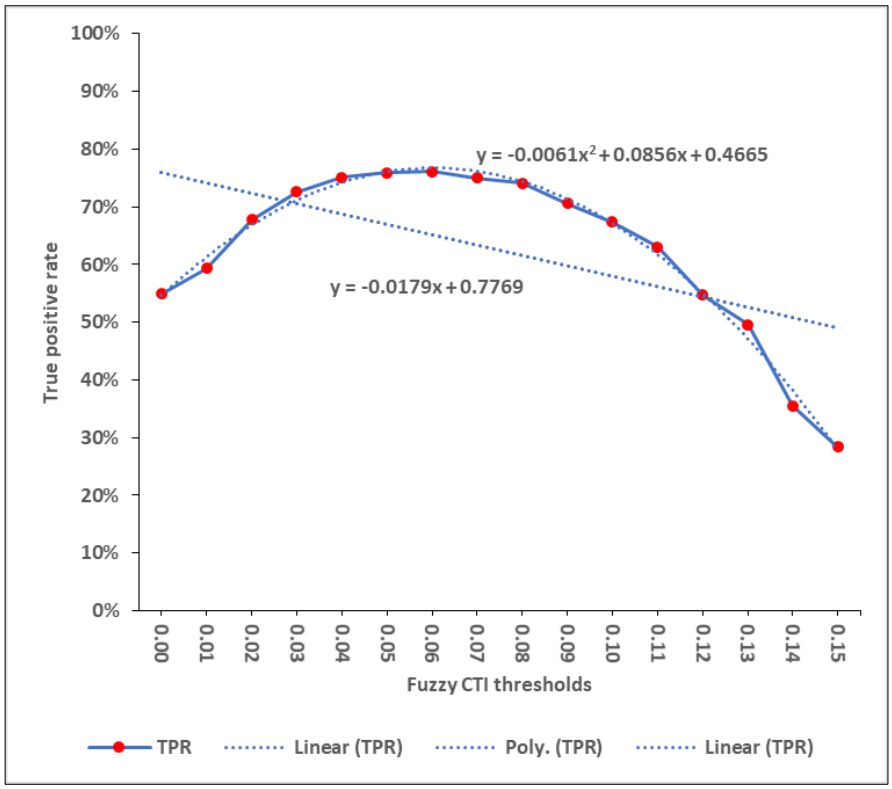

Figure 4.13. TPR as a function of value selected for the threshold fuzzy CTI.

These results show that the number of nodes with gullies correctly predicted peaks at a value of about 76% for fuzzy CTI cutoff value of 0.06. If a cutoff greater than 0.06 is selected, the *Sensitivity* declines. However, the data in the confusion matrix(Table 4.6) and curve in Figure 4.13 indicate that gullies are well predicted for the Eastern Cape Province for threshold fuzzy CTI values between $0.04 < \text{fuzzy CTI} \leq 0.08$.

4.6. **Discussion and conclusion**

With no minimum flow accumulation values (section 4.4.5), the fuzzy CTI outperformed the original CTI when applied to the Mount St Helens study area. Adding a minimum flow accumulation value in calculation of the CTI (section 4.4.5) produced a marked improvement in the predictive performance of the original CTI, but the improvement for the fuzzy CTI was smaller. As a result, CTI1_G1 performed slightly better than the fuzzy_CTI1_G1.

With a few exceptions, differences between the performance of the original and fuzzy CTIs decreased as grid size increased. Similarly, in nearly all cases for both fuzzy and original CTIs, predictive *Accuracy* declined as grid size increased. Exceptions to these general trends mostly concerned runs using the 10m DEM, which tended to perform less than those using the 15m DEM.

These results indicate that, when minimum values are used both in predicting and validating the lines of intense concentrated flow erosion (gullying) between 2003 and 2009, and the gully channels created or enlarged by that erosion, adding these critical values do improve predictive *Accuracy*. Achieving this depends on identification of appropriate minimum values for the accumulation of overland flow and the depth of concentrated flow erosion. For the Mount St Helens study area, an iterative, 'trial and error' process was used to arrive at threshold values of 1.5m for land lowering observed between 2003 and 2009, and 80m of flow accumulation upstream of a gully head. It must be borne in mind that these critical values represent a host of unmeasured and unknown variables that affect the susceptibility of a given swale to gully initiation and enlargement. Consequently, minimum values are site and probably season-specific and there is no way to establish or even guess their values without conducting detailed research like that reported above and in Chapter 3.

As a further example, when Parker *et al.* (2007) used new and historical data from the Ellis Farm site in Mississippi to test the utility of the original CTI, they qualitatively stated that it worked better with a threshold CTI value than without. That is conformed in this chapter, which demonstrates *Accuracy* was 93% with a threshold in comparison to 74% without. It was only possible to set a threshold CTI, however, thanks to extensive field observations and monitoring of gully processes. In applications where gully head locations and the lines of gully channels are unknown, it is problematic to set a minimum (critical) value for the minimum depth of surface erosion to define gullying, or the minimum flow accumulation necessary to initiate concentrated flow erosion, or the average CTI associated the locations of gully heads in the study area (which represents the threshold CTI for gully

initiation). When data does not exist on gully location, the results in this chapter suggest the researcher can still derive a threshold CTI value, provided the CTI model's true positive rate (*Sensitivity*) is high. Even better, it is possible to disaggregate the CTI into its component parts, identifying a critical value for the predominant topographic parameter – the flow accumulation - in areas with planform concavity (flow concentration). The researcher can optimise threshold CTI or critical flow accumulation to maximise *Sensitivity*. This essentially entails enhancing the level of agreement between prediction and ground truth, iteratively.

The reasons why the *Accuracy* of the fuzzy CTI is slightly lower than the original CTI stem from the capacity of the original, deterministic CTI to make better use of the detailed topographic representations provided by high resolution (< 15 m), LiDAR-derived DEMs with grid sizes in the range of 5 to 15m. When using 30 m DEM resolution, fuzzy_CTI1_G1 represented a statistically significant improvement in *Accuracy* over CTI1_G1, although it should be noted the actual improvement is very slight. This is because, with large grid squares, it is impractical to delineate or predict gully channels or lines of gully erosion, because these features are smaller than the resolution of the DEM. In lower resolution data the practical utility of the fuzzy CTI becomes much more cogent; however, variability in land-use, soil type and vegetation (not considered for traditional uses of CTI over much smaller areas) become problematic and are likely to partly explain the poor predictive power of the model. In other words, many of the false positives recorded in the validation of the fuzzy CTI are classified as such because no gully has been observed in the landscape. Even so, the area identified by the fuzzy CTI as being topographically-susceptible to concentrated flow erosion could still be subject to gullying following, for example, replacement of dense vegetation cover by cropland or bare earth.

The fuzzy CTI (and to a lesser extent the original CTI) indicate that wide areas of the landscape are topographically-susceptible to gullying. This implies, as suggested above, that other environmental information is needed to further constrain the model output if the intention is to predict the existence and locations of actual gullies. On the basis of these findings, it appears that the fuzzy CTI has the potential

to be a useful predictive tool for mapping topographic-susceptibility to gullying in the Nigerian Capital Territories, but this requires further exploration of the role of other environmental conditions, and this is addressed in Chapter 5.

CHAPTER 5: **CONTROLS ON WHETHER AND WHERE GULLIES ARE OBSERVED WITHIN A TOPOGRAPHICALLY-SUSCEPTIBLE AREA**

5.1. **Introduction**

In an area for which good quality topographic data is available, it is possible to use the CTI not only to identify areas that are topographically-susceptible to gullying, but also the paths that gullies are likely to follow. However, whether gullies are observed depends not only on topography but also on other environmental factors such as soil strength, vegetation and underlying geology, which also influence the locations where, and circumstances under which, gullies actually form. This is because environmental characteristics will determine whether a particular intensity of concentrated overland flow can overcome the stability of soils to erode a gully. Recognising this, it was recommended by Parker *et al*. (2007) that the CTI model be used to delineate areas with the *potential* for gully formation, and that other environmental factors should also be taken into account when predicting whether and where gullies will actually occur. This is particularly true when the CTI (or fuzzy CTI) is applied over large areas with variable soil strength and vegetative cover.

5.2. **Objective**

In exploring Parker et al.'s (2007) recommendation, the objective addressed in this chapter is (as stated in the Introduction in Chapter 1), to examine how other readily-available environmental descriptors can be combined with knowledge of the distribution of concentration of overland flow, to inform prediction of land surface susceptibility to concentrated flow erosion (e.g. gullying). This is explored using analysis of both the CTI1 and fuzzy-CTI1 models, based on the 30 m resolution DEMs for the Eastern Cape province of South Africa that was described and used in Chapter 4. The objective will be achieved by examining the predictive performance characteristics of the models within areas having different, specific classes of vegetation cover, soil texture and underlying geology.

5.3. **Literature review**

5.3.1. **Environmental influences on gullying**

A gully is instigated when the downslope flow of concentrated surface runoff has sufficient stream power per unit width to erode the land surface (Chapter 1). It is the topography that concentrates the surface runoff by generating high values of stream power per unit width where flow concentrates, but whether erosion occurs is also influenced by other environmental conditions. For example, areas of bare soil are likely to be eroded by concentrated overland flow at much lower specific stream powers than areas with dense vegetation cover, because plant roots strengthen soils (Gray and Barker, 2004). Recognising this, it has been recommended by many authors that the relationship between gully erosion and factors including soil properties (e.g. texture, bulk density, moisture, organic matter), vegetation cover, and climate should be established (Thorne *et al.*, 1984a; Thorne and Zevenbergen, 1984; Parker *et al.*, 2007). Factors influencing the formation of ephemeral gullies that were outlined by Zevenbergen (1989) are:

1. Overland flow discharge and duration, without which ephemeral gullies could not exist;
2. Slope and flow depth, which determine the magnitude of the flow's downslope component of weight and, therefore, the boundary shear stress exerted by the flowing water on the soil;
3. Planform curvature, which determines the local flow convergence and, therefore, the concentration of stress along a flow path or swale;
4. Soil characteristics, which affect both overland flow rates (through controlling infiltration capacity) and determine the erodibility of the soil;
5. Vegetation characteristics, which affect overland flow rates through interception and flow resistance and provide cover for the soil, reducing its susceptibility to erosion.

The nature of soils is undoubtedly also an important control on gullying. Soil formation and fabric are dependent on climate, parent material, organic matter, topography and time (Jenny (1994); (Simonson, 1995) and can be described as:

$$S = f(cl, o, r, p, t)$$ Equation 5.1

where, S = soil (soil properties), f = function of: cl = climate, p = parent material, o = soil organisms, r = relief, and t = time. This is a good point to start understanding the influence of environmental factors on soil characteristics. However, equation 5.1 does not necessarily indicate multiplication of the factors, or that there is a simple relationship between them, when describing soil formation. Actually, there have been concerted modelling efforts intended to work out how to combine environmental descriptors in order to predict soil types and soil erosion (Laflen and Flanagan, 2013). The numerous environmental influences on soil erosion, and the multitude of ways of quantifying these parameters, makes it challenging to account for environmental factors when predicting erosion. This is particularly true because each parameter requires a weighting as they do not have equal significance in affecting soil erosion, and their relative significance to each other (i.e. their weighting) changes, depending on local conditions. Some models have attempted to quantify the effects of these factors based on soil physics and chemistry (Bolstad *et al.*, 1998; Vandekerckhove *et al.*, 1998; McKenzie and Ryan, 1999; Laffan, 1999; Chagas *et al.*, 2016; Conoscenti *et al.*, 2016; Angileri *et al.*, 2016; Hengl *et al.*, 2017; Arabameri *et al.*, 2019b; Gayen *et al.*, 2019), while others, such as the USLE, have used a purely empirical approach to represent the influence of soil erodibility (k), plant cover (C), and erosion control practice (P).

5.3.2. **Influence of a soil property-based soil erodibility index on the threshold CTI**

Consideration of an appropriate soil erodibility index is likely to be important in successfully predicting gully initiation using the CTI. Several soil erodibility indices exist (Table 5.1), however it is those based on soil properties such as particle size distribution and organic matter content as it affects soil aggregation, that most strongly influence the structure of the soil and, hence, its erodibility by water erosion (Pieri, 1992; Bryan, 2000). Most soil erodibility indices are formulated from measured soil properties, with key properties typically being dispersion ratio, clay

ratio, organic matter content and sodium absorption ratio (SAR), each of which is reviewed below.

Table 5.1. List of soil erodibility indices in water and wind research. After Song et al. (2005)

Presenter	Date	Index	Method	Type
Bennet	1926	SiO_2/R_2O_3	1	water
Middlellon	1930	dispersion ratio, erosion ratio	1	water
Baver	1933	dispersion —permeability index	1	water
Bouyoucos	1935	(sand% + silt%) / clay%: clay ratio	1	water
Peel	1937	permeability, suspending, and dispersion rate	1	water
Anderson	1954	surface-aggregate ratio	1	water
De Leenheer L	1954	instability of aggregate	1	water
Zhu	1954	expansion coefficient, dispersion rate	1	water
Woodburn	1956	stability of aggregate, dispersion rate	1	water
Zhu	1960	the crumbling status of soil in static water	1	water
Tian	1964	dispersion ratio, erosion ratio, degree of aggregate, etc	1	water
Ekwue	1992	soil permeability	1	water
Yang	1992	erosion ratio, dispersion ratio, etc	1	water
Voznesenskil	1938	E = dh/a	2	water
Gussak	1946	the quantity of water needed in scouring lOOg soil	2	water
Elision	1947	separability and transportility of soil	2	water
Zhu	1960	the depth of water-scouring hole	2	water
Tang	1964	clay composition, microslructure	2	water
Subhash	1978	erosive coefficient: *K*	2	water
Bajracharya	1992	aggregate stability, anti-scour intensity	2	water
Jiang	1995	scouring coefficient	2	water
Amezketa	1996	soil structure, aggregate stability, shear strength, etc	2	water
Chen	2000	sodium-adsorption ratio, ion density in soil solution	2	water
Olson	1963	the soil loss per unit of the erosion index	3	water
Fanes	1985	the rate of air-dry of stable water aggregate	3	water
Zhou	1993	the soil loss per unit depth of runoff	3	water
Chepil	1942	water stable, dry clod structure	1.4	wind
Chepil	1950	dry aggregate structure, lump texture	1,4	wind
Chepil	1951	apparent density, mechanical stability of structure	1,4	wind
Chepil	1952	soil structure	1,4	wind
Chepil	1954	calcium carbonate, decomposed organic material	1,4	wind
Chepil	1955	ratio of sand, silt and clay	1,4	wind
Yakupof T	1955	mechanical composition, CaCOs. organic matter	1,4	wind
Skidmore	1982	particle composition	1.4	wind
Dong	1998	grain-size	1,4	wind

Note: 1 = measurement of physiochemical properties; 2 = measurement by scouring experiment; 3 = experiment in plot; 4 = wind tunnel experiment

5.3.3. **Dispersion Ratio**

Middleton (1930) examined the properties of soil that influence erosion, focusing particularly on sodic soils where the clay component is wet and the organic component is readily dispersible. This condition reduces soil aggregation and

structural stability. Therefore, dispersed and disaggregated soils are more prone to erosion than less disperse ones. Middleton (1930) developed a dispersion ratio as an index of soil erodibility, (which describes the rate at which soil particles disperse in water) by comparing the percentage silt and clay in soils before and after dispersion (Equation 5.2):

$$DR = \frac{[(\%\ \text{silt}\ +\ \%\ \text{clay})\text{in undispersed soil}]}{[(\%\ \text{silt} + \%\ \text{clay})\ \text{after Dispersion of soil in water})]} \qquad \text{Equation 5.2}$$

Distilled water is usually used to define the undispersed condition, whereas the dispersed condition is quantified by submerging soils in Calgon (sodium hexametaphosphate) or sodium hydroxide. Middleton (1930) found soils with dispersion ratios > 0.15 are erodible in nature.

The Dispersion ratio has been used to estimate soil erodibility by many researchers (Bajracharya and Lal, 1992; Igwe, 2003, 2005; Igwe and Udegbunam, 2008) and recent examples are replete in the literature (Mallo and Mgbanyi, 2013; Kusre *et al.*, 2018; Mittal *et al.*, 2019).

5.3.4. **Clay Ratio (CR)**

Bouyoucos (1935) developed the clay ratio (CR) as another method to represent the relative erodibility of soils. The CR depends on the granular composition of the soil and represents that composition based on the ratio of sand and silt to clay:

$$\text{CR} = \frac{\%\ Sand + \%Silt}{\%Clay} \qquad \text{Equation 5.3}$$

The reasoning behind this ratio is that sand and silt increase erodibility because the particles are small but noncohesive and so easily moved. In contrast, clay decreases soil erodibility because it is cohesive, binding soil particles together and making it hard to erode. Therefore, the lower the CR, the higher the resistance to erosion. CR has been found to be a suitable criterion for prediction of soil erodibility and it is

widely used. For example, Tarafdar and Ray (2005) identified that CR under trees was distinctly lower than in the barren soil.

5.3.5. **Modified Clay Ratio**

Correlations between soil properties suggest a modified clay ratio (MCR) gives a more precise prediction of soil erodibility than does the CR, especially in soils that have high organic content (Bhola and Mohan, 1982; Mukhi, 1988; Tarafdar and Ray, 2005). The MCR takes into account the fact that organic matter in soils can also increase their relative stability, even when clay content is low or zero. Therefore, the MCR incorporates the effect of organic matter in soils as:

$$\mathrm{MCR} = \frac{(\%\ \mathrm{sand}\ +\ \%\ \mathrm{silt})}{(\%\ \mathrm{clay}\ +\ \%\ \mathrm{organic\ matter})} \qquad \text{Equation 5.4}$$

5.3.6. **Critical Level of Soil Organic Matter Content**

Soils high in organic matter and clay have a stronger structure that is more erosion resistant than other soils. Soils with more sand and silt, and less organic matter and clay, are less stable and more susceptible to soil erosion and land degradation. Soil organic matter (SOM) serves as a soil binding agent promoting good structural development, particularly in the surface layer. Hence, high SOM serves to limit detachment of soil particles by erosive forces (Pieri, 1992; Tarafdar and Ray, 2005).

Pieri (1992, pp.252), relying on their experience that there is a critical level below which soil productivity declines, made the statement that, “The notion of the critical level is indispensable in practical agriculture in the Savannah as in another part of the world”. Pieri (1992, pp.253), based on work by Emerson (1967) and Jones (1976), postulated a relationship between the minimum SOM and the surface area of the mineral soil needed to adsorb chemicals effectively, below which maintenance of soil structure is no longer assured. Soil characteristics of the area had enough quotidian properties to enable them to come up with a critical SOM value defined as:

$$\mathrm{S}_t(\%) = \frac{(\mathrm{SOM})}{(Clay + Silt\ Content)} \times 100 \qquad \text{Equation 5.5}$$

Pieri (1992, pp.253) analysed 495 soil samples from West Africa to establish the relationship between SOM and the content of fine particles. He found that the more uniform the area of study, the closer the relationship between SOM and fine particle content. He also found that for 39 samples from the north of Togo the correlation coefficient for SOM versus fines content was r = 0.69 and that for 165 sites in Sefa (Casamance, Senegal) the correlation coefficient, r = 0.8. Values were also obtained from some poorly sites with poorly structured and/or eroded soils (e.g. Yatenga and others in Burkina Faso, Sine Saloun in Senegal, and N'Tarla in Mali), as well as sites where soils were judged to be in satisfactorily physical condition (e.g. Bebedjia in Chad and some compound areas in Burkina Faso). The results of these studies showed that where S_t < 5%, there is a loss of soil structure and high susceptibility to erosion. Where, S_t > 5% but < 7%, there is instability and a risk of loss of soil structure, and where S_t > 9% there is no immediate risk of structural decline and erosion (Pieri, 1992; Figure 5.1).

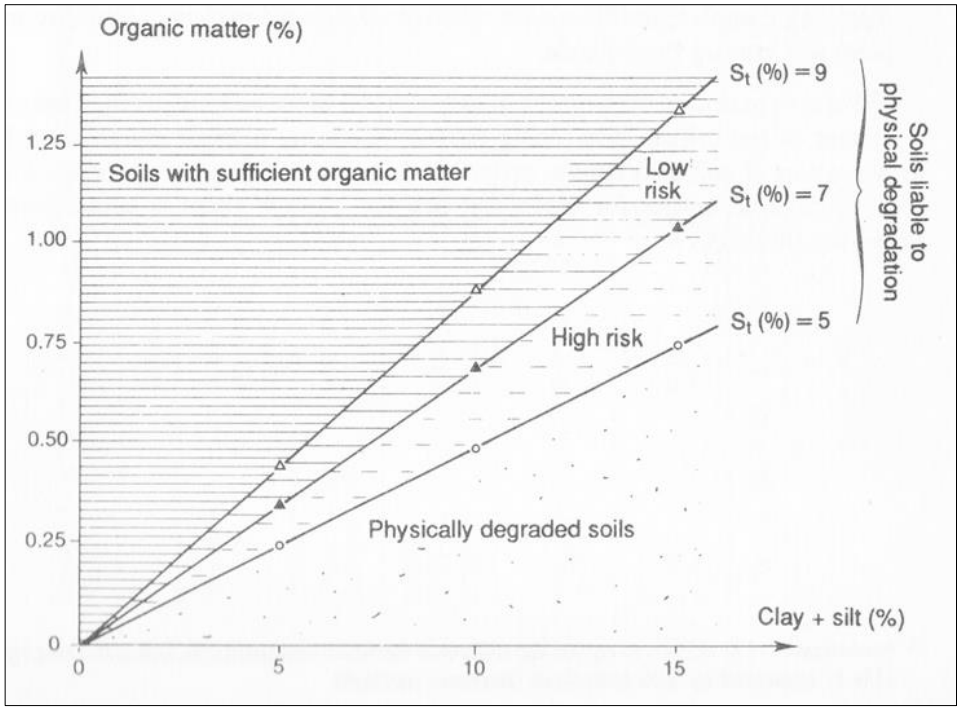

Figure 5.1. Critical organic matter levels for maintenance of physical soil stability and suppression of erosion/degradation. After Pieri (1992).

5.3.7. **Sodium absorption ratio (SAR) and exchangeable sodium percentage (ESP)**

Clay particles can either be dispersed, or flocculated into aggregates. Flocculation or aggregation describes the cementation of clusters of discrete sand, silt and clay particles into larger assemblages, and is desirable to allow water to move through the large pore spaces between the aggregates. Plant roots also grow mainly between aggregates.

Soil particles flocculate readily when negatively charged clay particles (anions) bond with divalent cations such as Calcium cations (Ca^{2+}) or magnesium cations (Mg^{2+}). Thus, Ca^{2+} and Mg^{2+} are good flocculants. In contrast, the Sodium cation (Na^{+}) is a poor flocculant that causes dispersion of the clay in the soil rather than flocculation. The ratio of poor to good flocculants is expressed by the sodium absorption ratio (SAR) as:

$$SAR = \frac{\mathrm{Na}^{+}}{\sqrt{(Ca^{2+} + Mg^{2+})/2}} \qquad \text{Equation 5.6}$$

Susceptibility to chemical dispersion of different soils upon wetting is high when SAR values are > 13 (SSSA, 1997). Therefore, when SAR > 13, the soil material loses its structure and cannot withstand the erosive forces generated by flowing water.

In addition to SAR, the quantity of dissolved ions in a soil is important to its erosion resistance. Dissolved ions conduct electricity, so the total amount of soluble soil ions can be estimated by measuring the electrical conductivity (EC) of a soil water extract. Soil with a high EC is salty. Soil with low EC is not. The stability of the soil structure, especially in the fine texture of clayey soils, depends on both the SAR and the amount of soluble salt in the soil – as represented by its EC. Therefore, the threshold value of SAR is dependent on the EC. In other words, if the soil contains sufficient calcium and magnesium, soil particles will flocculate, giving a low SAR and strengthening the soil. Whereas, if the soil contains high levels of sodium, soil particles will disperse, giving a high SAR and weakening the soil. When the EC is high, soil particles will flocculate at lower calcium and magnesium and/or higher sodium concentrations than when the EC is low. Therefore, when EC is low soils are more likely to disperse, while they are more likely to flocculate when EC is high.

Another major consideration when working on saline soils is that various salts provide nutrients to plants, although too much salt can interfere with plant water uptake. Salty or saline soils result from various sources of salt ions. For example, sodium chloride salt (NaCl) is a compound that contains a sodium cation and a chlorine anion (Na^+Cl^-). Consequently, its excessive presence in soils interferes with the functions of plant roots trying to take up water from the soil.

When there is an abundance of NaCl in the soil, water (H_2O) can react with it, yielding Sodium Hydroxide (NaOH) and Hydrogen Chloride (HCl), which results in plant roots being unable to uptake water. This is represented by the chemical reaction:

$$Na^+Cl^- + H_2O = NaOH + HCl \qquad \text{Equation 5.7}$$

5.3.8. **Land use and vegetation cover impacts on gullying**

Vegetated surfaces intercept raindrops, reducing their impact on the land surface and associated rates of soil detachment (Renard *et al.*, 1997; Zartl *et al.*, 2001). Plant roots also bind soils together, increasing the critical flow force required to mobilise soil particles. The stems of vegetation provide resistance to flow and reduce the impact of fluid shear stress in causing scour. Taking advantage of these mechanisms, vegetation has been widely used in applied geomorphology to stabilise slopes and improve soil structure (Thorne *et al.*, 1997). When land use/vegetation cover change takes place, especially on slopes, the soil surface can become exposed to the impacts of concentrated overland flow, increasing the likelihood of gully initiation (Thorne, 1984a). Different types of vegetation will have different influences, based on the characteristics of the plants, seasonality of foliage and growth periods. Broadly, the more complex the vegetation assemblage, the greater the stabilising influence (Institution of Civil, 1995).

5.4. **Methodology**

5.4.1. **Methodological overview**

In the investigations described in this chapter, the CTI1 and fuzzy-CTI1 models that were developed and tested in Chapter 4 were used together with available soil, land-use and geological data, to generate map layers for different areas of the study region of South Africa. The individual areas had differing land-uses, geologies and soil types. The predictive performances of the models were assessed using the ROC methodology that was applied in Chapter 4. The underlying hypothesis was that in areas where soil structure is strong, topography will not be as significant in driving gullying than it is in areas where soil structure is weak. If this hypothesis is true, it follows that in terms of predicting the existence of gullies, the CTI and/or fuzzy CTI models will perform relatively better in areas with weak soil, where topography is the dominant control on concentrated flow erosion, but relatively worse in areas where soils are either structurally strong (and erosion resistant) or protected by dense vegetation cover.

5.4.2. **Environmental descriptors**

A soil grid database (Hengl *et al.*, 2017) is available for the study area, from which environmental descriptors relating to the soil could be computed. Textural classes, (sand, silt and clay) were obtained from the soil grid data based on sand (50-2000 μm), silt (2 – 50 μm) and clay (< 2 μm) contents measured at 6 standard depths for two sets of Africa soil profile data (Hengl *et al.*, 2015). The textual classes were resampled to 30 m to match other existing data for the region, including CTI and fuzzy CTI values derived from 30 m resolution DEMs. The ‘extract multi-raster values to raster’ tool was used for this purpose. The resulting attribute table was exported to SAGA GIS, where a tool was available to both compute and reclassify soil texture, and generate the appropriate soil texture triangle diagram (Figure 5.2).

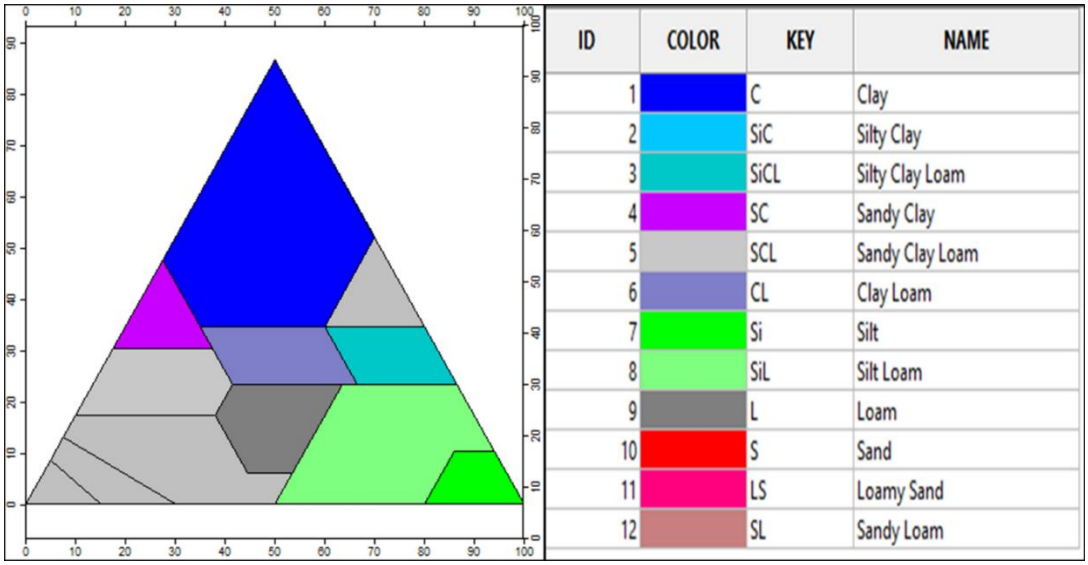

Figure 5.2. Soil Textural Class for the study area in the Eastern Cape province, South Africa.

Soil organic carbon content (quantified by either wet oxidation or dry combustion at 900 °C) at the same 6 standard depths was predicted using two sets of Africa soil profiles data (Hengl *et al.*, 2015) and was multiplied by 1.72 to obtain the soil organic matter content. The critical level of soil organic matter content (S_t) was computed using Equation 5.5. Based on expert knowledge presented in section 5.3.6 above, a reclassification of the critical level of soil organic matter content was developed, as set out in Table 5.2.

Table 5.2. Reclassification of critical level of soil organic matter content.

Class Number	S_t Thresholds	Interpretation of S_t Thresholds
1	0 - 5	there is loss of soil structure and great susceptibility to erosion (Physically degraded soil)
2	5 - 7	there is instability and risk of loss of soil structure (High risk)
3	7 - 9	there is no immediate risk of structural decline (Low risk)
4	>9	Soils with enough matter

The geology shapefile for Africa from which the geology of Eastern Cape province in South Africa was extracted can be obtained at the US Department of the Interior (USDI, 2019) or from the ORR & Associates website (ORRA, 2019). Land cover was

extracted from the land cover for Africa map, which was produced at 20 m, and based on 1 year of Sentinel -2A Observation. That map was published by the European Space Agency (ESA) (ESA, 2017). Land cover data was also resampled to the same spatial resolution as the USGS SRTM DEM of 30 m resolution. The digital soil map of the region was obtained from FAO GIS datasets (FAO, 2007). Soils can be visualised and identified by downloading the pdf version of the map at high definition (600 dpi). The hillslope form elements map was produced from the 30 m USGS SRTM DEM of the region based using the approach developed by Dikau (1989) for use in landform mapping (Dikau, 1988; Dikau, 1989; Pike *et al.*, 1995; Schmidt *et al.*, 2000; MacMillan and Shary, 2009; Dikau *et al.*, 2013; Messenzehl *et al.*, 2014). Geomorphological slope classes were mapped using the Young (1972) and Young and Clayton (1972) approach, as described in Chapter 2. Table 5.3 is a compilation of all the environmental descriptors, their substrates/classes and codes.

Table 5.3. Environmental descriptors and their substrates/classes.

Environmental descriptors	Classes	Codes
Predictive model(s)	CTI and Fuzzy CTI	Continous
Land cover	Tree cover	1
	Shrubs	2
	Grassland	3
	Cropland	4
	Lichens Mosses / Sparse vegetation	6
	Bare areas	7
Geology	Carboniferous and Devonian (CD)	1
	Cretaceous and Jurassic (JK)	2
	Devonian (undivided)(D)	3
	Mesozoic extrusive and intrusive rocks (Mi)	4
	Permian(P)	5
	Precambrian (undivided)(PC)	6
	Quaternary (undivided)(Q)	7
	Quaternary and Tertiary((QT)	8
	Silurian-Ordovician (SO)	9
	Tertiary(T)	10
	Triassic (Tr)	11
Soil type	Orthic Acrisols (Ao)	1
	Orthic Ferrasols (Fo)	2
	Rhodic Ferrasols (Fr)	3
	LITHOSOLS (I)	4
	Chromic Luvisols (Lc)	5

	Orthic Luvisols (Lo)	6
	Eutric Planosols (We)	7
	Solodic Planosols (Ws)	8
	Calcic Xerosols (Xk)	9
critical level of soil organic matter content	there is loss of soil structure and great susceptibility to erosion (Physically degraded soil)	1
	there is instability and risk of loss of soil structure (High risk)	2
	there is no immediate risk of structural decline (Low risk)	3
	Soils with enough matter	4
Real gullies/Ground truth	No gully	1
	Gully	2

5.5. **Results and discussion**

5.5.1. **Exploration of the benefits of considering land cover**

ROC curves were generated for CTI1 and Fuzzy_CTI1 for selected regions with specific and distinct land cover and soil conditions. When no threshold CTI was used, AUC values were all above 50%, but did not exceed 62% (Figure 5.3). The higher predictive performances were for areas characterised by crops, shrubs and trees. Comparison of the areas under the curves for the two models showed that, for all but one land cover category, the fuzzy CTI performed marginally better than the original CTI, in terms its performance in correctly predicting observed gullies.

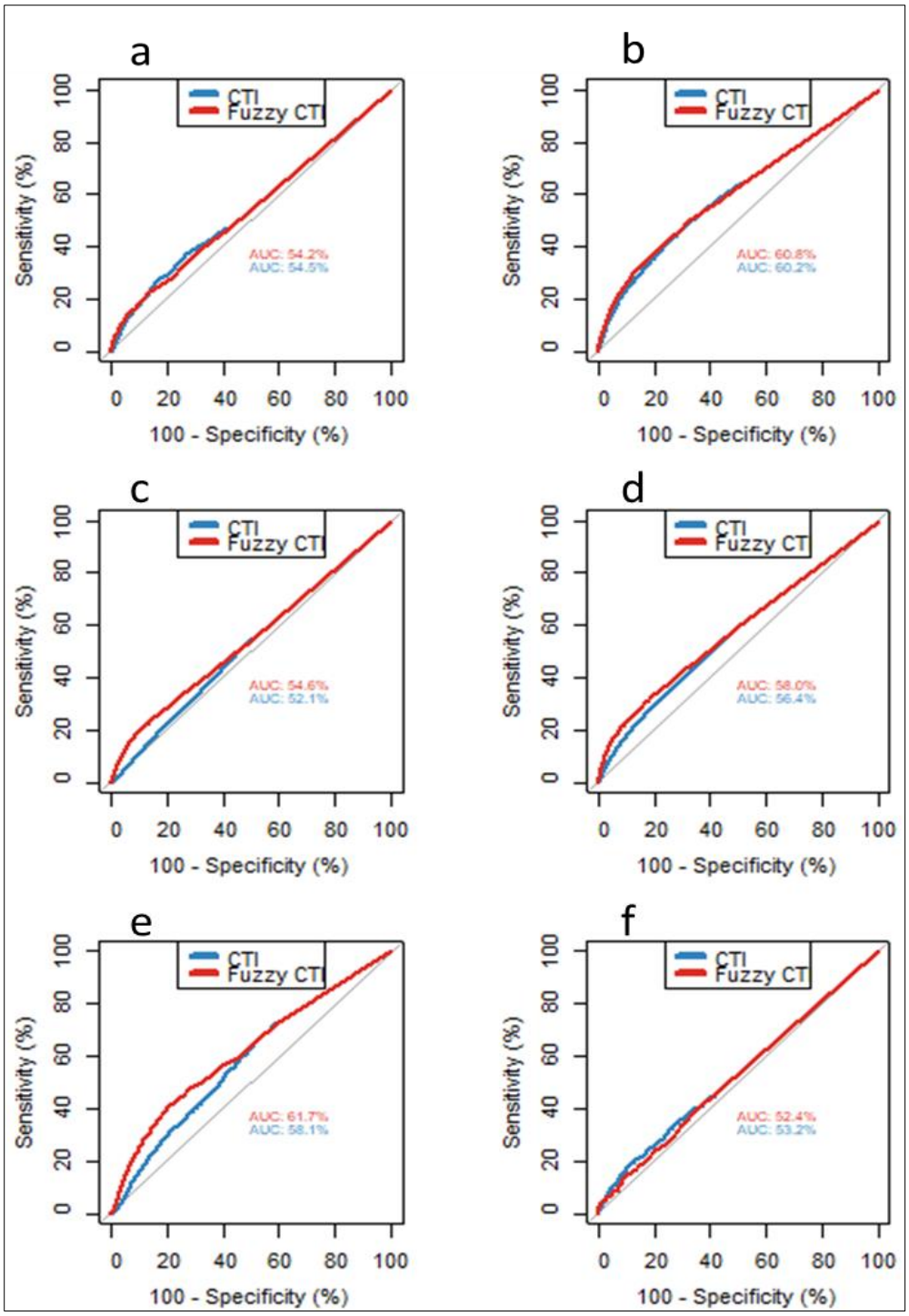

Figure 5.3. ROC curves for original and fuzzy CTI models (without threshold values) for the Eastern Cape Province specific to land covers of: (a) bare soil, (b) crops, (c) grass, (d) shrubs, (e) trees, and (f) lichens, mosses and sparse vegetation. In most cases, AUC values for fuzzy CTI are slightly higher than for the original CTI. While all AUCs are relatively low when no threshold CTI is used, fuzzy CTI out-performs the original CTI, albeit only by a small margin under all land covers except (f).

Further evaluation of the fuzzy CTI involved consideration of its *Accuracy* and *Sensitivity*, with respect to threshold values selected to set the lower limit on the intensity of concentrated overland flow necessary to initiate a gully, and in relation to the numbers of gullies actually observed in areas characterised by different land covers – as represented by their *Prevalence*.

Accuracy represents the overall performance of CTI in terms of the proportion of correct predictions of gullying and no gullying (TP and TN) it makes, as a percentage of the total number of cells in the DEM. As was set out in Chapter 3 (equation 3.3), this is computed as:

$$\text{Accuracy } = \left(\frac{TP+TN}{TP+TN+FP+FN}\right) \times 100$$

That is, the sum of true positives and true negatives, divided by the total number of cells in the DEM.

When fuzzy CTI was calculated without a threshold value, *Accuracy* was low (< 60%) for all land covers, and particularly so for trees (Table 5.3, Figure 5.4). However, in areas with tree cover the *Accuracy* of the fuzzy CTI improved sharply (from 44% to 63%) when a very low threshold fuzzy CTI of 0.01 was used. It then continued to rise steeply (to 83%) with a threshold fuzzy CTI value of 0.03, before rising a little more (to 89%) for the highest CTI threshold in the study (0.12). Small improvements in *Accuracy* were gained using relatively low threshold fuzzy CTI's (less than 0.03) for bare ground, crops, and shrubs, but not for grass (Table 5.3, Figure 5.4). These findings indicate that, with respect to model performance in terms of *Accuracy*, it is helpful to identify and select an appropriate threshold value for fuzzy CTI, especially in areas of tree cover.

Table 5.3. *Accuracy* and *Sensitivity* values for fuzzy CTI under different land covers, using no threshold CTI value and a range of possible threshold CTI values.

Threshold CTI	Bare	Cropland	Grassland	Shrubs	Trees
			Accuracy		
0.000	52.68%	57.23%	52.79%	54.68%	44.32%
0.010	55.20%	57.29%	49.44%	56.06%	62.98%
0.020	56.15%	55.19%	46.83%	56.21%	78.85%
0.030	55.39%	52.80%	44.72%	55.17%	83.46%
0.040	54.82%	50.97%	42.94%	54.02%	85.69%
0.050	54.05%	49.49%	41.68%	53.01%	86.81%
0.060	53.36%	48.12%	40.41%	51.93%	87.63%
0.070	53.25%	47.08%	39.56%	51.09%	88.12%
0.080	52.98%	46.34%	39.17%	50.58%	88.51%
0.090	52.75%	45.53%	38.62%	50.00%	88.95%
0.100	52.75%	45.13%	38.43%	49.77%	89.14%
0.110	52.75%	44.82%	38.29%	49.59%	89.34%
0.120	0.00%	44.59%	38.23%	49.45%	89.49%
			Sensitivity		
0.000	64.47%	60.99%	63.76%	54.90%	11.85%
0.010	55.37%	66.79%	67.22%	59.93%	13.88%
0.020	65.08%	74.84%	74.33%	69.01%	18.76%
0.030	70.41%	78.85%	78.67%	74.83%	20.65%
0.040	75.47%	81.02%	79.93%	78.44%	22.30%
0.050	73.61%	81.48%	80.77%	79.89%	22.76%
0.060	71.05%	82.89%	80.23%	80.94%	22.25%
0.070	76.00%	83.41%	79.27%	80.19%	20.72%
0.080	71.43%	83.17%	79.86%	79.21%	19.06%
0.090	50.00%	*83.29%*	74.05%	77.34%	16.13%
0.100	50.00%	82.14%	70.66%	75.52%	12.59%
0.110	50.00%	81.05%	65.15%	74.39%	11.61%
0.120	0.00%	82.19%	60.27%	66.41%	5.06%

Note: the highest values of Accuracy and Sensitivity for each land cover are highlighted in grey.

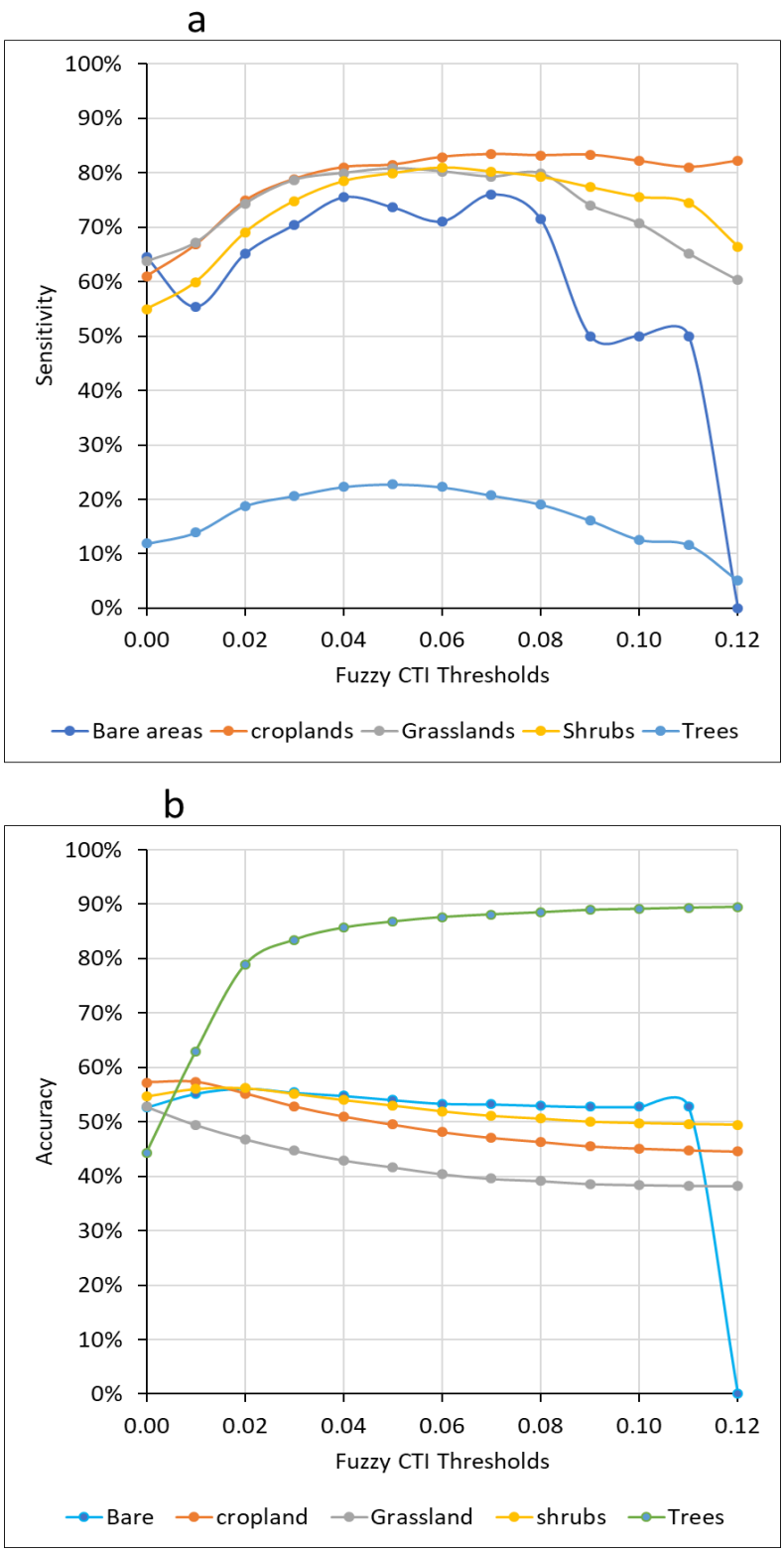

Figure 5.4. (a)Sensitivity and (b) Accuracy under different land covers for a range of threshold values for fuzzy CTI.

To investigate the contrasting performances of the fuzzy CTI in areas with different land covers, and how performance varied with the threshold CTI, *Sensitivity* was also explored. *Sensitivity* represents how often the CTI model correctly predicts gullies that were actually observed in the 'ground truth'. As set out in Chapter 3 (equation 3.1), it is calculated as:

$$\text{Sensitivity} = \left(\frac{TP}{TP + FN}\right) \times 100$$

That is: the number of true positives, divided by the number of true positives plus false negatives.

Without a threshold for the fuzzy CTI, *Sensitivity* values for bare ground, crops, grass and shrubs were in the range of 55 to 65%, but *Sensitivity* for tree cover was much lower (<12%). Introducing thresholds for fuzzy CTI ranging between 0.04 and 0.07 increased *Sensitivity* for all land covers, with values of 75% to 80% being achieved for bare ground, crops, grass and shrubs (Table 5.3, Figure 5.4). *Sensitivity* for tree cover was doubled to 23% when a threshold fuzzy CTI or 0.06 was used. These results demonstrate that with respect to model performance in terms of *Sensitivity*, it is helpful to identify and select an appropriate threshold value for fuzzy CTI, although the improvement is limited in areas of tree cover.

Accuracy and *Sensitivity* represent different aspects of the predictive performance of the fuzzy CTI when applied using a 30 m grid. *Accuracy* is the broader metric, indicating the overall success of the model in correctly predicting both where gullies formed by concentrated overland flow would, and would not, be expected in the 'ground truth' representation of the landscape. *Sensitivity* is the narrower metric, representing the performance of the model purely in terms of predicting locations where gullies would be expected, with no account of its success in predicting where gullies would not be expected. It follows that users should think carefully about how they are going to use predictions made using the fuzzy CTI and then optimise model performance by selecting the best value for the threshold fuzzy CTI.

If the most important goal is to correctly predict the concentrated flow paths along which gullies may be expected to form, then the threshold CTI that maximises *Sensitivity* is the one to use. For this purpose, the best threshold value is likely to be relatively high (e.g. in the case of land cover specific areas of the eastern Cape, 0.04 to 0.07, in a range extending between 0 and 0.12 – Table 5.3, Figure 5.4). With these thresholds, it was possible to achieve values of *Sensitivity* in the range 75% to 80% (Table 5.3, Figure 5.4) based on application of fuzzy CTI to a 30 m DEM and considering readily available information on the environmental descriptor of whether the land cover was bare ground, crops, grass and shrubs. However, the case of tree cover was exceptional, and is considered below.

If the user wishes to identify (and map) areas that are, and are not, susceptible to gullying, then it would be better to select the threshold value based on maximising the model's *Accuracy*. This is because the user is not trying to correctly predict the concentrated flow paths along which gullies may be expected to form, but areas in the landscape where gullies could form if, for example, there was extreme rainfall or a change of land use. For this purpose, the best threshold value is likely to be relatively low (e.g. in the case of land cover specific areas of the eastern Cape, 0.0 to 0.03 (Table 5.3, Figure 5.4), in a range extending between 0 and 0.12). With these thresholds, it was possible to achieve values of *Accuracy* in the range 53% to 57% based on application of fuzzy CTI using a DEM with a 30 m grid and taking into account the environmental descriptor of whether the land cover was bare ground, crops, grass and shrubs. However, as with *Sensitivity*, the case of tree cover was exceptional, and is considered below.

But before moving on to consider the results for areas with tree cover, it is necessary to point out that the *Accuracy* values for the other land covers are all greater than 50% and (based on the analyses performed in Chapter 4), they are likely to be statistically significant. That said, these values of *Accuracy* are clearly lower than *Sensitivity.* This is acceptable because the fuzzy CTI is not being used to predict the locations of existing gullies; it is being optimised to differentiate between areas that are topographically-susceptible to gullying and areas that are not. Hence, the model's relatively weak (but still significant) performance in terms

of predicting where gullies were and were not observed in 'ground truth', is not a problem.

The performance of the fuzzy CTI when applied to areas with tree cover differed from that in the other four land cover types. To explain why, it is necessary to consider the how the *Prevalence* of gullies in areas with tree cover differed from that in the other areas. This performance parameter is the percentage of cells in the 'ground truth' observations that actually had gullies. As set out in Chapter 3 (Equation 3.4), this is calculated as:

$$\text{Prevalence} = \left(\frac{TP + FN}{TP + TN + FP + FN}\right) \times 100$$

Values of *Prevalence* for gullies in the five land use types are listed in Table 5.4.

Table 5.4. Values of FN, FP, TN, TP and *Prevalence* for the five land use types

Land use	FN	FP	TN	TP	Totals	**Prevalence**
Bare areas	661	560	794	574	2589	**47.70**
Cropland	4240	4845	4577	7581	21243	**55.65**
Grassland	11838	8114	8018	14284	42254	**61.82**
Shrubs cover areas	11677	13574	13912	16563	55726	**50.68**
Tree cover areas	278	5438	3827	733	10276	**9.84**
Total number of cells					132088	

Consideration of *Prevalence* reveals that gullies were largely absent from the area with tree cover (<10%) compared to the other land covers (48 to 62%), which is expected given the high level of erosion protection provided by forests. *Accuracy* values generated using the fuzzy CTI consequently trended toward a very high levels (>89% - Table 5.3, Figure 5.4) asymptotically as threshold CTI values increased to a high level (0.12), due to large and increasing numbers of True Negative (TN) predictions, which resulted from exclusion of more and more cells in the tree cover area that did not have a gully even though they did experience concentrated overland flow. This explains why the tree cover area had unusually high *Accuracy:* it was simply because >90% of the tree cover area was correctly predicted as 'no gully'.

Conversely, *Sensitivity* for the tree cover area was low because the model incorrectly predicts gullies in areas of concentrated flow where gullies did not form, due to the protective effects of the tree cover. Given the small percentage of DEM cells (<10% - Table 5.4) that had gullies according to 'ground truth', it is unsurprising that the fuzzy CTI produced relatively few of the 'True Positives' necessary to produce a high *Sensitivity*. In contrast, areas with over covers have higher *Sensitivity* values when the appropriate threshold CTI is used, because gullies were observed in a large percentage of the area where topography concentrates the flow, due to lack of protective vegetation cover. Conversely, *Accuracy* is lower in under land covers than it is for tree cover, because the model still predicts that gullies could form in areas where concentrated overland occurs, where no gully was observed in the 'ground truth' data.

5.5.2. **Exploration of the benefits of considering soil conditions**

The same procedure as described in Section 5.5.1 was undertaken for different levels of soil organic matter content. The results are listed in Table 5.5 and graphed in Figure 5.5. The pattern of results that emerged for soil organic matter content was broadly similar to that for land cover, with model *Accuracy* varying inversely to *Sensitivity*.

A critical level of soil organic matter in category 1 (S_t1), representing weak soils, had a high Prevalence for gullying (55%). In the S_t1 area, fuzzy CTI performed with low *Accuracy* (<55%), but high *Sensitivity* (>75%) when optimum threshold values were selected. If the user wished to predict the gullies observed in the 'ground truth', the threshold CTI should be set at 0.06. However, if the aim was to delineate areas topographically-susceptible gullying caused by concentrated flow erosion of these weak, erosion prone soils, either no (or a very low) threshold value (0 or 0.01) should be selected.

Table 5.5. Accuracy and Sensitivity values for fuzzy CTI in areas with different levels of soil organic matter content, using no threshold CTI and a range of possible threshold CTI values.

Threshold Fuzzy CTI	st1	st2	st3	st4
Accuracy				
0.00	53.69%	47.25%	47.04%	46.41%
0.01	54.36%	66.97%	67.96%	68.51%
0.02	54.24%	82.63%	85.00%	86.74%
0.03	52.97%	88.57%	90.56%	95.58%
0.04	51.74%	90.82%	93.33%	96.13%
0.05	50.72%	92.08%	94.81%	96.69%
0.06	49.66%	92.80%	96.11%	98.90%
0.07	48.89%	93.25%	96.67%	98.90%
0.08	48.44%	93.97%	96.85%	-
0.09	47.92%	94.15%	97.04%	-
0.10	47.71%	94.69%	97.22%	-
0.11	47.55%	94.78%	97.78%	-
0.12	47.45%	94.78%	97.78%	-
Sensitivity				
0.00	55.74%	5.37%	2.74%	0.00%
0.01	60.17%	6.16%	3.43%	0.00%
0.02	68.58%	7.36%	5.06%	0.00%
0.03	73.32%	10.75%	6.38%	0.00%
0.04	75.81%	10.00%	9.38%	0.00%
0.05	76.62%	11.36%	9.09%	0.00%
0.06	76.74%	13.89%	7.69%	0.00%
0.07	75.68%	11.11%	10.00%	0.00%
0.08	74.76%	11.76%	11.11%	0.00%
0.09	71.38%	7.69%	0.00%	0.00%
0.10	68.14%	14.29%	0.00%	0.00%
0.11	63.75%	0.00%	0.00%	0.00%
0.12	55.62%	0.00%	0.00%	0.00%

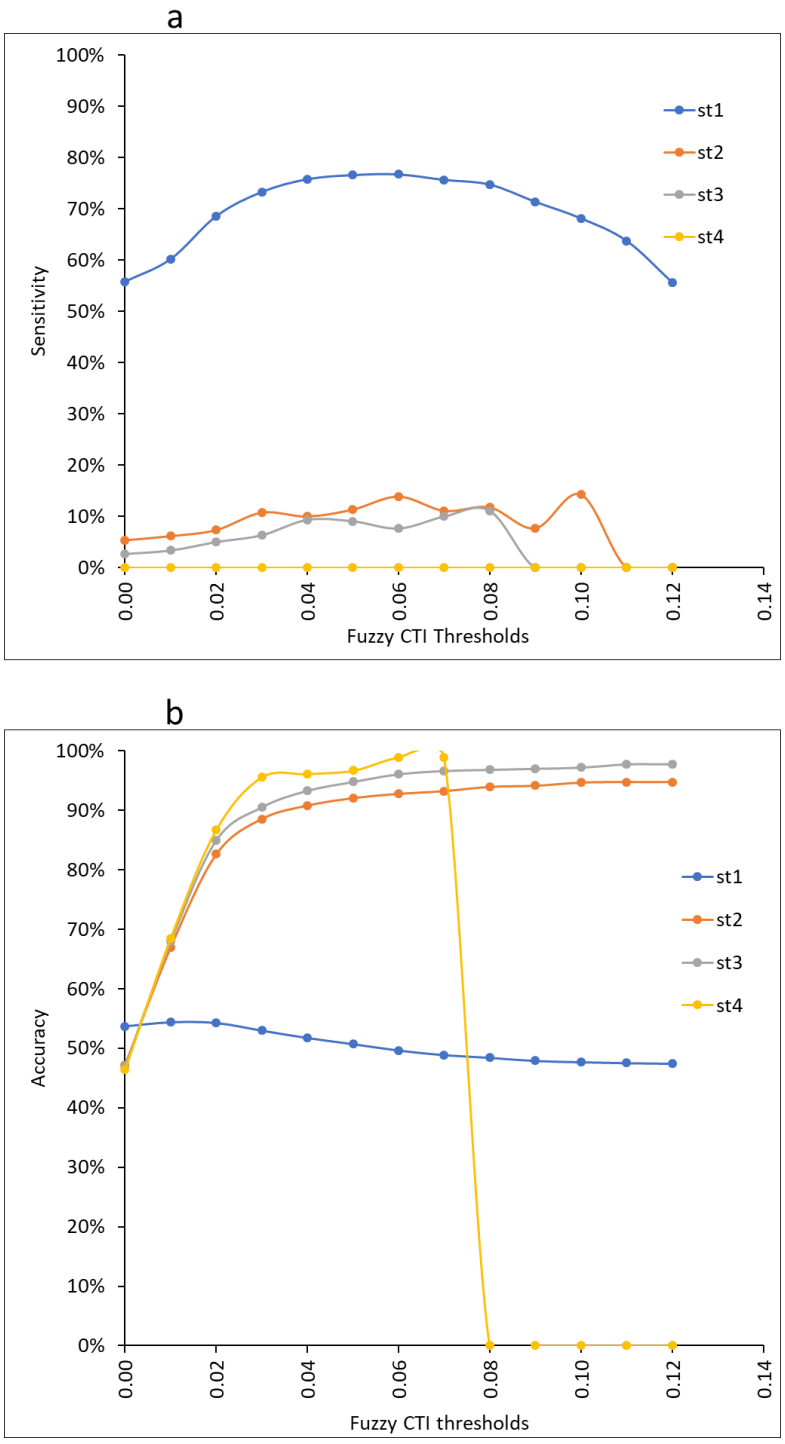

Figure 5.5. (a)Sensitivity and (b) Accuracy under levels of soil organic matter content for a range of threshold values for fuzzy CTI. Note: St1 = loss of soil structure and high susceptibility to erosion (i.e. physically degraded soil), St2 = instability and high risk of loss of soil structure, St3 = no/low immediate risk of structural decline, and, St4 = soils with enough organic matter.

Areas with soils catorgorised as St2 and St3 had very few gullies, with Prevalence values being <5% and <2%, respectively (Table 5.6). Very low numbers of cells with gullies in the 'ground truth' limited the number of 'True Positives' that were possible, meaning that *Sensitivity* was maximised when the threshold CTI was set at high values (0.1 and 0.08, respectively). Due to the very small *Prevalence* of gullies, *Accuracy* approached 100% as the threshold fuzzy CTI was increased to its highest value.

At the top end of the range of organic matter categories, no gullies at all were observed in the St4 area (which had the strongest, least erodible soils). Consequently, *Sensitivity* was zero for all threshold fuzzy CTI values, simply because there could be no 'True Positive' predictions. As no gullies were actually observed, even in the area most topographically-susceptible to gulling, the predictive performance of the fuzzy CTI as represented by *Accuracy* approached 100% asymtopically as the threshold fuzzy CTI was increased to 0.07.

Table 5.6. Values of FN, FP, TN, TP and *Prevalence* for the four soil organic matter contents

Soil critical organic matter	FN	FP	TN	TP	Grand Total	**Prevalence**
S_t1	29207	31942	30777	40161	132087	**52.52**
S_t2	22	570	504	32	1128	**4.79**
S_t3	2	284	250	8	544	**1.84**
S_t4	0	96	84	0	180	**0**
Total number of cells					133939	

5.5.3. **Prediction of gullies at sub-Provincial scale in the Eastern Cape Province**

Applying the CTI approach to the entirety of the East Cape Province demonstrates the currently limited capacity of the method to predict gullies observed in large areas of the landscape (Chapter 4; *Accuracy* ~50%). However, in practice, it is likely that the model would be applied over smaller areas, such as particular administrative districts. To evaluate how the original and fuzzy CTI analyses performed at smaller scales, they were applied to selected administrative units within the Eastern Cape province of South Africa. These administrative units were: Alfred Nzo, Amathole, Buffalo City, Chris Hani, Joe Gqabi, Nelson Mandela Bay, ORT

Tambo, and Sarah Baartman. The resulting ROC curves are plotted in Figure 5.6, while Figure 5.7 allows direct comparison of the performances of the two versions of the CTI, with the results plotted in terms of ascending order of AUC. In these applications, based on a coarse (30 m DEM and for which no threshold CTI values were tested), fuzzy CTI was again found to be very marginally better than the original CTI, though the model's power to predict the locations of observed gullies is only low to moderate in all cases. Based on the results reported in the preceding sections of this chapter, CTI performance could have been substantially improved by accounting for other environmental descriptors (e.g. land cover, soil organic matter content) and testing a range of possible threshold values, and iteratively selecting the one with the highest *Sensitivity* (if the goal is gully prediction) or *Accuracy* (for delineating areas topographically-susceptible to gullying).

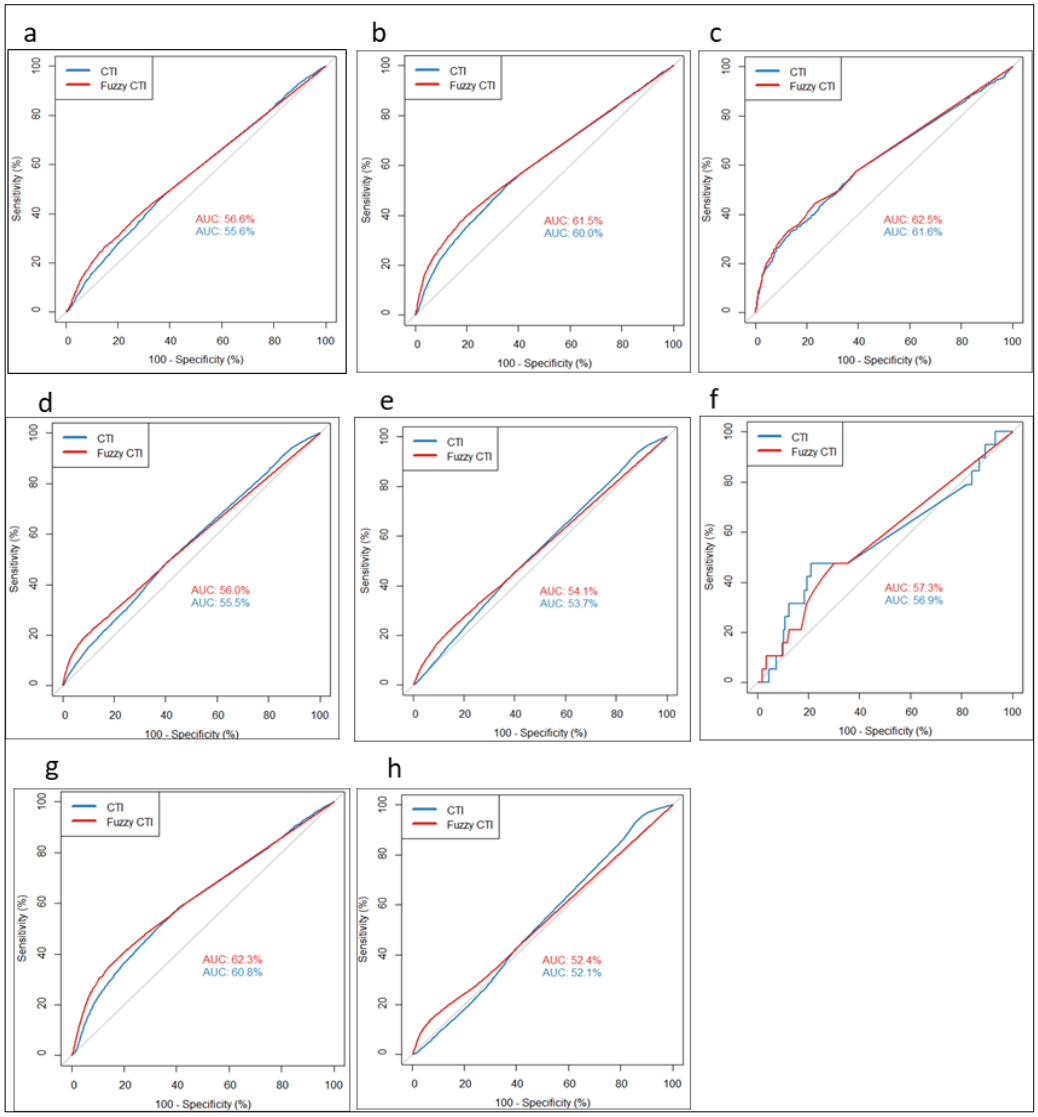

Figure 5.6. ROC curves for original and fuzzy CTI (with no threshold CTI value) applications in selected administrative districts of the Eastern Cape: (a) Alfred_Nzo, (b) Amathole; (c) Buffalo City (d) Chris Hani, (e) Joe Gqabi, (f) Nelson Mandela Bay, (g) OR Tambo, and (h) Sarah Baartma.

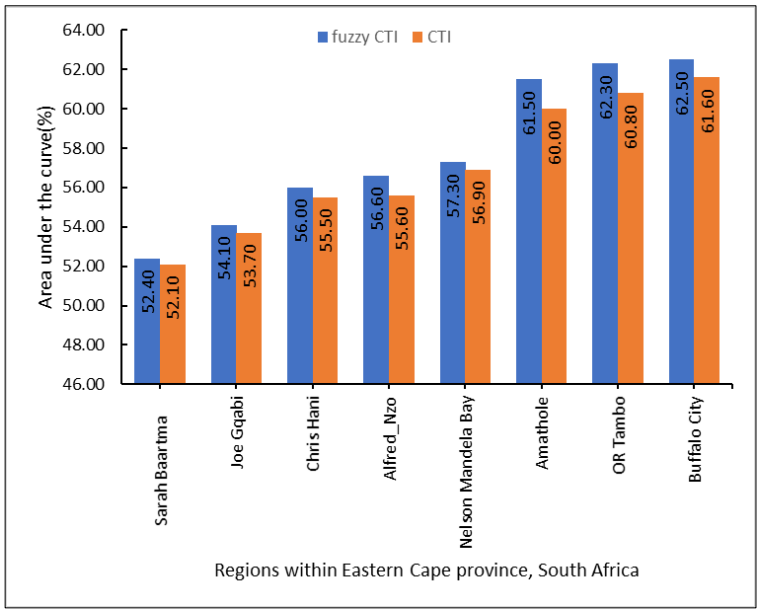

Figure 5.7. Bar chart allowing direct comparison of the predictive performances of the original and fuzzy CTI models (as indicated by area under the ROC curve) when applied in selected administrative units of the Eastern Cape province of South Africa.

5.5.4. **Analysis of variance of fuzzy CTI with subsets of environmental descriptors**

Sections 5.5.1 and 5.5.2 explored whether considering land-cover or critical organic matter content improved model performance in predicting observed gullies. The results reported above indicate that the predictive performance of the fuzzy CTI does vary between different land cover, and that the same is true for different levels of critical soil organic matter content. However, investigation was not made as to whether fuzzy CTI values vary *significantly* between different environmental descriptors.

In this section, further analyses are therefore performed to test the null hypothesis that there is no statistically significant variation in mean values of the fuzzy CTI when different subsets of environmental descriptors are taken into consideration.

The complete descriptive statistics computed for applications considering different environmental descriptors are voluminous and so are presented in an appendix (Appendix D), with a summary of the ANOVA results is included here in the main text in Table 5.7.

The results of the ANOVA analyses using the least small difference (LSD) approach indicate that there is a statistically significant variation ($p < 0.05$) in the mean values of fuzzy CTI with classes of the different environmental descriptors. The results of the *post hoc* ANOVA for level of soil organic content (Appendix E) indicate a statistically significant variation between S_t1 and S_t2 ($p = 0.003$), S_t1 and S_t3 ($p = 0.044$) and S_t1 and S_t4 ($p = 0.029$). However, there was no statistically significant variation between S_t2 and S_t3 ($p = 0.977$), S_t2 and S_t4 ($p = 0.358$) and S_t3 and S_t4 ($p = 0.381$). For the land cover the post hoc ANOVA presented Appendix Table E.2 indicate that the mean difference is statistically significant at the 0.05 alpha level for all the pair of land use(Appendix E). Post hoc ANOVA for soil type presented in Appendix Table E.4(Appendix E) indicates that the mean difference is statistically significant(Sig.< 0.05) at the 0.05 level for comparison between two soil types except between the Ao and Fr, Ao and We, Fo and Lo and Fr and We that there is no statistically significant difference(Sig.>0.05).

As mean fuzzy CTI values do in fact vary between the various environmental descriptors, the null hypothesis must be rejected. Therefore, it is concluded that fuzzy CTI values do vary significantly between different environmental descriptor sub-areas within the Eastern Cape study area(

Table 5.7. Summary results for fuzzy CTI applications with different Environmental Descriptors, based on post hoc tests for multiple comparisons of means of fuzzy CTI using the least small difference (LSD) approach.

Environmental descriptor	Group type	Sum of Squares	Df	Mean Square	F	Sig.
Level of Soil Organic Content	Between Groups Within Groups Total	0.007 53.473 53.480	3 133786 133789	0.002 0.000	5.757	0.0006
Land Cover	Between Groups Within Groups Total	0.215 53.265 53.480	5.0000 133784 133789	0.043 0.000	108.149	0.0000
Soil Types	Between Groups Within Groups Total	0.766 52.715 53.480	8 133781 133789	0.096 0.000	242.894	0.0000

5.5.5. **Discussion and Conclusion**

When measured by ROC-AUC, the fuzzy CTI has been shown to perform slightly better than the original CTI in predicting the locations of observed gullies when applied at 30 m resolution in the study area of South Africa. The results of exploratory analyses performed under different land uses/covers, and for soils with a range of critical levels of soil organic matter, suggest that croplands have the highest vulnerability to concentrated flow erosion (i.e. highest *Prevalence*), probably due to a combination of lack of protective vegetation cover coupled with loss of soil structure in arable fields (i.e. S_t1 conditions). Conversely, very few gullies were observed in areas with trees and no gullies at all were observed in areas with a high content of critical organic matter (S_t4).

Mean values of fuzzy CTI were found to differ significantly between different Environmental Descriptors, indicating that consideration of such descriptors does affect fuzzy CTI values calculated within a large region.

The predictive performance of the fuzzy CTI varied across different land cover types and different categories of critical soil organic matter. *Accuracy* was highest in tree covered areas and lowest in croplands and bare soils, but *Sensitivity* had the opposite trend. This was shown to be the result of there being widely different percentages of cells with gullies (as represented by *Prevalence*) in the tree covered versus the other study areas. For example, low *Sensitivity* for forested areas indicates the fuzzy CTI substantially over-predicted the number of cells with observed gullies, because few gullies had actually formed - even in areas where topographic-susceptibility to gullying was high and concentrated overland flow occurred. Conversely, high *Sensitivity* in croplands indicates that the fuzzy CTI correctly predicted most of the observed gullies, most likely because even at fairly low intensities, concentrated overland flow was easily able to overcome the low erosion resistance of unprotected soils with weak structures, to form gullies in most of the areas where concentrated flow occurred.

Using an iterative approach to identifying the optimum threshold value of fuzzy CTI enhanced predictive performance (as inferred by considering either *Accuracy* or *Sensitivity,* the choice depending on the purpose of the fuzzy CTI application). This finding clearly demonstrates that, in data sparse regions where only a coarse DEM is available and where no basis exists for selecting a suitable threshold value *a priori*, consideration of land cover and soil erosion resistance (for which data are readily available even in LEDCs), together with use of an iterative approach to selecting the threshold fuzzy CTI value, can substantially improve the performance of the fuzzy CTI in predicting both gully locations and susceptibility to gullying.

CHAPTER 6: DISCUSSION AND CONCLUSIONS

6.1. Major findings of the study and their implications

The substantial and detailed data inputs required to model and predict gullying are unavailable in many of the areas of the World where such model applications are most needed. Thus, there is an urgent need for investigation into the efficacy of simpler approaches to identifying gully susceptibility in data-sparse regions, and this was the main motivation for the research reported in this thesis. The underpinning hypothesis was that the data requirements currently specified for application of terrain analysis to gully prediction are stringent because of a desire to predict the precise locations, extents and sizes of gullies. It followed that focusing instead on identification of areas *susceptible* to gullying could greatly reduce data requirements for successful application of terrain analysis, opening the possibility for erosion avoidance and sustainable agricultural development based on better decision-making with respect to land use and soil conservation. The major findings of the study are summarised according to objectives as follows:

The first objective was, *to determine how different measures of slope affect terrain analysis, and the implications of DEM resolution and terrain ruggedness for slope calculation.* The outcome of this research shows that there can be considerable differences in the prediction of topographic attributes and gullying, when using different slope values. Determining which slope value was more accurate was confounded by the difficulty of quantifying the 'true' slope in the field. However, ruggedness was found to remain low (i.e. VRM <0.4) across DEMs with relatively coarse grid sizes of the type available in data sparse regions. This finding could not fully inform the choice of slope method. However the Zevenbergen and Thorne (1987) method was selected as the terrain analysis to be used for the global-datasets used in this research because the intent was to develop a method applicable to large regions (for which ruggedness values are always low and where Z&T has been generally recommended by previous researchers) and for the purposes of remaining in tandem with original spirit of the CTI.

The second objective was *to determine the effect of a Digital Elevation Model (DEM) grid resolution when calculating the Compound Topographic Index (CTI), which for decades has proved useful in identifying pathways for concentrated overland flow*. Research tests performed herein confirm previous work indicating that the CTI works well with high resolution DEMS (grid size < 5 m), but less well for coarser grids. Previous research described model performance qualitatively. Research performed here, for the first time quantifies predictive performance (AUC, *Accuracy* and *Sensitivity)* and shows how this becomes progressively poorer as the resolution coarsens. At 30 m grid size, quantitative accuracy using the original CTI was broadly 50%, which is unsatisfactory for practical use in predicting the locations of gullies.

The third objective was *to explore how fuzzification of the CTI affects its accuracy when applied using fine and coarse resolution DEMs.* To enhance the performance of the CTI for predicting topographic-susceptibility to gullying as well as gully locations in the landscape), a fuzzy logic approach was developed and tested. While this did not dramatically improve the power of the original CTI model to predict the locations of gullies when used with high resolution data, there was a very small, but consistent improvement in prediction for coarse resolution DEMs. This hints at the possibility of greater improvements if the fuzzy approach is further developed. Both models performed relatively poorly when no threshold CTI was selected, and/or no critical (minimum) value was set for the upstream contributing drainage area. The predictive ability of both models improved when threshold values were applied, and the fuzzy CTI continued to perform very marginally better than the original CTI.

The fourth objective was *to examine how other readily available environmental descriptors can be combined with knowledge of the distribution of concentration of overland flow, to inform prediction of topographic-susceptibility to concentrated flow erosion (e.g. gullying) and the likelihood of gullies being observed in the landscape.* The predictive performance of the fuzzy CTI (measured by *Sensitivity* when trying to predict the locations of gullying and *Accuracy* when trying to delineate areas susceptible and not susceptible to gulling) was improved

substantially when applied to areas characterised by specific environmental descriptors (e.g. categories of land cover and critical soil organic matter content). Interpreting the results of exploratory applications of the fuzzy CTI in the Eastern Cape province of South Africa was complicated by the fact that the *Prevalence* of gullies varied widely between areas with different land covers and soil properties, because *Prevalence* strongly affects the predictive performance of fuzzy CTI in terms of *Accuracy* and *Sensitivity*. Consequently, both *Accuracy* and *Sensitivity* must be computed and considered when selecting the appropriate threshold CTI value for a data-sparse region, where the threshold CTI is not known *a priori*. Results obtained in the Easter Cape province showed that it is possible to generate high values of *Sensitivity* (>75% to 80%) and statistically significant levels of Accuracy (>55%) using a 30 m grid DEM, when other environmental descriptors are taken into account and threshold values are optimised iterively.

6.2. **Fuzzy CTI and constraints on modelling**

Quantitative analyses performed herein established that the original CTI performed well with high resolution DEMs but, more poorly with coarser resolution DEMs, as was expected on the basis of previous, qualitative research. In an attempt to remedy this, the CTI was fuzzified, but tests using both high and low resolution DEMs for selected study areas at Mount St Helens, USA and the Eastern Cape Province of South Africa, failed to deliver substantially improved model performance. Whilst the fuzzy CTI successfully predicted gullies in the landscape (i.e. high *Sensitivity*), with statistically significant results, it also predicted gullies in areas without gullies (False Positives), which substantially reduce model *Accuracy* and limit its practical utility in predicting the locations of gullies featured in 'ground truth' observations or measurements. This was related to three factors:

1. to substantially improve the performance of the CTI in gully prediction it is necessary to set a suitable critical value, in terms of the minimum upstream contributing area required to initiate gullying, or in terms of a threshold value for the CTI itself. The problem that arises is in identifying the threshold

or critical value, which is problematic as values are likely to be specific to a particular region and unknown *a priori* for data sparse regions.

2. Fuzzy CTI values indicate where there is a possibility of gullying, due to concentration of overland flow, even where that probability of a gully actually forming is very small. Therefore, setting a threshold fuzzy CTI value becomes extremely important as, otherwise, such a method will predict gullying over larger areas than those where gullying is actually likely to occur.
3. The CTI fundamentally only focuses on the topography and, it identifies only where the topography could generate gullies – that is areas that are 'topographically-susceptible' to gullying. It is likely that high False Positive rates for the fuzzy CTI are not indicative of incorrect predictions, but instead reflect the fact that there exist many other factors that influence whether gullying actually occurs in areas subjected to concentrated surface runoff. In other words, large areas are likely *susceptible* to gullying based on their topography alone but, gullying does not occur because of other controls such as soil strength, vegetation cover and anthropogenic protection.

Therefore, a limitation in this study was the necessity to validate the model regarding the presence or absence of observed gullies, in areas which the model predicts to be *susceptible* to gullying. The subtle difference between these measures is critically important, and there may be limited opportunities to validate and optimise model predictions in data sparse regions.

The alternative approach, explored herein, is to validate the model separately in areas characterised by different land cover and soil structure categories. The results demonstrate that fuzzy CTI with either no, or a very low, threshold value performs best in areas of weak soil strength and little vegetation cover. This is logical as, in these areas, there is little surface protection and low resistance to erosion, so that topography will be the key driver of where and whether gullies form. However, in areas of tree cover and/or structurally-stable soils, fuzzy CTI performs poorly in predicting the actual occurrence of gullies, due to the fact that there are few (and in

some case no) gullies in the 'ground truth' observations. This is because the topography indicates *susceptibility* to gullying, but gullies are unlikely to occur because of the stability imparted by the other environmental factors. In such areas, if gullies are to be predicted, it is essential to employ a threshold value for the fuzzy CTI in order to increase the model's predictive performance, which should be expressed using *Sensitivity*. However, if it is only necessary to identify the *potential* for gullying should the land cover be removed or the soil structure deteriorate, then fuzzy CTI is suitable for this application and its performance in mapping areas as being susceptible to gullying should be gauged using *Accuracy*.

The point here is that fuzzy CTI can be used to avoid the serious gullying likely to occur if, for example, deforestation reduces erosion protection and soil strength in areas subjected to intense, concentrated overland flow. However, this requires that the results of topographic analysis are used to inform wise land use management and soil conservation decisions.

The impact of land cover and soil structure on modelling gullying has two important implications. The first is its importance to successful monitoring of gullying and the need to incorporate these parameters into topographic models of erosion, at least over large areas where such parameters may vary substantially. The second is the implications of land use change. The results presented here suggest that where soil structure is strong and vegetation complex, the topography is not a significant control on the occurrence and locations of gullies whereas, where soil is weak and vegetation minimal, topography is a dominant control and modelling using only topographic information is strong. Given that the fuzzy CTI maps *susceptibility to gullying* over large regions of the landscape based on the topography alone, this reinforces the view that land cover and soil health are key in preventing gullying and, if soil structure is diminished or forest cover lost, the potential for gullying increases dramatically.

6.3. **Implications for land management**

The impacts of land cover and soil structure on gully *Prevalence* and reducing model performance when no threshold CTI is used clearly have serious implications for sustainable land management. The fuzzy CTI with no (or a very low) threshold performs relatively well for areas with shrubs and croplands, indicating that these areas are vulnerable to gullying. It performs less well for forested areas and areas with soil that feature high organic matter content and a strong soil structure. Such areas are still topographically-susceptible to gullying, and gullies could form in these regions under extreme rainfall events, even though there is little evidence of gullies in the landscape. As mentioned above, False Positives in these areas do not indicate incorrect predictions in terms of susceptibility to concentrated flow erosion, but rather indicate that though these areas are topographically sensitive to gullying, other environmental factors, such as vegetation, are currently preventing gullies from being instigated. Therefore, if these forest areas are converted to cropland and/or the soil structure is weakened, gullies become more likely to form. Consequently, poor land management could lead to severe soil loss in such areas.

The aim of this thesis was *to develop a GIS-based approach that identifies (at a regional scale) areas that are susceptible to gullying*, with which to inform and enhance decision making regarding where land use changes take place; i.e. helping to identify where forest should be left intact, and where it is safe to remove it for farming or other types of development. However, what was unexpected is that the fuzzy CTI predicts gully susceptibility over very large areas of the landscape. This is less useful for land use optimisation, as it indicates that forest removal and soil structure weakening is likely to lead to gullying in many places, and it is rare for scenarios to exist where such land use changes would not be likely to lead to at least some chance of gullying.

Results in Chapter 5 suggest that spatial optimisation can be improved with higher spatial resolution topographic information, allowing more specifically to determine where gullies are more, or less, to form. In this context, understanding and being able to set clear threshold values for fuzzy CTI, below which the risk is considered

minimal, is desirable and possibly achievable, but this requires better data for model calibration and validation, particularly in the form of field measurements of environmental descriptors and reliable 'ground truth'. More generally, incorporating soil stability and land use into such models explicitly has been shown to also improve optimisation through iterative selection of threshold values for CTI and this points the way to providing a potentially useful land-use planning tool.

6.4. **Future research**

This study has explored in detail the ability of terrain analysis to predict gullies and gully susceptibility in data sparse regions. Important new insights and understanding have been generated, and the importance and utility of reliable threshold values for gully initiation have been confirmed. In short, progress towards a practical model suitable for use in data sparse regions has been made, though such a model has not successfully been created.

However, this thesis has elucidated some of the key issues and limitations with the original CTI, and the fuzzy CTI exhibits promise as a 'next-generation' version. Hence, original contributions to knowledge have been made even though they have not led to a practical tool within the timeframe allowed for doctoral study. Notwithstanding this, progress has been made and, with further research, the fuzzy could yield a tool for the prediction of both gully susceptibility and gully occurrence, based on the fresh framework of the fuzzy CTI.

In this context, five suggestions are made for future research:

1. The way that slope is calculated has been found to be crucial to reliable terrain modelling. While it was not possible to identify whether the Horn and Zevenbergen and Thorne approaches to slope calculation is better suited to computing CTI, further research is needed to resolve this question, especially with respect to whether terrain is rugged or smooth.
2. The resolution of DEMs is a barrier to prediction, with the CTI working well on higher resolution surfaces. New imagery and topographic products are becoming available, including at 12.5 m DEM of much of the global surface

(Tadono *et al.*, 2014; Takaku *et al.*, 2014; Takaku *et al.*, 2016; Tadono *et al.*, 2016; Takaku and Tadono, 2017; Jaxa, 2019). Such datasets could dramatically improve gully predicting in data sparse regions, though, based on the findings of Chapter 2, they could lead to issues of incorrect slope calculation associated with variable ruggedness. More work is needed to identify the best slope algorithm to select in different terrains and, ideally, a composite method should be developed, where the best slope algorithm is selected automatically, based on the ruggedness of the landscape.

3. The accuracy of the fuzzy CTI in predicting gullying (and less so susceptibility to gullying) is dependent on reliable identification of threshold values, with an appropriate threshold substantially improving predictive ability. However, the magnitude of these threshold values is hard to define and are likely to be region specific. The analysis in Chapter 5, using proportions of ROC curves to assess where best predictive ability lies, is a potentially useful mechanism to objectively define and identify these thresholds; however, more work specifically focused on tuning threshold values for the best result, in different regions, would be beneficial in this regard.
4. There is a great deal of work on how soil structure and land cover impact soil erosion and gullying. However, their inclusion in terrain-based modelling approaches is difficult. In Chapter 5, their importance is demonstrated, with differential model accuracy representing the different relative significance of topography alone in generating gullying. Incorporating additional controls on gullying into topography driven models, such as the CTI, is more difficult because the significance of these variables relative to topography, and each other, is not known and likely to be variable, depending on geographical context. Values are also likely to be seasonal. The fuzzy logic framework provides a useful starting point and development environment, but factor weighting, or threshold values need to be determined. Further research is needed to achieve this.

5. Another avenue that was explored but not included in this thesis but, which is worth revisiting is combining concentrated flow erosion equations (such as the CTI) and models of soil strength and structure (such as S_t). Simply multiplying such values together implies they are equally important and ignores mismatches in data scaling and weighting. Fuzzy logic could provide an opportunity to transform variables based on their relative (fuzzy) importance, especially for continuous data. The availability of values for the critical level of soil organic matter in gridded continuous surface data for the study area means it could be fuzzified such that both the S_t and the CTI vary in the same direction. In this way, the susceptibility to concentrated flow erosion increases as both the critical level of soil organic matter and CTI increase. Concentrated flow erosion is then estimated by a fuzzy overlay of the fuzzy membership of St ($\mu_A(s_t)$) and the fuzzy CTI by the Mamdani fuzzy overlay approach as in Equation 6:1.

$$CFE = \min[(CTI), \mu_A(s_t)] \qquad \text{Equation 6:1}$$

6. A key finding here is that the fuzzy CTI reveals that much of the landscape has the potential to suffer gullying – i.e. there is sufficient planform and/or profile curvature to concentrate and accelerate overland flow. What this indicates is that in most of the landscape there is a relatively low upper limit to the contributing area necessary to initiate a gully. The relative lack of gullying in the landscape, which was used to validate the CTI models and indicates relatively poor performance, is because gullying is determined by factors other than topography alone. This has important implications for land management, especially in rapidly developing areas, because either soil degradation and loss of soil structure, or removal of natural vegetation and, especially forests, could rapidly lead to widespread gullying based on the occurrence of concentrated overland flow driven by the topography. Whilst not necessarily a surprising finding in itself, the spatial extent over which this is the case, is larger than expected, which is concerning and supports

the justification for this work and further research. It reinforces the need identified at the outset of this doctoral study, which is for relatively simple, widely applicable predictor of gullying, for use in data sparse regions.

APPENDICES

Appendix A. **Comparison of rasterized slopes**

Appendix Table A.1**.** Correlation and paired-sample t-test results for H and Z&T slope methods from a raster-based scatter plot generated in SAGA GIS

Statistics for each slope	1m	5m	10m	15m	20m	25m	30m
Mean H slope	34.440	31.619	29.980	29.104	28.055	27.540	26.881
Mean Z&T slope	34.640	32.115	30.545	29.792	28.775	28.274	27.637
N of H slopes	25207	25200	25472	25610	25429	26309	26370
N of Z&T slopes	25207	25200	25472	25610	25429	26309	26370
H Variance	1209.510	917.198	790.249	741.688	672.592	644.239	614.193
Z&T Variance	1236.390	958.533	825.283	788.205	708.498	683.909	652.306
Degrees of freedom	25206	25199	25471	25609	25428	26308	26369
P(T<=t) one-tail	0.000	0.000	0.000	0.000	0.000	0.000	0.000
P(T<=t) two-tail	0.000	0.000	0.000	0.000	0.000	0.000	0.000
Correlation coeff. (r)	0.999	0.995	0.993	0.992	0.992	0.992	0.991
Coeff. determination (r^2)	0.998	0.990	0.986	0.984	0.984	0.984	0.982
t_{Crit} - one-tail	1.640	1.645	1.645	1.645	1.645	1.645	1.645
t_{Crit} - two-tail	1.960	1.960	1.960	1.960	1.960	1.960	1.960
t-statistic	17.017	24.965	26.884	31.010	33.168	34.737	35.342
Kurtosis (Z&T slope)	63.041	14.439	4.142	9.377	1.915	1.676	1.570
Kurtosis (H slope)	52.642	10.781	3.382	4.332	1.448	1.272	1.200
Max Z&T (slope)	1074.763	579.746	299.769	556.769	263.203	226.010	207.570
Max (H slope)	997.071	494.873	269.564	409.853	211.020	202.426	197.540
Median (Z&T slope)	26.272	24.122	23.099	22.460	21.778	21.359	20.830
Median (H slope)	26.068	23.766	22.654	21.908	21.202	20.784	20.220
Min Z&T (slope)	0.000	0.000	0.000	0.000	0.000	0.000	0.000
Min (H slope)	0.000	0.000	0.000	0.000	0.000	0.000	0.000
Mode (Z&T slope)	0.000	0.000	0.000	0.000	0.000	0.000	0.000
Mode (H slope)	0.000	0.000	0.000	0.000	0.000	0.000	0.000
Range (Z&T slope)	1074.763	579.746	299.769	556.769	263.203	226.010	207.570
Range (H slope)	997.071	494.873	269.564	409.853	211.020	202.426	197.540
Skewness (Z&T slope)	4.193	2.138	1.453	1.666	1.193	1.171	1.170
Skewness (H slope)	3.863	1.912	1.369	1.392	1.141	1.119	1.120
Std dev (Z&T slope)	35.162	30.960	28.728	28.075	26.618	26.152	25.540
Std dev (H slope)	34.778	30.285	28.111	27.234	25.934	25.382	24.780
Std error (Z&T slope)	0.221	0.195	0.180	0.175	0.167	0.161	0.160
Std error (H slope)	0.219	0.191	0.176	0.170	0.163	0.156	0.150

Appendix B. **slope validation**

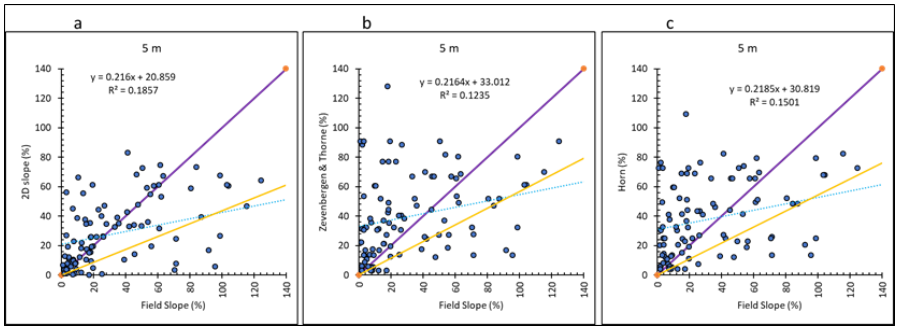

Appendix Figure B.1. Comparisons of field and computed slopes along cross-section NF100 at 5m resolution. (a)2D Slope vs field slope, (b)Zevenbergen & Thorne vs field slope and (c) Horn vs Field slope. Purple line = 1:1 line of perfect agreement, Yellow line = the regression line passing through the origin, light blue line = the regression line pass through the y- intercept.

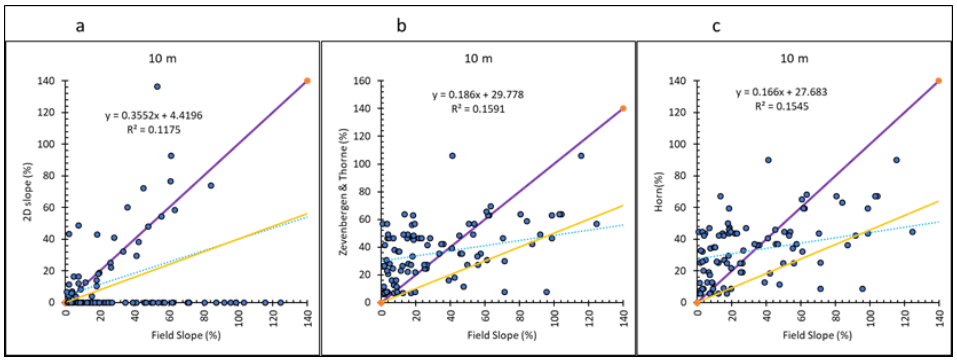

Appendix Figure B.2. Comparisons of field and computed slopes along cross-section NF100 at 10m resolution. (a)2D Slope vs field slope, (b)Zevenbergen & Thorne vs field slope and (c) Horn vs Field slope. Purple line = 1:1 line of perfect agreement, Yellow line = the regression line passing through the origin, light blue line = the regression line pass through the y- intercept.

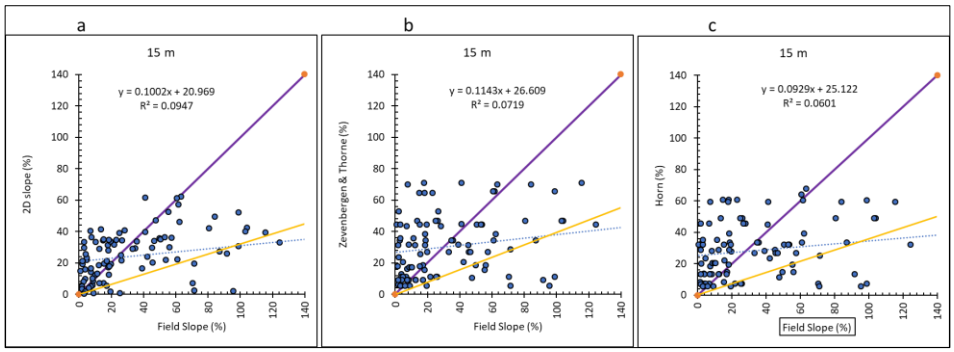

Appendix Figure B.3. Comparisons of field and computed slopes along cross-section NF100 at 15m resolution. (a)2D Slope vs field slope, (b)Zevenbergen & Thorne vs field slope and (c) Horn vs Field slope. Purple line = 1:1 line of perfect agreement, Yellow line = the regression line passing through the origin, light blue line = the regression line pass through the y- intercept.

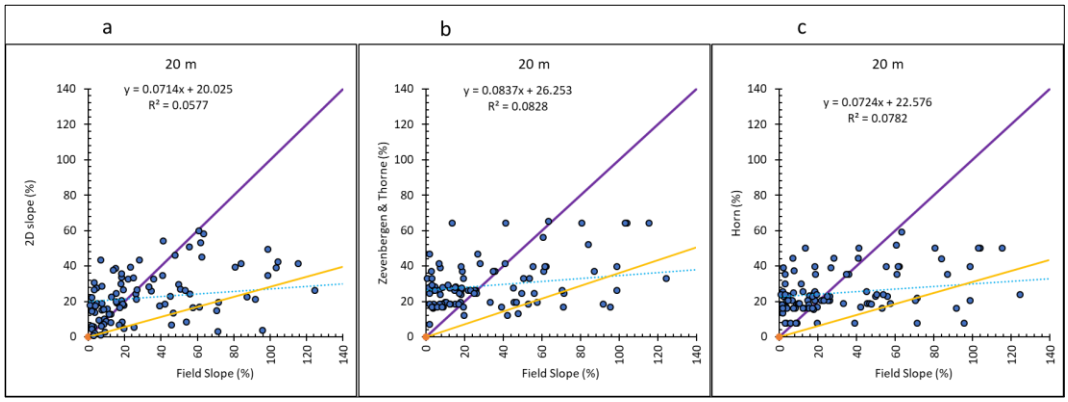

Appendix Figure B.4. Comparisons of field and computed slopes along cross-section NF100 at 20m resolution. (a)2D Slope vs field slope, (b)Zevenbergen & Thorne vs field slope and (c) Horn vs Field slope. Purple line = 1:1 line of perfect agreement, Yellow line = the regression line passing through the origin, light blue line = the regression line pass through the y- intercept.

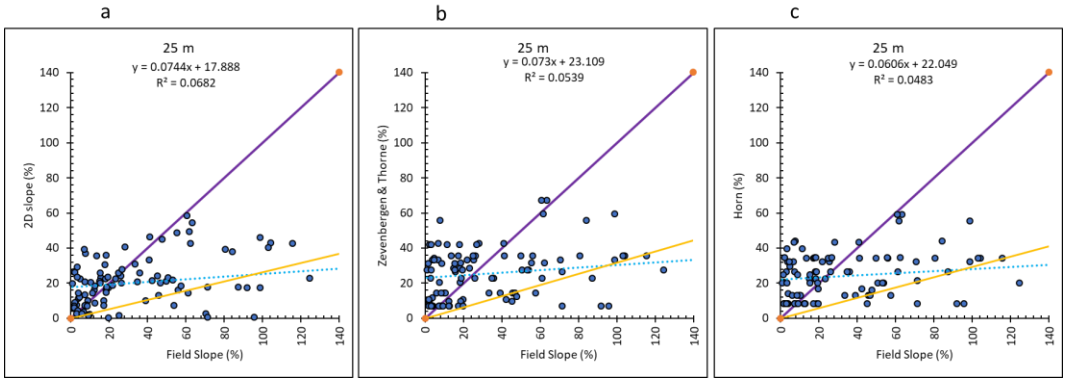

Appendix Figure B.5. Comparisons of field and computed slopes along cross-section NF100 at 25m resolution. (a)2D Slope vs field slope, (b)Zevenbergen & Thorne vs field slope and (c) Horn vs Field slope. Purple line = 1:1 line of perfect agreement, Yellow line = the regression line passing through the origin, light blue line = the regression line pass through the y- intercept.

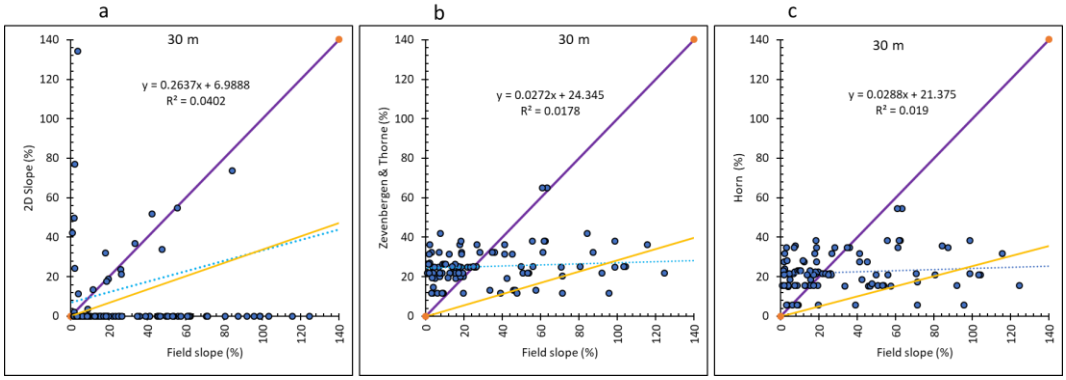

Appendix Figure B.6. Comparisons of field and computed slopes along cross-section NF100 at 30m resolution. (a)2D Slope vs field slope, (b)Zevenbergen & Thorne vs field slope and (c) Horn vs Field slope. Purple line = 1:1 line of perfect agreement, Yellow line = the regression line passing through the origin, light blue line = the regression line pass through the y- intercept.

To extend the comparison further, data from cross-sections NF100, NF110, NF300 and NF310 were merged and also compared at resolutions ranging between 1m and 30m. The resulting graphs are shown in Figures 2.39 to 2.45. The results are very similar to those for NF100, with the H and Z&T methods yielding almost identical r^2 values, and those values falling rapidly as grid resolution coarsens.

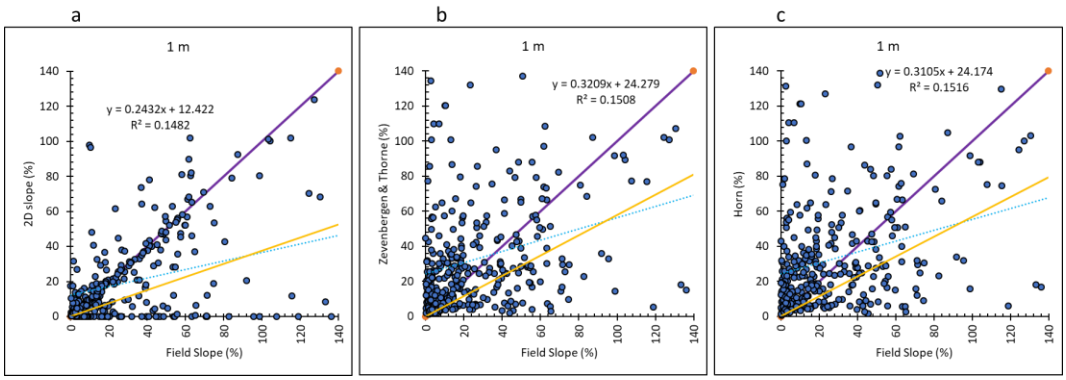

Appendix Figure B.7. Comparisons of field and computed slopes along 4 cross-sections, at 1m resolution. .(a)2D Slope vs field slope, (b)Zevenbergen & Thorne vs field slope and (c) Horn vs Field slope. Purple line = 1:1 line of perfect agreement, Yellow line = the regression line passing through the origin, light blue line = the regression line pass through the y- intercept.

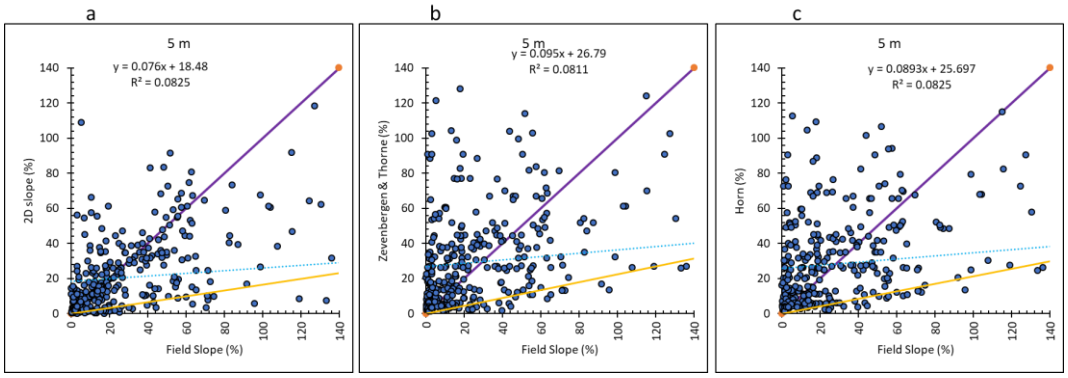

Appendix Figure B.8. Comparisons of field and computed slopes along 4 cross-sections, at 5m resolution. .(a)2D Slope vs field slope, (b)Zevenbergen & Thorne vs field slope and (c) Horn vs Field slope. Purple line = 1:1 line of perfect agreement, Yellow line = the regression line passing through the origin, light blue line = the regression line pass through the y- intercept.

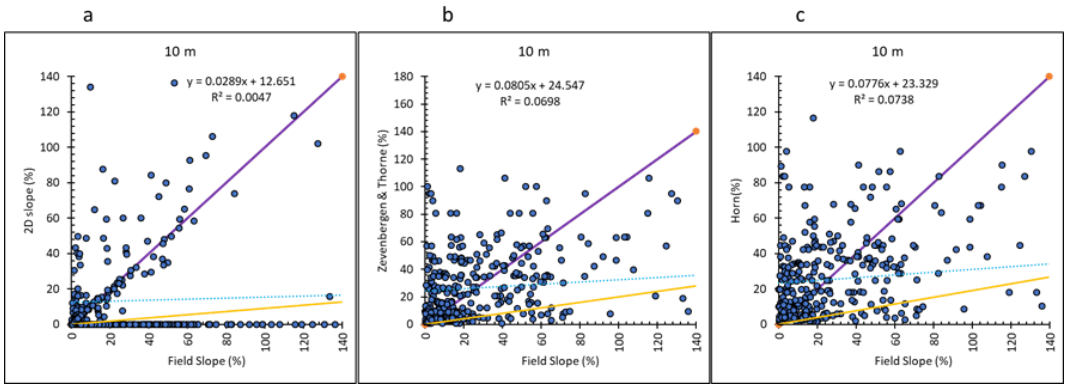

Appendix Figure B.9. Comparisons of field and computed slopes along 4 cross-sections, at 10m resolution. (a)2D Slope vs field slope, (b)Zevenbergen & Thorne vs field slope and (c) Horn vs Field slope. Purple line = 1:1 line of perfect agreement, Yellow line = the regression line passing through the origin, light blue line = the regression line pass through the y- intercept.

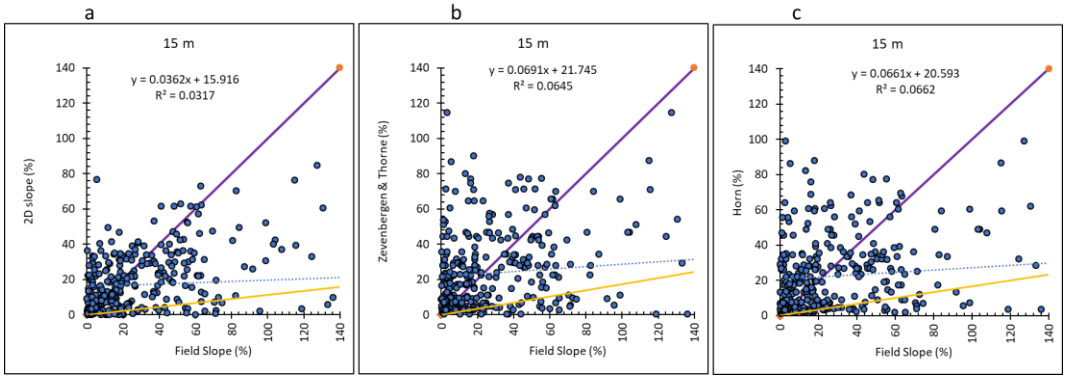

Appendix Figure B.10. Comparisons of field and computed slopes along 4 cross-sections, at 15m resolution. (a)2D Slope vs field slope, (b)Zevenbergen & Thorne vs field slope and (c) Horn vs Field slope. Purple line = 1:1 line of perfect agreement, Yellow line = the regression line passing through the origin, light blue line = the regression line pass through the y- intercept.

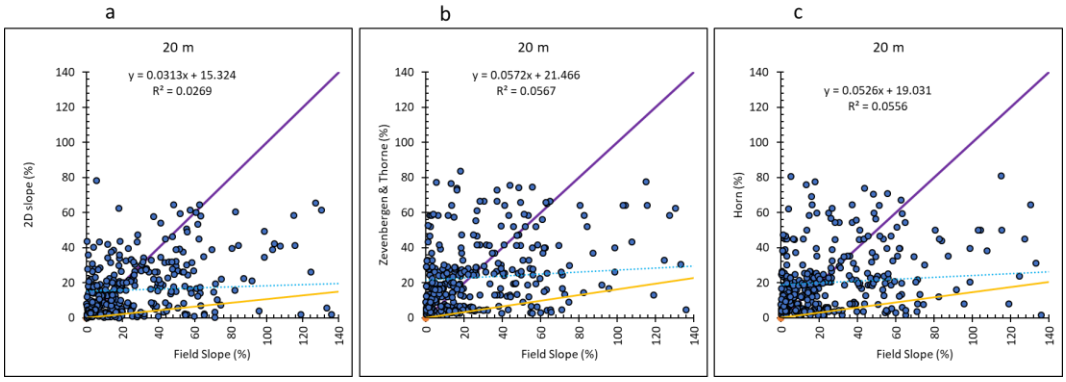

Appendix Figure B.11. Comparisons of field and computed slopes along 4 cross-sections, at 20m resolution. (a)2D Slope vs field slope, (b)Zevenbergen & Thorne vs field slope and (c) Horn vs Field slope. Purple line = 1:1 line of perfect agreement, Yellow line = the regression line passing through the origin, light blue line = the regression line pass through the y- intercept.

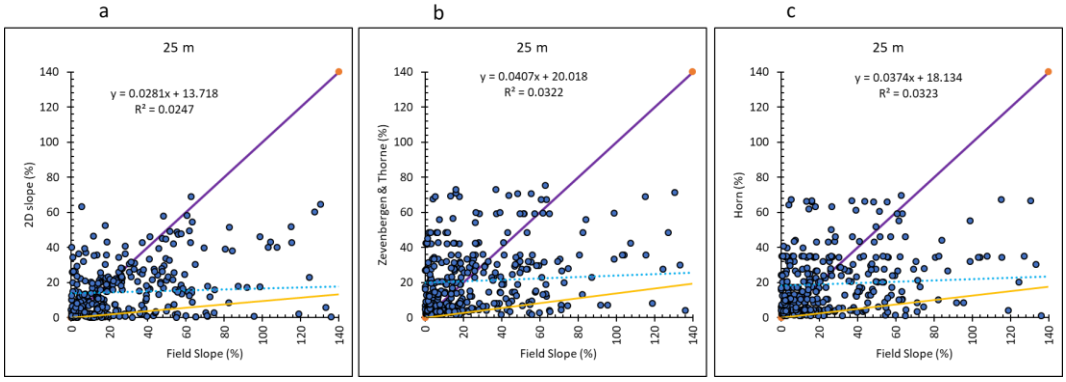

Appendix Figure B.12. Comparisons of field and computed slopes along 4 cross-sections, at 25m resolution. (a)2D Slope vs field slope, (b)Zevenbergen & Thorne vs field slope and (c) Horn vs Field slope. Purple line = 1:1 line of perfect agreement, Yellow line = the regression line passing through the origin, light blue line = the regression line pass through the y- intercept.

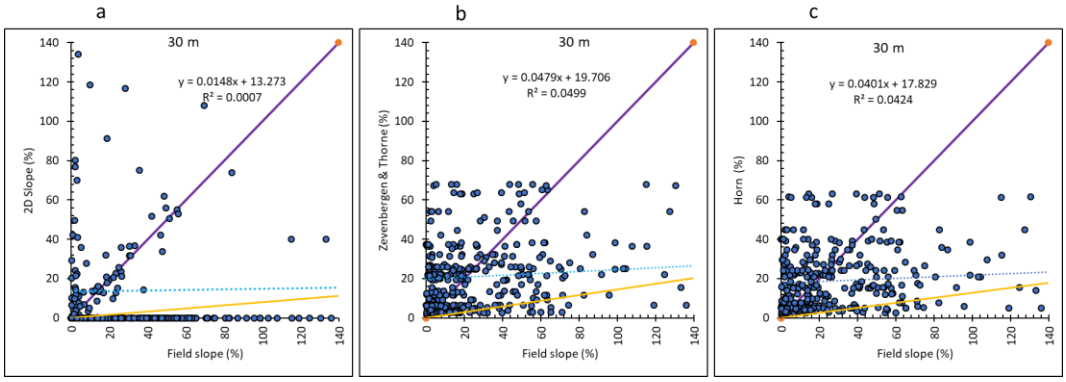

Appendix Figure B.13. Comparisons of field and computed slopes along 4 cross-sections, at 30m resolution. .(a)2D Slope vs field slope, (b)Zevenbergen & Thorne vs field slope and (c) Horn vs Field slope. Purple line = 1:1 line of perfect agreement, Yellow line = the regression line passing through the origin, light blue line = the regression line pass through the y- intercept.

Appendix C. **ROC: Sensitivity, specificity and Accuracy across region**

Appendix Table C.1. Sensitivity, specificity and Accuracy the fuzzy CTI model across Administrative areas in the Eastern Cape Province of South Africa.

Districts	Area (sqkm	FN	FP	TN	TP	Grand Total	Sensitivity	specificity	Accuracy
Aberdeen	6863.38	1780	1229	2194	995	6198	35.86	64.10	44.77
Adelaide	1556.22	95	306	457	114	972	54.55	59.90	21.50
Albany	4375.74	270	920	1221	287	2698	51.53	57.03	20.64
Albert	3909.21	2058	726	1164	1452	5400	41.37	61.59	65.00
Alexandria	2240.3	5	384	593	6	988	54.55	60.70	1.11
Aliwal North	1993.66	1394	354	567	1219	3534	46.65	61.56	73.94
Barkly East	3749.6	89	793	1017	150	2049	62.76	56.19	11.66
Bathurst	1367.93	8	250	373	4	635	33.33	59.87	1.89
Bedford	2753.89	516	573	818	581	2488	52.96	58.81	44.09
Bizana	1913.63	178	386	531	278	1373	60.96	57.91	33.21
Butterworth	698.37	209	154	193	295	851	58.53	55.62	59.22
Cala	938.49	207	191	261	236	895	53.27	57.74	49.50
Cathcart	2574.72	232	544	736	254	1766	52.26	57.50	27.52
Cofimvaba	2119.04	715	437	649	830	2631	53.72	59.76	58.72
Cradock	6062.89	1076	1162	1791	993	5022	47.99	60.65	41.20
East London	1268.68	79	226	312	103	720	56.59	57.99	25.28
Elliot	1965.7	165	424	594	235	1418	58.75	58.35	28.21
Elliotdale	690.71	10	139	182	14	345	58.33	56.70	6.96
Engcobo	2686.98	1424	545	769	1435	4173	50.19	58.52	68.51
Flagstaff	1130.06	87	214	305	155	761	64.05	58.77	31.80
Fort Beaufort	1276.97	61	257	359	76	753	55.47	58.28	18.19
Graaff-Reinet	6792.87	1073	1367	2034	692	5166	39.21	59.81	34.17
Hankey	1643.69	3	341	418	5	767	62.50	55.07	1.04
Hewu	1018.94	142	217	303	181	843	56.04	58.27	38.32
Hofmeyr	2433.93	725	438	792	468	2423	39.23	64.39	49.24
Humansdorp	3487.63	13	627	926	15	1581	53.57	59.63	1.77

Idutywa	1239.92	432	247	368	544	1591	55.74	59.84	61.35
Indwe	702.79	152	156	213	170	691	52.80	57.72	46.60
Jansenville	4523.6	1736	835	1351	1080	5002	38.35	61.80	56.30
Joubertina	1336.28	11	312	415	6	744	35.29	57.08	2.28
Keiskammahoek	576.26	107	122	184	84	497	43.98	60.13	38.43
Kentani	1085.64	75	222	287	107	691	58.79	56.39	26.34
King William's Town	631.93	59	136	201	93	489	61.18	59.64	31.08
Kirkwood	1639.5	36	327	481	35	879	49.30	59.53	8.08
Komga	1402.28	32	261	381	40	714	55.56	59.35	10.08
Lady Frere	2662.32	1141	500	784	1304	3729	53.33	61.06	65.57
Lady Grey	1386.34	479	270	408	462	1619	49.10	60.18	58.12
Libode	1474.49	285	337	447	616	1685	68.37	57.02	53.47
Lusikisiki	2393.31	42	512	647	101	1302	70.63	55.82	10.98
Maclear	2301.98	197	453	649	176	1475	47.18	58.89	25.29
Maluti	1699.58	613	337	501	532	1983	46.46	59.79	57.74
Mdantsane	498.98	34	87	138	70	329	67.31	61.33	31.61
Middelburg	5570.06	1906	1058	1645	1345	5954	41.37	60.86	54.60
Middledrift	762.91	161	144	236	176	717	52.23	62.11	47.00
Molteno	2028.41	812	381	637	629	2459	43.65	62.57	58.60
Mpofu	792.99	50	167	223	61	501	54.95	57.18	22.16
Mqanduli	1237.97	82	272	335	247	936	75.08	55.19	35.15
Mt Fletcher	2982.62	2281	603	764	2193	5841	49.02	55.89	76.60
Mt Ayliff	880.57	538	216	232	576	1562	51.71	51.79	71.32
Mt Frere	1852	1773	394	424	1894	4485	51.65	51.83	81.76
Ngqueleni	1393.21	120	301	456	384	1261	76.19	60.24	39.97
Nqamakwe	1287.89	534	244	391	706	1875	56.94	61.57	66.13
Ntabethemba	485.5	80	84	151	78	393	49.37	64.26	40.20
Pearston	2645.91	750	487	828	497	2562	39.86	62.97	48.67
Peddie	1605.91	115	312	473	248	1148	68.32	60.25	31.62
Port Elizabeth	1317.77	3	186	367	3	559	50.00	66.37	1.07
Port St Johns	614.85	1	109	156		266	0.00	58.87	0.38
Queenstown	1897.14	205	373	558	184	1320	47.30	59.94	29.47

Qumbu	1494.29	1235	285	383	1346	3249	52.15	57.34	79.44
Somerset East	5610.95	1767	1142	1651	1661	6221	48.45	59.11	55.10
Sterkspruit	1701.72	1221	325	445	1340	3331	52.32	57.79	76.88
Sterkstroom	1660.84	315	314	482	286	1397	47.59	60.55	43.02
Steynsburg	2695.77	1862	473	751	1291	4377	40.95	61.36	72.04
Steytlerville	3647.17	1035	721	1059	907	3722	46.70	59.49	52.18
Stutterheim	1566.38	158	323	455	245	1181	60.79	58.48	34.12
Tabankulu	1501.4	804	312	435	1083	2634	57.39	58.23	71.64
Tarka	3083.62	880	588	902	631	3001	41.76	60.54	50.35
Tsolo	1820.78	1030	351	529	1138	3048	52.49	60.11	71.13
Tsomo	1097.71	598	231	313	621	1763	50.94	57.54	69.14
Uitenhage	3078.84	63	670	924	63	1720	50.00	57.97	7.33
Umtata	1778.83	731	379	491	1055	2656	59.07	56.44	67.24
Venterstad	1963.95	628	373	634	462	2097	42.39	62.96	51.98
Victoria East	1036.36	150	233	279	183	845	54.95	54.49	39.41
Willowmore	7683.61	1354	1492	2348	853	6047	38.65	61.15	36.50
Willowvale	1382.55	45	289	358	91	783	66.91	55.33	17.37
Wodehouse	3071.05	1021	602	922	936	3481	47.83	60.50	56.22
Zwelitsha	1545.71	250	323	493	367	1433	59.48	60.42	43.06
Grand Total	167846	42603	33075	48744	40273	164695	48.59	59.58	50.32

Appendix D. **Descriptive statistics**

Appendix Table D.1. Descriptive by Land use/cover.

Statistic	Bare areas	Cropland	Grassland	Lichens Mosses /sparse vegetation	Shrubs	Tree cover
5% Trimmed Mean	0.00497	0.01071	0.00829	0.00541	0.00857	0.00936
Interquartile Range	0.009	0.01683	0.0135	0.01006	0.0135	0.01492
Kurtosis	12.79041	7.11565	9.18699	13.25499	9.62641	14.79414
Lower Bound	0.00674	0.01374	0.01104	0.00678	0.01152	0.01249
Maximum	0.11135	0.19722	0.18451	0.11728	0.20418	0.23732
Mean	0.00727	0.01404	0.01122	0.00745	0.01168	0.01291
Median	0	0.00636	0.0045	0	0.0045	0.00636
Minimum	0	0	0	0	0	0
N	2616	21250	42331	1490	55811	10292
Range	0.11135	0.19722	0.18451	0.11728	0.20418	0.23732
Skewness	3.21955	2.49515	2.74246	3.10015	2.81012	3.35939
Std. Deviation	0.01386	0.02227	0.01892	0.01321	0.01979	0.02195
Std. Error of Kurtosis	0.0957	0.0336	0.0238	0.1267	0.0207	0.0483
Std. Error of Mean		0.0002	0.0001	0.0003	0.0001	0.0002
Std. Error of Mean	0.0003					
Std. Error of Skewness	0.0479	0.0168	0.0119	0.0634	0.0104	0.0241
Upper Bound	0.0078	0.01434	0.0114	0.00812	0.01185	0.01334
Variance	0.00019	0.0005	0.00036	0.00017	0.00039	0.00048

Appendix Table D.2. Descriptions by Soil types/units.

Row Labels	Ao	Fo	Fr	I	Lc	Lo	We	Ws	Xk
5% Trimmed Mean	0.00887	0.01199	0.00966	0.00754	0.01116	0.01292	0.00927	0.00714	0.00675
95% CI Lower Bound	0.01124	0.01473	0.01126	0.01033	0.01425	0.01578	0.01197	0.00974	0.00937
95% CI Upper Bound	0.01286	0.01658	0.01403	0.01092	0.01475	0.01667	0.01264	0.01035	0.0097
Interquartile Range	0.0135	0.01909	0.01558	0.01272	0.01799	0.01961	0.01558	0.0119	0.01102
Kurtosis	13.08214	9.03466	9.2061	14.57234	7.21573	6.07633	8.91492	11.8546	11.24505
Maximum	0.1684	0.18123	0.14463	0.23101	0.1912	0.19514	0.20418	0.20328	0.23732
Mean	0.01205	0.01566	0.01264	0.01062	0.0145	0.01622	0.0123	0.01005	0.00953
Median	0.00636	0.00779	0.00636	0.0045	0.00636	0.00779	0.0045	0.0045	0
Minimum	0	0	0	0	0	0	0	0	0
N	2352	2646	805	16375	30762	10974	13474	13564	42838
Range	0.1684	0.18123	0.14463	0.23101	0.1912	0.19514	0.20418	0.20328	0.23732
Skewness	3.18189	2.72311	2.7097	3.29672	2.50609	2.29322	2.66838	3.04375	2.98864
Std. Deviation	0.02001	0.0242	0.02002	0.01904	0.02228	0.02372	0.01997	0.01799	0.01726
Std. Error of Kurtosis	0.1009	0.0951	0.1721	0.0383	0.0279	0.0468	0.0422	0.0421	0.0237
Std. Error of Mean	0.0004	0.0005	0.0007	0.0001	0.0001	0.0002	0.0002	0.0002	0.0001
Std. Error of Skewness	0.0505	0.0476	0.0862	0.0191	0.014	0.0234	0.0211	0.021	0.0118
Variance	0.0004	0.00059	0.0004	0.00036	0.0005	0.00056	0.0004	0.00032	0.0003

NB: Orthic Acrisols (Ao), Chromic Luvisols (Lc), Orthic Ferrasols (Fo), Rhodic Ferrasols (Fr), Solodic Planosols (Ws)
Eutric Planosols (We), Calcic Xerosols (Xk), Orthic Luvisols (Lo) and LITHOSOLS (I).

Appendix Table D.3.Descriptions according to Geological units.

Row Labels	Carbonif	Cretaceous	Devonian	Mesozoic	Permian	Precambr	Quaterna	Silurian	Tertiary	Triassic
5% Trimmed Mean	0.0072	0.00697	0.00756	0.00993	0.00836	0.00892	0.00473	0.00759	0.00595	0.00928
95% CI Lower Bound	0.00965	0.00905	0.00972	0.01289	0.01116	0.01123	0.00626	0.01	0.00514	0.01233
95% CI Upper Bound	0.01076	0.01095	0.01109	0.01405	0.01151	0.01262	0.00784	0.01117	0.00984	0.01264
Interquartile Range	0.01102	0.01102	0.01102	0.01558	0.0135	0.01423	0.009	0.01272	0.0119	0.01492
Kurtosis	11.01495	9.98742	7.69172	11.74091	9.85955	13.99365	23.588	17.14113	8.08463	8.85465
Maximum	0.16387	0.13396	0.12401	0.23101	0.19514	0.23732	0.1416	0.1912	0.05864	0.20418
Mean	0.0102	0.01	0.01041	0.01347	0.01134	0.01193	0.00705	0.01058	0.00749	0.01249
Median	0.0045	0	0.0045	0.00636	0.0045	0.0045	0	0.0045	0.0045	0.0045
Minimum	0	0	0	0	0	0	0	0	0	0
N	4233	1439	2672	5684	46032	3195	1227	3766	89	65453
Range	0.16387	0.13396	0.12401	0.23101	0.19514	0.23732	0.1416	0.1912	0.05864	0.20418
Skewness	3.0264	2.94036	2.65122	3.02611	2.81338	3.0465	4.16059	3.5717	2.47517	2.71409
Std. Deviation	0.01833	0.01838	0.01806	0.02231	0.01917	0.01999	0.01413	0.01833	0.01116	0.0207
Std. Error of Kurtosis	0.0753	0.1289	0.0947	0.065	0.0228	0.0866	0.1396	0.0798	0.5056	0.0191
Std. Error of Mean	0.0003	0.0005	0.0003	0.0003	0.0001	0.0004	0.0004	0.0003	0.0012	0.0001
Std. Error of Skewness	0.0376	0.0645	0.0474	0.0325	0.0114	0.0433	0.0698	0.0399	0.2554	0.0096
Variance	0.00034	0.00034	0.00033	0.0005	0.00037	0.0004	0.0002	0.00034	0.00012	0.00043

Appendix Table D.4. Descriptive statistics for the fuzzy CTI with critical levels of soil organic matter.

Name statistics	1	2	3	4
	Statistics			
5% Trimmed Mean	0.00878	0.00718	0.00732	0.00664
95% CI Lower Bound	0.01179	0.00908	0.00866	0.0067
95% CI Upper Bound	0.01201	0.01119	0.01166	0.01061
Interquartile Range	0.01423	0.0119	0.01272	0.01231
Kurtosis	9.81459	15.54657	16.62553	8.67885
Maximum	0.23732	0.16189	0.14514	0.07805
Mean	0.0119	0.01013	0.01016	0.00866
Median	0.0045	0.0045	0.0045	0.0045
Minimum	0	0	0	0
N	131958	1111	540	181
Range	0.23732	0.16189	0.14514	0.07805
Skewness	2.81413	3.45591	3.54145	2.64886
Std. Deviation	0.02003	0.0179	0.01774	0.01332
Std. Error	0.0001			
Std. Error of Kurtosis	0.0135	0.1466	0.2099	0.3593
Std. Error of mean		0.0005	0.0008	0.001
Std. Error of Skewness	0.0067	0.0734	0.1051	0.1806
Variance	0.0004	0.00032	0.00031	0.00018

Appendix E. **Post hoc ANOVA**

Appendix Table E.1. Post Hoc Tests for Multiple Comparisons of means Dependent Variable: Fuzzy CTI LSD.

(I) Critical levels of soil organic matter content		Mean Difference (I-J)	Std. Error	Sig.	95% Confidence Interval	
					Lower Bound	Upper Bound
S_t1	S_t 2	0.0018*	0.001	0.003	0.0006	0.0029
	S_t 3	0.0017*	0.001	0.044	0.0000	0.0034
	S_t 4	0.0032*	0.001	0.029	0.0003	0.0062
S_t 2	S_t 1	-0.0018*	0.001	0.003	-0.0029	-0.0006
	S_t 3	0.0000	0.001	0.977	-0.0021	0.0020
	S_t 4	0.0015	0.002	0.358	-0.0017	0.0046
S_t 3	S_t 1	-0.0017*	0.001	0.044	-0.0034	0.0000
	S_t 2	0.0000	0.001	0.977	-0.0020	0.0021
	S_t 4	0.0015	0.002	0.381	-0.0019	0.0049
S_t 4	S_t 1	-0.0032*	0.001	0.029	-0.0062	-0.0003
	S_t 2	-0.0015	0.002	0.358	-0.0046	0.0017
	S_t 3	-0.0015	0.002	0.381	-0.0049	0.0019
*. The mean difference is significant at the 0.05 level.						

Appendix Table E.2. Post Hoc Tests for Multiple Comparisons of means of fuzzy CTI under different Land use/Land cover class using the least small difference (LSD) approach.

(I) Land use/Land cover		Mean Difference (I-J)	Std. Error	Sig.	95% Confidence Interval	
					Lower Bound	Upper Bound
Tree cover	Shrubs	0.0012	0.000	0.000	0.0008	0.0017
	Grassland	0.0017	0.000	0.000	0.0013	0.0021
	Cropland	-0.0011	0.000	0.000	-0.0016	-0.0007
	Bare areas	0.0056	0.000	0.000	0.0048	0.0065
Shrubs	Tree cover	-0.0012	0.000	0.000	-0.0017	-0.0008
	Grassland	0.0005	0.000	0.000	0.0002	0.0007
	Cropland	-0.0024	0.000	0.000	-0.0027	-0.0020
	Bare areas	0.0044	0.000	0.000	0.0036	0.0052
Grassland	Tree cover	-0.0017	0.000	0.000	-0.0021	-0.0013
	Shrubs	-0.0005	0.000	0.000	-0.0007	-0.0002
	Cropland	-0.0028	0.000	0.000	-0.0031	-0.0025
	Bare areas	0.0040	0.000	0.000	0.0032	0.0047
Cropland	Tree cover	0.0011	0.000	0.000	0.0007	0.0016
	Shrubs	0.0024	0.000	0.000	0.0020	0.0027
	Grassland	0.0028	0.000	0.000	0.0025	0.0031
	Bare areas	0.0068	0.000	0.000	0.0060	0.0076
Bare areas	Tree cover	-0.0056	0.000	0.000	-0.0065	-0.0048
	Shrubs	-0.0044	0.000	0.000	-0.0052	-0.0036
	Grassland	-0.0040	0.000	0.000	-0.0047	-0.0032
	Cropland	-0.0068	0.000	0.000	-0.0076	-0.0060
*. The mean difference is significant at the 0.05 level.						

Appendix Table E.3. Post Hoc Tests for Multiple Comparisons of means of fuzzy CTI under different Geological units using the least small difference (LSD) approach.

(I) Geological units		Mean Difference (I-J)	Std. Error	Sig.	95% Confidence Interval	
					Lower Bound	Upper Bound
Carboniferous and Devonian	Cretaceous and Jurassic	0.00020	0.001	0.743	-0.0010	0.0014
	Devonian (undivided)	-0.00020	0.000	0.679	-0.0012	0.0008
	Mesozoic extrusive and intrusive rocks	-0.00327	0.000	0.000	-0.0041	-0.0025
	Permian	-0.00114	0.000	0.000	-0.0018	-0.0005
	Precambrian (undivided)	-0.00172	0.000	0.000	-0.0026	-0.0008
	Quaternary (undivided)	0.00344	0.001	0.000	0.0018	0.0051
	Quaternary and Tertiary	0.00282	0.001	0.002	0.0011	0.0046
	Silurian-Ordovician	-0.00040	0.000	0.394	-0.0013	0.0005
	Tertiary	0.00270	0.002	0.204	-0.0015	0.0069
	Triassic	-0.00228	0.000	0.000	-0.0029	-0.0017
Cretaceous and Jurassic	Carboniferous and Devonian	-0.00020	0.001	0.743	-0.0014	0.0010
	Devonian (undivided)	-0.00040	0.001	0.536	-0.0017	0.0009
	Mesozoic extrusive and intrusive rocks	-0.00347	0.001	0.000	-0.0046	-0.0023
	Permian	-0.00134	0.001	0.012	-0.0024	-0.0003
	Precambrian (undivided)	-0.00192	0.001	0.002	-0.0032	-0.0007
	Quaternary (undivided)	0.00324	0.001	0.001	0.0014	0.0051
	Quaternary and Tertiary	0.00262	0.001	0.008	0.0007	0.0046
	Silurian-Ordovician	-0.00060	0.001	0.348	-0.0018	0.0006
	Tertiary	0.00250	0.002	0.249	-0.0018	0.0068
	Triassic	-0.00248	0.001	0.000	-0.0035	-0.0014
Devonian (undivided)	Carboniferous and Devonian	0.00020	0.000	0.679	-0.0008	0.0012

	Cretaceous and Jurassic	0.00040	0.001	0.536	-0.0009	0.0017
	Mesozoic extrusive and intrusive rocks	-0.00306	0.000	0.000	-0.0040	-0.0021
	Permian	-0.00093	0.000	0.019	-0.0017	-0.0002
	Precambrian (undivided)	-0.00152	0.001	0.004	-0.0025	-0.0005
	Quaternary (undivided)	0.00365	0.001	0.000	0.0019	0.0054
	Quaternary and Tertiary	0.00302	0.001	0.001	0.0012	0.0048
	Silurian-Ordovician	-0.00020	0.001	0.727	-0.0012	0.0008
	Tertiary	0.00290	0.002	0.175	-0.0013	0.0071
	Triassic	-0.00208	0.000	0.000	-0.0029	-0.0013
Mesozoic extrusive and intrusive rocks	Carboniferous and Devonian	0.00327	0.000	0.000	0.0025	0.0041
	Cretaceous and Jurassic	0.00347	0.001	0.000	0.0023	0.0046
	Devonian (undivided)	0.00306	0.000	0.000	0.0021	0.0040
	Permian	0.00213	0.000	0.000	0.0016	0.0027
	Precambrian (undivided)	0.00154	0.000	0.000	0.0007	0.0024
	Quaternary (undivided)	0.00671	0.001	0.000	0.0051	0.0083
	Quaternary and Tertiary	0.00609	0.001	0.000	0.0044	0.0078
	Silurian-Ordovician	0.00289	0.000	0.000	0.0021	0.0037
	Tertiary	0.00598	0.002	0.005	0.0018	0.0102
	Triassic	0.00098	0.000	0.000	0.0004	0.0015
Permian	Carboniferous and Devonian	0.00114	0.000	0.000	0.0005	0.0018
	Cretaceous and Jurassic	0.00134	0.001	0.012	0.0003	0.0024
	Devonian (undivided)	0.00093	0.000	0.019	0.0002	0.0017
	Mesozoic extrusive and intrusive rocks	-0.00213	0.000	0.000	-0.0027	-0.0016
	Precambrian (undivided)	-0.00060	0.000	0.108	-0.0013	0.0001
	Quaternary (undivided)	0.00458	0.001	0.000	0.0030	0.0061
	Quaternary and Tertiary	0.00396	0.001	0.000	0.0023	0.0056

	Silurian-Ordovician	0.00075	0.000	0.026	0.0001	0.0014
	Tertiary	0.00390	0.002	0.069	-0.0003	0.0080
	Triassic	-0.00115	0.000	0.000	-0.0014	-0.0009
Precambrian (undivided)	Carboniferous and Devonian	0.00172	0.000	0.000	0.0008	0.0026
	Cretaceous and Jurassic	0.00192	0.001	0.002	0.0007	0.0032
	Devonian (undivided)	0.00152	0.001	0.004	0.0005	0.0025
	Mesozoic extrusive and intrusive rocks	-0.00154	0.000	0.000	-0.0024	-0.0007
	Permian	0.00060	0.000	0.108	-0.0001	0.0013
	Quaternary (undivided)	0.00517	0.001	0.000	0.0035	0.0068
	Quaternary and Tertiary	0.00454	0.001	0.000	0.0028	0.0063
	Silurian-Ordovician	0.00134	0.000	0.005	0.0004	0.0023
	Tertiary	0.00444	0.002	0.039	0.0002	0.0086
	Triassic	-0.00060	0.000	0.123	-0.0013	0.0002
Quaternary (undivided)	Carboniferous and Devonian	-0.00344	0.001	0.000	-0.0051	-0.0018
	Cretaceous and Jurassic	-0.00324	0.001	0.001	-0.0051	-0.0014
	Devonian (undivided)	-0.00365	0.001	0.000	-0.0054	-0.0019
	Mesozoic extrusive and intrusive rocks	-0.00671	0.001	0.000	-0.0083	-0.0051
	Permian	-0.00458	0.001	0.000	-0.0061	-0.0030
	Precambrian (undivided)	-0.00517	0.001	0.000	-0.0068	-0.0035
	Quaternary and Tertiary	-0.00060	0.001	0.587	-0.0029	0.0016
	Silurian-Ordovician	-0.00382	0.001	0.000	-0.0055	-0.0022
	Tertiary	-0.00070	0.002	0.747	-0.0051	0.0037
	Triassic	-0.00572	0.001	0.000	-0.0073	-0.0042
Quaternary and Tertiary	Carboniferous and Devonian	-0.00282	0.001	0.002	-0.0046	-0.0011
	Cretaceous and Jurassic	-0.00262	0.001	0.008	-0.0046	-0.0007
	Devonian (undivided)	-0.00302	0.001	0.001	-0.0048	-0.0012

	Mesozoic extrusive and intrusive rocks	-0.00609	0.001	0.000	-0.0078	-0.0044
	Permian	-0.00396	0.001	0.000	-0.0056	-0.0023
	Precambrian (undivided)	-0.00454	0.001	0.000	-0.0063	-0.0028
	Quaternary (undivided)	0.00060	0.001	0.587	-0.0016	0.0029
	Silurian-Ordovician	-0.00320	0.001	0.000	-0.0050	-0.0014
	Tertiary	-0.00010	0.002	0.963	-0.0046	0.0044
	Triassic	-0.00510	0.001	0.000	-0.0067	-0.0035
Silurian-Ordovician	Carboniferous and Devonian	0.00040	0.000	0.394	-0.0005	0.0013
	Cretaceous and Jurassic	0.00060	0.001	0.348	-0.0006	0.0018
	Devonian (undivided)	0.00020	0.001	0.727	-0.0008	0.0012
	Mesozoic extrusive and intrusive rocks	-0.00289	0.000	0.000	-0.0037	-0.0021
	Permian	-0.00075	0.000	0.026	-0.0014	-0.0001
	Precambrian (undivided)	-0.00134	0.000	0.005	-0.0023	-0.0004
	Quaternary (undivided)	0.00382	0.001	0.000	0.0022	0.0055
	Quaternary and Tertiary	0.00320	0.001	0.000	0.0014	0.0050
	Tertiary	0.00310	0.002	0.148	-0.0011	0.0073
	Triassic	-0.00190	0.000	0.000	-0.0026	-0.0012
Tertiary	Carboniferous and Devonian	-0.00270	0.002	0.204	-0.0069	0.0015
	Cretaceous and Jurassic	-0.00250	0.002	0.249	-0.0068	0.0018
	Devonian (undivided)	-0.00290	0.002	0.175	-0.0071	0.0013
	Mesozoic extrusive and intrusive rocks	-0.00598	0.002	0.005	-0.0102	-0.0018
	Permian	-0.00390	0.002	0.069	-0.0080	0.0003
	Precambrian (undivided)	-0.00444	0.002	0.039	-0.0086	-0.0002
	Quaternary (undivided)	0.00070	0.002	0.747	-0.0037	0.0051
	Quaternary and Tertiary	0.00010	0.002	0.963	-0.0044	0.0046
	Silurian-Ordovician	-0.00310	0.002	0.148	-0.0073	0.0011

	Triassic	-0.00500	0.002	0.018	-0.0091	-0.0008
Triassic	Carboniferous and Devonian	0.00228	0.000	0.000	0.0017	0.0029
	Cretaceous and Jurassic	0.00248	0.001	0.000	0.0014	0.0035
	Devonian (undivided)	0.00208	0.000	0.000	0.0013	0.0029
	Mesozoic extrusive and intrusive rocks	-0.00098	0.000	0.000	-0.0015	-0.0004
	Permian	0.00115	0.000	0.000	0.0009	0.0014
	Precambrian (undivided)	0.00060	0.000	0.123	-0.0002	0.0013
	Quaternary (undivided)	0.00572	0.001	0.000	0.0042	0.0073
	Quaternary and Tertiary	0.00510	0.001	0.000	0.0035	0.0067
	Silurian-Ordovician	0.00190	0.000	0.000	0.0012	0.0026
	Tertiary	0.00500	0.002	0.018	0.0008	0.0091
Based on observed means. The error term is Mean Square (Error) = .000. *. The mean difference is significant at the 0.05 level.						

Appendix Table E.4. **Post Hoc Tests** for **Multiple Comparisons of** means of **fuzzy CTI** under different Soil types/units **using** the least small difference (**LSD**) approach.

(I) Soil types/units		Mean Difference (I-J)	Std. Error	Sig.	95% Confidence Interval	
					Lower Bound	Upper Bound
Ao	Fo	-0.00361	0.0006	0.0000	-0.0047	-0.0025
	Fr	0.00000	0.0008	0.4605	-0.0022	0.0010
	I	0.00142	0.0004	0.0012	0.0006	0.0023
	Lc	-0.00245	0.0004	0.0000	-0.0033	-0.0016
	Lo	-0.00418	0.0005	0.0000	-0.0051	-0.0033
	We	0.00000	0.0004	0.5607	-0.0011	0.0006
	Ws	0.00200	0.0004	0.0000	0.0011	0.0029
	Xk	0.00251	0.0004	0.0000	0.0017	0.0033
Fo	Ao	0.00361	0.0006	0.0000	0.0025	0.0047
	Fr	0.00301	0.0008	0.0002	0.0014	0.0046
	I	0.00503	0.0004	0.0000	0.0042	0.0058
	Lc	0.00116	0.0004	0.0040	0.0004	0.0019
	Lo	0.00000	0.0004	0.1871	-0.0014	0.0003
	We	0.00335	0.0004	0.0000	0.0025	0.0042
	Ws	0.00561	0.0004	0.0000	0.0048	0.0064
	Xk	0.00612	0.0004	0.0000	0.0053	0.0069
Fr	Ao	0.00000	0.0008	0.4605	-0.0010	0.0022
	Fo	-0.00301	0.0008	0.0002	-0.0046	-0.0014
	I	0.00202	0.0007	0.0048	0.0006	0.0034
	Lc	-0.00185	0.0007	0.0089	-0.0032	-0.0005
	Lo	-0.00358	0.0007	0.0000	-0.0050	-0.0022
	We	0.00000	0.0007	0.6367	-0.0011	0.0018
	Ws	0.00260	0.0007	0.0003	0.0012	0.0040
	Xk	0.00311	0.0007	0.0000	0.0017	0.0045
I	Ao	-0.00142	0.0004	0.0012	-0.0023	-0.0006
	Fo	-0.00500	0.0004	0.0000	-0.0058	-0.0042
	Fr	-0.00202	0.0007	0.0048	-0.0034	-0.0006
	Lc	-0.00387	0.0002	0.0000	-0.0043	-0.0035
	Lo	-0.00560	0.0002	0.0000	-0.0061	-0.0051
	We	-0.00168	0.0002	0.0000	-0.0021	-0.0012
	Ws	0.00058	0.0002	0.0122	0.0001	0.0010
	Xk	0.00109	0.0002	0.0000	0.0007	0.0014
Lc	Ao	0.00245	0.0004	0.0000	0.0016	0.0033
	Fo	-0.00116	0.0004	0.0040	-0.0019	-0.0004
	Fr	0.00185	0.0007	0.0089	0.0005	0.0032
	I	0.00387	0.0002	0.0000	0.0035	0.0043
	Lo	-0.00172	0.0002	0.0000	-0.0022	-0.0013
	We	0.00219	0.0002	0.0000	0.0018	0.0026
	Ws	0.00445	0.0002	0.0000	0.0041	0.0049
	Xk	0.00496	0.0001	0.0000	0.0047	0.0053
Lo	Ao	0.00418	0.0005	0.0000	0.0033	0.0051
	Fo	0.00000	0.0004	0.1871	-0.0003	0.0014
	Fr	0.00358	0.0007	0.0000	0.0022	0.0050
	I	0.00560	0.0002	0.0000	0.0051	0.0061
	Lc	0.00172	0.0002	0.0000	0.0013	0.0022
	We	0.00392	0.0003	0.0000	0.0034	0.0044
	Ws	0.00618	0.0003	0.0000	0.0057	0.0067
	Xk	0.00669	0.0002	0.0000	0.0063	0.0071
We	Ao	0.00000	0.0004	0.5607	-0.0006	0.0011

	Fo	-0.00335	0.0004	0.0000	-0.0042	-0.0025
	Fr	0.00000	0.0007	0.6367	-0.0018	0.0011
	I	0.00168	0.0002	0.0000	0.0012	0.0021
	Lc	-0.00219	0.0002	0.0000	-0.0026	-0.0018
	Lo	-0.00392	0.0003	0.0000	-0.0044	-0.0034
	Ws	0.00226	0.0002	0.0000	0.0018	0.0027
	Xk	0.00277	0.0002	0.0000	0.0024	0.0032
Ws	Ao	-0.00200	0.0004	0.0000	-0.0029	-0.0011
	Fo	-0.00561	0.0004	0.0000	-0.0064	-0.0048
	Fr	-0.00260	0.0007	0.0003	-0.0040	-0.0012
	I	-0.00058	0.0002	0.0122	-0.0010	-0.0001
	Lc	-0.00445	0.0002	0.0000	-0.0049	-0.0041
	Lo	-0.00618	0.0003	0.0000	-0.0067	-0.0057
	We	-0.00226	0.0002	0.0000	-0.0027	-0.0018
	Xk	0.00051	0.0002	0.0089	0.0001	0.0009
Xk	Ao	-0.00251	0.0004	0.0000	-0.0033	-0.0017
	Fo	-0.00612	0.0004	0.0000	-0.0069	-0.0053
	Fr	-0.00311	0.0007	0.0000	-0.0045	-0.0017
	I	-0.00109	0.0002	0.0000	-0.0014	-0.0007
	Lc	-0.00496	0.0001	0.0000	-0.0053	-0.0047
	Lo	-0.00669	0.0002	0.0000	-0.0071	-0.0063
	We	-0.00277	0.0002	0.0000	-0.0032	-0.0024
	Ws	-0.00051	0.0002	0.0089	-0.0009	-0.0001

Based on observed means. The error term is Mean Square (Error) = 0.000.
*. The mean difference is significant at the 0.05 level.

REFERENCES

Aguilar, F. J., Aguilar, M. A., Aguera, F. and Sanchez, J. 2006. The accuracy of grid digital elevation models linearly constructed from scattered sample data. *International Journal of Geographical Information Science,* 20**,** 169-192.

Aiello, A., Adamo, M. and Canora, F. 2015. Remote sensing and GIS to assess soil erosion with RUSLE3D and USPED at river basin scale in southern Italy. *Catena,* 131**,** 174-185.

Aksoy, H. and Kavvas, M. L. 2005. A review of hillslope and watershed scale erosion and sediment transport models. *Catena,* 64**,** 247-271.

Angileri, S. E., Conoscenti, C., Hochschild, V., Marker, M., Rotigliano, E. and Agnesi, V. 2016. Water erosion susceptibility mapping by applying Stochastic Gradient Treeboost to the Imera Meridionale River Basin (Sicily, Italy). *Geomorphology,* 262**,** 61-76.

Antoniol, G., Ceccarelli, M., Maratea, A. and ... 2003. Classification of digital terrain models through fuzzy clustering: An application. *International Workshop on ….*

Arabameri, A., Chen, W., Blaschke, T., Tiefenbacher, J. P., Pradhan, B. and Tien Bui, D. 2020. Gully Head-Cut Distribution Modeling Using Machine Learning Methods—A Case Study of NW Iran. *Water,* 12**,** 16.

Arabameri, A., Chen, W., Loche, M., Zhao, X., Li, Y., Lombardo, L., Cerda, A., Pradhan, B. and Bui, D. T. 2019a. Comparison of machine learning models for gully erosion susceptibility mapping. *Geoscience Frontiers*.

Arabameri, A., Pradhan, B. and Rezaei, K. 2019b. Gully erosion zonation mapping using integrated geographically weighted regression with certainty factor and random forest models in GIS. *Journal of Environmental Management,* 232**,** 928-942.

Arnold, J., Williams, J., Griggs, R. and Sammons, N. 1991. SWRRBWQ–A Basin Model 5 for Assessing Management Impacts on Water Quality (Draft), USDA ARS, Grassland. *Soil, and Water Research Laboratory, Temple, TX*.

Arnold, J. G., Williams, J., Nicks, A. and Sammons, N. 1990. SWRRB; a basin scale simulation model for soil and water resources management. *SWRRB; a basin scale simulation model for soil and water resources management.*

Arrell, K. E., Fisher, P. F., Tate, N. J. and Bastin, L. 2007. A fuzzy c-means classification of elevation derivatives to extract the morphometric classification of landforms in Snowdonia, Wales. *Computers & Geosciences,* 33**,** 1366-1381.

Arun, P. V. 2013. A comparative analysis of different DEM interpolation methods. *The Egyptian Journal of Remote Sensing and Space Science,* 16**,** 133-139.

Avand, M., Janizadeh, S., Naghibi, S. A., Pourghasemi, H. R., Khosrobeigi Bozchaloei, S. and Blaschke, T. 2019. A Comparative Assessment of Random Forest and k-Nearest Neighbor Classifiers for Gully Erosion Susceptibility Mapping. *Water,* 11**,** 2076.

Bajracharya, R. and Lal, R. 1992. Seasonal soil loss and erodibility variation on a Miamian silt loam soil. *Soil Science Society of America Journal,* 56**,** 1560-1565.

Bbcnews. 2019. *Disappearing village* [Online]. @BBCNews. Available: https://www.bbc.com/news/av/world-africa-48463191/our-village-is-disappearing-due-to-erosion [Accessed].

Beasley, D. B., Huggins, L. F. and Monke, E. J. 1980. Answers - a Model for Watershed Planning. *Transactions of the Asae,* 23**,** 938-944.

Beasom, S. L., Wiggers, E. P. and Giardino, J. R. 1983. A Technique for Assessing Land Surface Ruggedness. *Journal of Wildlife Management,* 47**,** 1163-1166.

Bellman, R. E. and Zadeh, L. A. 1970. Decision-Making in a Fuzzy Environment. *Management Science Series B-Application,* 17**,** B141-B164.

Bergonse, R. and Reis, E. 2016. Controlling factors of the size and location of large gully systems: A regression-based exploration using reconstructed pre-erosion topography. *Catena,* 147**,** 621-631.

Bhola, S. and Mohan, S. 1982. Soil erodibility of black soils of Bellary district. *Indian journal of soil conservation*.

Biesemans, J., Van Meirvenne, M. and Gabriels, D. 2000. Extending the RUSLE with the Monte Carlo error propagation technique to predict long-term average off-site sediment accumulation. *Journal of Soil and Water Conservation,* 55**,** 35-42.

Bigdeli, B., Samadzadegan, F. and Reinartz, P. 2015. Fusion of hyperspectral and LIDAR data using decision template-based fuzzy multiple classifier system. *International Journal of Applied Earth Observation and Geoinformation,* 38**,** 309-320.

Bingner, R. L., Wells, R. R., Momm, H. G., Rigby, J. R. and Theurer, F. D. 2016. Ephemeral gully channel width and erosion simulation technology. *Natural Hazards,* 80**,** 1949-1966.

Bock, A. 2010. *Multiscale Landform Characterization for Land Use Evaluation using Fuzzy Sets*, scholar.colorado.edu.

Bolstad, P. V., Swank, W. and Vose, J. 1998. Predicting Southern Appalachian overstory vegetation with digital terrain data. *Landscape Ecology,* 13**,** 271-283.

Borah, D. 1989. Sediment discharge model for small watersheds. *Transactions of the ASAE,* 32**,** 874-0880.

Bouyoucos, G. 1935. 1789001. The clay ratio as a criterion of susceptibility of soils to erosion. *Agronomy journal,* 27**,** 738-741.

Bryan, R. B. 2000. Soil erodibility and processes of water erosion on hillslope.

Bui, E. N. 2004. Soil survey as a knowledge system. *Geoderma,* 120**,** 17-26.

Burrough, P. A. 1989. Fuzzy Mathematical-Methods for Soil Survey and Land Evaluation. *Journal of Soil Science,* 40**,** 477-492.

Burrough, P. A., Van Gaans, P. F. M. and Macmillan, R. A. 2000. High-resolution landform classification using fuzzy k-means. *Fuzzy Sets and Systems,* 113**,** 37-52.

Cadell, W. 2002. Report on the generation and analysis of DEMs for spatial modelling. *The James Hutton Institute (formerly The Macaulay Land Use Research Institute),* 28.

Cappadonia, C., Coco, L., Buccolini, M. and Rotigliano, E. 2016. From Slope Morphometry to Morphogenetic Processes: An Integrated Approach of Field Survey, Geographic Information System Morphometric Analysis and Statistics in Italian Badlands. *Land Degradation & Development,* 27**,** 851-862.

Capra, A., Mazzara, L. M. and Scicolone, B. 2005. Application of the EGEM model to predict ephemeral gully erosion in Sicily, Italy. *CATENA,* 59**,** 133-146.

Carre, F. and Girard, M. C. 2002. Quantitative mapping of soil types based on regression kriging of taxonomic distances with landform and land cover attributes. *Geoderma,* 110**,** 241-263.

Casalí, J., Loizu, J., Campo, M. A., De Santisteban, L. M. and Álvarez-Mozos, J. 2006. Accuracy of methods for field assessment of rill and ephemeral gully erosion. *Catena,* 67**,** 128-138.

Casalí, J., López, J. J. and Giráldez, J. V. 1999. Ephemeral gully erosion in southern Navarra (Spain). *CATENA,* 36**,** 65-84.

Chagas, C. D., De Carvalho, W., Bhering, S. B. and Calderano, B. 2016. Spatial prediction of soil surface texture in a semiarid region using random forest and multiple linear regressions. *Catena,* 139**,** 232-240.

Chu, T. and Tsai, T. 1995. Comparison of accuracy and algorithms of slope and aspect measures from DEM. *Proceedings of GIS AM/FM ASIA'95*, 21-24.

Cochrane, T. A. and Flanagan, D. C. 1999. Assessing water erosion in small watersheds using WEPP with GIS and digital elevation models. *Journal of Soil and Water Conservation,* 54, 678-685.

Cochrane, T. A. and Flanagan, D. C. 2003. Representative hillslope methods for applying the WEPP model with DEMS and GIS. *Transactions of the Asae,* 46, 1041-1049.

Conoscenti, C., Agnesi, V., Angileri, S., Cappadonia, C., Rotigliano, E. and Märker, M. 2013. A GIS-based approach for gully erosion susceptibility modelling: a test in Sicily, Italy. *Environmental Earth Sciences,* 70, 1179-1195.

Conoscenti, C., Angileri, S., Cappadonia, C., Rotigliano, E., Agnesi, V. and Marker, M. 2014. Gully erosion susceptibility assessment by means of GIS-based logistic regression: A case of Sicily (Italy). *Geomorphology,* 204, 399-411.

Conoscenti, C., Rotigliano, E., Cama, M., Caraballo-Arias, N. A., Lombardo, L. and Agnesi, V. 2016. Exploring the effect of absence selection on landslide susceptibility models: A case study in Sicily, Italy. *Geomorphology,* 261, 222-235.

Cooke, R. and Doornkamp, J. 1990. Geomorfology in Enviroment Management: a new introduction. Oxford: Clarendon Press.

Coughlan, K. J. and Rose, C. 1997. *new soil conservation methodology and application to cropping systems in tropical steeplands*, Australian Centre for International Agricultural Research.

Cucchiaro, S., Cavalli, M., Vericat, D., Crema, S., Llena, M. and ... 2019. Geomorphic effectiveness of check dams in a debris-flow catchment using multi-temporal topographic surveys. *Catena*.

D'oleire-Oltmanns, S., Marzolff, I., Tiede, D. and Blaschke, T. 2014. Detection of Gully-Affected Areas by Applying Object-Based Image Analysis (OBIA) in the Region of Taroudannt, Morocco. *Remote Sensing,* 6, 8287-8309.

Daggupati, P., Douglas-Mankin, K. R. and Sheshukov, A. Y. 2013. Predicting Ephemeral Gully Location and Length Using Topographic Index Models. *Transactions of the Asabe,* 56, 1427-1440.

Daggupati, P., Mankin, K. R. D., Barnes, P. L., Nelson, P. C. N. O., Delvin, D. L. and Frees, L. D. 2009. Identifying Potential Ephemeral Gully Locations at a Watershed Scale.

Daggupati, P., Sheshukov, A. Y. and Douglas-Mankin, K. R. 2014. Evaluating ephemeral gullies with a process-based topographic index model. *Catena,* 113**,** 177-186.

De Roo, A. and Jetten, V. 1999. Calibrating and validating the LISEM model for two data sets from the Netherlands and South Africa. *Catena,* 37**,** 477-493.

De Roo, A., Offermans, R. and Cremers, N. 1996. LISEM: A single-event, physically based hydrological and soil erosion model for drainage basins. II: Sensitivity analysis, validation and application. *Hydrological processes,* 10**,** 1119-1126.

Desmet, P. J. J. 1997. Effects of interpolation errors on the analysis of DEMs. *Earth Surface Processes and Landforms,* 22**,** 563-580.

Desmet, P. J. J., Poesen, J., Govers, G. and Vandaele, K. 1999. Importance of slope gradient and contributing area for optimal prediction of the initiation and trajectory of ephemeral gullies. *Catena,* 37**,** 377-392.

Dewitte, O., Daoudi, M., Bosco, C. and Van Den Eeckhaut, M. 2015. Predicting the susceptibility to gully initiation in data-poor regions. *Geomorphology,* 228**,** 101-115.

Dietrich, C. R., Green, T. R. and Jakeman, A. J. 1999. An analytical model for stream sediment transport: application to Murray and Murrumbidgee river reaches, Australia. *Hydrological Processes,* 13**,** 763-776.

Dikau, R. 1988. Case studies in the development of derived geomorphic maps. *Geologisches Jahrbuch A,* 104**,** 329-338.

Dikau, R. 1989. The application of a digital relief model to landform analysis in geomorphology. *Three dimensional applications in geographical information systems***,** 51-77.

Dikau, R., Rasemann, S. and Schmidt, J. 2013. Hillslope, Form. *Encyclopedia of Geomorphology***,** 516-521.

Dillard, A., Thomas, A., Snyder, W. and ... 1992. Interpolation of topographic attributes using sliding polynomials. *Applied Engineering in …*.

Dragut, L. and Blaschke, T. 2006. Automated classification of landform elements using object-based image analysis. *Geomorphology,* 81**,** 330-344.

Drăguţ, L. and Blaschke, T. 2006. Automated classification of landform elements using object-based image analysis. *Geomorphology,* 81**,** 330-344.

Dumitriu, D. 2016. Geomorphic Effectiveness of Floods on Trotus River Channel (Romania) between 2000 and 2012. *Carpathian Journal of Earth and Environmental Sciences,* 11**,** 181-196.

Eppl 1987. Environmental Planning and Programming Language User's Guide. Minnesota State Planning Agency, St. Paul, Minnesota, U.S.A.

Esa. 2017. *Prototype Land Cover map over Africa at 20m released | ESA CCI Land cover website* [Online]. Available: https://www.esa-landcover-cci.org/?q=node/187 [Accessed 19/01/2019 2019].

Evans, I. 1998. *What do terrain statistics really mean*, John Wiley and Sons.

Evans, I. S. 1979. Statistical Characterization of Altitude Matrices by Computer. Report 6. An Integrated System of Terrain Analysis and Slope Mapping. DURHAM UNIV (ENGLAND) DEPT OF GEOGRAPHY.

Evans, I. S. 1980. An integrated system of terrain analysis and slope mapping. *Zeitschrift fur Geomorphologie,* 36**,** 274-295.

Evans, I. S. 2012. Geomorphometry and landform mapping: What is a landform? *GEOMOR Geomorphology,* 137**,** 94-106.

Fao. 2007. *Digital Soil Map of the World* [Online]. Available: http://www.fao.org/geonetwork/srv/en/metadata.show%3Fid=14116 [Accessed 14/06/2016 2016].

Ferro, V. and Porto, P. 2000. Sediment delivery distributed (SEDD) model. *Journal of hydrologic engineering,* 5**,** 411-422.

Finlayson, B. and Statham, I. 1980. *Hillslope analysis*, Butterworth-Heinemann.

Fisher, P., Wood, J. and Cheng, T. 2004. Where is Helvellyn? Fuzziness of multi-scale landscape morphometry. *Transactions of the Institute of British Geographers,* 29**,** 106-128.

Fleming, M. D. and Hoffer, R. M. 1979. Machine processing of Landsat MSS data and DMA topographic data for forest cover type mapping. *LARS Technical Reports***,** 80.

Florinsky, I. V. 1998a. Accuracy of local topographic variables derived from digital elevation models. *International Journal of Geographical Information Science,* 12**,** 47-61.

Florinsky, I. V. 1998b. Combined analysis of digital terrain models and remotely sensed data in landscape investigations. *Progress in Physical Geography,* 22**,** 33-60.

Florinsky, I. V. and Kuryakova, G. A. 1996. Influence of topography on some vegetation cover properties. *Catena,* 27**,** 123-141.

Florinsky, I. V. and Pankratov, A. N. 2015. Digital terrain modeling with the Chebyshev polynomials. 1-10.

Florinsky, I. V. and Pankratov, A. N. 2016. A universal spectral analytical method for digital terrain modeling. *International Journal of Geographical Information Science,* 30**,** 2506-2528.

Foster, G. R. and Wischmeier, W. H. 1974. Evaluating Irregular Slopes for Soil Loss Prediction. *Transactions of the Asae,* 17**,** 305-309.

Frank, S. 2011. *Using fuzzy logic and spectral responses to estimate and digitally map soil organic carbon in a recently glaciated loess mantled landscape*, search.proquest.com.

Garosi, Y., Sheklabadi, M., Conoscenti, C., Pourghasemi, H. R. and Van Oost, K. 2019. Assessing the performance of GIS- based machine learning models with different accuracy measures for determining susceptibility to gully erosion. *Science of The Total Environment,* 664**,** 1117-1132.

Gayen, A., Pourghasemi, H. R., Saha, S., Keesstra, S. and Bai, S. 2019. Gully erosion susceptibility assessment and management of hazard-prone areas in India using different machine learning algorithms. *Science of The Total Environment,* 668**,** 124-138.

Gerrard, A. J. W. and Robinson, D. A. 1971. Variability in Slope Measurements. A Discussion of the Effects of Different Recording Intervals and Micro-Relief in Slope Studies. *Transactions of the Institute of British Geographers***,** 45.

Godone, D. and Garnero, G. 2013. *The role of morphometric parameters in Digital Terrain Models interpolation accuracy: a case study*, researchgate.net.

Goñi, U. 2015. *When nature says 'Enough!': the river that appeared overnight in Argentina* [Online]. @guardian. Available: http://www.theguardian.com/world/2018/apr/01/argentina-new-river-soya-beans [Accessed].

Goodchild, M. F. 1980. Fractals and the Accuracy of Geographical Measures. *Journal of the International Association for Mathematical Geology,* 12**,** 85-98.

Goodchild, M. F. and Mark, D. M. 1987. The Fractal Nature of Geographic Phenomena. *Annals of the Association of American Geographers,* 77**,** 265-278.

Gorsevski, P. V., Donevska, K. R., Mitrovski, C. D. and Frizado, J. P. 2012. Integrating multi-criteria evaluation techniques with geographic information systems for landfill site selection: A case study using ordered weighted average. *Waste Management,* 32**,** 287-296.

Grams, P., Buscombe, D., Topping, D. and ... 2019. How many measurements are required to construct an accurate sand budget in a large river? Insights from analyses of signal and noise. *Earth Surface …*.

Gray, D. H. and Barker, D. 2004. Root-soil mechanics and interactions. *Riparian vegetation and fluvial geomorphology,* 8**,** 113-123.

Grohmann, C. H. 2015. Effects of spatial resolution on slope and aspect derivation for regional-scale analysis. *Computers & Geosciences,* 77**,** 111-117.

Guesgen, H. W., Albrecht, J. and Grundner, S. Erosion Modeling in a Raster-Based GIS with Fuzzy Logic. FLAIRS Conference, 2000. 266-270.

Guisado-Pintado, E., Jackson, D. and Rogers, D. 2019. 3D mapping efficacy of a drone and terrestrial laser scanner over a temperate beach-dune zone. *Geomorphology*.

Haider, V. L., Kropacek, J., Dunkl, I., Wagner, B. and Von Eynatten, H. 2015. Identification of peneplains by multi-parameter assessment of digital elevation models. *Earth Surface Processes and Landforms,* 40**,** 1477-1492.

Hanley, J. A. and Mcneil, B. J. 1982. The meaning and use of the area under a receiver operating characteristic (ROC) curve. *Radiology,* 143**,** 29-36.

Hanley, N., Faichney, R., Munro, A. and Shortle, J. S. 1998. Economic and environmental modelling for pollution control in an estuary. *Journal of Environmental management,* 52**,** 211-225.

Haralick, R. M. 1983. . Pattern recognition and classification. Manual of Remote Sensing. American Society of Photogrammetry.

Heerdegen, R. G. and Beran, M. A. 1982. Quantifying source areas through land surface curvature and shape. *Journal of Hydrology,* 57**,** 359-373.

Hengl, T. and Evans, I. S. 2009. Mathematical and Digital Models of the Land Surface. *Geomorphometry: Concepts, Software, Applications,* 33**,** 31-63.

Hengl, T., Heuvelink, G. B. M., Kempen, B., Leenaars, J. G. B., Walsh, M. G., Shepherd, K. D., Sila, A., Macmillan, R. A., De Jesus, J. M., Tamene, L. and Tondoh, J. E. 2015. Mapping Soil Properties of Africa at 250 m Resolution: Random Forests Significantly Improve Current Predictions. *Plos One,* 10**,** e0125814.

Hengl, T., Mendes De Jesus, J., Heuvelink, G. B., Ruiperez Gonzalez, M., Kilibarda, M., Blagotic, A., Shangguan, W., Wright, M. N., Geng, X., Bauer-Marschallinger, B., Guevara, M. A., Vargas, R., Macmillan, R. A., Batjes, N. H., Leenaars, J. G., Ribeiro, E., Wheeler, I., Mantel, S. and Kempen, B. 2017. SoilGrids250m: Global gridded soil information based on machine learning. *PLoS One,* 12**,** e0169748.

Hengl, T. and Reuter, H. I. 2009. Geomorphometry concepts, software, applications.

Heuvelink, G. 1998. *Error propagation in environmental modelling with GIS*, books.google.com.

Heuvelink, G. 2002. Analysing uncertainty propagation in GIS: why is it not that simple. *Uncertainty in remote sensing and GIS*.

Heuvelink, G. B. and Burrough, P. A. 1993. Error propagation in cartographic modelling using Boolean logic and continuous classification. *International Journal of Geographical Information Systems,* 7**,** 231-246.

Hobson, R. 1972. Surface roughness in topography: quantitative approach. Methuen.

Hodgson, M. E. 1995. What cell size does the computed slope/aspect angle represent? *Photogrammetric Engineering and Remote Sensing,* 61**,** 513-517.

Hoffman, M. T. and Todd, S. 2000. A National Review of Land Degradation in South Africa: The Influence of Biophysical and Socio-Economic Factors. *Journal of Southern African Studies,* 26**,** 743-758.

Hofierka, J. and Cebecauer, T. 2007. Spatial interpolation of elevation data with variable density: A new methodology to derive quality DEMs. *Ieee Geoscience and Remote Sensing Letters,* 4**,** 117-121.

Hofle, B., Griesbaum, L. and Forbriger, M. 2013. GIS-Based Detection of Gullies in Terrestrial LiDAR Data of the Cerro Llamoca Peatland (Peru). *Remote Sensing,* 5**,** 5851-5870.

Horn, B. K. P. 1981. Hill Shading and the Reflectance Map. *Proceedings of the Ieee,* 69**,** 14-47.

Igwe, C. 2003. Erodibility of soils of the upper rainforest zone, southeastern Nigeria. *Land degradation & development,* 14**,** 323-334.

Igwe, C. 2005. Erodibility in relation to water-dispersible clay for some soils of eastern Nigeria. *Land Degradation & Development,* 16**,** 87-96.

Igwe, C. and Udegbunam, O. 2008. Soil properties influencing water-dispersible clay and silt in an Ultisol in southern Nigeria. *International Agrophysics,* 22**,** 319-325.

Institution of Civil, E. 1995. *Vegetation and slopes : stabilisation, protection and ecology,* London, Thomas Telford.

Irvin, B. J., Ventura, S. J. and Slater, B. K. 1997. Fuzzy and isodata classification of landform elements from digital terrain data in Pleasant Valley, Wisconsin. *Geoderma,* 77**,** 137-154.

Jakeman, A., Littlewood, I. and Whitehead, P. 1990. Computation of the instantaneous unit hydrograph and identifiable component flows with application to two small upland catchments. *Journal of hydrology,* 117**,** 275-300.

Jakeman, A. J., Post, D. A. and Beck, M. B. 1994. From data and theory to environmental model: the case of rainfall runoff. *Environmetrics,* 5**,** 297-314.

Jaxa. 2019. *ALOS Global Digital Surface Model "ALOS World 3D - 30m" (AW3D30)* [Online]. Available: https://www.eorc.jaxa.jp/ALOS/en/aw3d30/index.htm [Accessed].

Jenness, J. 2013. DEM surface tools for ArcGIS. *Jenness Enterprises***,** 1-96.

Jenness, J. S. 2004. Calculating landscape surface area from digital elevation models. *Wildlife Society Bulletin,* 32**,** 829-839.

Jenny, H. 1994. *Factors of soil formation: a system of quantitative pedology*, Courier Corporation.

Johanson, R., Imhoff, J. and Davis, H. 1980. Users Manual for the Hydrologic Simulation Program—Fortran (HSPF) version No. 5.0. *Athens, GA: USA EPA Environmental Research Laboratory*.

Johnson, B. E., Julien, P. Y., Molnar, D. K. and Watson, C. C. 2000. THE TWO-DIMENSIONAL UPLAND EROSION MODEL CASC2D-SED 1. *JAWRA Journal of the American Water Resources Association,* 36**,** 31-42.

Jones, K. 1998a. A comparison of two approaches to ranking algorithms used to compute hill slopes. *GeoInformatica*.

Jones, K. H. 1998b. A comparison of algorithms used to compute hill slope as a property of the DEM. *Computers & Geosciences,* 24**,** 315-323.

Kakembo, V., Xanga, W. W. and Rowntree, K. 2009. Topographic thresholds in gully development on the hillslopes of communal areas in Ngqushwa Local Municipality, Eastern Cape, South Africa. *Geomorphology,* 110**,** 188-194.

Kinnell, P. and Risse, L. 1998. USLE-M: empirical modeling rainfall erosion through runoff and sediment concentration. *Soil Science Society of America Journal,* 62**,** 1667-1672.

Kinnell, P. I. A. 2010. Event soil loss, runoff and the Universal Soil Loss Equation family of models: A review. *Journal of Hydrology,* 385**,** 384-397.

Knighton, A. D. 1999. Downstream variation in stream power. *Geomorphology,* 29**,** 293-306.

Knisel, W. and Foster, G. 1981. CREAMS [Chemicals, runoff, and erosion from agricultural management systems]: a system for evaluating best management practices [Mathematical models, pollution].

Kornejady, A., Ownegh, M. and Bahremand, A. 2017. Landslide susceptibility assessment using maximum entropy model with two different data sampling methods. *Catena,* 152**,** 144-162.

Korzeniowska, K. and Korup, O. 2016. Mapping gullies using terrain-surface roughness.

Korzeniowska, K., Pfeifer, N. and Landtwing, S. 2018. Mapping gullies, dunes, lava fields, and landslides via surface roughness. *Geomorphology,* 301**,** 53-67.

Kosko, B. and Toms, M. 1993. *Fuzzy thinking: The new science of fuzzy logic*, Hyperion New York.

Kusre, B., Ghosh, P. and Nath, K. 2018. Prioritization of soil conservation measures using erodibility indices as criteria in Sikkim (India). *Journal of Earth System Science,* 127**,** 81.

Ladson, A. R. and Moore, I. D. 1992. Soil-Water Prediction on the Konza Prairie by Microwave Remote-Sensing and Topographic Attributes. *Journal of Hydrology,* 138**,** 385-407.

Laffan, S. 1999. *Spatially assessing model error using geographically weighted regression*, geocomputation.org.

Laflen, J., Elliot, W., Simanton, J., Holzhey, C. and Kohl, K. 1991a. WEPP: Soil erodibility experiments for rangeland and cropland soils. *Journal of Soil and Water Conservation,* 46**,** 39-44.

Laflen, J., Franti, T. and Watson, D. 1985. Effect of tillage systems on concentrated flow erosion. *Soil Conservation and Productivity,* 2**,** 798-809.

Laflen, J. M. and Flanagan, D. C. 2013. The development of U. S. soil erosion prediction and modeling. *International Soil and Water Conservation Research,* 1**,** 1-11.

Laflen, J. M., Lane, L. J. and Foster, G. R. 1991b. WEPP: A new generation of erosion prediction technology. *Journal of Soil and Water Conservation,* 46**,** 34-38.

Lecours, V., Devillers, R., Simms, A. E., Lucieer, V. L. and Brown, C. J. 2017. Towards a framework for terrain attribute selection in environmental studies. *Environmental Modelling & Software,* 89**,** 19-30.

Leduc, P., Peirce, S. and Ashmore, P. 2019. *Challenges and applications of structure-from-motion photogrammetry in a physical model of a braided river*, earth-surf-dynam.net.

Li, H., Cruse, R. M., Bingner, R. L., Gesch, K. R. and Zhang, X. 2016. Evaluating ephemeral gully erosion impact on Zea mays L. yield and economics using AnnAGNPS. *Soil and Tillage Research,* 155**,** 157-165.

Lin, P., Liu, X. L., Hu, S. Y. and Li, P. J. 2016. Large Deformation Analysis of a High Steep Slope Relating to the Laxiwa Reservoir, China. *Rock Mechanics and Rock Engineering,* 49**,** 2253-2276.

Lindsay, J. The whitebox geospatial analysis tools project and open-access GIS. Proceedings of the GIS Research UK 22nd Annual Conference, The University of Glasgow, 2014. 16-18.

Lindsay, J. B. 2009. Geomorphometry in TAS GIS. *Geomorphometry: Concepts, Software, Applications,* 33**,** 367-386.

Littleboy, M., Freebairn, D., Hammer, G. and Silburn, D. 1992a. Impact of soil erosion on production in cropping systems. II. Simulation of production and erosion risks for a wheat cropping system. *Soil Research,* 30**,** 775-788.

Littleboy, M., Silburn, D., Freebairn, D., Woodruff, D., Hammer, G. and Leslie, J. 1992b. Impact of soil erosion on production in cropping systems. I. Development and validation of a simulation model. *Soil Research,* 30**,** 757-774.

Lopes, V. and Lane, L. 1988. Modeling sedimentation processes in small watersheds. *Sediment Budgets.* IAHS Publication.

Lopes, V. L. 1987. *A numerical model of watershed erosion and sediment yield.* University of Arizona Tucson.

Macmillan, R. A., Pettapiece, W. W., Nolan, S. C. and Goddard, T. W. 2000. A generic procedure for automatically segmenting landforms into landform elements using DEMs, heuristic rules and fuzzy logic. *Fuzzy Sets and Systems,* 113**,** 81-109.

Macmillan, R. A. and Shary, P. A. 2009. Landforms and Landform Elements in Geomorphometry. *Geomorphometry: Concepts, Software, Applications,* 33**,** 227-254.

Mallo, I. and Mgbanyi, L. 2013. Assessment of Soil erodibility Indices and Soil wash in a miniature badlands at Gada Biyu, FCT Nigeria. *Ethiopian Journal of Environmental Studies and Management,* 6**,** 135-142.

Mamdani, E. H. 1974. Application of Fuzzy Algorithms for Control of Simple Dynamic Plant. *Proceedings of the Institution of Electrical Engineers-London,* 121**,** 1585-1588.

Mamdani, E. H. and Assilian, S. 1975. An experiment in linguistic synthesis with a fuzzy logic controller. *International journal of man-machine studies,* 7**,** 1-13.

Mararakanye, N. 2015. *A comparative study of gully erosion contributing factors in two tertiary catchments in Mpumalanga, South Africa*, repository.up.ac.za.

Mararakanye, N. and Le Roux, J. 2012. Gully location mapping at a national scale for South Africa. *South African Geographical Journal,* 94**,** 208-218.

Mararakanye, N. and Sumner, P. D. 2017. Gully erosion: A comparison of contributing factors in two catchments in South Africa. *Geomorphology,* 288**,** 99-110.

Marzolff, I. and Poesen, J. 2009. The potential of 3D gully monitoring with GIS using high-resolution aerial photography and a digital photogrammetry system. *Geomorphology,* 111**,** 48-60.

Maxwell, A. E., Warner, T. A. and Strager, M. P. 2016. Predicting Palustrine Wetland Probability Using Random Forest Machine Learning and Digital Elevation Data-Derived Terrain Variables. *Photogrammetric Engineering and Remote Sensing,* 82**,** 437-447.

Mcbratney, A. B., Santos, M. L. M. and Minasny, B. 2003. On digital soil mapping. *Geoderma,* 117**,** 3-52.

Mccullagh, M. 1998. Quality, use and visualisation in terrain modelling. *Landform Monitoring, Modeling and Analysis***,** 95-117.

Mckenzie, N. J. and Ryan, P. J. 1999. Spatial prediction of soil properties using environmental correlation. *Geoderma,* 89**,** 67-94.

Mcneill, D. and Freiberger, P. 1994. *Fuzzy logic: The revolutionary computer technology that is changing our world*, Simon and Schuster.

Merritt, W. S., Letcher, R. A. and Jakeman, A. J. 2003. A review of erosion and sediment transport models. *Environmental Modelling & Software,* 18**,** 761-799.

Messenzehl, K., Hoffmann, T. and Dikau, R. 2014. Sediment connectivity in the high-alpine valley of Val Müschauns, Swiss National Park — linking geomorphic field mapping with geomorphometric modelling. *Geomorphology,* 221**,** 215-229.

Minar, J. and Evans, I. S. 2008. Elementary forms for land surface segmentation: The theoretical basis of terrain analysis and geomorphological mapping. *Geomorphology,* 95**,** 236-259.

Mitášová, H. and Hofierka, J. 1993. Interpolation by regularized spline with tension: II. Application to terrain modeling and surface geometry analysis. *Mathematical Geology*.

Mitasova, H., Hofierka, J., Zlocha, M. and Iverson, L. R. 1996. Modelling topographic potential for erosion and deposition using GIS. *International Journal of Geographical Information Systems,* 10**,** 629-641.

Mitra, B., Scott, H. D., Dixon, J. C. and Mckimmey, J. M. 1998. Applications of fuzzy logic to the prediction of soil erosion in a large watershed. *Geoderma,* 86**,** 183-209.

Mittal, D., Shukla, R., Verma, S., Sagar, A., Verma, K. S., Pandey, A., Negi, Y. S., Saini, R. V. and Saini, A. K. 2019. Fire in pine grown regions of Himalayas depletes cultivable plant growth promoting beneficial microbes in the soil. *Applied Soil Ecology,* 139**,** 117-124.

Momm, H., Bingner, R., Wells, R. and ... 2011a. Analysis of topographic attributes for identification of ephemeral gully channel initiation in agricultural watersheds. *… , Kentucky, August 7-10 …*.

Momm, H., Bingner, R., Wells, R., Dabney, S. and Bhuiyan, F. 2011b. Methods for gully characterization in agricultural croplands using ground-based light detection and ranging. *Sediment Transport—Flow and Morphological Processes*.

Momm, H. G., Bingner, R. L., Wells, R. R., Rigby, J. R. and Dabney, S. M. 2013. Effect of Topographic Characteristics on Compound Topographic Index for Identification of Gully Channel Initiation Locations. *Transactions of the Asabe,* 56**,** 523-537.

Montgomery, D. R. and Dietrich, W. E. 1989. Source areas, drainage density, and channel initiation. *Water Resources Research,* 25**,** 1907-1918.

Moore, I. and Nieber, J. 1989. *Landscape assessment of soil erosion and nonpoint source pollution*, agris.fao.org.

Moore, I. D., Burch, G. J. and Mackenzie, D. H. 1988a. Topographic Effects on the Distribution of Surface Soil-Water and the Location of Ephemeral Gullies. *Transactions of the Asae,* 31**,** 1098-1107.

Moore, I. D., Grayson, R. B. and Ladson, A. R. 1991. Digital Terrain Modeling - a Review of Hydrological, Geomorphological, and Biological Applications. *Hydrological Processes,* 5**,** 3-30.

Moore, I. D., Oloughlin, E. M. and Burch, G. J. 1988b. A Contour Based Topographic Model for Hydrological and Ecological Applications. *Earth Surface Processes and Landforms,* 13**,** 305-320.

Moore, R. and Thompson, J. 1996. Are water table variations in a shallow forest soil consistent with the TOPMODEL concept? *Water Resources Research*.

Morgan, R. 2005. Soil erosion and conservation. National Soil Resources Institute. Cranfield University. Blackwell Publishing, UK.

Morgan, R., Qinton, J., Smith, R., Govers, G., Poesen, J., Auerswald, K., Chisci, G., Torri, D. and Styczen, M. 1999. The European soil erosion model (EUROSEM): A dynamic approach for predicting sediment transport from fields and small catchments-Reply. *Earth Surface Processes and Landforms,* 24**,** 567-568.

Morgan, R., Quinton, J., Smith, R., Govers, G., Poesen, J., Auerswald, K., Chisci, G., Torri, D. and Styczen, M. 1998a. The European Soil Erosion Model (EUROSEM): a dynamic approach for predicting sediment transport from fields and small catchments. *Earth Surface Processes and Landforms: The Journal of the British Geomorphological Group,* 23**,** 527-544.

Morgan, R., Quinton, J., Smith, R., Govers, G., Poesen, J., Auerswald, K., Chisci, G., Torri, D., Styczen, M. and Folly, A. 1998b. The European Soil Erosion Model (EUROSEM): documentation and user guide. 124-124.

Morgan, R. P. C. 2009. *Soil erosion and conservation*, John Wiley & Sons.

Morgan, R. P. C. and Nearing, M. A. 2011. *Handbook of erosion modelling*, Wiley Online Library.

Morino, C., Conway, S., Balme, M. and ... 2019. Debris-flow release processes investigated through the analysis of multi-temporal LiDAR datasets in north-western Iceland. *Earth Surface …*.

Mosbrucker, A. 2014. High-resolution digital elevation model of Mount St. Helens crater and upper North Fork Toutle River basin, Washington, based on an airborne lidar survey of September 2009. *Data Series.* Reston, VA.

Mosbrucker, A. R., Spicer, K. R., Major, J. J., Saunders, D. R., Christianson, T. S. and Kingsbury, C. G. 2015. Digital database of channel cross-section surveys, Mount St. Helens, Washington. US Geological Survey.

Mukhi, A. 1988. Erodibility of some vertisols. *Journal of the Indian Society of Soil Science,* 36**,** 532-536.

Murphy, P. N. C., Ogilvie, J. and Arp, P. 2009. Topographic modelling of soil moisture conditions: a comparison and verification of two models. *European Journal of Soil Science,* 60**,** 94-109.

Nearing, M., Foster, G., Lane, L. and Finkner, S. 1989. A process-based soil erosion model for USDA-Water Erosion Prediction Project technology. *Transactions of the ASAE,* 32**,** 1587-1593.

Negnevitsky, M. 2005. *Artificial intelligence: a guide to intelligent systems*, Pearson Education.

Nisar Ahamed, T. R., Gopal Rao, K. and Murthy, J. S. R. 2000. Fuzzy class membership approach to soil erosion modelling. *Agricultural Systems,* 63**,** 97-110.

Noto, L. V., Bastola, S., Dialynas, Y. G., Arnone, E. and Bras, R. L. 2017. Integration of fuzzy logic and image analysis for the detection of gullies in the Calhoun Critical Zone Observatory using airborne LiDAR data. *Isprs Journal of Photogrammetry and Remote Sensing,* 126**,** 209-224.

O'loughlin, E. 1986. Prediction of surface saturation zones in natural catchments by topographic analysis. *Water Resources Research,* 22**,** 794-804.

Onorati, G. and Poscolieri, M. The Italian mean heights archive, a digital data set useful for thematic mapping and geomorphological units analysis. Proc. 8th Symposium EARSeL, Capri, Italy, 1988. 451-466.

Orra. 2019. *USGS Geology of Africa | Orr & Associates* [Online]. Available: https://www.orrbodies.com/resource/usgs-geology-africa/ [Accessed].

Parker, C., Clifford, N. J. and Thorne, C. R. 2011. Understanding the influence of slope on the threshold of coarse grain motion: Revisiting critical stream power. *Geomorphology,* 126**,** 51-65.

Parker, C., Thorne, C., Bingner, R., Wells, R. and Wilcox, D. 2007. Automated mapping of potential for ephemeral gully formation in agricultural watersheds. *US Department of Agriculture, Agricultural Research Service, National Sedimentation Laboratory Research Report, Oxford, MS*.

Pieri, C. J. M. G. 1992. *Fertility of soils: a future for farming in the West African savannah,* Berlin, Springer-Verlag.

Pike, R., Wood, W. and Dikau, R. 1995. *Advances in geomorphometry: proceedings of the Walter F. Wood memorial symposium: Third International Conference on Geomorphology, McMaster …*, Gebrüder Borntraeger.

Pipaud, I. and Lehmkuhl, F. 2017. Object-based delineation and classification of alluvial fans by application of mean-shift segmentation and support vector machines. *Geomorphology,* 293**,** 178-200.

Poesen, J., Nachtergaele, J., Verstraeten, G. and Valentin, C. 2003. Gully erosion and environmental change: importance and research needs. *Catena,* 50**,** 91-133.

Poesen, J., Torri, D. and Vanwalleghem, T. 2011. Gully erosion: procedures to adopt when modelling soil erosion in landscapes affected by gullying. *Handbook of erosion modelling.* Wiley Online Library.

Poesen, J., Vandekerckhove, L., Nachtergaele, J., Wijdenes, D. O., Verstraeten, G. and Van Wesemael, B. 2002. 8 Gully Erosion in Dryland Environments. *Dryland rivers: Hydrology and geomorphology of semi-arid channels*, 229.

Prosser, I., Rustomji, P., Young, B., Moran, C. and Hughes, A. 2001a. Constructing river basin sediment budgets for the National Land and Water Resources Audit. *Land and Water Technical Report, CSIRO, Canberra*.

Prosser, I., Young, W., Rustomji, P., Hughes, A. and Moran, C. 2001b. A model of river sediment budgets as an element of river health assessment.

Pu, R. L. and Bell, S. 2013. A protocol for improving mapping and assessing of seagrass abundance along the West Central Coast of Florida using Landsat TM and EO-1 ALI/Hyperion images. *Isprs Journal of Photogrammetry and Remote Sensing,* 83, 116-129.

Qi, F., Zhu, A. X., Harrower, M. and Burt, J. E. 2006. Fuzzy soil mapping based on prototype category theory. *Geoderma,* 136, 774-787.

Rahmati, O., Tahmasebipour, N., Haghizadeh, A., Pourghasemi, H. R. and Feizizadeh, B. 2017. Evaluation of different machine learning models for predicting and mapping the susceptibility of gully erosion. *Geomorphology,* 298, 118-137.

Renard, K., Foster, G., Weesies, G., Mccool, D. and Yoder, D. 1997. *Predicting soil erosion by water: a guide to conservation planning with the Revised Universal Soil Loss Equation (RUSLE)*.

Renard, K. G., Foster, G. R., Weesies, G. A. and Porter, J. P. 1991. Rusle - Revised Universal Soil Loss Equation. *Journal of Soil and Water Conservation,* 46, 30-33.

Rhind, D. W. 1972. One-Sided Constraints in Automated Contouring of Drift Thickness. *Geological Society of America Bulletin,* 83, 2525-&.

Riley, S. J. 1999. Index that quantifies topographic heterogeneity. *intermountain Journal of sciences,* 5, 23-27.

Ritter, P. 1987. A Vector-Based Slope and Aspect Generation Algorithm. *Photogrammetric Engineering and Remote Sensing,* 53, 1109-1111.

Robinson, G. J. 1994. The Accuracy of Digital Elevation Models Derived from Digitized Contour Data. *Photogrammetric Record,* 14, 805-814.

Ruiz, E. V. T., Yuan, Y., Bingner, R., Acevedo, A. P., Y Rafael, J. L. a. M. and Alcántara, P. 2007 EVALUATION OF THE COMPOUND TOPOGRAPHIC INDEX (CTI) FOR THE LOCATION OF EPHEMERAL GULLIES ON OLIVE ORCHARDS AT A MICROCATCHMENT SCALE.

Saleh, A. and Belal, A. A. 2014. Delineation of site-specific management zones by fuzzy clustering of soil and topographic attributes: A case study of East Nile Delta, Egypt. *8th International Symposium of the Digital Earth (Isde8),* 18.

Salski, A. 1992. Fuzzy knowledge-based models in ecological research. *Ecological modelling,* 63**,** 103-112.

Santisteban, L. D., Casalí, J., López, J. and ... 2005. Exploring the role of topography in small channel erosion. *Earth Surface ….*

Sappington, J. M., Longshore, K. M. and Thompson, D. B. 2007. Quantifying landscape ruggedness for animal habitat analysis: A case study using bighorn sheep in the Mojave Desert. *Journal of Wildlife Management,* 71**,** 1419-1426.

Schmidt, J., Hennrich, K. and Dikau, R. 2000. Scales and similarities in runoff processes with respect to geomorphometry. *Hydrological Processes,* 14**,** 1963-1979.

Schmidt, J. and Hewitt, A. 2004. Fuzzy land element classification from DTMs based on geometry and terrain position. *Geoderma,* 121**,** 243-256.

Schwindt, S., Pasternack, G., Bratovich, P. and ... 2019. Hydro-morphological parameters generate lifespan maps for stream restoration management. *Journal of environmental ….*

Sekaluvu, L., Sheshukov, A. Y. and Hutchinson, S. L. Accuracy of Topographic Index Models at Prediction of Ephemeral Gullies. 2015 ASABE Annual International Meeting, 2015. American Society of Agricultural and Biological Engineers, 1.

Sharpnack, D. A. 1969. An algorithm for computing slope and aspect from elevations. *Photogrammetric Engineering,* 35**,** 247-248.

Shary, P. A., Sharaya, L. S. and Mitusov, A. V. 2002. Fundamental quantitative methods of land surface analysis. *Geoderma,* 107**,** 1-32.

Sheshukov, A. Y. 2015. Predicting location and length of ephemeral gullies with a process-based Topographic Index model. *Proceedings of the International Association of Hydrological Sciences,* 367**,** 93-98.

Sheshukov, A. Y., Sekaluvu, L. and Hutchinson, S. L. 2018. Accuracy of topographic index models at identifying ephemeral gully trajectories on agricultural fields. *Geomorphology,* 306**,** 224-234.

Shi, X., Zhu, A. X., Burt, J. E., Oi, F. and Simonson, D. 2004. A case-based reasoning approach to fuzzy soil mapping. *Soil Science Society of America Journal,* 68**,** 885-894.

Silvan-Cardenas, J. L. and Wang, L. 2014. On quantifying post-classification subpixel landcover changes. *Isprs Journal of Photogrammetry and Remote Sensing,* 98**,** 94-105.

Simons, M., Podger, G. and Cooke, R. 1996. IQQM—a hydrologic modelling tool for water resource and salinity management. *Environmental Software,* 11**,** 185-192.

Simonson, R. W. 1995. *Factors of soil formation. A system of quantitative pedology*.

Skidmore, A. K. 1989. A comparison of techniques for calculating gradient and aspect from a gridded digital elevation model. *International journal of geographical information systems,* 3**,** 323-334.

Smith, L. M. 1993. Investigation of ephemeral gullies in loessial soils in Mississippi. DTIC Document.

Sriti, M., Thibaud, R. and Claramunt, C. 2005. A fuzzy identity-based temporal GIS for the analysis of geomorphometry changes. *Journal on Data Semantics Iii,* 3534**,** 81-99.

Storm, B. and Jorgensen, G. 1987. Simulation of water flow and soil erosion processes with a distributed physically-based modelling system. *Forest hydrology and watershed management/edited by RH Swanson, PY Bernier & PD Woodard*.

Summerell, G. K., Vaze, J., Tuteja, N. K., Grayson, R. B., Beale, G. and Dowling, T. I. 2005. Delineating the major landforms of catchments using an objective hydrological terrain analysis method. *Water Resources Research,* 41.

Svidzinska, D. 2011. *Mapping of landscape spatial dynamics patterns by the fuzzy clustering analysis*, agro.icm.edu.pl.

Tadono, T., Ishida, H., Oda, F., Naito, S., Minakawa, K. and Iwamoto, H. 2014. Precise global DEM generation by ALOS PRISM. *ISPRS Annals of the Photogrammetry, Remote Sensing and Spatial Information Sciences,* 2**,** 71.

Tadono, T., Nagai, H., Ishida, H., Oda, F., Naito, S., Minakawa, K. and Iwamoto, H. 2016. GENERATION OF THE 30 M-MESH GLOBAL DIGITAL SURFACE MODEL BY ALOS PRISM. *International Archives of the Photogrammetry, Remote Sensing and Spatial Information Sciences,* 4.

Taguas, E., Yuan, Y. P., Pena, A. and Ayuso, J. L. 2010. Prediction of Ephemeral Gullies by Using the Combined Topographical Index in a Micro-Catchment of Olive Groves in Andalucia, Spain. *Agrociencia,* 44**,** 409-426.

Takagi, T. and Sugeno, M. 1985. Fuzzy identification of systems and its applications to modeling and control. *IEEE Transactions on Systems, Man, and Cybernetics*, 116-132.

Takaku, J. and Tadono, T. Quality updates of 'AW3D' global DSM generated from ALOS PRISM. 2017 IEEE International Geoscience and Remote Sensing Symposium (IGARSS), 23-28 July 2017 2017. 5666-5669.

Takaku, J., Tadono, T. and Tsutsui, K. 2014. GENERATION OF HIGH RESOLUTION GLOBAL DSM FROM ALOS PRISM. *ISPRS Annals of Photogrammetry, Remote Sensing & Spatial Information Sciences,* 2.

Takaku, J., Tadono, T., Tsutsui, K. and Ichikawa, M. 2016. Validation of" AW3D" global DSM generated from Alos Prism. *ISPRS Annals of the Photogrammetry, Remote Sensing and Spatial Information Sciences,* 3**,** 25.

Takken, I., Beuselinck, L., Nachtergaele, J., Govers, G., Poesen, J. and Degraer, G. 1999. Spatial evaluation of a physically-based distributed erosion model (LISEM). *Catena,* 37**,** 431-447.

Tang, J. and Pilesjö, P. 2011. Estimating slope from raster data: a test of eight different algorithms in flat, undulating and steep terrain. *River Basin Management VI*.

Tarafdar, P. and Ray, R. 2005. Effect of trees on improvement of physical environment and fertility in soils of West Bengal. *Bull. Natl. Inst. Ecol,* 16**,** 129-136.

Thorne, C. 1984a. *Prediction of soil loss due to ephemeral gullies in arable fields*, dspace.library.colostate.edu.

Thorne, C., Amarasinghe, I., Gardiner, J., Gardiner, C. and ... 1997. *Bank protection using vegetation with special reference to the use of willows*, Rep.

Thorne, C., Chang, H. and Hey, R. 1988. *Prediction of hydraulic geometry of gravel-bed streams using the minimum stream power concept*.

Thorne, C., Grissinger, E. and Murphey, J. 1984a. Field study of ephemeral cropland gullies in northern Mississippi. *Paper-American Society of Agricultural Engineers (USA)*.

Thorne, C., Grissinger, E. and Murphey, J. 1984b. *Field study of ephemeral cropland gullies in northern Mississippi*, agris.fao.org.

Thorne, C. and Zevenbergen, L. 1984. On-site prediction of ephemeral gully erosion. Report to the US Department of Agriculture. *Agricultural Research and Soil Conservation Services*.

Thorne, C., Zevenbergen, L., Burt, T. and Butcher, D. 1987. Terrain analysis for quantitative description of zero-order basins. *IN: Erosion and Sedimentation in the Pacific Rim. IAHS Publication*.

Thorne, C., Zevenbergen, L. W., Grissinger, E. and Murphey, J. Ephemeral gullies as sources of sediment. Proceedings of the Fourth Federal Interagency Sedimentation Conference March 24-27, 1986, Las Vegas, Nevada., 1986.

Thorne, C. R. 1984b. Prediction of soil loss due to ephemeral gullies in arable fields. *Colorado State University Publications*.

Thorne, C. R. and Zevenbergen, L. W. 1990a. Prediction of Ephemeral Gully Erosion on Cropland in the South-Eastern United-States. *Soil Erosion on Agricultural Land***,** 447-460.

Thorne, C. R. and Zevenbergen, L. W. 1990b. Prediction of ephemeral gully erosion on cropland in the southeastern United States. *Soil erosion on agricultural land***,** 447-460.

Thorne, C. R., Zevenbergen, L. W., Grissinger, E. H. and Murphey, J. B. 1984c. Calculator program and nomograph for on-site prediction of ephemeral gully erosion. *CER; 84/85-36*.

Tobler, W. R. 1969. An analysis of a digitalized surface. *A study of the land type, Final Report on Contract No. DA-31-124-ARO-D-456 to US Army Research Office, Durham, NC, ed. CM Davis***,** 59-83.

Torri, D. and Poesen, J. 2014. A review of topographic threshold conditions for gully head development in different environments. *Earth-Science Reviews,* 130**,** 73-85.

Torri, D., Poesen, J., Borselli, L., Bryan, R. and Rossi, M. 2012. Spatial variation of bed roughness in eroding rills and gullies. *Catena,* 90**,** 76-86.

Travis, M. R., Elsner, G. H., Iverson, W. D. and Johnson, C. G. 1975. VIEWIT: computation of seen areas, slope, and aspect for land-use planning. *Gen. Tech. Rep. PSW-GTR-11. Berkeley, CA: Pacific Southwest Research Station, Forest Service, US Department of Agriculture: 70 p,* 11.

Unwin, D. J. 1981. *Introductory spatial analysis*, Taylor & Francis.

Usdi. 2019. *Surficial geology of Africa (geo7_2ag) - Shapefile - Data.gov* [Online]. Available: https://catalog.data.gov/dataset/surficial-geology-of-africa-geo7-2ag/resource/96d6e5e1-92f4-4eba-8494-23874159da8e [Accessed July 4, 2019 2019].

Valentin, C., Poesen, J. and Li, Y. 2005. Gully erosion: Impacts, factors and control. *Catena,* 63**,** 132-153.

Vandaele, K. and Poesen, J. 1995. Spatial and Temporal Patterns of Soil-Erosion Rates in an Agricultural Catchment, Central Belgium. *Catena,* 25**,** 213-226.

Vandaele, K., Poesen, J., Desilva, J. R. M., Govers, G. and Desmet, P. 1997. Assessment of factors controlling ephemeral gully erosion in Southern Portugal and Central Belgium using aerial photographs. *Zeitschrift Fur Geomorphologie,* 41**,** 273-287.

Vandaele, K., Poesen, J., Govers, G. and Vanwesemael, B. 1996a. Geomorphic threshold conditions for ephemeral gully incision. *Geomorphology,* 16**,** 161-173.

Vandaele, K., Poesen, J., Silva, J. D. and ... 1996b. *Rates and predictability of ephemeral gully erosion in two contrasting environments*, persee.fr.

Vandekerckhove, L., Poesen, J., Oostwoud Wijdenes, D., Nachtergaele, J., Kosmas, C., Roxo, M. and De Figueiredo, T. 2000. Thresholds for gully initiation and sedimentation in Mediterranean Europe. *Earth Surface Processes and Landforms,* 25**,** 1201-1220.

Vandekerckhove, L., Poesen, J., Wijdenes, D. O. and De Figueiredo, T. 1998. Topographical thresholds for ephemeral gully initiation in intensively cultivated areas of the Mediterranean. *Catena,* 33**,** 271-292.

Vanegas, M. C., Bloch, I. and Inglada, J. 2016. Fuzzy constraint satisfaction problem for model-based image interpretation. *Fuzzy Sets and Systems,* 286**,** 1-29.

Veitinger, J., Purves, R. S. and Sovilla, B. 2016. Potential slab avalanche release area identification from estimated winter terrain: a multi-scale, fuzzy logic approach. *Natural Hazards and Earth System Sciences,* 16**,** 2211-2225.

Vendrusculo, L. G. 2014. Classical gully spatial identification and slope stability modeling using high-resolution elevation and data mining technique.

Vertessy, R. A., Watson, F. G., Rahman, J. M., Cuddy, S. M., Seaton, S. P., Chiew, F. H., Scanlon, P. J., Marston, F. M., Lymburner, L. and Jeannelle, S. New software to aid water quality management in the catchments and waterways of the south-east Queensland region. Proceedings of the Third Australian Stream Management Conference, August, 2001. Citeseer, 27-29.

Viloria, J. and Pineda, M. 2016. Neuro-fuzzy Classification of the Landscape for Soil Mapping in the Central Plains of Venezuela. *Geopedology*.

Viney, N. R. and Sivapalan, M. 1999. A conceptual model of sediment transport: application to the Avon River Basin in Western Australia. *Hydrological Processes,* 13**,** 727-743.

Watson, C., Kargel, J. and Tiruwa, B. 2019. UAV-Derived Himalayan Topography: Hazard Assessments and Comparison with Global DEM Products. *Drones*.

Watson, F., Rahman, J. and Seaton, S. Deploying environmental software using the Tarsier modelling framework. Proceedings of the Third Australian Stream Management Conference, Brisbane, 2001. 631-637.

Wells, R. R., Momm, H. G., Bennett, S. J., Gesch, K. R., Dabney, S. M., Cruse, R. and Wilson, G. V. 2016. A Measurement Method for Rill and Ephemeral Gully Erosion Assessments. *Soil Science Society of America Journal,* 80**,** 203-214.

Wheaton, J. M. 2008. Uncertainty in morphological sediment budgeting of rivers. *Unpublished PhD, University of Southampton, Southampton,* 412.

Wicks, J. and Bathurst, J. 1996. SHESED: a physically based, distributed erosion and sediment yield component for the SHE hydrological modelling system. *Journal of Hydrology,* 175**,** 213-238.

Wicks, J. M. 1988. Physically-based mathematical modelling of catchment sediment yield.

Williams, R. D. 2012. DEMs of Difference. *Geomorphological Techniques,* 2**,** 1-17.

Wischmeier, W. H., Johnson, C. B. and Cross, B. V. 1971. Soil Erodibility Nomograph for Farmland and Construction Sites. *Journal of Soil and Water Conservation,* 26**,** 189-+.

Wischmeier, W. H. and Smith, D. D. 1978. Predicting rainfall erosion losses-A guide to conservation planning. *Predicting rainfall erosion losses-A guide to conservation planning*.

Wise, S. 1998. *The effect of GIS interpolation errors on the use of digital elevation models in geomorphology*, Wiley, Chichester.

Wolock, D. M. and Price, C. V. 1994. Effects of Digital Elevation Model Map Scale and Data Resolution on a Topography-Based Watershed Model. *Water Resources Research,* 30**,** 3041-3052.

Wong, W. V. C., Tsuyuki, S., Ioki, K. and Phua, M.-H. 2014. *Accuracy assessment of global topographic data (SRTM & ASTER GDEM) in comparison with lidar for tropical montane forest*.

Wood, J. 1994. *Visualizing contour interpolation accuracy in digital elevation models*.

Wood, J. 1996. The geomorphological characterisation of digital elevation models. *Ph. D. Dissertation***,** 160-160.

Wood, J. D. and Fisher, P. F. 1993. Assessing Interpolation Accuracy in Elevation Models. *Ieee Computer Graphics and Applications,* 13**,** 48-56.

Woodward, D. E. 1999. Method to predict cropland ephemeral gully erosion. *Catena,* 37**,** 393-399.

Xu, M. X., Li, Q. and Wilson, G. 2016. Degradation of soil physicochemical quality by ephemeral gully erosion on sloping cropland of the hilly Loess Plateau, China. *Soil & Tillage Research,* 155**,** 9-18.

Yan, C. Q., Yue, T. X., Liu, J. M., Zhao, C. Y., Li, H. and Chen, C. F. 2015. A Comparison of Methods for Solving High Accuracy Surface Modeling in DEM Construction. *Journal of Algorithms & Computational Technology,* 9**,** 377-388.

Yang, C. T. 1979. Unit Stream Power Equations for Total Load. *Journal of Hydrology,* 40**,** 123-138.

Yang, X., Chapman, G., Young, M. and Gray, J. Using compound topographic index to delineate soil landscape facets from digital elevation models for comprehensive coastal assessment. MODSIM 2005 International Congress on Modelling and Simulation. Modelling and Simulation Society of Australia and New Zealand, 2005. 1511-1517.

Yang, X., Chapman, G. A., Gray, J. M. and Young, M. A. 2007. Delineating soil landscape facets from digital elevation models using compound topographic index in a geographic information system. *Australian Journal of Soil Research,* 45**,** 569-576.

Young, A. 1972. Slopes: Edinburgh. *Oliver and Boyd,* 288.

Young, A. 1999. Is there really spare land? A critique of estimates of available cultivable land in developing countries. *Environment, Development and Sustainability,* 1**,** 3-18.

Young, A. and Clayton, K. M. 1972. *Slopes*, Longman.

Young, M. 1978. Terrain Analysis: Program Documentation. Report 5 on Grant DA-ERO-591-73-60040. Statistical characterization of altitude matrices by computer. European Research Office. *US Army. IS Evans, Principal Investigator. University of Durham, England*.

Young, R. A., Onstad, C. A., Bosch, D. D. and Anderson, W. P. 1989. Agnps - a Nonpoint-Source Pollution Model for Evaluating Agricultural Watersheds. *Journal of Soil and Water Conservation,* 44**,** 168-173.

Yu, B., Rose, C., Ciesiolka, C., Coughlan, K. and Fentie, B. 1997. Toward a framework for runoff and soil loss prediction using GUEST technology. *Soil Research,* 35**,** 1191-1212.

Yunkai, L., Yingjie, T., Zhiyun, O., Lingyan, W., Tingwu, X., Peiling, Y. and Huanxun, Z. 2010. Analysis of soil erosion characteristics in small watersheds with particle swarm optimization, support vector machine, and artificial neuronal networks. *Environmental Earth Sciences,* 60**,** 1559-1568.

Zadeh, L. A. 1965. Information and control. *Fuzzy sets,* 8**,** 338-353.

Zadeh, L. A. 1976. A fuzzy-algorithmic approach to the definition of complex or imprecise concepts. *Systems Theory in the Social Sciences.* Springer.

Zadeh, L. A. 1983. A Computational Approach to Fuzzy Quantifiers in Natural Languages. *Computers & Mathematics with Applications,* 9**,** 149-184.

Zadeh, L. A. 1996a. Fuzzy logic = computing with words. *IEEE Transactions on Fuzzy Systems,* 4**,** 103-111.

Zadeh, L. A. 1996b. Fuzzy logic, neural networks, and soft computing. *Fuzzy Sets, Fuzzy Logic, And Fuzzy Systems: Selected Papers by Lotfi A Zadeh.* World Scientific.

Zadeh, L. A. 1997. Toward a theory of fuzzy information granulation and its centrality in human reasoning and fuzzy logic. *Fuzzy Sets and Systems,* 90**,** 111-127.

Zakerinejad, R. and Maerker, M. 2015. An integrated assessment of soil erosion dynamics with special emphasis on gully erosion in the Mazayjan basin, southwestern Iran. *Natural Hazards,* 79**,** S25-S50.

Zartl, A. S., Klik, A. and Huang, C. 2001. Soil detachment and transport processes from interrill and rill areas. *Physics and Chemistry of the Earth Part B-Hydrology Oceans and Atmosphere,* 26**,** 25-26.

Zevenbergen, L. 1987. *Erosion modelling using terrain analysis*.

Zevenbergen, L. W. 1989. *Modelling erosion using terrain analysis.* Thesis presented for the degree of Doctors of Philosophy in the University of London.

Zevenbergen, L. W. and Thorne, C. R. 1987. Quantitative-Analysis of Land Surface-Topography. *Earth Surface Processes and Landforms,* 12**,** 47-56.

Zhao, W. and Li, A. N. 2015. A Review on Land Surface Processes Modelling over Complex Terrain. *Advances in Meteorology,* 2015**,** 1-17.

Zheng, S., Thorne, C. R., Wu, B. S. and Han, S. S. 2017. Application of the Stream Evolution Model to a Volcanically Disturbed River: The North Fork Toutle River, Washington State, USA. *River Research and Applications,* 33**,** 937-948.

Zhou, Q. M. and Liu, X. J. 2004. Analysis of errors of derived slope and aspect related to DEM data properties. *Computers & Geosciences,* 30**,** 369-378.

Zhu, A. X., Hudson, B., Burt, J., Lubich, K. and Simonson, D. 2001. Soil mapping using GIS, expert knowledge, and fuzzy logic. *Soil Science Society of America Journal,* 65**,** 1463-1472.

Zweig, M. H. and Campbell, G. 1993. Receiver-operating characteristic (ROC) plots: a fundamental evaluation tool in clinical medicine. *Clinical chemistry,* 39**,** 561-577.